12-2004

The Synthesis and Characterization of Mesoporous Uranium Oxide Catalysts for Oxidative Destructions of Volatile Organic Compounds and Clean Air Protection

Cyrus Khezr Riahi-Nezhad
University of Tennessee, Knoxville

To the Graduate Council:

I am submitting herewith a thesis written by Cyrus Khezr Riahi-Nezhad entitled "The Synthesis and Characterization of Mesoporous Uranium Oxide Catalysts for Oxidative Destructions of Volatile Organic Compounds and Clean Air Protection." I have examined the final electronic copy of this thesis for form and content and recommend that it be accepted in partial fulfillment of the requirements for the degree of Master of Science, with a major in Environmental Engineering.

<div align="right">

Terry L. Miller, Major Professor

</div>

We have read this thesis and recommend its acceptance:

Chris D. Cox, Randall W. Gentry

<div align="right">

Accepted for the Council:
<u>Carolyn R. Hodges</u>

Vice Provost and Dean of the Graduate School

</div>

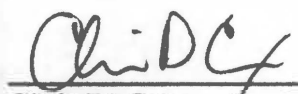(Original signatures are on file with official student records.)

To the Graduate Council:

I am submitting herewith a thesis written by Cyrus Khezr Riahi-Nezhad entitled "The Synthesis and Characterization of Mesoporous Uranium Oxide Catalysts for Oxidative Destructions of Volatile Organic Compounds and Clean Air Protection." I have examined the final paper copy of this thesis for form and content and recommend that it be accepted in partial fulfillment of the requirements for the degree of Master of Science, with a major in Environmental Engineering.
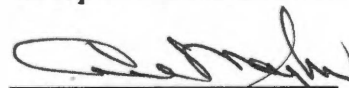
Terry L. Miller, Major Professor

We have read this thesis
and recommend its acceptance:

Chris D. Cox

Randall W. Gentry

Accepted for the Council:

Vice Chancellor and
Dean of Graduate Studies

THE SYNTHESIS AND CHARACTERIZATION OF MESOPOROUS URANIUM OXIDE CATALYSTS FOR OXIDATIVE DESTRUCTIONS OF VOLATILE ORGANIC COMPOUNDS AND CLEAN AIR PROTECTION

**A Thesis
Presented for the
Master of Science
Degree
The University of Tennessee, Knoxville**

Cyrus Khezr Riahi-Nezhad

December 2004

ACKNOWLEDGMENTS

Writing a thesis is hard even this my second thesis, but acknowledging all of the people and organizations that helped for this thesis can be even harder. You don't want to forget anyone who provided original, administrative, technical, editorial and financial support. You want to show enthusiasm and let them to know that you couldn't have completed this thesis without their help. You want the readers to know that the thesis they are reading evolved from the collective effort of many talented people.

The author wishes to thank Oak Ridge National Laboratory for providing the financial support which made this work possible. Several people contributed in significant measure to this program. The author's deepest appreciation and thanks go to the following people:

Dr. Terry L. Miller, major professor, for his invaluable guidance, technical advice and friendship.

Dr. Steven H. Overbury, group leader, supervisor and the leader for exploring possible applications for DU catalysts at ORNL, for his support and suggestion of preparing and characterizing the catalyst. The knowledge about catalysis that I have learned through conversations with Dr. Overbury is immeasurable.

Dr. Chris D. Cox, committee member, for his comments, contributions, kindness and suggestions.

Dr. Randall W. Gentry, committee member, for his kindness, encouragement, understanding and suggestions.

Jane E. Taylor at University of Tennessee, Dee Dee L. Greene at Oak Ridge National Laboratory for their secretarial services.

Finally, I would like to express my appreciation of my parents for their support, love, and encouragement to pursue my education which resulted in this work.

ABSTRACT

The overall goal of this research was to investigate a new class of mesoporous uranium oxide catalyst used to destroy a range of volatile organic compounds (VOCs), including aromatics and chlorinated organic compounds under conditions which are applicable for U.S. Department of Energy (DOE) facilities and U.S industries.

Uranium oxides are known to have high efficiency and long-term stability when used to destroy volatile organic compounds (VOCs) when compared with some of the commercial catalysts, such as precious metals, TiO_2, and Co_3O_4 catalysts. Two key factors limiting catalytic activities of uranium oxides prepared by conventional methods are small *surface area* and *pore size*. To overcome these limitations, mesoporous uranium oxides dispersed on mesoporous oxide hosts were synthesized and tested for VOC destruction efficiency.

This research work consisted of synthesizing potential depleted uranium catalysts, as well as testing and structural characterization. A plug flow microreactor was built and used to measure the catalytic performance of toluene, chlorobenzene, and trichloroethylene (TCE) vs. catalyst temperature. These data result in so-called 'light-off' curves. Destruction efficiency generally increases with temperature. These VOCs were chosen as typical of those found in anticipated air pollution controls applications.

The catalysts have been tested for the destruction of VOCs at space velocities of 84,000 $mlg^{-1}h^{-1}$. A gas chromatograph and a sampling mass spectrometer were used to measure conversion and reaction by-products. The X-ray diffraction (XRD), transmission electron microscope (TEM) and Brunauer-Emmett-Teller (BET) adsorption-

desorption isotherm surface area measurements were used to provide information about the compositions present in the catalyst.

Catalysts were synthesized using a variety of methods, most notably a method that includes template-moderated co-synthesis of mesoporous oxides. Catalyst activity was improved by supporting the uranium oxide on silica. Dopants (e.g., Cr, Co, K, Br, Fe, Ca, Mg, Cu, Pt, La, Ce, Sr) were added to the urania to improve the catalytic activity. Catalyst performance was compared with that of conventional catalysts. Further improvement was made by supporting uranium on titanium oxide. This co-assembled formulated catalyst was found to be competitive with noble metal catalysts for catalytic oxidation of VOCs and chlorinated VOCs. The variation in the U:Ti ratio indicates that optimal activity for oxidation of toluene, chlorobenzene, and trichloroethylene was obtained for U:Ti ratio of 1:20 at calcinations temperature of 600 °C. It was stable to deactivation and operates effectively in the presence of large amounts of water.

The gained experiences of this project can be used in the clean up of emissions from soil vapor extraction wells, which are in use to remove VOCs from ground water at DOE's Hanford and Savannah River sites.

This work was conducted under the auspices of the U.S. Department of Energy's (EM-21) Depleted Uranium uses Research and Development Program.

TABLE OF CONTENTS

LIST OF TABLES

LIST OF FIGURES

LIST OF SYNTHESIS CALCULATIONS

CHAPTER 1

INTRODUCTION

One of the inadvertent consequences of the industrial age is the creation of waste products and byproducts, which are often released to the air, land or water. The sources of these emissions include automobiles, polymers, paints, process vents, process vent leaks, transfer operations, storage vessels, waste water treatment, and equipment leaks [1]. Volatile organic compound (VOC) abatement has gained recent attention due to a better understanding of the effects of releasing these compounds into the environment. Both the magnitude and hazards of emissions of toxic compounds have led to public health concern and recent government regulations to reduce emissions.

Volatile organic compounds (VOCs) are the most common and significant atmospheric pollutants due to their toxicity and odorous nature [2]. They are defined as "any compound of carbon, excluding carbon monoxide, carbon dioxide, carbonic acid, metallic carbides or carbonates, and ammonium carbonate, which participates in atmospheric photochemical reactions" [3]. If, however, the photochemical reactivity of an organic compound is negligible, it can be excluded from classification as a VOC.

The Clean Air Act Amendments of 1990 (CAAA) changed the air quality regulations in the United States. A major component of the CAAA concerns the emissions of hazardous air pollutants (HAPs). After the rules have been implemented by U.S Environmental Protection Agency (EPA), U.S. industries and U.S. Department of Energy must manage and modify their operations and emission control systems for off

1

gas wastes consisting of complex volatile organic compounds to meet the regulatory challenges [4]. This title calls for a 90% reduction in the emissions of 189 toxic chemicals which are mainly VOCs, by 1998.

Each year, approximately, 706000 tons of organic pollutants are discharged to the atmosphere from US alone and twice that of U.S are worldwide discharges [5]. Approximately, 70% of these compounds are VOCs. This release has been linked to the depletion of ozone layer [6] and production of ground-level ozone [7] and photochemical smog [8].

More than 2,500 soil and ground water plumes are contaminated with organic source solvents, such as alkanes, aromatics, and chlorinated organics compounds. The organic compounds are not readily degraded by microorganisms and thus persist in environmental media. Many technologies are available for the treatment of VOCs [9]. Pump-and-treat and vacuum-extraction techniques have been developed and are commonly used for remediating contaminated soils and ground water [10-13]. Adsorption has been used widely by using zeolite or carbon type adsorbents which create considerable waste and the low gas hourly space velocity is a limiting factor for the VOCs adsorption system (14, 15), and also the small pore size of zeolite materials could be problematic when large waste polymer molecules are emitted with VOCs in the real industries. Thermal oxidation or incineration [16, 17] is very common technique in which requires very high temperature up to 1000 °C. This is a fuel intensive technique with small control over the conditions of products which may result the formation of NO_x, dioxins and furans. Therefore, it is very important to establish an effective method

2

to abate these organic compounds to reduce the emission of pollution without overwhelming economic growth.

In contrast, catalytic oxidation is a promising method for energy consumption and has a better temperature control over the products. The catalytic reaction occurs at the fluid-solid interface and a large surface area is very helpful in attaining a significant reaction rate. This surface area is provided by many fine pores in a porous structure and these pores provide the necessary area for high rate of reaction [18]. Another distinct advantage of catalytic oxidation is that it can operate with very dilute pollutant concentration (<1%), which can be thermally combusted without additional fuel.

Several alternative and clean methods, such as catalytic oxidation over noble metals and transition metal oxides are proposed in the literature for destruction of VOCs [19-22]. Supported noble metal catalyst, primarily platinum and palladium, show high combustion activity for the oxidation of many VOCs; however, they are relatively expensive, susceptible to poisoning even at low contaminant levels, and in some cases show poor stability. Metal oxide catalyst (such as TiO_2 and Co_3O_4) can tolerate relatively high levels of poisons; however, the activity shown by these oxides is generally lower than precious metal catalysts (23, 24). It is therefore recognized that the slow reaction kinetics and low destruction efficiency of VOCs have been limiting steps to remediate VOC-contaminated soils and groundwater or other mixed waste stream.

A high-activity oxide catalyst that can operate at a relatively low temperature (<450 °C) is highly desirable. Uranium oxides based catalysts are thermally stable, destroy low concentrations and mixtures of VOCs and lifetime studies indicate that deactivation during oxidation of chlorinated of VOCs did not occurre [24, 25]. Uranium

3

oxide based catalysts have also shown relatively high activity for carbon monoxide oxidation [26]. Two key factors limiting catalytic activities of uranium oxides prepared by conventional methods are small surface area and pore size [27]. The porous material is the best candidate as supports for dispersed catalysts. Ordered mesoporous materials are one of the most exciting discoveries in the field of materials synthesis over the past decade [28]. The most interesting feature of mesoporous materials is its regular pore structure, which consists of a hexagonal array with a pore dimension of 2-10 nm (29). This property offers a very high surface area with very regular pore size dimensions allowing the deposition of active phases, such as transition metal complexes and oxides, and the transport of organics in catalytically active sites [30].

Previously, uranium oxides have been considered as a waste in our environment; however, here we show that we can prepare catalysts made of uniform U_3O_8 nanocrystals incorporated into a mesoporous oxide matrix, which result in high activity for the destruction of volatile organic compounds. This can be effectively used to provide a solution to a major problem affecting our environment such as VOC, including alkanes, aromatics, and chlorinated organic compounds under industrially relevant flow rates and temperatures. Since uranium oxides are nonvolatile and catalytic reactions only involve gas/solid heterogeneous reactions, there is no potential risk of leaching radioactive materials into the environment during thermal reaction.

1.1 Problem Statement and Research Objectives

The overall goal of this research is to investigate a new class of mesoporous uranium oxide catalyst to destroy a range of volatile organic contaminants, including alkanes, aromatics, and chlorinated organic compounds, through the reutilization of depleted uranium. This study is motivated by the high efficiency and long-term performance of uranium-oxide-based catalyst in degrading many contaminant organic substrates as compared with some precious metal catalysts, and by the needs for efficient disposal or reutilization of spent uranium at many DOE facilities. Current uranium-oxide catalyst (e.g. U_3O_8), prepared by conventional solid-state syntheses, have very small surface area (<1 m^2/g). A large surface area is essential to increase the surface-adsorption capacity of VOCs on catalysts, which is a pre-condition for any efficient heterogeneous catalytic reactions. Furthermore, conventional uranium-oxide catalysts are basically non-porous materials, implying that the bulk of the uranium-oxide catalysts are not involved in catalytic reactions because they are inaccessible to reactant molecules. Accordingly, any increase in surface area will greatly increase the catalytic efficiency of the uranium oxides in the destruction of VOCs. Using co-assembly synthesis methodology, our specific objectives are as follows:

- Synthesize the mesoporous uranium oxide (U_3O_8) and mesoporous supports (silica, titania) doped with uranium compounds through a novel surfactant template synthetic method.

- Characterize the mesoporous uranium oxide (U_3O_8) and uranium oxides supported by mesoporous materials (e.g. silica, titania).

- Determine the kinetics, mechanisms, pathways, and rate-limiting steps of the surface catalyzed thermal oxidation processes on the mesoporous uranium oxide and mesoporous hosts loaded with uranium oxides.

1.2 Thesis Organization

This thesis is organized into eight chapters. After this introductory chapter, Chapter 2 presents a review of pertinent literature. Basic concept and fundamentals in catalyst preparations are described in chapter 3. Experimental setup and procedures, catalyst preparations are described in Chapter 4. Theoretical considerations such as gas adsorption on solid, classification of adsorption isotherm and adsorption hysteresis are presented in chapter 5. Results and discussion will cover catalyst activities (BET, XRD, and Mass Spectrometer), effect of VOCs concentration, kinetics and mechanism. This will be presented in chapter 6. Summary and conclusions are presented in chapter 7. Avenues for future works are suggested in chapter 8.

CHAPTER 2

REVIEW OF PERTINENT LITERATURE

This chapter provides an overview of end-of-pipe abatement technologies for VOCs. For each technology, the overview includes basic operating theory, general applicability issues, advantages, and disadvantages.

2.1 Pump and Treat Remediation

Pump and treat is one of the most widely used groundwater remediation technologies. Groundwater contaminated with dissolved organic contaminants can be pumped out of the aquifer using a series of extraction wells and be treated on the surface of the ground to remove the contaminants. The treated groundwater can either be returned to the pumped aquifer, or dispose of it off site. Hence, this method is referred to as pump-and-treat [31]. The pump-and treat remediation approach is used at about three-quarters of the Superfund sites where ground water is contaminated and most sites where cleanup is required by the Resource Conservation and Recovery Act (RCRA) and National Research Council (NRC).

Pump-and-treat systems are used primarily to control the movement of contaminated ground water, preventing the continued expansion of the contaminated zone and reduce the dissolved contaminant concentrations in ground water sufficiently that the aquifer complies with cleanup standards and restore the aquifer [33]. The major advantage of pump-and-treat is removing the contaminated ground water with a variety

of dissolved materials, including VOCs, SVOCs, fuel, UXO (i.e., explosive compounds) and dissolved metals. However, this method suffers from serious disadvantages, due a series of subsurface processes. One of the major disadvantages of pump and treat is that the degree of contaminant removal is highly dependant on the chemical nature of the contaminant and the subsurface geology. Additional factors come into play when debating the possible use of pump-and-treat for aquifer remediation. Remediation by pump-and-treat is a slow process and cleanup times are often very long [34].

2.2 Soil Vapor Extraction

Soil vapor extraction (SVE), also known as volatilization or vacuum extraction, is an effective technique in removing of volatile organic compounds (VOCs) and certain semi-volatile organic compounds (SVOCs) found in vapor-phase of petroleum contaminants from the unsaturated (vadose) zone [35]. SVE consists of a system of small diameter vertical wells and lateral trenches linked to piping network that ends in a vacuum pump at the wellhead. Soil vapor extraction works by creating negative pressure gradients in a series of zone within the unsaturated soil. This negative pressure causes a subsurface airflow. The air in the soil is replaced with fresh air that strips the vapor phase hydrocarbons from spaces between soil particles in the vadose zone [36]. The extracted vapors are treated, as necessary, and discharged to the atmosphere or possibly reinjected to the subsurfaces by applicable state laws. Some of the factors that determine the effectiveness of SVE are: Temperature, depth to groundwater, soil moisture, soil porosity, and volatility of the contaminant [37]. The major advantages of SVE is the

performance and availability of equipment with minimal disturbances to site operations. It can be applied at sites with competitive cost and combined with other technologies such as charcoal adsorption or catalytic oxidation. It is effective only to treat unsaturated-zone soils and concentration reductions greater than 90% are difficult to achieve. Soil with high moisture requires higher vacuum, hindering the operation of SVE system. SVE will not remove heavy oils, metals, PCBs, or dioxins. Air emission permits are generally required.

2.3 Thermal Desorption

Thermal desorption is a physical separation process, not as a form of incineration [38]. Thermal desorption systems are made up of three parts: the pretreatment and material handling system, the desorption unit, and the post-treatment sytems. Pretreatment and material handling system is used to remove large blocks and foreign objects. In the desorption unit system, soil is heated to volatize water, organic contaminants and certain metals. A carrier gas or vacuum system transports vaporized water and organics to the desorption unit system. The chamber temperatures and residence time aims to volatize the contaminants but not to oxidize them. Offgas from the desorber is usually processed to take out particulate matter in the gas stream after the desorption step. The vaporized contaminants in this offgas requires further treatments.

Two common thermal desorption designs are the rotary dryer and thermal screw conveyor. Rotary dryer is cylindrical in shape, arranged horizontally and rotates around its axis. In thermal screw units, screw conveyors or hollow augers are used to transport

9

the medium through an enclosed trough. Hot oil or steam circulates through the auger to indirectly heat the soil.

Based on the operating temperature of the desorber, thermal desorption processes can be categorized into two groups: high temperature thermal desorption (HTTD) and low temperature thermal desorption (LTTD). In high temperature thermal desorption, wastes are heated to 320 to 560 ^{0}C. HTTD is frequently used in combination with incineration, solidification/stabilization, or dechlorination, depending upon site-specific conditions. In low temperature thermal desorption, wastes are heated to between 90 and 320 ^{0}C. This is a full-scale technology that has been proven successful for remediating petroleum hydrocarbon contamination in all types of soil.

Treatment and control of air emissions from thermal desorption operations is extremely important consideration. There should be no emissions of metals, certain polycyclic aromatic hydrocarbons and dioxins/furans. Mercury emissions are very difficult to control, and using an afterburner is unaccepted. Dust and organic matter in the soil increase the difficulty of treating off-gas. Clay and silty soils and high humic content soils increase reaction time as a result of binding of contaminants [39].

2.4 Adsorption

Adsorption has been used throughout history as a water treatment process since biblical times. This process involves mass transfer of a molecule from the gas or liquid phase onto the surface of a solid substrate. The ancient Hindus filtered their water with

10

charcoal and in the thirteen century, carbon materials were used in a process to purify sugar solution.

Two types of adsorption phenomena have been known: physical adsorption takes place when intermolecular forces (Van der Waals) attract and hold the gas molecules to the solid surface and it is similar in character to condensation of vapor molecules onto a liquid of the same composition [40]. Chemisorption occurs when a chemical bond forms between the gas molecule and the solid surface. The removal of a chemisorbed component is more difficult and requires more energy input. A physically adsorbed molecule can be removed readily from the adsorbent surface due to its weaker bond. Physical adsorption on activated carbon is of particular interest here for treatment of VOCs.

Carbon adsorption is a remediation technology in which pollutants are removed from air by means of physical adsorption. Carbon is activated for this purpose by processing the carbon to create porous particles with a large surface area of 300 to 2,500 m^2 per gram of carbon that attracts and adsorbs organic molecules as well as metal and inorganic molecules. It is porous, and the size of the pores is important in determining the effectiveness of the adsorbent [41]. Contaminated air is passed through one or more vessels containing activated carbon. Contaminants sorb onto the surfaces of the activated carbon grains. The activated carbon attracts and adsorbs organic and inorganic molecules. When the concentration of contaminants in the air exiting the vessels exceeds a certain level, the carbon must be replaced. Spent carbon can be regenerated in place; removed and regenerated at an off-site facility or disposed [42, 43]. Some degradation products such as vinyl chloride and smaller molecules are not sorbed well, and they must

11

be monitored carefully. Spent carbon transport may require hazardous waste handling. Relative humidity greater than 50% and elevated temperatures from soil vapor extraction (SVE) pumps greater than 38 °C reduces carbon capacity.

2.5 HEPA Filters

High Efficiency Particulate Attenuation (HEPA) filters are used to prevent the emissions of particulates and mists into the environment. Filters are often made of 0.013-inch thick glass fiber materials. These filters are efficient to capture 99.97% of 0.3 micron diameter aerosol particles. Water is the major problem for HEPA. Usually, a preheater is installed in the air ducts of waste stream to prevent condensation which damage the HEPA. Construction of HEPA with sintered stainless steel will provide a filter which is not subject to water damage and can be installed with built in water jets to wash the filter to reduce radiation and to eliminate the dirt accumulation. Preliminary tests showed that the use of such filters gives the same efficiency as filtration with a fiberglass filter medium. This medium resulted in data indicating that it was efficient to capture 99.97% of aerosol with 0.3 micron in diameter. Test data indicated that removal of water from the clean side of the filter is required for normal filter operation. Water on the clean side of filter flows by gravity and air movement out of the bottom of the cylindrical filter. Using a vacuum pump, clean air will be drawn out of the cylindrical filter. Water sprayed on the dirty side of a vertical filter flushes the accumulated aerosol down the dirty side. One of the advantages is the formation of a very thin filter medium which stops particle transmission at the exposed surface of the medium. The collected

particles can be easily removed from the relatively smooth surface compared to a thicker medium, such as wire mesh. In addition, the stainless steel construction makes the filter resistant to mechanical damage, high pressure, and temperature. On the other hand, washing the dirty side of filter increases the waste volume.

2.6 Electro-Filtration

The removal of sub-micron particles from processed waste streams is ineffective and requires a significant amount of energy. Several reports on investigations of electrically enhanced aerosol filtration in fiber filters have been published. Silverman [44], Thomas and Woodfin [45] empirically showed that fiber filtration efficiency was enhanced by the application of an electric field. They used a bank of metal screens [44] and several layers of nylon hosiery [45] placed between high voltage electrodes as a filter. They measured filtration efficiency with and without electric field. The filtration efficiency was much higher with electric field.

Bogardus [46] and Fielding [47] studied the performance of commercial fiber filters when placed in an electric field. Their experiment showed great improvements of filtration efficiency over non-electrified filters.

Granular filtration (deep-bed filtration) is mechanically simple and consumes little energy. However, it relies principally on the mechanisms of interception, sedimentation, diffusion, inertia, and surface forces, which yield low collision efficiency between particle and collectors [48]. It is well known that the efficiency of aerosol filtration in fiber mats [44] and in granular beds [49] can be improved by the application

13

of an electric field to the filter media. Filtration efficiency greater than 99% are repoted in the literature [50].

A granular electrofilter is simply a bed of coarse particles (diameter ≈1mm), with electrodes arranged so that a strong electric field can be applied to the bed. The electric field polarizes the packing granules, and the combined electric field causes the charged suspended particles to deviate from the fluid streamline and be collected on the oppositely charged surface of the granules. In a different concept of electrofiltration, the electric charge is applied directly to the granules [51]. In this case, the granular electrofilter operates much like an electrostatic precipitator, but with more complex flow paths. This type of electrofiltration is more suitable with less densely packed beds, such as fiber filled beds. The filter media is also restricted to a conducting medium.

Applied electric field across fibrous filters have enhanced performance with gas filtration, and successful mathematical analyses have been presented [52, 53]. There are two differences between fibrous and granular filters: first, the geometry of the collecting solids, and second, in fibrous filtration of gaseous streams, the drag on suspending particles is more likely to be dominated by inertial rather than viscous forces.

Local electric fields are essentially in the direction of the applied field and important deviations occur near the granule or fiber packing. If the granules/fiber packing are non-conducting, the field lines will be diverted around the granules or fibers. If the packing is a better conductor than the fluid, the field lines will be diverted toward the granules or fibers. Since the electric forces on the particulates act along the electric field lines, it is desirable to have the lines diverted into (rather than around) the granules or fibers. This is similar to the concept of using conducting granules or fibers which can

14

be considered to have a very high dielectric constant than the fluid. When both fluid and packing are conductors, it is desirable for the granules or fibers to have a higher conductivity than the fluid. In the case, the packing materials are highly conductive, more or less packed fibers may be needed to prevent unnecessary current through the bed. Cleaner granules could be obtained by vigorously backwashing, but the particles could be obtained in a more concentrated suspension by slow backwashing when the field is off [54].

In summary, many parameters can have a major effect on the electric filtration process such as geometry of packing and density, orientation and strength of the electric field, particle charge, dielectric constant and conductivity of the packing material and fluid, and particle size. It is in our best interest to take all of the major parameters into account in order to achieve the highest separation efficiency.

2.7 Thermal Oxidation

Thermal oxidation or thermal incineration, is the process of oxidizing combustible materials in the exhaust gas from air strippers and SVE system by raising their temperature above the autoignition point in the presence of oxygen and maintaining them at high temperature for sufficient time to complete combustion to CO_2 and H_2O. Time, temperature, turbulence, and the amount of oxygen affect the rate and efficiency of the combustion process.

Thermal oxidation units are typically single chamber, refractory-lined oxidizer equipped with a propane or natural gas burner, a fan to move volatile organic compound (VOC) laden air; a filter-mixer to mix the VOC-laden air and a stack. Thermal oxidizers

15

are often equipped with heat exchangers where combustion gas is used to preheat the incoming contaminated gas. Operating temperatures range from 760 to 871 C, and gas residence times are typically 1 second or less. Thermal oxidation units typically are used to treat halogenated and nonhalogenated VOCs and semivolatile organic compounds (SVOCs) and polychlorinated biphenyls (PCBs) in a gas stream. Thermal oxidation is most efficiently applied for treating off-gass containing 1,000 to 5000 ppmv of combustibles.

In general, thermal oxidizers are not well suited to exhaust streams with low concentration (>1000 ppmv) and highly variable flow rates because of the reduced residence time and poor mixing resulting from high flow rates that decrease the completeness of combustion. This causes the combustion chamber temperature to fall, decreasing the destruction efficiency. Thermal combustion system usually has very high capital cost [55].

CHAPTER 3

FUNDAMENTALS IN CATALYST PREPARATION

The objectives of this chapter are to develop an understanding of what it can be expected to do or not to do by a catalyst, catalyst organization within industrial and academic fields, and classification according to the preparation procedure. We start the discussion with a definition: *A catalyst is a substance that increases the rate at which a chemical reaction approaches equilibrium without itself becoming permanently involved in the reaction* [56].

Enzymes Catalysis is involved the application of enzymes for biochemical reactions. Enzymes are protein molecules of colloidal size and they are between the molecular homogeneous and the macroscopic heterogeneous catalyst. They are characterized by tremendous efficiencies and selectivities [57].

Homogeneous catalysis concerns processes in which a catalyst is the same phase as the reactants and products [58]. An example of homogeneous catalysis is the industrial Oxo process for manufacturing normal isobutyl-aldehyde. It has propylene, carbon monoxide, and hydrogen as the reactants and a liquid-phase cobalt complex as the catalyst.

Heterogeneous Catalysis involves more than one phase; usually solid catalysts are used with gaseous or liquid reactants, sometimes both. Much of the benzene production in US is manufactured from the dehydrogenation of cyclohexane using platinum-on-alumina as the catalyst. The heterogeneous catalytic reaction occurs at or very near the

17

fluid-solid interface [18]. A heterogeneous catalyst is a composite material, characterized by: (a) the active species, physical and/or chemical promoters, and supports; (b) shape; (c) size; (d) pore volume and distribution; (e) surface area. They are convenient to use commercially. Easily prepared solid catalyst pellets, packed in tubes through which reactants flow, satisfy process requirements for simple construction and dependable operation. Majority of industrial catalytic processes adopt this approach.

For many years, the development and preparations of heterogeneous catalyst were considered more as alchemy than science [59], with the predominance of trial and error experiments. However, this approach is expensive, time-consuming, does not offer assurances on the final results and discourages oscillation between catalysis and other related sciences, such as analytical or solid state chemistry, spectroscopy, etc. Thus, it is not surprising that catalysis followed an isolated route up until the 1070, when the idea of scientific bases for the preparation of catalysts began to develop [60], with significant incorporation and overlapping between the different sciences.

The wide number of variables in preparing heterogeneous catalysts can be reduced to a series of elementary steps, which present quite strongly marked analogies from one catalyst to another, and may be described in a general way. It must be noted that all these steps may not always be required, since a new catalyst may consist only of minor modifications of an existing catalyst. A wide ranging approach is always necessary. However, all the preparation steps must be considered even though scale-up may not be required.

The fundamental aspects in the preparation of heterogeneous catalysts starting from catalyst design up to the catalyst in its final form are briefly described, with focus

on the key factors in each preparation step. The main properties of mesoporous uranium oxide based catalysts and their preparation methods are also reported, considering their relevance for environmental applications.

3.1 Catalyst design

The design of a catalyst covers all aspects from choice of the active phases to the method of forming particles. It can be rigorous and detailed, starting from fundamentals to get the best catalyst for a new process, however, in many cases the design of a new catalyst is only an improvement and structural modification of an existing industrial catalyst [61, 62, 63, 64, 65]. The procedure may be difficult but is a fairly straightforward application of many principles as mentioned earlier. Addition of promoters may modify the catalyst structure, or improving the stability and enhance the catalytic reactions to give better activity or selectivity. However, the nature of the active species is always the most important factor. The optimum catalyst is the one that provides the necessary combination of properties such as activity, selectivity, lifetime, ease of regeneration and toxicity at an acceptable cost.

3.2 Methods of Catalyst preparation

Successful preparation of the catalysts can proceed through a series of mysterious steps, or unit operations, which present marked analogies and can be described in a general ways [66, 67]. Most of catalysts are either a finely divided metal supported on a carrier such as alumina or silica, or a metal oxide either on a carrier or unsupported.

Either of two types of processes are named *precipitation* and *impregnation* method for making the catalysts.

3.2.1. Precipitation

This method involves the precipitation of a solid from a liquid solution, as either a precipitate or gel which is a precursor and its nature determines the structure and properties of the final solid catalyst. The precursor may be a crystalline or a gel. The precipitation of a crystalline solid can be divided into three steps: Supersaturation, nucleation and growth. In the supersaturation region, the system is unstable and precipitation occurs as a result of any small perturbation. Supersaturation is reached by means of chemical process (addition of bases or acids) or physical transformations (change in temperature). Formation of the solid phase occurs in two elementary steps: (i) nucleation, and (ii) growth or agglomeration of the particles. Under conditions of high supersaturation, the rate of nucleation is much higher than the rate of crystal growth and leads to the formation of numerous but small particles. In this condition amorphous precipitates can be obtained [67, 68, 69].

Precipitation is one of the most widely employed preparation methods and may be used to prepare either single component catalysts and supports or mixed catalysts. Usually, catalysts with specific properties such as the nature of the phase formed, chemical composition, purity, particle size, surface area, pore size, etc., as well as downstream processes (drying, palletizing or calcinations) are desired. The PH of final solution plays a major role in the final product and it has to be adjusted and kept constant.

Hydroxides and carbonates are the preferred precipitates because of their low solubility, easy decomposition and minimal toxicity and environmental problems [70].

3.2.2 Sol-Gel Process

The sol-gel process refers to formation of an interconnected three dimensional network by hydrolysis and condensation of metal alkoxide precursors. Sol-gel method is a homogeneous process and it has several promising advantages over precipitation. Many different products have been prepared using sol-gel techniques including micro and mesoporous materials, mixed oxides, composite powders and ceramic oxides [71].

Four main steps are identified in sol-gel preparation: formation of a hydrogel, its ageing, removal of solvent and heat treatment. Hydrophilic colloidal solutions are formed of micelles that remain separated because of electrical charges on their surfaces and in the surrounding solution. If the charge is high, particles effectively repel one another and avoid contact. If it is low, then thermal motion leads to collision and coalescence. The hydrogel formation (gelation) depends on the micelle concentration, temperature, ionic strength of the solution and especially the pH. With low pH acid solutions, the equilibrium is driven toward positive surfaces. The surface becomes less positive and finally negative as the pH increases. The chemistry of the processes can be expressed as follows:

$$- M - OR + H_2O \Rightarrow -M - OH + R - OH \qquad \text{(hydrolysis)} \qquad (3.1)$$

$$- M - OH + XO - M \Rightarrow -M - O - M + X - OH \qquad \text{(condensation)} \qquad (3.2)$$

where X can be either H or alkyl group R. However, this description oversimplifies the overall process because it does not represent the nature of the intermediates and end products. The two key factors are the relative rates of hydrolysis and condensation, due to their impact on the properties of the product [72, 73].

3.2.3 Impregnation

Impregnation known as 'incipient wetness' is the simplest and most direct method of deposition (74). The object is to fill the pores of inorganic supports with a solution of metal salt of sufficient concentration to give the correct loading. The impregnation technique requires less equipment since the filtering and forming steps are eliminated. It is the preferred process in preparing supported noble metal catalysts for which it is usually economically desirable to spread out the metal in as finely divided a form as possible. The supported material may be prepared in a variety of ways, but all suffer major problems: (i) no control of the location of catalytic particles on support surfaces, (ii) potential aggregation of particles, and (iii) poly-dispersion of particle sizes. Large-particle-size distributions limit the tenability and selectivity of the nano-particle catalysts and make it difficult to correlate experimental test results with particle sizes. The particles isolated on external surfaces of the supports are susceptible to aggregation, which eventually destroys the ultra-dispersion and catalytic efficiency [75]. The concentration profile of the impregnated compound depends on the mass transfer conditions within the pores during impregnation and drying [62, 70, 76].

Drying is necessary to crystallize the salt on the pore surface. If the rate of drying is too slow, evaporation occurs at the meniscus, which retreats down the pore. Some salt deposition occurs but most of the solute merely concentrates deeper in the pore. After crystallization, the salt is located at the bottom or center of the particle. When the drying rate is too fast, a temperature gradient occurs and the solutions are forced outside the pores. The ideal situation is when crystallization is slow enough to form uniform deposits.

Calcination is very important. Crystallized salt redisolves when the dehydrated catalyst is exposed to moist environments. Calcination converts the salt to an oxide or metal and immobilizes the distribution.

3.2.4 Ion-Exchange Reaction Method

The ion-exchange reaction has been extensively used to prepare novel intercalate materials [75]. It consists of replacing an ion in an electrostatic interaction with the surface of a support by another ion species [76]. The general reaction mechanism can be written in terms of:

$$m(S\text{-}O^-)M_1^+ + M_2^{m+} = (S\text{-}O^-)_m M_2^{m+} + mM_1^+ \tag{3.3}$$
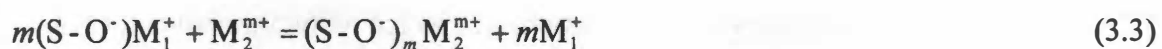
where $(S\text{-}O^-)$ is a surface anionic group in inorganic materials, such as the galleries of pillared materials, M_1^+ a singlely-charged cation in as-synthesized materials, and M_2^{m+} new cationic species needed to be intercalated into the above materials. This type of ion-exchange reaction has been previously used to organize CdS and ZnS clusters in crystalline zeolites with diameter less than 10 A^o [77, 78]. Ordered mesoporous materials

synthesized by the use of cationic surfactants have the same structural feature as those of ionic intercalate materials. In this case, the group of (S-O⁻) corresponds to the SiO⁻ of the mesopore surface, while M^+ is a cationic surfactant ion. The cationic surfactant ions are organized in a form of a cylindrical micellar structure with hydrophilic positive ends coulombically interacting silica pore surfaces. The weak coulombic interaction can be easily broken or replaced by abother cation through ion exchange (see eqn. 3.3). In fact, this exchanging reaction has been employed to remove surfactant molecules from the ordered inorganic materials synthesized through surfactant templating method [79].

3.2.5 Co-Assembly Synthesis Method

The methodology in this synthesis is based on the $I^+M^-S^+$ scheme for the synthesis of mesoporous supports in an acid medium [80, 81]. The positively charged surfactant molecules (S^+), such as protonated block copolymers, interact with positively charged inorganic oxide precursors (I^+) through a negatively charged mediator M^-. The mediator M^- in our case is the anionic complex of uranyl, depending on precursor uranium oxidation states. Nitric acid is used in our synthesis to increase the solubility of uranyl nitrate in the sol-gel inorganic precursor solution such as tetraethylorthorsilicon (TEOS). The nitrate complexes of uranyl ions are known to be very stable and dominant species under high nitrate concentration in several different solvent systems [82]. Their superior location at the interface between silica and surfactants may prevent excessive disruption of the silica wall during the formation of mesostructure.

3.2.6 Ionic-Adsorption Method

Adsorption is an excellent method for depositing of a precursor solution on the solid support. The term adsorption is used to describe all processes where ionic species from aqueous solutions are attracted electrostatically by charged sites on a solid surface. Adsorption is cationic or anionic depending on the surface properties. Zeolites are strong cationic exchangers, silica is a weak cationic adsorber, alumina adsorbs both cations and anions weakly, magnesia is a strong anion adsorber and carbon prefers to form charge-transfer complexes with electron donation but also weakly adsorb cations [83].

As an example, chloroplatinic acid, H_2PtCl_6, a commonly used platinum reagent, is strongly adsorbed on alumina or activated carbon but not on silica gel. Its application to alumina by the incipient-wetness method leads to the deposition of a thin shell of platinum on the outer portions of the particle. To obtain a more uniform dispersion, the adsorptivity of $PtCl_6^{2-}$ ions may be reduced by competitive adsorption by adding nitric or hydrochloric acid to the solution, resulting in a more uniform deposit. Alternatively, platinum could be applied to alumina as $Pt(NH_3)_4Cl_2$, in which case platinum is in the form of a cation. It is then less readily adsorbed on alumina, but more strongly adsorbed on silica gel. If a halogen-free catalyst preparation is desired, a compound such as platinum diaminodinitrite, $Pt(NH_3)_2(NO_2)_2$, may be used. It is also possible to embed the catalytically active material as a layer slightly inside the catalyst particle by adding an organic acid such as citric acid to the impregnation solution [84]. Such a structure may be desired for prolongation of catalyst life in an application where poisons are deposited

on the ouside surface of a porous catalyst support. An example is supported platinum catalysts for oxidation of pollutants in automobile engine exhaust.

3.3 Hydrothermal Treatments

Hydrothermal treatments refer to treatments of precipitates, flocculates or gels carried out at low temperature such as 300 °C, under ageing or ripening in the presence of the mother liquor [85]. The variables for a given solid are pH, temperature, pressure, time and concentration. The main difference between ageing and hydrothermal treatments regards the reaction conditions (such as T, P and time), ageing being performed at room temperature and pressure for longer times. All textural or structural hydrothermal transformations follow the thermodynamic laws and thus proceed toward a decrease in free energy of the system. Increasing attention has been devoted in the last decades to the synthesis of zeolites and mesoporous materials, in which the original amorphous gels crystallize in hydrothermal conditions around different templating agents [86]. Most hydrothermal treatments are performed in the presence of a liquid phase (mother liquor); however they also include the steam stabilization procedure of Y zeolites [87].

3.4 Solid-Phase Recovery

Separation of the solid phase from the mother liquor can be performed by decantation, filtration and centrifugation, followed by washing with distilled water to remove completely the mother liquor and eliminate impurities [62, 68]. The separation

26

operations are easy for crystalline precipitates, difficult for flocculates and useless for hydrogels. Choice of the separation method depends on the particle size of the solids, since for example, small particles may require filtration or centrifugation. When washing flocculates, problems may arise since removal of counterions reverts flocculates to sol, thus care must be taken not to wash too much or allow the settling time to become too long.

3.5 Thermal Treatments

The thermal treatments of catalysts include drying, calcinations and activation [56]. *Drying* is necessary to remove the large volume of water in the hydrogel. Drying occurs through evaporation of moisture from the outside surface of the hydrogel that contains up to 90% water. The mass transfer during drying is controlled by temperature, relative humidity, flow rate of air over surface, and size of the filtrate. The process continues until over 50% of the moisture content is removed and the obtained solids are called xerogels. Continued moisture loss occurs with a declining rate, in which evaporation is controlled by capillary forces. The saturation point decreases as pores becomes smaller and evaporation slows until water is forced into larger pores by concentration gradients. If removal of moisture is blocked by smaller pores, an internal pressure of steam develops and the structure collapses, with loss of pore volume and surface area. High temperature gradients in the sample must be avoided. Gel breakage may be reduced by lowering the temperature gradient, increasing the relative humidity of the drying medium or decreasing the air flow through the gel bed [89]. Vacuum drying such as rotary, lamp-heated evaporator at lower temperature is a satisfactory laboratory

device. Dried xerogels encapsulated in fine pores or chemically bound to the oxide. At this state, it is easier to form the material into pellets and extrudates.

Calcination is further heat-treatment beyond drying without the formation of a liquid phase. It is carried out in air at temperatures higher than those used in the catalytic reaction or catalyst regeneration. Several processes occur during calcinations: (i) loss of chemically bound water or CO_2, (ii) changes in pore size distribution, (iii) active phase generation, (iv) surface conditioning, and (v) stabilization of mechanical properties [76].

If a metallic catalyst is the ultimate goal, conversion to the oxide form is frequently sought prior to reduction. If a mixed oxide catalyst is the goal, a substantially elevated firing temperature may be required to cause mixing by diffusion of individual species to form a desired compound or crystal phase. In many event the catalyst should be heated under controlled conditions to a temperature at least as high as will be encountered in the plant reactor to remove bound water, carbon dioxide, etc. If these decompositions occur to a significant extent in the plant, they may cause structural weaknesses in pellets, leading to breakup, dusting, and so on, that may cause excessive pressure drop and premature reactor shutdown. Therefore, calcinations temperature must be properly chosen to obtain phases that are stable in the reaction and regeneration conditions.

Activation is the final step in producing the active component through physical and chemical changes. This typically involves heating to cause calcinations or decomposition, followed by reduction if a metallic catalyst is desired. In reduction, the deposited oxide is converted to the metal by treating with hydrogen, CO or hydrazine. The amount of produced metal depends on which oxidic compounds are present. The

temperature of reduction is also important. Another factor is the purity of hydrogen. The presence of steam, even in small amounts, influences the rate and extent of reduction. The sensitivity of these parameters introduces serious doubts concerning control and reproducibility of reduction procedures [90]. Very careful instructions must be followed for satisfactory results. In many cases a supported-metal catalyst is pyrophoric, and reduction is carried out in the plant reactor rather than by the catalyst manufacturer to avoid hazards upon shipping and reactor loading.

3.6 Catalyst Forming

The shaping of catalysts and supports is a key step in the catalyst preparation procedure. The shape and size of the catalyst particles should promote catalytic activity, strengthen the particle resistance to crushing and abrasion, minimize the bed pressure drop, lessen fabrication costs and distribute dust build-up uniformly [91]. Unfortunately, some of these objectives are mutually exclusive. For instance, small particle size increases activity, but also increases bed pressure drop. Thus, the best operational catalysts have the shape and size that represent an optimum economic trade-off [92]. The choice of the shape and size is mainly driven by the type of reactor. Moreover, for a given reactor the best shape and size of the catalyst particle depends on the hydrodynamics and heat and mass transfer limitations. Here, we consider the principle factors in the production of common forms of particles.

Pellets or pill is essentially powder compression in a pelleting press. Powder is poured into a cylindrical cavity that shapes it into pellets or rings and a piston applies pressures [88]. Plasticizing agents and die lubricants such as stearic acid, talc, and

mineral oil are usually added to the mixture, and the process can only be used with those powder mixtures that are free flowing and that cohere upon pressing [93]. Fibers such as polymers are also added to improve thermal conductivity in or out of the pellet. Factors such as the ultimate tensile strength of the materials, mesoporosity of the grains, and moisture content are important. Compared to the other shaping methods tableting is quite an expensive method.

Spheres Hydrogels such as alumina, silica, and silica-alumina are formed into spheres using column method. In this method, the hydrogel is forced through holes in a plate at the top of a column containing oil in which the gel is immiscible. The drop falls slowly through the oil, hardening as it ages. At the bottom, the spheres are separated, dried, calcined, and sieved [94].

Extrusion is the most economic and commonly applied shaping technique for catalysts and supports [69]. A slurry of the catalyst powder is fed from a hopper into the screw drive. The screw forces the slurry through holes in the end plate. Some additives such as peptizing agents (dilute acetic or nitric acid) are added to deagglomerate the particles [95]. As the ribbon of slurry emerges from hole, it begins to dry and harden to maintain its shape. Special shapes (trilobites, rings, hollow cylinders, monoliths or honeycombs) can be obtained using proper dies. The operating variables include mixing time, additive content, water content, ageing, and extrusion temperature.

Granules are produced simply by grinding and screening with diameter ranging from 1 to 20 mm [68]. They usually cause a higher pressure drop in a packed bed than pellets of the same size. They may also cause thermal effects that can destroy some materials, such as some zeolites.

Powders (50-500 μm) and *microspheres* (<1 mm) are used in fluidized bed and slurry reactors. They are produced by spray-drying. Hydrogel is sprayed through nozzles into a heated zone. Drying and calcinations occurs rapidly as the small drops fall. Important process parameters are the viscosity of the liquid, the film-forming characteristics, type of atomizer, the temperature and the gas velocity [70].

CHAPTER 4

EXPERIMENTAL PROCEDURES

4.1 Experimental Setup

The primary objective of this research project is to investigate a new class of mesoporous uranium oxide and mesoporous sol-gel catalyst loaded with uranium oxides to destroy a range of volatile organic contaminants, including alkanes, aromatics, and chlorinated organic compounds, through the reutilization of depleted uranium. To accomplish this objective, an experimental setup was designed to carry out a series of experiments to:

- Synthesize an active, stable, poison-resistant mesoporous uranium oxide (U_3O_8) and mesoporous supports (e.g. silica, titania) doped with uranium compounds through a novel surfactant template synthetic method.

- Characterize the mesoporous uranium oxide (U_3O_8) and uranium oxides supported by mesoporous materials (e.g. silica, titania).

Using the experimental setup described below, a sequence of procedures was followed in each experiment in order to ensure repeatable results.

The experimental setup for this study is shown schematically in figures 4.1, and 4.2. Catalytic thermal oxidation of volatile organic compounds (VOCs) were carried out under conditions appropriate for the treatment of industrial effluent streams

Reactor Set-up for Catalytic Testing
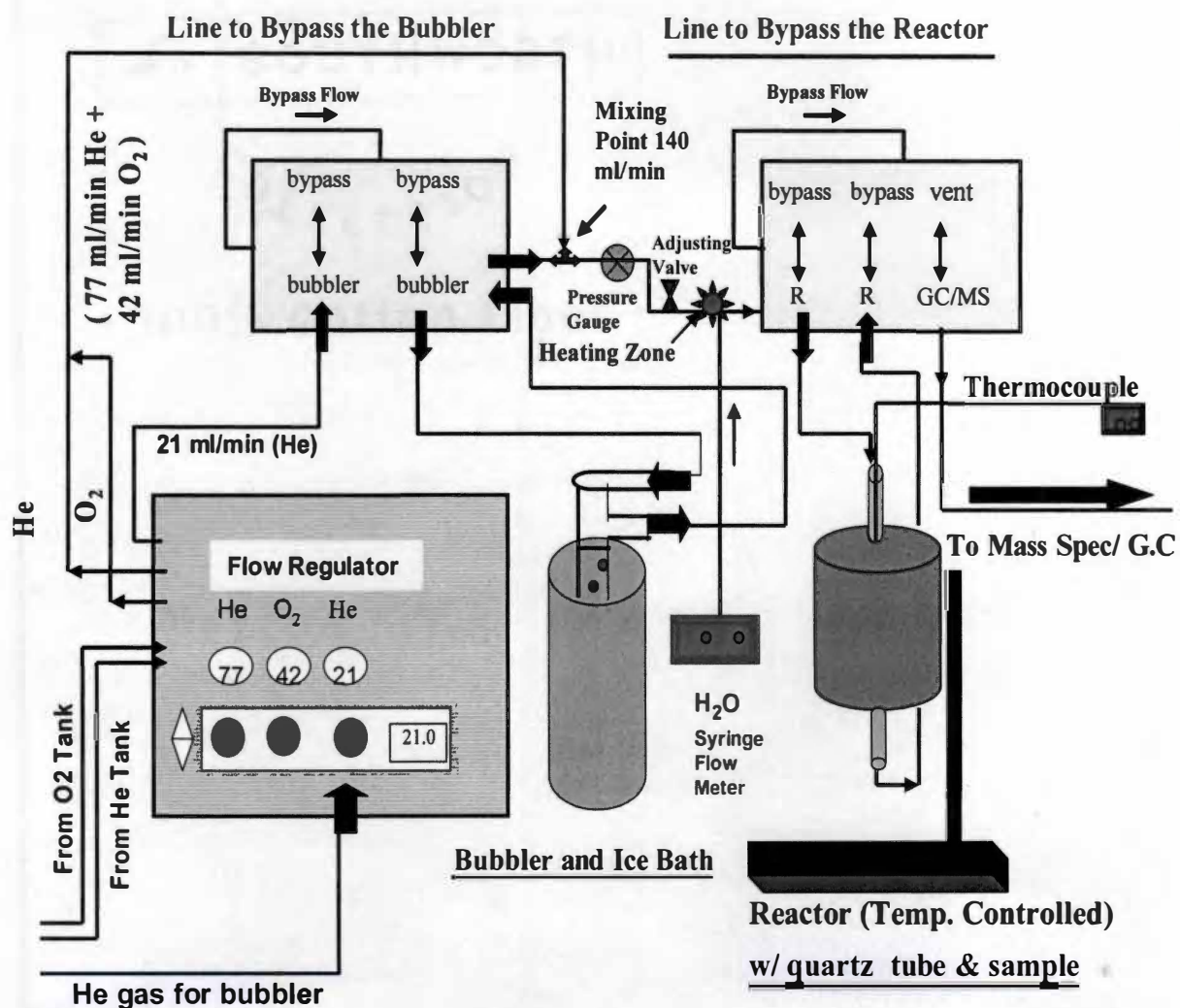
Figure 4.1: Schematic drawing of the analytical arrangements for the laboratory set-up.
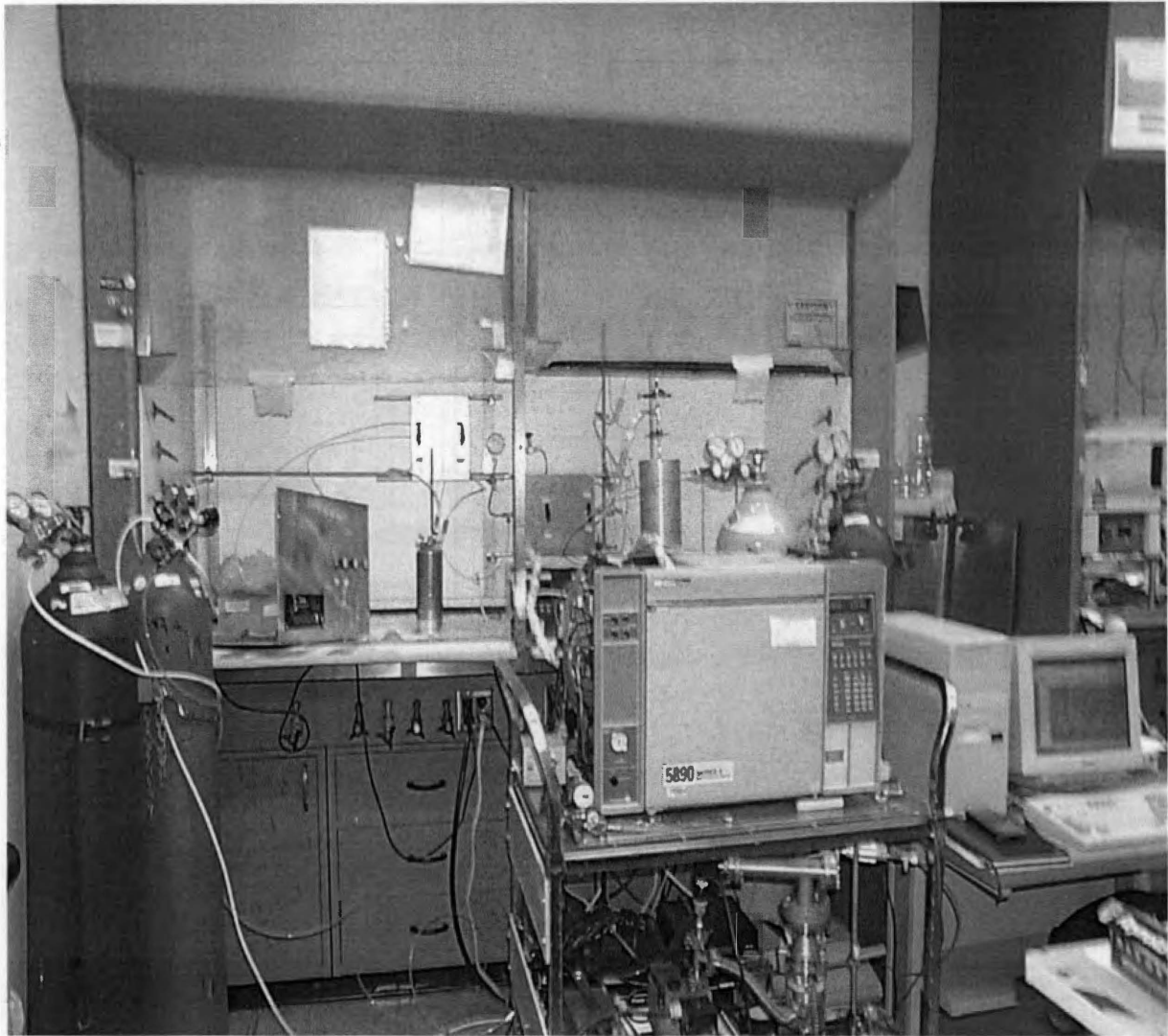
Figure 4.2: Photograph of experimental setup used in this study.

and soil vapor extractions. All reactions were carried out with flow rate of 140 ml/min and space velocity of approximately 84,000 $mlg^{-1}hr^{-1}$. All gases including air, He, O_2, and H_2 were supplied from high pressure cylinders and were regulated by mass flow controllers. Gas flow rates were regulated by electronic mass flow controllers (MKS type 247). A pressure gauge (Ashcroft) was installed to monitor the pressure build up in the system. A needle valve was installed to adjust the pressure drop through the reactor systems. VOC was introduced to the reactor by the passage of a He stream at flow rate of 21 ml/min through a single saturator (Figure 4.3) maintained at ice bath (0 ^{o}C) temperature. The saturated stream was mixed with O_2 at flow rate of 42 ml/min and He (balance) to achieve the desired concentrations, preheated by a stainless steel coil, and introduced to the reactor.

The reaction temperature was measured using a K-type thermocouple projecting into the catalyst bed. Each run utilized approximately 100 mg of the catalyst in the form of 150 μm particles to obtain a better defined range of particles sized to reduce mass transfer problems. The plug flow microreactor was a vertical single pass quarts tube with 6.3 mm OD and 42 cm long and placed in the center of the furnace, where the temperature was most uniform (Figure 4.4). The top and bottom of the reactor tube was connected to inlet and outlet tubing by Cajon Ultra-Torr fittings. The fittings were sealed with Viton O-rings. The catalyst bed section was normally 5 cm OD and 30 cm long. It was supported by medium size frit at the middle of the reactor tube to prevent the catalyst particles from being carried away with the flow. The inlet and outlet reactor tubing was steel (6.3 mm OD) which was traced with a heating tape to reduce effects of condensation of VOC in the system. The temperature of heating tape was adjusted by a Thermolyne
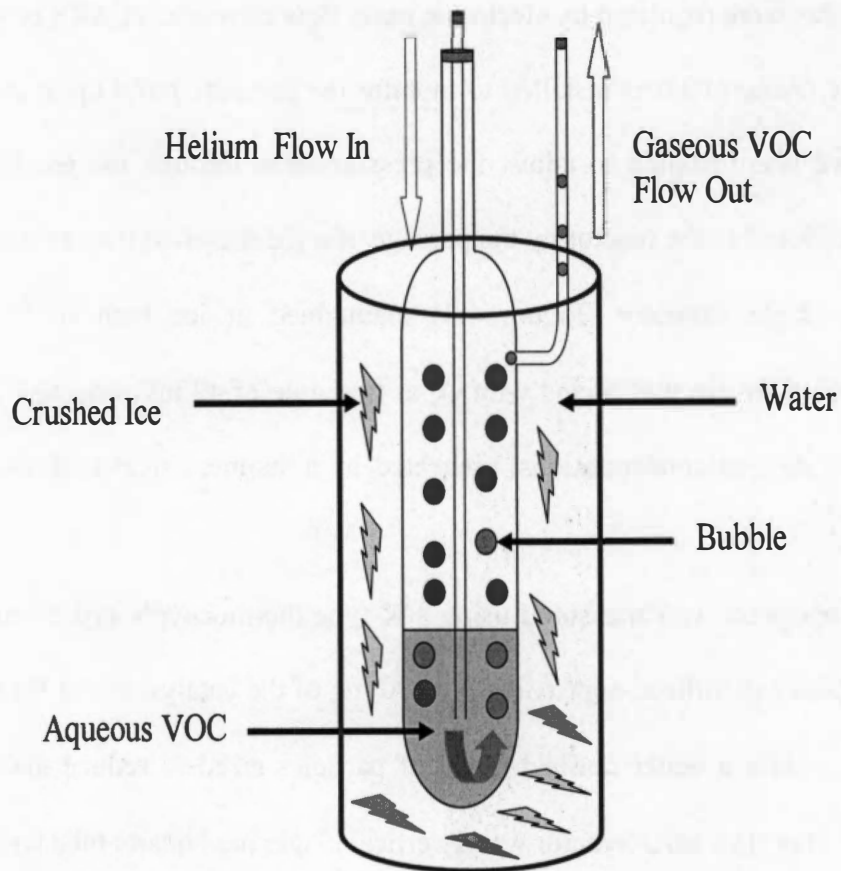
Figure 4.3: Schematic diagram of the Ice-Bath and experimental Bubbler (Saturator).

Flow In

Furnace
Wall

Teflon Frit

Flow Out

Thermocouple

Catalyst

Quartz
Microreactor

Cajon Ultra-Torr
Fitting
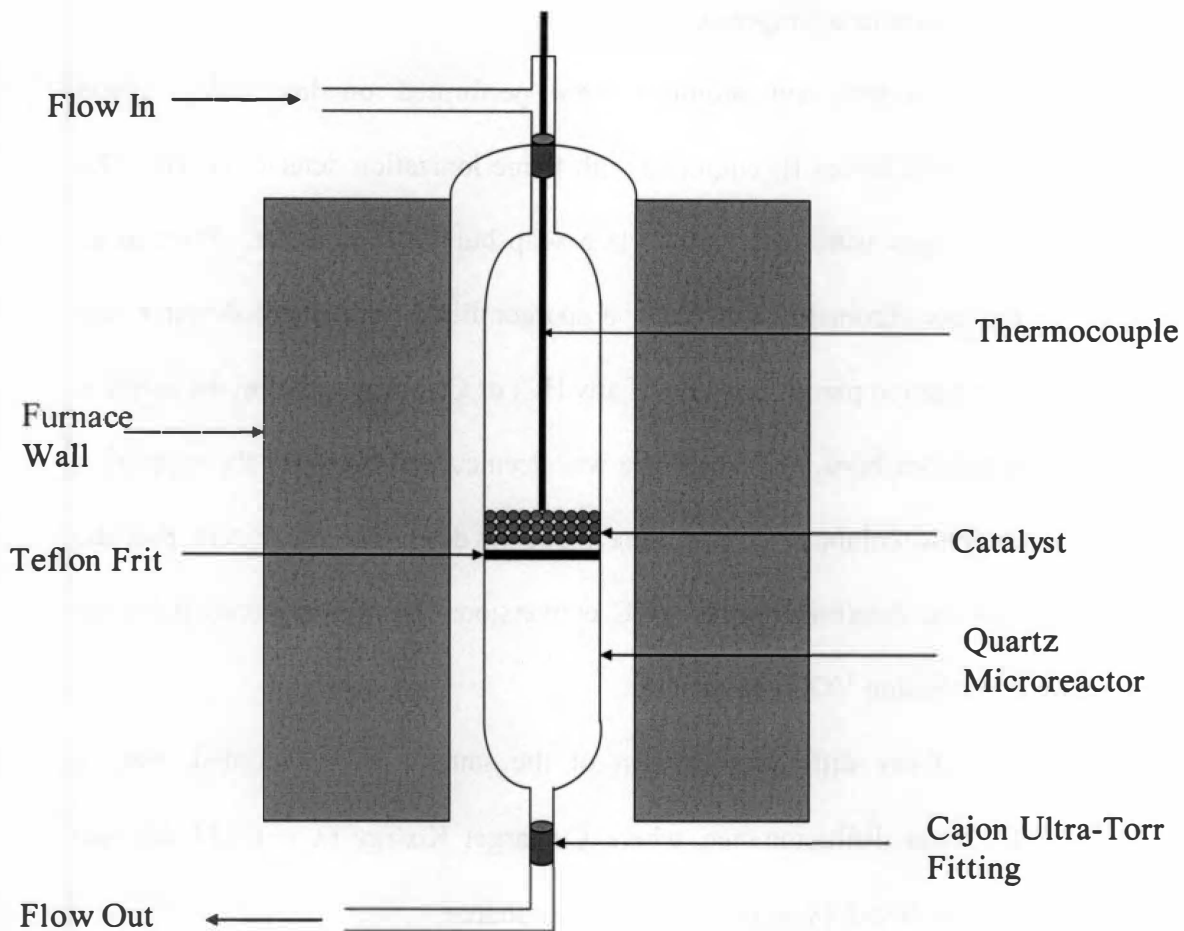
Figure 4.4: Schematic diagram of the laboratory plug flow microreactor showing the furnace and flow system.

(Type 45500). The reactor was heated with a tubular furnace, vertically mounted with a heated zone 30 cm long and 8 cm in diameter. A Digi-Sense Temperature Controller was used for controlling the furnace temperature.

Analysis of reactants and products were performed on line using a gas chromatograph (HP 5890 Series II) equipped with flame ionization detector (FID). The inlet and outlet flow rates were determined via a soap bubble flow meter. Prior to its introduction to the gas chromatograph (GC), a sparger filled with distilled water was incorporated downstream to permit trapping of any HCl or Cl_2 formed during the reaction with halogenated hydrocarbons. This measure was deemed necessary for the protection of the chromatographic columns. Tests were made to determine the extent that the sparger would alter the determination of VOC conversion. Preliminary tests indicated that it is possible to measure VOC conversion.

The powder X-ray diffraction pattern of the sample were recorded using a SIEMENS D5005 X-rat diffractometer, where Cu target $K\alpha$-ray (λ = 0.154 nm and operating at 40 kV and 40 mA) was used as the X-ray source.

Nitrogen adsorption-desorption isotherm were measured on a micromeritics Gemini 2375^{TM} surface area analyzer at 77 $^\circ$K. The samples were dried at 75 C for two hours prior to the measurement. The total pore volume was calculated by converting the volume of nitrogen adsorbed at P/P_0 = 0.99 into the volume of liquid nitrogen, using a converting factor of 0.001546. The specific surface area was computed using the Brunauer-Emmet-Teller (BET) method.

A Dycore Quadrupole Mass Spectrometer was used to analyze the residual gases such as CO_2, CO and unwanted VOC reaction products. A gas sampler consisting of

a 1 m capillary entry column was installed in an entry port into a high vacuum system of Quadrupole Mass Spectrometer. Since the proposed application is for the catalytic destruction of VOCs under realistic conditions, it is required to allow the addition of water to the reactant stream. For this purpose, a water injection syringe (Thermo Orion Model M 361) was used to introduce water into the reactant heated lines up-stream from reactor to see the effect of water on the activity of catalyst.

Finally, the conversion of VOC was calculated as follows:

$$\% \text{ conv. of VOC} = \frac{(\text{VOC concen.})_{\text{bypass exit}} - (\text{VOC concen.})_{\text{reactor exit}}}{(\text{VOC concen.})_{\text{bypass exit}}} \tag{4.1}$$

4.2 Gas Chromatography

Chromatography was first employed by Ramsey [96] in 1905. It is the separation of a mixture of compounds (solutes) into separate components. By separating the sample into individual components, it is easier to identify and measure the amount of the various sample components. The separation process involves the distribution of a sample between two phases. One of these phases is a stationary bed of large surface area, and the other phase is a gas which penetrates through the stationary bed.

Gas chromatography is a technique for separating volatile substances by infiltrating a gas stream over a stationary phase [97]. For this work, a compound must have sufficient volatility and thermal stability. The sample is vaporized and injected onto

39

chromatographic columns and then separated into many components. The elution is brought about by the flow of an inert gaseous mobile phase. The carrier gas such as helium serves as the mobile phase that elutes the components of a mixture from a column containing an immobilized stationary phase. In contrast to most other types of chromatography, the mobile phase does not interact with molecules of the analytes.

As solutes are eluted from the gas chromatography column, they interact with the detector. The GC detector converts this interaction into an electrical signal that is sent to the data system. The magnitude of the signal is plotted versus time (from the time of injection) and a chromatogram is generated.

A GC HP 5890 Series II (figure 4.5) with flame ionization detector (FID) was used to identify solutes as they exit the column. The essential components are: (1) carrier gas, (2) flow controller and pressure regulator, (3) injection port, (4) column, (5) FID, (6) thermostat, (7) recorder [98].

Carriers gas must be chemically inert. A pressure regulator is used to assure a uniform pressure to the column inlet, and thereby a constant rate of gas flow. At a given temperature, this constant rate of flow will elute components at a characteristic time (the retention time). The choice of carrier gas is often dependent upon the type of detector. Commonly used gases are helium, argon, and nitrogen.

Pressure and flow-Rate Regulator – Standard pressure reduction valves are used on the gas cylinders to regulate the pressure and flow of gas emerging from the tank. Flow rates ranging between twenty and thirty milliliters per minute (carrier + make up) are used normally through the capillary column. The flow rate can be measured at the outlet of the column by a simple soap bubble flowmeter.
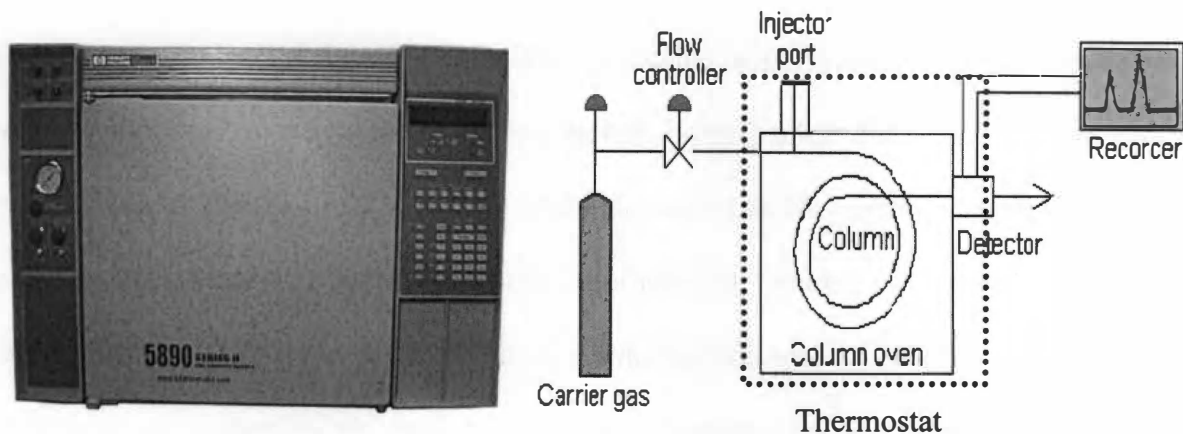
Figure 4.5: (a) GC HP 5890 Series II, (b) Schematic Drawing of GC System

Sample injection port – The sample should not be too large and should be introduced instantaneously as a "plug" of vapor onto the column. Slow injection of large samples causes band broadening and loss of resolution. Gases are usually introduced by gas-tight syringes or by-pass sample loops. Liquids are handled with syringes. For packed columns, sample size ranges from tenths of a microliter up to 20 microliters. Capillary columns, on the other hand, need much less sample, typically around 10^{-3} µl. For capillary GC, split/splitless injection is used. The injector can be used in one of two modes; split or splitless. The injector contains a heated chamber containing a glass liner into which the sample is injected through the septum. The carrier gas enters the chamber and can leave by three routes (when the injector is in split mode). The sample vaporizes to form a mixture of carrier gas, vaporized solvent and vaporized solutes. A proportion of this mixture passes onto the column, but most exits through the split outlet. The

41

septum purge outlet prevents septum bleed components from entering the column as shown in Figure 4.6 (a).

Column – There are two types of column, packed and capillary. Packed columns contain a finely divided, inert, solid support material such as diatomaceous earth coated with liquid stationary phase. Most packed columns are 1.5 – 10 m in length and have an internal diameter of 2 – 4 mm. In order to separate and analyze extremely small samples, the diameter of the gas chromatographic column must be reduced to a small value. Moreover, a packed chromatographic column often does not operate at its theoretical efficiency. Capillary columns operate at a much greater efficiency, making them excellent for difficult separations. Capillary columns have an internal diameter of a few tenths of a millimeter. They can be one of two types; wall-coated open tubular or support-coated open tubular. Wall-coated columns consist of a capillary tube whose walls are coared with liquid stationary phase. In supported-coated columns, the inner wall of the capillary is lined with a thin layer of support material such as diatomaceous earth, onto which the stationary phase has been adsorbed.

The column tubing can be made from copper, stainless steel, aluminum, and glass tubing. In 1979, a new type of wall-coated open tubular column such as fused silica open tubular column was devised. They have much thinner walls than the glass capillary columns, and are given strength by the polyimide coating. These columns are flexible and can be wound into coils as shown in Figure 4.6 (b). They have the advantages of physical strength, flexibility and reactivity.

Detector – The detector indicates the presence and measures the amount of components in the column effluent. There are many detectors which can be used in gas

The split / splitless injector

- Rubber septum
- Septum purge outlet
- Carrier gas inlet
- Split outlet
- Heated metal block
- Glass liner
- Vapourisation chamber
- Column
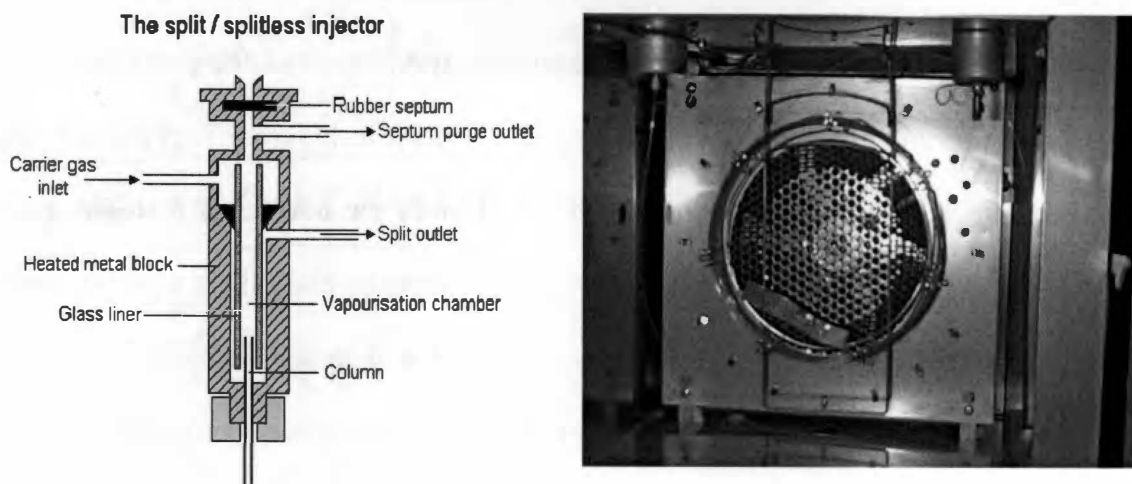
Figure 4.6: (a) Schematic diagram of split/splitless injector. (b) Fused silica coils column.

chromatography. Different detectors will give different types of selectivity. A non-selective detector responds to all compounds except the carrier gas, a selective detector responds to a range of compounds with a common physical or chemical property and a specific detector responds to a single chemical compound. Detectors can also be grouped into concentration dependant detectors and mass flow dependant detectors. The signal from a concentration dependant detector is related to the concentration of solute in the detector, and does not usually destroy the sample. Dilution of with make-up gas will lower the detectors response. Mass flow dependant detectors usually destroy the sample, and the signal is related to the rate at which solute molecules enter the detector. The response of a mass flow dependant detector is unaffected by make-up gas.

Flame Ionization Detector – When using the flame ionization detector (FID), the effluent from the column is mixed with hydrogen and air, and ignited. Organic compounds burning in the flame produce ions and electrons which can conduct electricity

43

through the flame. A large electrical potential is applied at the burner tip, and a collector electrode is located above the flame. The current resulting from the pyrolysis of any organic compounds is measured. This process is shown in Figure 4.7. FIDs are mass sensitive rather than concentration sensitive; this gives the advantage that changes in mobile phase flow rate do not affect the detector's response. The FID is a useful general detector for the analysis of organic compounds; it has high sensitivity, a large linear response range, and low noise. It is also robust and easy to use, but unfortunately, it destroys the sample.

Recorder – The signal from most gas chromatographic detectors is an electrical current or a voltage. The currents are usually exceedingly small. The signal is usually amplified and then fed to a readout or printout device.

4.3 Quadrupole Mass Spectrometer

Mass spectrometer is one of most powerful techniques used by the modern chemist. It continues to be actively developed. It uses the difference in mass-to-charge ratio (m/e) of ionized atoms or molecules to separate them from each other. Mass spectrometry is therefore useful for quantitation of atoms or molecules and also for determining chemical and structural information about molecules. Molecules have distinctive fragmentation patterns that provide structural information to identify structural components.

Our choice of the Dycor Quadrupole Mass Spectrometer, Model Dycor M 250 made by Ametek as shown in Figure 4.8, was influenced by the experience of other colleagues with this equipment in their research at Oak Ridge Natoal Laboratory.

44
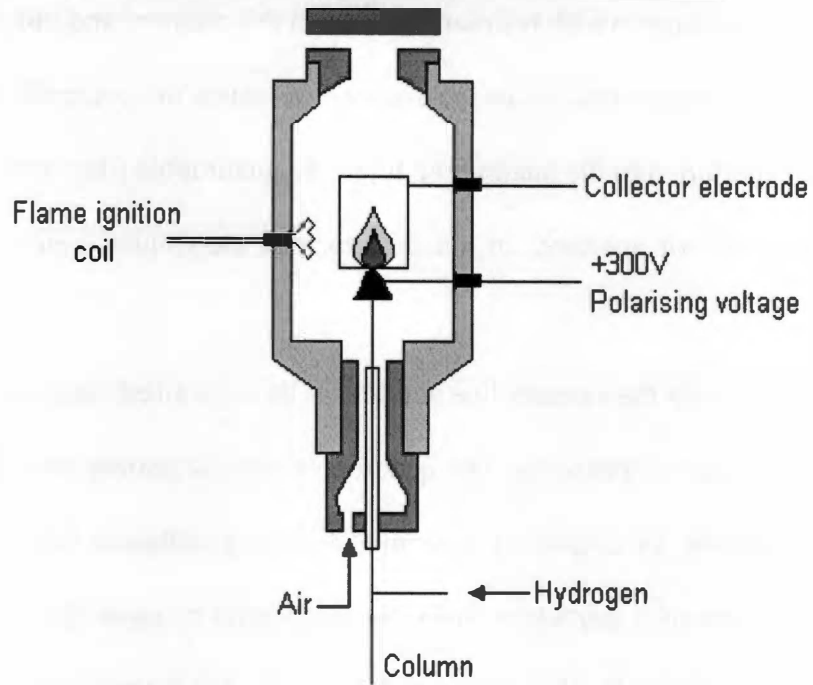
Figure 4.7: Schematic diagram of flame ionization detector.
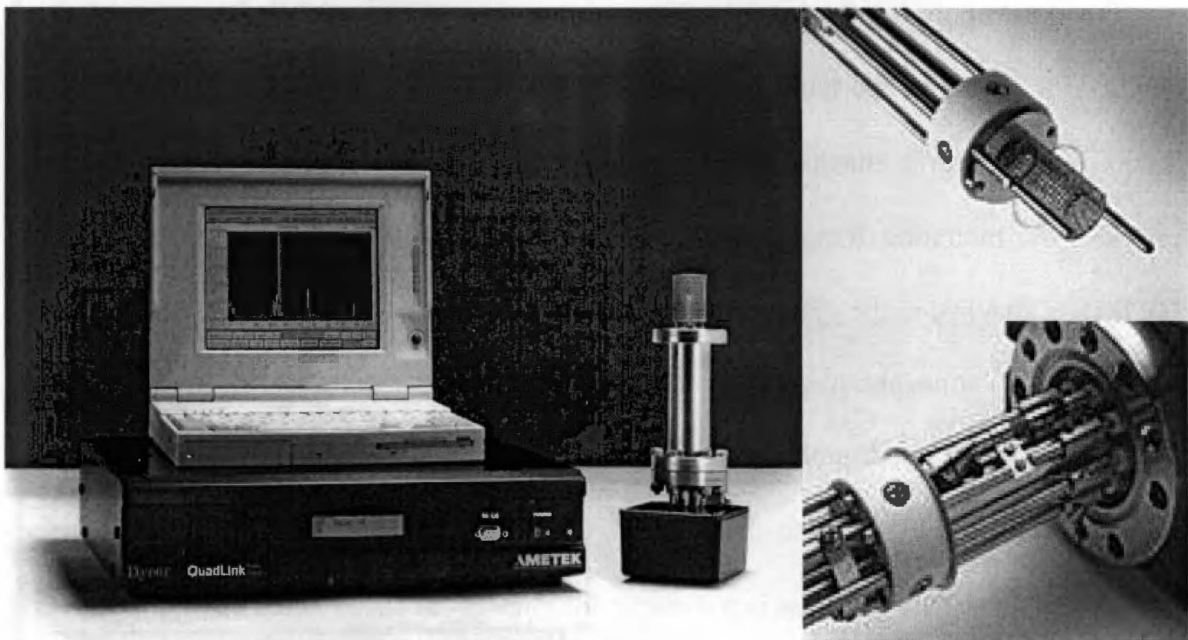
Figure 4.8: Ametek Quadrulink and Quadrupole Mass Spectrometer.

The Quadrupole Mass Spectrometer shows many advantages over the traditional magnetic-sector instrument which is described later in this chapter, and this is reflected in its popularity. The unit consist of an ion source, ion optics to accelerate and focus the ions through an aperture into the quadrupole filter, the quadrupole filter itself with control voltage supplies, an exit aperture, an ion detector and electronics, and a high-vacuum system.

Gas is admitted into the vacuum line and bleeds through a leak into the high vacuum region. Gas molecules approaching the quadrupole can be ionized and the motion of these ions through the quadrupole is determind by the quadrupole field. For selected field conditions, ions of a particular mass-to-charge ratio traverse the quadrupole and strike the detector, while all other ions are defocused. Ion currents are amplified and passed to the monitor for visual display [99, 100].

The quadrupole is pumped by a Varian Macro Torr (Turbo V-70 D), mounted at a height of 5 cm above the table, and backed by an oil pump (Edwards-1, 2 stages). The mouth of the pump is attached through a reduction flange to a high-vacuum tee and this provides the mounting flange for the quadrupole. A Hastings Vacuum Gauge model CVT-16 is attached to the system to monitor the pressure.

The M250 atmospheric system is used as an atmospheric pressure gas inlet system to house the Dycor quadrupole head in its required high vacuum environment. The pumping station is attached to the M250 via a 4 1/2" conflat-type flange using copper gasket supplied. The gas inlet is a 1-meter long length of fused silica capillary with an inside diameter of 10 microns. The low conductance of the capillary is used to decrease the sample gas pressure from atmospheric to about E^{-6} Torr at the quadrupole sensor.

46

The advantages of the capillary are that gas travels through system in continuous laminar flow. A bakeable valve is found at the end of the capillary which can be used to turn off the flow of gas to the high vacuum region. The valve can be closed to look at the system background spectrum. The inlet gas can be heated to prevent condensation. This can be done by wrapping with heating tape. The capillary is sealed to the sampling system using a graphitized vespel ferrule [99]. The schematic diagram of M250 pressure sampling system is shown in Figure 4.9.

4.4 Details of Catalyst Preparation

In this section, the preparations of all major catalysts of interest in this project are discussed briefly.

4.4.1 U_3O_8

High-purity uranium oxide (U_3O_8) spheres of 150 μm was prepared by the thermal decomposition of uranyl nitrate hexahydrate ($UO_2(NO_3)_2 \cdot 6 H_2O$) at 800 °C in static air for 24 hours.

4.4.2 Mesoporous Silica (SiO_2)

Using co-assembly synthesis, transparent mesostructured silica-block co-polymer composites were prepared by mixing tetraethoxysilane (TEOS) and pluronic F127 (BASF) in a mixture of ethanol, butanol, cyclohexane. The initial mass ratio was: F127
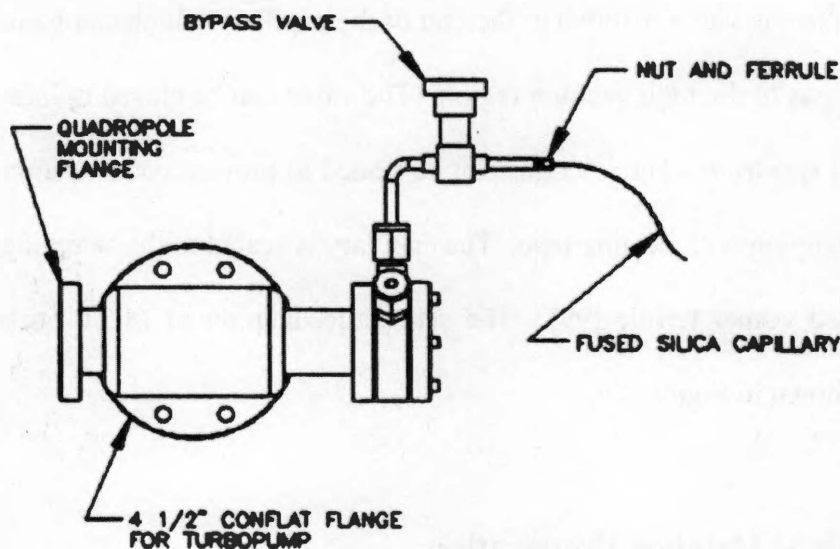
Figure 4.9: The schematic diagram of M250 pressure sampling system.

(0.75 g) : TEOS (2 ml) : butanol (0.50 ml) : cyclohexane (0.50 ml) : ethanol (2 ml). Monolithic structure materials were formed after a week polymerization and gelation. The mesoporous silica materials were obtained by calcinations at 300 °C for 2 hours and then at 800 oC for 8 hours. The overall reaction is shown schematically in Figure 4.10. Detailed synthesis calculations are given in appendix B.1.

4.4.3 U-Meso-5 (Uranium Mesoporous Silica)

Mesoporous silica-block copolymer composite doped with UO_2^{2+} was prepared by mixing HNO_3 (0.05 M) with tetraethoxysilane (TEOS) and $UO_2(NO_3)_2.6H_2O$. The mixture (U:Si=1:10) was added to a solution of Pluronic F127 (BASF), ethanol, butanol, and cyclohexane. The initial mass ratio was F127 (0.75 g): butanol (0.50 ml) : ethanol

48

Figure 4.10: Scheme illustrating the rout to new mesoporous silica.

(2.00 ml) : cyclohexane (0.50 ml) : HNO_3/H_2O (2.00 ml) : TEOS (2.00 ml) : $UO_2(NO_3)_2.6H_2O$ (0.45 g). The monolithic mesoscopic gel was formed after 1 week of condensation and gelation. The mesoporous silica material incorporating U_3O_8 nanoparticles were obtained by calcinations, first at 150 C for 6 h and then at 350 C for 6 h and finally at 800 C for additional 6 h in air to remove template. The overall reaction is shown schematically in Figure 4.11. Detailed synthesis calculations are given in appendix B.2.

4.4.4 U-Meso-6 (Uranium Mesoporous Silica)

A new type of catalyst, U-Meso-6, was synthesized and compared with previous one with modified mole ratio of U:Si = 1:20. In a typical synthesis, transparent

TEOS
Pluronic F127
UO_2^{2+}
HNO_3

Co-assemble →

Silica Network

$UO_2(NO_3)_3^-$

Protonated F127
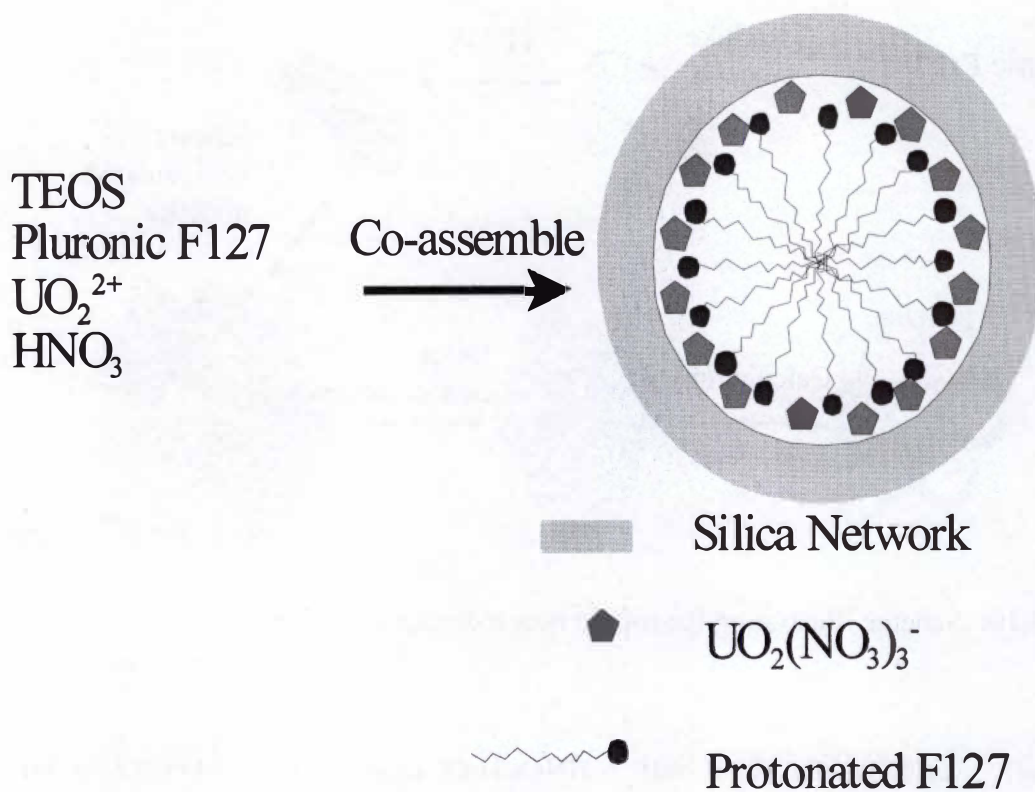
Figure 4.11: Schematic diagram of Silica Network.

mesostructured silica-block copolymer composite doped with UO_2^{2+} was prepared by mixing HNO_3 (0.05 M) with tetraethoxysilane (TEOS) and $UO_2(NO_3)_2.6H_2O$. The mixture was added to a solution of Pluronic F127 (BASF), ethanol, butanol, and cyclohexane. The initial mass ratio was F127 (0.75 g): butanol (0.50 ml) : ethanol (2.00 ml) : cyclohexane (0.50 ml) : HNO_3/H_2O (2.00 ml) : TEOS (2.00 ml) : $UO_2(NO_3)_2.6H_2O$ (0.225 g). The monolithic mesoscopic gel was formed after 1 week of condensation and gelation. The mesoporous silica material incorporating U_3O_8 nanoparticles was obtained by calcinations, first at 150 °C for 6 h and then at 350 °C for 6 h and finally at 800 °C for 6 h in air to remove template. Detailed synthesis calculations are given in appendix B.3.

4.4.5 U-Meso-9 (Uranium Mesoporous Silica)

The method of co-synthesis for this catalyst is similar to U-Meso-6 except the mole ratio of U:Si was 1:30. 0.15 g of uranyl nitrate hexahydrate was dissolved in a vial by using 2 ml ethanol and 2 ml 0.04 M HNO_3. Then 2 ml TEOS was added to the mixture. When the mixture was transparent, 0.75 g of F127 was added to the solution. For enhancing the dissolution process, 0.5 ml cyclohexane and 0.5 ml butanol was added to the solution. After drying in room's temperature, it was calcined at 350 °C for 6 hours then at 800 °C for additional 6 hours. The final product was dark green color. Detailed synthesis calculations are given in appendix B.4

4.4.6 U-Meso-10 (Potassium+Uranium Mesoporous Silica)

Emphasis was placed on studying the effects of doping the mesoporous uranium catalysts with other materials such as potassium. The goal was to find a way to enhance, i.e to promote the activity of the uranium oxide catalysts. Potassium was used because it is a commonly used promoter for various catalysts including iron catalysts used in Fischer-Tropsch catalysts and as a promoter in certain oxidation catalysts. Using incipient wetness synthesis method, HNO_3 (0.05 M) with tetraethoxysilane (TEOS) and $UO_2(NO_3)_2 \cdot 6H_2O$ were mixed. The mixture was added to a solution of Pluronic F127 (BASF), ethanol, butanol, cyclohexane and potassium nitrite. The initial mass ratio was F127 (0.75 g): butanol (0.50 ml) : ethanol (2.00 ml) : cyclohexane (0.50 ml) : HNO_3/H_2O (2.00 ml) : TEOS (2.00 ml) : $UO_2(NO_3)_2 \cdot 6H_2O$ (0.235 g) : KNO_2 (0.04 g). Material was

calcined first at 150 °C for 6 h and then at 350 °C for 6 h and finally at 600 °C for 6 h in air to remove template.

4.4.7 U-Meso-11 (Potassium+Uranium Mesoporous Silica)

The synthesis of U-Meso-11 is identical with U-Meso-10 except that potassium oxalate ($K_2C_2O_4$) was used instead potassium nitrite. The initial mass ratio was F127 (0.75 g): butanol (0.50 ml) : ethanol (2.00 ml) : cyclohexane (0.50 ml) : HNO_3/H_2O (2.00 ml) : TEOS (2.00 ml) : $UO_2(NO_3)_2.6H_2O$ (0.235 g) : $K_2C_2O_4$ (0.084 g). Material was calcined first at 150 °C for 6 h and then at 350 °C for 6 h and finally at 600 °C for 6 h in air to remove template.

4.4.8 U-Meso-12 (Bromide+Uranium Mesoporous Silica)

The synthesis of U-Meso-12 is identical with U-Meso-11 except that potassium bromide (KBr) was used instead potassium oxalate. The initial mass ratio was F127 (0.75 g): butanol (0.50 ml) : ethanol (2.00 ml) : cyclohexane (0.50 ml) : HNO_3/H_2O (2.00 ml) : TEOS (2.00 ml) : $UO_2(NO_3)_2.6H_2O$ (0.235 g) : KBr (0.055 g). Material was calcined first at 150 °C for 6 hours and then at 350 °C for 6 hours and finally at 600 °C for additional 6 hours in air to remove template.

4.4.9 U-Meso-13 (Fe+Mg+Uranium Mesoporous Silica)

Iron and magnesium were tried as an additive into standard synthesis of mesoporous uranium oxide catalyst. Iron was added as nitrate and magnesium was added

as acetate. The initial mass ratio was F127 (0.75 g): butanol (0.50 ml) : ethanol (2.00 ml) : cyclohexane (0.50 ml) : HNO_3/H_2O (2.00 ml) : TEOS (2.00 ml) : $UO_2(NO_3)_2.6H_2O$ (0.235 g) : $Fe(NO_3)_3. 6H_2o$ (0.10 g): $Mg(C_2H_3O_2). 4H_2O$(0.05 g). Material was calcined first at 150 °C for 6 hours and then at 350 °C for 6 hours and finally at 600 °C for 6 hours in air to remove template.

4.4.10 U-Meso-14 (Fe+Ca+Uranium Mesoporous Silica)

Iron and calcium were tried as an additive into standard synthesis of mesoporous uranium oxide catalyst. Iron was added as nitrate and calcium was added as acetate. The initial mass ratio was F127 (0.75 g): butanol (0.50 ml) : ethanol (2.00 ml) : cyclohexane (0.50 ml) : HNO_3/H_2O (2.00 ml) : TEOS (2.00 ml) : $UO_2(NO_3)_2.6H_2O$ (0.235 g) : $Fe(NO_3)_3. 6H_2O$ (0.10 g): $Ca(NO_3)_2. 4H_2O$ (0.06 g). Material was calcined first at 150 °C for 6 hours and then at 350 °C for 6 hours and finally at 600 °C for 6 hours in air to remove template.

4.4.11 U-Meso-15 (Uranium Mesoporous Silica)

The method of co-synthesis for this catalyst is similar to U-Meso-9 except the mole ratio of U:Si was 1:40. 0.11 g of uranyl nitrate hexahydrate was dissolved in a vial by using 2 ml ethanol and 2 ml 0.04 M HNO_3. Then 2 ml TEOS was added to the mixture. When the mixture was transparence, 0.75 g of F127 was added to the solution. For enhancing dissolving process, 0.5 ml cyclohexane and 0.5 ml butanol was added to

the solution. After drying in room's temperature, it was calcined at 350 °C for 6 hours then at 800 °C for additional 6 hours. Detailed synthesis calculations are given in appendix B.5.

4.4.12 U-Meso-18 (Uranium Mesoporous Silica)

The method of co-synthesis for this catalyst is similar to U-Meso-15 except the mole ratio of U:Si was 1:50. 0.09 g of uranyl nitrate hexahydrate was dissolved in a vial by using 2 ml ethanol and 2 ml 0.04 M HNO_3. Then 2 ml TEOS was added to the mixture. When the mixture was transparence, 0.75 g of F127 was added to the solution. For enhancing dissolving process, 0.5 ml cyclohexane and 0.5 ml butanol was added to the solution. After drying in room's temperature, it was calcined at 350 °C for 6 hours then at 800 °C for additional 6 hours. Detailed synthesis calculations are given in appendix B.6.

4.4.13 U-Cr-Meso-19 (Chromium + Uranium Mesoporous Silica)

Using incipient wetness synthesis method (impregnation), 0.025 g of $CrCl_3.6H_2O$ was dissolved in 2 ml HNO_3 (0.05 M) and 2 ml ethanol. Then, 0.40 g of previously made U-Meso-6 was added to the same solution. Stirring for two days did not dissolve the solid U-Meso-6. The sample was dried naturally at room temperature, then it was calcined at 600 °C for 5 hours. The final sample is black in color.

4.4.14 U-Co-Meso-20 (Cobalt + Uranium Mesoporous Silica)

Using incipient wetness synthesis method (impregnation), 0.025 g of $CoCl_2.6H_2O$ was dissolved in 2 ml HNO_3 (0.05 M) and 2 ml ethanol. Then, 0.40 g of previously made U-Meso-6 was added to the same solution. Stirring for two days did not dissolve the solid U-Meso-6. The sample was dried naturally at room temperature, then, it was calcined at 600 $^{\circ}$C for 5 hours. The final sample is black in color.

4.4.15 U-Cr-Meso-21 (Chromium + Uranium Mesoporous Silica)

Using co-assembly synthesis for this catalyst, transparent mesostructured silica-block copolymer composite doped with UO_2^{2+} was prepared by mixing HNO_3 (0.05 M) with tetraethoxysilane (TEOS), $CrCl_3.6$ H_2O and $UO_2(NO_3)_2.6H_2O$. The mixture was added to a solution of Pluronic F127 (BASF), ethanol, butanol, and cyclohexane. The initial mass ratio was F127 (0.75 g): butanol (0.50 ml) : ethanol (2.00 ml) : cyclohexane (0.50 ml) : HNO_3/H_2O (2.00 ml) : TEOS (2.00 ml) : $UO_2(NO_3)_2.6H_2O$ (0.235 g) : $CrCl_3.6$ H_2O (0.025 g). The monolithic mesoscopic gel was formed after 1 week of condensation and gelation. The mesoporous silica material incorporating Cr_2O_3 and U_3O_8 nanoparticles was obtained by calcinations, first at 150 $^{\circ}$C for 6 h and then at 350 $^{\circ}$C for 6 h and finally at 800 $^{\circ}$C for 6 h in air to remove template. Detailed synthesis calculations are given in appendix B.7.

4.4.16 MesoCr-22 (Chromium + Mesoporous Silica)

The method of co-synthesis for this catalyst is similar to U-Meso-21 except no uranium in this catalyst. 0.025 g $CrCl_3 \cdot 6 H_2o$ was dissolved in a vial by using 2 ml ethanol and 2 ml 0.04 M HNO_3. Then 2 ml TEOS was added to the mixture. When the mixture was transparence, 0.75 g of F127 was added to the solution. For enhancing dissolving process, 0.5 ml cyclohexane and 0.5 ml butanol was added to the solution. After drying in room's temperature, it was calcined at 350 °C for 6 hours then at 800 °C for additional 6 hours. The final product was orange color.

4.4.17 U-Co-Meso-23 (Cobalt + Uranium Mesoporous Silica)

The method of synthesis for this catalyst is similar to U-Meso-21. 0.2355 g of uranyl nitrate hexahydrate and 0.025 g $CoCl_2 \cdot 6H_2O$ was dissolved in a vial by using 2 ml ethanol and 2 ml 0.04 M HNO_3. Then 2 ml TEOS was added to the mixture. When the mixture was transparent, 0.75 g of F127 was added to the solution. For enhancing dissolving process, 0.5 ml cyclohexane and 0.5 ml butanol was added to the solution. After drying in room's temperature for 4 days or so, it was calcined at 350 C for 6 hours then at 800 C for additional 6 hours. The final product was olive or dark green in color.

4.4.18 MesoCo-24 (Cobalt + Mesoporous Silica)

The method of co-synthesis for this catalyst is similar to U-Meso-23 except no uranium in this catalyst. 0.025 g $CoCl_2 \cdot 6H_2O$ was dissolved in a vial by using 2 ml ethanol and 2 ml 0.04 M HNO_3. Then 2 ml TEOS was added to the mixture. When the

mixture was transparent, 0.75 g of F127 was added to the solution. For enhancing dissolving process, 0.5 ml cyclohexane and 0.5 ml butanol was added to the solution. After drying in room's temperature for 4 days or so, it was calcined at 350 C for 6 hours then at 800 C for additional 6 hours. The final product was dark green in color. The detail of calculation is given in appendix B.8.

4.4.19 U-Cr-Meso-25 (Chromium + Uranium Mesoporous Silica)

The method of co-synthesis for this catalyst is similar to U-Meso-21 except the mole ratio of U:Si was 1:30. 0.2355 g of uranyl nitrate hexahydrate and 0.025 g $CrCl_3$. 6 H_2o was dissolved in a vial by using 2 ml ethanol and 2 ml 0.04 M HNO_3. Then 2 ml TEOS was added to the mixture. When the mixture was transparence, 0.75 g of F127 was added to the solution. For enhancing dissolving process, 0.5 ml cyclohexane and 0.5 ml butanol was added to the solution. After drying in room's temperature, it was calcined at 350 $^\circ$C for 6 hours then at 800 $^\circ$C for additional 6 hours. The final product was orange color.

4.4.20 U-La-Meso-27 (Lanthanum + Uranium Mesoporous Silica)

Using co-assembly synthesis for this catalyst, transparent mesostructured silica-block copolymer composite doped with UO_2^{2+} was prepared by mixing HNO_3 (0.05 M) with tetraethoxysilane (TEOS), $La(NO_3)_3$.6 H_2O and $UO_2(NO_3)_2$.6H_2O. The mixture was added to a solution of Pluronic F127 (BASF), ethanol, butanol, and cyclohexane. The initial mass ratio was F127 (0.75 g): butanol (0.50 ml) : ethanol (2.00 ml) : cyclohexane

(0.50 ml) : HNO$_3$/H$_2$O (2.00 ml) : TEOS (2.00 ml) : UO$_2$(NO$_3$)$_2$.6H$_2$O (0.235 g) : La(NO$_3$)$_3$.6 H$_2$O (0.10 g). The monolithic mesoscopic gel was formed after 1 week of condensation and gelation. The mesoporous silica material incorporating La$_2$O$_3$ and U$_3$O$_8$ nanoparticles was obtained by calcinations, first at 150 $^\circ$C for 6 h and then at 350 $^\circ$C for 6 h and finally at 800 $^\circ$C for 6 h in air to remove template.

4.4.21 U-Ce-Meso-28 (Cerium + Uranium Mesoporous Silica)

The method of co-synthesis for this catalyst is similar to U-Meso-27. 0.10 g Ce(NO$_3$)$_3$. 6H$_2$O and 0.2355 g of uranyl nitrate hexahydrate was dissolved in a vial by using 2 ml ethanol and 2 ml 0.04 M HNO$_3$. Then 2 ml TEOS was added to the mixture. When the mixture was transparent, 0.75 g of F127 was added to the solution. For enhancing dissolving process, 0.5 ml cyclohexane and 0.5 ml butanol was added to the solution. After drying in room's temperature for 4 days or so, the mesoporous silica material incorporating CeO$_2$ and U$_3$O$_8$ nanoparticles was obtained by calcinations at 350 $^\circ$C for 6 hours then at 800 $^\circ$C for additional 6 hours.

4.4.22 MesoCu-29 (Copper + Mesoporous Silica)

Using co-assembly synthesis for this catalyst, 0.54 g Cu(NO$_3$)$_2$. 3 H$_2$o was dissolved in a vial by using 2 ml ethanol and 2 ml 0.04 M HNO$_3$. Then 2 ml TEOS was added to the mixture. When the mixture was transparence, 0.75 g of F127 was added to the solution. For enhancing dissolving process, 0.5 ml cyclohexane and 0.5 ml butanol was added to the solution. After drying in room's temperature, the mesoporous silica

58

material incorporating CuO was calcined at 350 °C for 6 hours then at 800 °C for additional 6 hours. The final product was black color.

4.4.23 U-Cu-Meso-30 (Copper + Uranium Mesoporous Silica)

The method of co-synthesis for this catalyst is similar to MesoCu-29, except uranium was added. 0.54 g $Cu(NO_3)_2$. 3 H_2o and 0.2355 g of uranyl nitrate hexahydrate was dissolved in a vial by using 2 ml ethanol and 2 ml 0.04 M HNO_3. Then 2 ml TEOS was added to the mixture. When the mixture was transparence, 0.75 g of F127 was added to the solution. For enhancing dissolving process, 0.5 ml cyclohexane and 0.5 ml butanol was added to the solution. After drying in room's temperature, the mesoporous silica material incorporating CuO and U_3O_8 nanoparticles was calcined at 350 °C for 6 hours then at 800 °C for additional 6 hours. Detailed synthesis calculations are given in appendix B.14.

4.4.24 U-Sr-Meso-33 (Strontium + Uranium Mesoporous Silica)

The idea was to add a small amount of the strontium to increase the activity of the uranium oxide catalyst. Using co-assembly synthesis for this catalyst, transparent mesostructured silica-block copolymer composite doped with UO_2^{2+} was prepared by mixing HNO_3 (0.05 M) with tetraethoxysilane (TEOS), $SrCl_2.6$ H_2O and $UO_2(NO_3)_2.6H_2O$. The mixture was added to a solution of Pluronic F127 (BASF), ethanol, butanol, and cyclohexane. The initial mass ratio was F127 (0.75 g): butanol (0.50 ml) : ethanol (2.00 ml) : cyclohexane (0.50 ml) : HNO_3/H_2O (2.00 ml) : TEOS
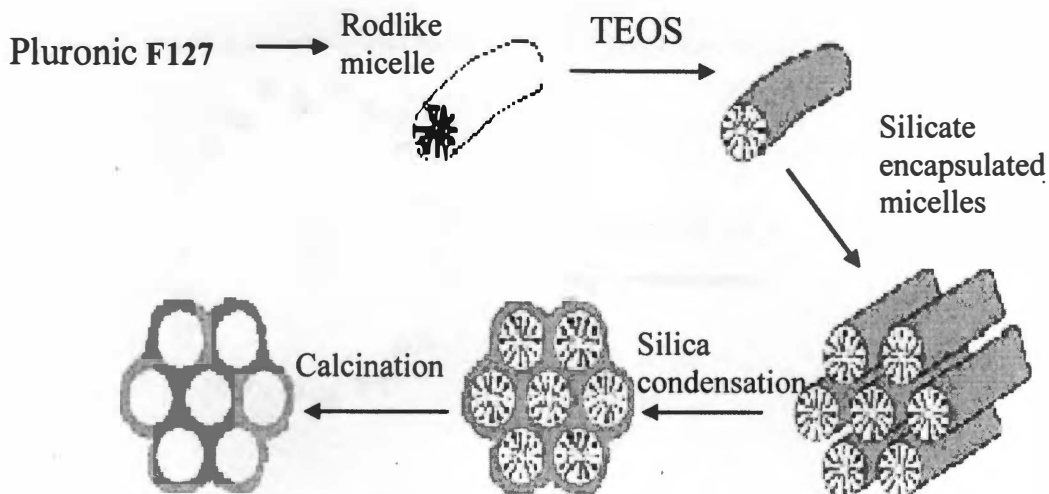
(2.00 ml) : $UO_2(NO_3)_2.6H_2O$ (0.235 g) : $SrCl_2.6 H_2O$ (0.12 g). The monolithic mesoscopic gel was formed after 1 week of condensation and gelation. The mesoporous silica material incorporating SrO and U_3O_8 nanoparticles was obtained by calcinations, first at 150 °C for 6 h and then at 350 °C for 6 h and finally at 800 °C for 6 h in air to remove template. Detailed synthesis calculations are given in appendix B.15.

4.4.25 MesoSr-34 (Strontium + Mesoporous Silica)

The method of co-synthesis for this catalyst is similar to U-MesoSr-33 except no uranium in this catalyst. 0.12 g $SrCl_2$. 6 H_2O was dissolved in a vial by using 2 ml ethanol and 2 ml 0.04 M HNO_3. Then 2 ml TEOS was added to the mixture. When the mixture was transparence, 0.75 g of F127 was added to the solution. For enhancing dissolving process, 0.5 ml cyclohexane and 0.5 ml butanol was added to the solution. After drying in room's temperature, the mesoporous silica material incorporating SrO was calcined at 350 °C for 6 hours then at 800 °C for additional 6 hours.

4.4.26 U-Ti-Si-39 (Uranium + Titanium + Mesoporous Silica)

Using co-assembly method, the following materials were used: 2 ml of 0.04M HNO_3 and 2 ml of tetraethyl orthosilicate (TEOS) were mixed very well in a vial. Then, 0.2355 g $UO_2(NO_3)_2.6H_2O$ was added to the solution. Stirring the solution for 30 minutes. After the solution was transparence, 0.75 g of F127 surfactant, 2 ml ethanol, 0.3 ml Butanol, and 0.3 ml Cyclohexane was added to the mixture. Then, 0.118 g of $Ti(OC_2H_5)_4$ was added to the same container. Mixing for over night and letting to dry for a week. The dried solid material (gel) was clear yellow and was calcined at 350 °C for 6

hrs. After 350 °C calcinations, the sample was light yellow. Then it was divided into three equal weights. 1/3 was kept as U-Ti-Si-39 (350 °C), the other two were calcined at 600 °C and 800 °C individually for 6 hrs. I call them U-Ti-Si-39 (600 °C) and U-Ti-Si-39 (800 °C) respectively. U-Ti-Si-39 (600 °C) was a light brown but calcinations at 800 °C was dark brown.

4.4.27 U-Pt-Si-40 (Uranium + Platinum mesoporous Silica)

Using co-assembly method, 2 ml of 0.04M HNO_3 and 2 ml of tetraethyl orthosilicate (TEOS) were mixed very well in a vial. Then, 0.2355 g $UO_2(NO_3)_2.6H_2O$ was added to the solution. Stirring the solution for 30 minutes. After the solution was transparence, 0.75 g of F127 surfactant, 2 ml ethanol, 0.3 ml Butanol, and 0.3 ml Cyclohexane was added to the mixture. Then, 0.035 g of $Pt(NH_3)_4(NO_3)_2$ was added to the same container. Mixing for over night and letting to dry for a week, gave a clear yellow gel. The dried solid (gel) was calcined at 350 °C for 6 hrs giving a black powder. Then it was divided into three equal weights. 1/3 was kept as U-Pt-Si-40 (350 °C), the other two were calcined at 600 °C and 800 °C individually for 6 hrs. I named them U-Pt-Si-40 (600 °C) and U-Pt-Si-40 (800 °C) respectively.

4.4.28 TiO₂-41 (Mesoporous Titanium Oxide)

Titanium oxide was prepared in the following method: 1 g of Pluronic P123 was dissolved in 12 g absolute ethanol. This solution was added to a solution containing 2.7 ml concentrated hydrochloric acid and 3.88 ml titanium(IV) ethoxide. After 2 hours

stirring, the solution was transferred into a big Petri Dish to dry at room temperature for 3-7 days before the calcinations. The as synthesized catalyst was calcined at 400 °C for 6 hours giving a white powder. 1/3 was kept as TiO_2-41 (400), the other two were calcined at 600 °C and 800 °C individually for 6 hours. I named them TiO_2-41 (600), and TiO_2-41 (800) respectively. Detailed synthesis calculations are given in appendix B.9.

4.4.29 U-Ti-Meso-42 (Mesoporous Uranium + Titanium)

A new type of catalyst was synthesized by co-assembly of uranyl nitrate with tetraethoxy titanium, and using a Pluronic P123 as a surfactant in strong acid solution. This synthesis has been reported in the literature for rare earth ions [101] and the present work is the first time this has been attempted with uranyl ions. The atom ratio of U:Ti was 1:10. 1.25 g of P123 as a surfactant was dissolved in 14 g of 2-propanol and stirring for 2 hours. Then, it was mixed with a precursor solution prepared by mixing 3 g of Titanium (IV) ethoxide and 0.53 g of 2,4-pentanedione and 4 g of 2-propanol with stirring for 2 hours. Based on mole ratio of U:Ti = 1:10, 0.53 g $UO_2(NO_3)_2.6H_2O$ was added to the mixture. The obtained solution was hydrolyzed at low PH=2 condition by addition of 4 ml HNO_3 (0.05 M). After stirring the light transparent solution for 2 days, it was transferred to an open container, gelation under ambient conditions for 10 days. The trunk sample was annealed at 150 °C for 72 hours, then at 400 °C for 24 hours in oven to remove the template. Detailed synthesis calculations are given in appendix B.10.

62

4.4.30 U-Ti-Meso-43 (Mesoporous Uranium + Titanium)

The method of co-synthesis for this catalyst is similar to U-Ti-Meso-42 except the mole ratio of U:Ti = 1:20. 1.25 g of P123 as a surfactant was dissolved in 14 g of 2-propanol and stirring for 2 hours. Then, it was mixed with a precursor solution prepared by mixing 3 g of Titanium (IV) ethoxide and 0.53 g of 2,4-pentanedione and 4 g of 2-propanol with stirring for 2 hours. Based on mole ratio of U:Ti = 1:20, 0.265 g $UO_2(NO_3)_2.6H_2O$ was added to the mixture. The obtained solution was hydrolyzed at low PH=2 condition by addition of 4 ml HNO_3 (0.05 M). After stirring the light transparent solution for 2 days, it was transferred to an open container, gelation under ambient conditions for 10 days. The trunk sample was annealed at 150 °C for 72 hours, then at 400 °C for 24 hours in oven to remove the template. The prepared catalyst was divided into three equal portions. The first portion was named U-Ti-Meso-43 (400). The other two portions were calcined at 600 °C and 800 °C respectively. I named them U-Ti-Meso-43 (600) and U-Ti-Meso-43 (800) respectively. Detailed synthesis calculations are given in appendix B.11.

4.4.31 U-Ti-Meso-44 (Mesoporous Uranium + Titanium)

The method of co-synthesis for this catalyst is similar to U-Ti-Meso-43 except the mole ratio of U:Ti = 1:30. 1.25 g of P123 as a surfactant was dissolved in 14 g of 2-propanol and stirring for 2 hours. Then, it was mixed with a precursor solution prepared by mixing 3 g of Titanium (IV) ethoxide and 0.53 g of 2,4-pentanedione and 4 g of 2-propanol with stirring for 2 hours. Based on mole ratio of U:Ti = 1:30, 0.18 g

$UO_2(NO_3)_2.6H_2O$ was added to the mixture. The obtained solution was hydrolyzed at low PH=2 condition by addition of 4 ml HNO_3 (0.05 M). After stirring the light transparent solution for 2 days, it was transferred to an open container, gelation under ambient conditions for 10 days. The trunk sample was annealed at 150 °C for 72 hours, then at 400 °C for 24 hours in oven to remove the template. Detailed synthesis calculations are given in appendix B.12.

4.4.32 U-Ti-Meso-45 (Mesoporous Uranium + Titanium)

The method of co-synthesis for this catalyst is similar to U-Ti-Meso-44 except the mole ratio of U:Ti = 1:40. 1.25 g of P123 as a surfactant was dissolved in 14 g of 2-propanol and stirring for 2 hours. Then, it was mixed with a precursor solution prepared by mixing 3 g of Titanium (IV) ethoxide and 0.53 g of 2,4-pentanedione and 4 g of 2-propanol with stirring for 2 hours. Based on mole ratio of U:Ti = 1:40, 0.13 g $UO_2(NO_3)_2.6H_2O$ was added to the mixture. The obtained solution was hydrolyzed at low PH=2 condition by addition of 4 ml HNO_3 (0.05 M). After stirring the light transparent solution for 2 days, it was transferred to an open container, gelation under ambient conditions for 10 days. The trunk sample was annealed at 150 °C for 72 hours, then at 400 °C for 24 hours in oven to remove the template. Detailed synthesis calculations are given in appendix B.13.

4.4.33 K-U-SBA15-46 (Mesoporous SBA-15)

SBA-15 silica was prepared using Pluronic P123 (Aldrich) and tetraethylorthosilicate (TEOS, Aldrich) according to the procedure described in literature [102]. Typically, 16 g of P123 was dissolved in 250 g of deioned water and 100 g of concentrated HCl (Aldrich). After the P123 was completely dissolved, an extra 250 g of deioned water was added followed by the addition of 34.4 g of TEOS. The mixture was stirred for extra 2 hours at room temperature before it was placed in a 35°C oven under static conditions for 24 hours, and then heated at 100 °C for an extra 24 hours under static conditions. The white fine powder of the SBA-15 product was filtered without washing and dried in an oven at 70 °C for the whole night. The product was washed with ethanol and diluted HCl solutions and dried again, and then calcined to remove the surfactant of P123 at 550 °C for 4 hours with a heating rate of 1.5 °C/min in air.

Using incipient wetness synthesis method (impregnation), 0.05 g of KNO_3 was dissolved in 2 ml ethanol in a vial. Then, 0.385 g of U-SBA-15 (previously made) was added to the mixture of ethanol and KNO_3. After steering for over night, the sample was dried at room temperature. The dried sample was then calcined at 600 C for three hours.

4.4.34 U-SBA15-47 (Mesoporous SBA-15 + Uranium)

Using incipient wetness synthesis method (impregnation), 0.1 g $UO_2(NO_3)_2.6H_2O$ was dissolved in 4 ml ethanol. When the mixture was transparence, 0.385 g of SBA-15 was added to the solution. After stirring for 6 hours, the sample was dried at room's temperature for 4 days, then, it was calcined at 800 °C for 3 hours.

4.4.35 U-MCM41-49 (Mesoporous MCM-41 + Uranium)

The following materials were used for the preparation of the mesoporous MCM-41 silicate: fumed silica (99.8%, Aldrich), tetraethyl orthosilicate (TEOS; Aldrich, 98%), tetramethylammonium hydroxide (TMAOH; Aldrich, 25 wt.%), cetyltrimethylammonium bromide (CTAB; Aldrich, 99%), sodium hydroxide (NaOH; Loba, 98%), and distilled water.

The siliceous MCM-41 was synthesized hydrothermally according to a procedure outlined [103, 104, 105] as follows: In a Teflon-lined stainless steel autoclaves, a typical gel with molar composition of $10SiO_2:1.35 (CTA)_2 O :0.75(TMA)_2O:1.3Na_2O:680H_2O$ was synthesized at 100 ^{o}C for 24 h. The as-synthesized sample was calcined at 550 ^{o}C in a flow of N_2, for an hour followed by 6 h in air.

Using incipient wetness synthesis method (impregnation), 0.1 g $UO_2(NO_3)_2.6H_2O$ was dissolved in 4 ml ethanol. When the mixture was transparence, 0.385 g of MCM-41 (calcined at 550 ^{o}C) was added to the solution. After stirring for 6 hours, the sample was dried at room's temperature for 4 days, then, it was calcined at 800 ^{o}C for 3 hours.

4.4.36 K-U-MCM41-50 (Mesoporous MCM-41 + Potassium)

Using incipient wetness synthesis method (impregnation), 0.05 g KNO_2 was dissolved in 4 ml ethanol, then, 0.385 g of U-MCM-41 (calcined at 550 ^{o}C) was added to the solution. After stirring for 6 hours, the sample was dried at room's temperature for 4 days, then, it was calcined at 800 ^{o}C for 3 hours.

4.4.37 U-Ti-La-51 (Mesoporous Uranium + Titanium + Lanthanum)

Using the method of co-synthesis for this catalyst, 1.25 g of P123 as a surfactant was dissolved in 14 g of 2-propanol and stirring for 2 hours. Then, it was mixed with a precursor solution prepared by mixing 3 g of Titanium (IV) ethoxide, 0.1 g La(NO$_3$)$_3$. 6H$_2$O, 0.53 g of 2,4-pentanedione, and 4 g of 2-propanol with stirring for 2 hours. Based on mole ratio of U:Ti = 1:20, 0.265 g UO$_2$(NO$_3$)$_2$.6H$_2$O was added to the mixture. The obtained solution was hydrolyzed at low PH=2 condition by addition of 4 ml HNO$_3$ (0.05 M). After stirring the light transparent solution for 2 days, it was transferred to an open container, gelation under ambient conditions for 10 days. The mesoporous titania materials incorporating La$_2$O$_3$ and U$_3$O$_8$ were annealed at 150 ^{o}C for 72 hours, then at 400 ^{o}C for 24 hours in oven to remove the template.

4.4.38 La-U-52 (Uranium + Lanthanum)

This catalyst was synthesized by IPC (in-situ polymerizable complex) method. This method was first developed by Pechini in 1967 to prepare capacitor materials focusing only on niobates, titanates and zirconates [106]. The basic chemistry involved in the IPC method is related to the formation of metal complexes as well as the dehydration reaction of an α-hydroxycarboxylic acid and a polyhydroxy alcohol. All the studies previously reported have clearly indicated that the IPC method is quite suitable for producing highly pure and homogeneous oxides at reduced temperatures (400-900 ^{o}C). Having this in mind, 0.01 mole La (NO$_3$)$_3$. 6H$_2$O was mixed with 0.4 mole ethylene glycol. Separately, 0.1 mole citric acid and 0.01 mole uranyl nitrate hexahydrate were

mixed well. The two above solutions were transferred into a different quarts vial. During well mixing, it was heated to 60 °C. Later, condensing the citrate complex at 130 °C and polyesterification, it was gradually heated to 200 °C. The dried sample was heated to 800 °C for 6 hours.

4.4.39 La-Ti-53 (Lanthanum + Titanium)

This catalyst was synthesized by IPC (in-situ polymerizable complex) method. 0.01 mole La $(NO_3)_3$. $6H_2O$ was mixed with 0.4 mole ethylene glycol. Separately, 0.1 mole citric acid and 0.01 mole $Ti(OPr)_4$ were mixed well. The two above solutions were transferred into a different quarts vial. During well mixing, it was heated to 60 °C. Later, condensing the citrate complex at 130 °C and polyesterification, it was gradually heated to 200 °C. The dried sample was heated to 800 °C for 6 hours.

4.4.40 La$_2$O$_3$-54 (Lanthanum Oxide)

La$_2$O$_3$ was prepared by the thermal decomposition of La $(NO_3)_3$. 6H2O at 800 °C in static air for 24 hours.

4.4.41 CeO$_2$-55 (Cerium Oxide)

CeO$_2$ was prepared by the thermal decomposition of Ce $(NO_3)_3$. 6H2O at 800 °C in static air for 24 hours.

4.4.42 Pt/TiO$_2$-56 (Platinum over Titanium Oxide)

Using incipient wetness synthesis method (impregnation), 0.036 g Pt(NH$_3$)$_4$(NO$_3$)$_2$ was dissolved in 2 ml ethanol and 2 ml 0.04M HNO$_3$. Then, 0.122 g of powder TiO$_2$ (calcined at 500 °C) was added to the solution. After stirring for 6 hours, the sample was dried at room's temperature for 4 days, then, it was calcined at 500 °C for 3 hours.

4.4.43 Pt/U$_3$O$_8$-57 (Platinum over Uranium Oxide)

Impregnation method was used to synthesize this catalyst. UO$_2$(NO$_3$)$_2$.6H$_2$O was calcined to provide U$_3$O$_8$. 0.06 g Pt(NH$_3$)$_4$(NO$_3$)$_2$ was dissolved in 2 ml ethanol and 2 ml 0.04M HNO$_3$. Then, 0.4 g powder U$_3$O$_8$ was added to the solution. After stirring for 6 hours, the sample was dried at room's temperature for 4 days, then, it was calcined at 500 °C for 3 hours.

4.4.44 Pt(0.1%)/γ Alumina-59 (Platinum over γ Alumina)

This is also a commercial catalyst. It was purchased from Alfa Aesar Chemical Company.

CHAPTER 5

THE FUNDAMENTALS OF GAS ADSORPTION

Gas adsorption measurements are widely used for determining the surface area and pore size distribution of a variety of different solid materials, such as industrial sorbents, catalysts, pigments, ceramics, and building materials. Two types of adsorption phenomena have been recognized in principle for many years: Physical adsorption and chemical adsorption, or chemisorption. Physical adsorption is caused by secondary (van der Wals) attractive forces such as dipole-dipole interaction and induced dipoles and is similar in character to condensation of vapor molecules onto a liquid of the same composition. Chemisorption involves chemical bonding, is similar in character to a chemical reaction, and involves transfer of electrons between adsorbent and adsorbate. Physical adsorption is of particular interest here because it provides a method of measuring the surface area of a catalyst and determining its average pore size and pore-size distribution.

The term sorption proposed by McBain [107] in 1909 embraces adsorption as process in which adsorptive molecules are transferred to, and accumulate in the interfacial layer on a surface and absorption by penetration into the lattice of the solid, and capillary condensation within the pores. The designation adsorption is frequently employed to denote uptake whether by capillary condensation or by surface adsorption. In such an experiment the material actually adsorbed by the solid (the adsorbent) is termed the adsorbate. Adsorption is brought about by the forces acting between the solid

and the molecules of the gas. These forces of two main kinds (physical and chemical) and they give rise to physisorption (or van der Waals) and chemisorption respectively.

The specific surface area of a particular sample is defined as the amount of surface contained on a specific quantity (i.e. volume or mass) of sample. Methods of obtaining the specific surface area of solid particles have been discussed by Adamson [108]. Such methods include optical and electron microscopic inspection, adsorption from solution, and indirectly by mercury intrusion porosimetry. Most commonly, adsorption of inert gases is used for this purpose, since this method does not make assumptions concerning the overall shape of the particles. It is also relatively straightforward in application and has been proven valid for many systems.

There are two types of isotherms to determine surface area of porous solids: Langmuir isotherm and Brunauer-Emmett-Teller (BET) isotherm. The mass of adsorbate, N, located at the interface between solid and gaseous phases is a function of temperature and pressure, $N = f(T, P)$. Experimentally, one can obtain adsorption data by determining N as a function of pressure at constant temperature, $N = f(P)_T$, in which case an "isotherm" can be constructed. Alternatively, one can vary the temperature of the adsorbing system at constant pressure, $N = f(T)_P$, resulting in an "isobaric plot". For experimental convenience, the most common measurements of adsorption are isotherms. An adsorption isotherm is the relationship at constant temperature between the partial pressure of the adsorbate and the amount adsorbed at equilibrium. This varies from zero at $P/P_o = 0$ to infinity as P/P_o reaches 1 provided that the contact angle of the condensed vapor is zero, i.e., the surface area is completely wetted.

71

5.1 The Langmuir Isotherm

The Langmuir adsorption isotherm model [109] was developed in 1918 for submonolayer adsorption under equilibrium conditions. Equilibrium between a vapor and the adsorbed state is defined in this case as being reached when the rate at which molecules leave the surface (desorb) is matched by the rate at which molecules are captured on a bare site on the surface (adsorb). Langmuir had to make several assumptions in order to describe the adsorption process. First, he assumed that the factors affecting adsorption and desorption of adsorbate molecules were constant as the coverage of the surface approached completion of one monolayer. Second, he assumed that the surface consisted of energetically homogeneous adsorption sites. Third, each site can adsorb only one adsorbate molecules, thereby limiting the adsorbed film to one monolayer in thickness.

If the fractions of occupied sites and unoccupied sites on the surface are θ_1 and θ_0, respectively, the total surface is described by

$$\theta_1 + \theta_0 = 1 \tag{5.1}$$

the rate of adsorption (k_a) on unit area of surface is then

$$k_a = P\,\alpha_1\,\kappa\,\theta_0 \tag{5.2}$$

where α_1 is the condensation coefficient (the fraction of the molecules hitting the surface that actually adsorb) and P is the partial pressure of the adsorbate in the carrier gas. κ is a constant given by the kinetic theory of gases, i.e.

$$\kappa = \frac{0.5\,L}{\sqrt{M\,R\,L}} \tag{5.3}$$

where L is Avogadro's number, M is the molar mass of the adsorbate, R is the gas constant, and T is the temperature (K).

The adsorption of a molecule from the surface is an activated process requiring an input of energy essentially equal to the isosteric heat of adsorption (ΔH_{iso}). The rate of desorption (k_d) from unit area of surface is equel to

$$K_d = Z_m\,\theta_l\,\upsilon_l\,exp\left(\frac{-\Delta H_{iso}}{R\,T}\right) \tag{5.4}$$

where Z_m is the number of sites per unit area of surface ($Z_m\,\theta_l$ = the number of adsorbed molecules per unit area of surface) and is the frequency of the oscillation of the molecule in the direction perpendicular to the surface. At equilibrium $k_a = k_d$ so that

$$P\,\alpha_l\,k\,\theta_o = Z_m\,\theta_l\,\upsilon_l\,exp\left(\frac{-\Delta H_{iso}}{R\,T}\right) \tag{5.5}$$

or

$$P\,\alpha_l\,k\,(1-\theta_l) = Z_m\,\theta_l\,\upsilon_l\,exp\left(\frac{-\Delta H_{iso}}{R\,T}\right) \tag{5.6}$$

solving this equation for θ_l leads to

$$\theta_l = \frac{\alpha_1\,\kappa\,P}{\alpha_1\,\kappa\,P + Z_m\upsilon_1\,exp\left(\dfrac{-\Delta H_{iso}}{R\,T}\right)} \tag{5.7}$$

if N is the mass of adsorbate per gram of adsorbent and N_m is the monolayer capacity, then, $\theta_l = N/N_m$ as long as $N \le N_m$. Thus,

$$\frac{N}{N_m} = \frac{B\,P}{1+B\,P} \tag{5.8}$$

Where

$$B = \frac{k_a}{k_d} = \frac{\alpha_1 k}{Z_m \upsilon_1} \exp\left(\frac{\Delta H_{iso}}{R T}\right)$$ (5.9)

Equation (5.8) is the well known langmuir equation. This equation shows that a chemisorption-type isotherm (Figure 5.1) is obtained from this theory. At small value of P, where P in the denominator can be neglected compared with B, equation (5.8) reduced to a simple proportionality between θ and P, and this behavior is that corresponding to the initial steep rise of the isotherm curve. At higher pressures the value of P in the denominator contributes appreciably, and the increasing denominator leads to values of θ_l that do not increase proportionality with increases in P. For sufficiently large values of P, θ_l approaches the constant value of unity.

5.2 The Brunauer-Emmett-Teller (BET) Isotherm

The Langmuir isotherm disregards the possibility that initial overlayer may act as a substrate for further adsorption to give a multilayer adsorbate. Instead of the isotherm leveling off to some saturated value at high pressures in these cases one expects it to continue to rise indefinitely because there is no limit to the amount of material that may condense. The most popular isotherm dealing with multilayer adsorption is the one due to Brunauer, Emmett, and Teller, the BET isotherm. The derivation is an extension of the Langmuir argument, and it assumes that each layer with an exposed surface is in equilibrium with the gas.
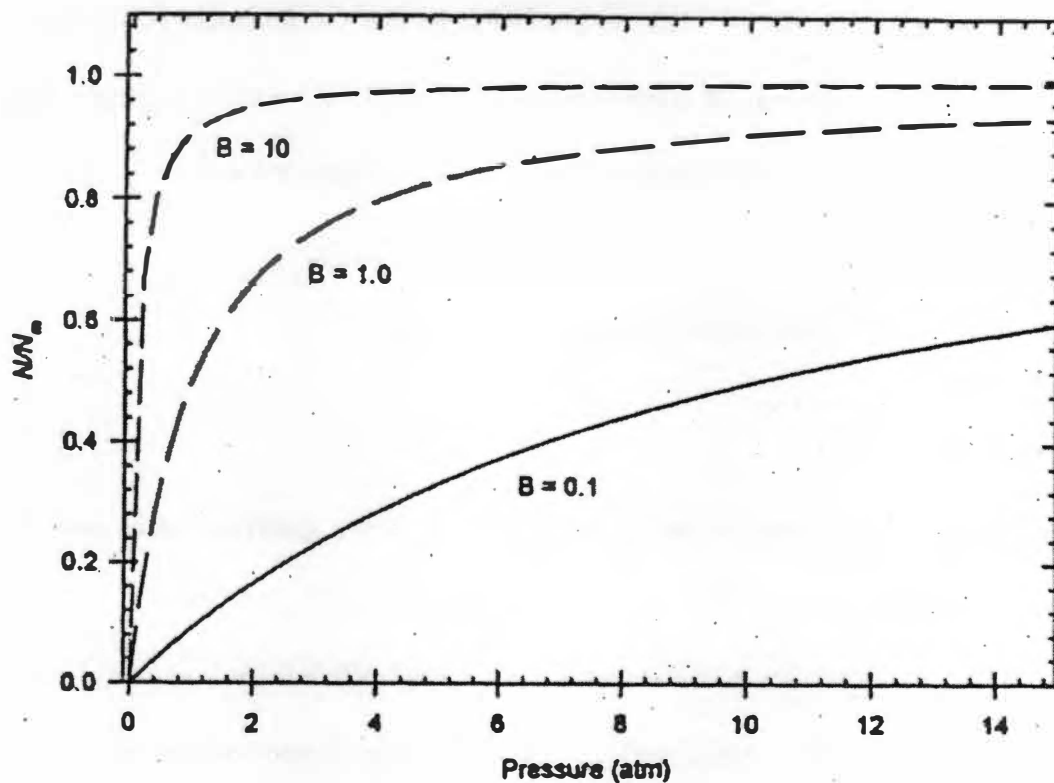
Figure 5.1: Plot of (N/N_m) vs. P (atm) as a function of B.

On most surfaces, contrary to the assumption inherent in the Langmuir isotherm, adsorption does not cease after a monolayer of adsorbate is completed. In most cases, multilayer adsorption can take place on the surface. In 1938, Brunauer, Emmet, and Teller [110] extended the Langmuir model to include the adsorption of multiple molecular layers on a surface. These researchers developed a method by which the monolayer coverage could be calculated from adsorption data obtained in the multilayer region of the isotherm. The "BET" model, as it is now called, states that, at any pressure

below the saturation vapor pressure (P_o), the fractions of the surfaces covered with 1, 2, ..., i molecules will be θ_1, θ_2, ..., θ_i respectively, so that the thickness of the adsorbed layer will not be constant at all points on the surface. On the surface corresponding to one gram of adsorbent the total number of molecules (N_T) adsorbed will be

$$N_T = A_d Z_m (\theta_1 + 2\theta_2 + ... + i\theta_i) \tag{5.10}$$

so that N, the amount adsorbed in grams, will be given by

$$N = \frac{MA_d Z_m \sum (i\,\theta_i)}{L} \tag{5.11}$$

where M is the molar mass of the adsorbate and A_d is the specific surface area of the adsorbent (m_2/g).

Since the molecules in each layer are in slightly different environments, each will have its own value of α, ΔH_{iso}, and ν. Thus, in order to perform the summation in equation (5.10), Brunauer et al. made several simplifying assumptions:

a. First, in all layers of adsorbate except the first, the heat of adsorption is equal to the molar heat of liquefaction (ΔH_L), i.e.,

$$\Delta H_{iso,2} = \Delta H_{iso,3} = ... = \Delta H_{iso,i} = \Delta H_L$$

b. Second, the desorption/ adsorption behavior of the adsorbate molecules in the second and higher layers is the same as that of the adsorbate in the liquid state, i.e.,

$$\nu_2 = \nu_3 = ... = \nu_i$$

and

$$\alpha_2 = \alpha_3 = ... = \alpha_i$$

76

c. Third, when the vapor is saturated with the adsorbate ($P = P_0$), the adsorbate condenses to a bulk liquid on the surface and the number of layers approaches infinity. Given the above assumptions, the summation of terms in Equation (5.10) leads to Equation (5.12), *the BET Equation*.

$$\frac{N}{N_m} = \frac{C(P/P_0)}{(1-P/P_0)\{1-(1-C)(P/P_0)\}} \qquad (5.12)$$

for convenience of plotting, it is rewritten as:

$$\frac{1}{N\left(\dfrac{P_0}{P}-1\right)} = \frac{1}{N_m C} + \frac{C-1}{N_m C}\left(\frac{P}{P_0}\right) \qquad (5.12)$$

The parameter C in Equation (5.12), which is related exponentially to the enthalpy of adsorption in the first adsorbed layer, is given by

$$C = \frac{\alpha_1 v_2}{\alpha_2 v_2} \exp\left(\frac{\Delta H_{iso} - \Delta H_L}{RT}\right) \qquad (5.14)$$

however, in practice the C constant is nearly always taken as

$$C = \exp\left(\frac{\Delta H_{iso} - \Delta H_L}{RT}\right) \qquad (5.15)$$

The factor $(\Delta H_{iso} - \Delta H_L)$ is the net heat of adsorption of the adsorbate on the surface at absolute temperature T.

If plotted as N/N_m against P/P_0, equation (5.12) gives a curve having the shape of a *type II* isotherm as $C > 2$ (Figure 5.2). The shape of the knee depends on the volume of C, becoming sharper as the value of C becomes larger. A high value of C ($\cong 100$) is
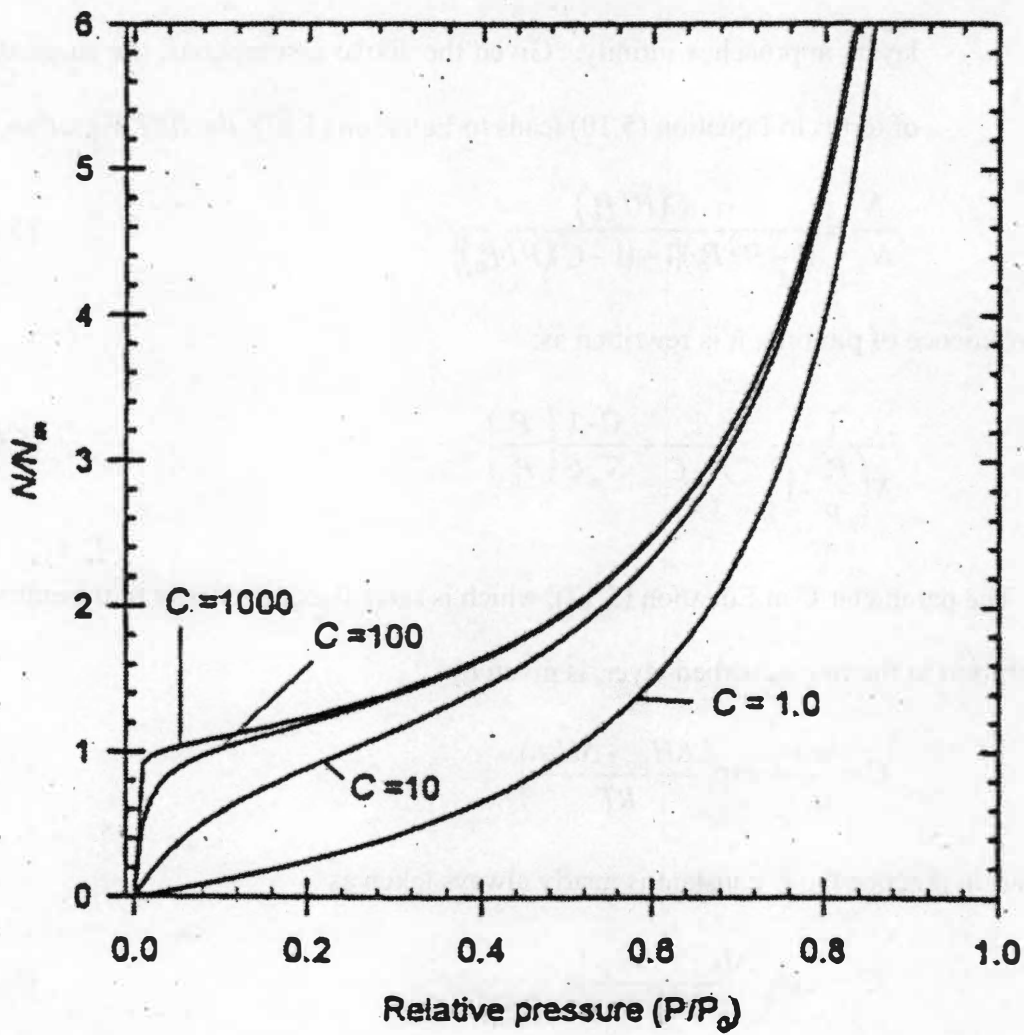
Figure 5.2: Curves of N/Nm against P/Po, calculated from the BET equation (5.12) for different values

associated with a sharp knee on the isotherm. On the other hand, if C is low (≤ 20) point

B can not be identified as a single point on the isotherm.

By plotting $\{N(P_0/P-1)\}^{-1}$ verses (P/P_0) (a so-called "BET plot"), the amount of

adsorbate (N_m) in a monolayer can be obtained. The slope of the resulting line should be

equal to $[(C-1)/N_mC]$ and the line should have an intercept of $[1/N_mC]$. Thus,

$$N_m = \frac{1}{\text{slope} + \text{intercept}} \tag{5.16}$$

and

$$C = \frac{\text{slope}}{\text{intercept}} + 1 \tag{5.17}$$

The specific surface area of the sample is calculated using

$$A_d = \frac{N_m L \sigma}{MS} \tag{5.18}$$

where σ is the cross-sectional area of the adsorbate and S is the mass of the sample.

Although several simplifying assumptions were necessary in deriving the BET

equation, it has been a highly successful model for the calculation of the monolayer

coverage of adsorbate. Even though the BET plot frequently shows deviation from

linearity in the multilayer region of the isotherm ($P/P_o > 0.35$), linearity of the BET plot

over some portion of the low partial pressure regime can usually be expected.

In addition to the assumption listed above, it is easy to overlook the fact the BET

equation can only be applied to certain types of adsorption isotherms. The general types

of adsorption isotherms as suggested by Brunauer, Deming, and Teller [111] are illustrated in Figure 5.3. Of these, adsorption conditions which produce isotherms of *Types III* and *V* can be analyzed with the BET treatment, nor can the BET equation be used in cases where the *C* constant is very small.

5.3 Classification of Adsorption Isotherm

A search of the literature on the van der Waals adsorption of gases reveals that there exist five different types of isotherms. To give an example of each type we may mention the adsorption of oxygen on charcoal at -183 $^{\circ}$C (Type I), nitrogen on iron catalysts at -195 $^{\circ}$C (Type II), bromine on silical gel at 79 $^{\circ}$C (Type III), benzene on ferric oxide gel at 50 $^{\circ}$C (Type IV), and water vapor on charcoal at 100 $^{\circ}$C (Type V). Figure 5.3 illustrates these five types of isotherms, they are imaginary, not real isotherms. The reversible *Type I* isotherm is concave to the p/p_o axis and N approaches a limiting values as $p/p_o \rightarrow 1$. Type I isotherms are given by microporous solids having relatively small surface areas (e.g. activated carbons, molecular sieve zeolites and certain porous oxides), the limiting uptake being governed by the accessible micropore volume rather than by the internal surface area. The reversible Type II isotherm is the normal form of isotherm obtained with a non-porous or macroporous adsorbent. The *Type II* isotherm represents unrestricted monolayer-multilayer adsorption. The beginning of the isotherm is often taken to indicate the stage at which monolayer coverage is complete and multilayer adsorption begin. The reversible *Type III* isotherm is convex to the p/p_o axis over its entire range. Isotherms of this type are not common, but there are a number of
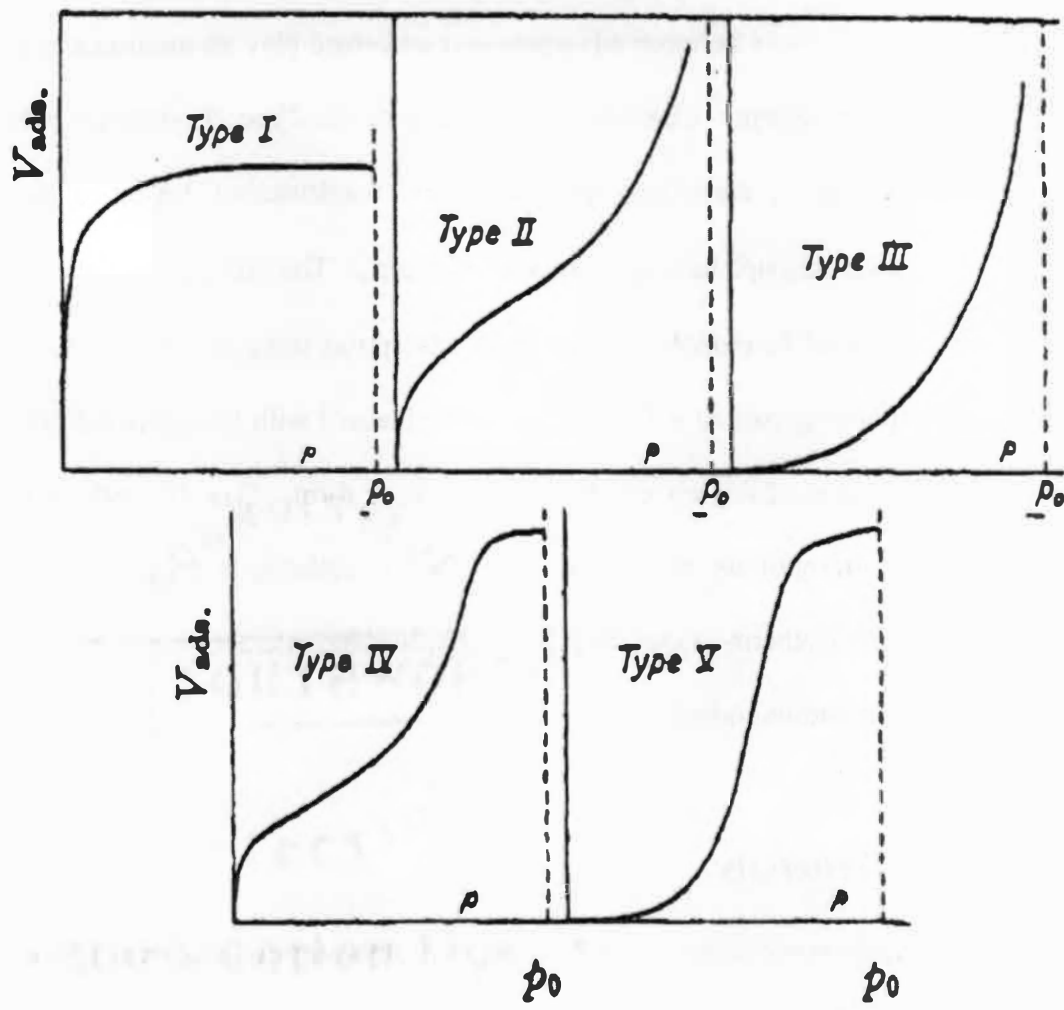
Figure 5.3: The five types of adsorption isotherm

systems (e.g. nitrogen on polyethylene) which give isotherms gradual curvature. In such cases, very weak interactions between adsorbent and adsorbate play an important role in the formation of the isotherm. Characteristic features of the *Type IV* isotherm are its hysteresis loop, which is associated with capillary condensation taking place in mesopores and the limiting uptake over a range of high p/p_o. The initial part of the *Type IV* isotherm is attributed to monolayer-multilayer adsorption since it follows the same path as the corresponding part of a *Type II* isotherm obtained with the given adsorptive on the same surface area of the adsorbent in a non-porous form. *Type IV* isotherms are observed for many mesoporous adsorbents. The *Type V* isotherm is uncommon. It is related to the *Type III* isotherm in that the adsorbent-adsorbate interaction is weak, but is obtained with certain porous sorbents.

5.4 Adsorption Hysteresis

Hysteresis appearing in the multilayer range of physisorption isotherm is usually associated with capillary condensation in mesoporous structures. Such hysteresis loops may exhibit a wide variety of shapes. Two extreme types are shown *H1* and *H4* in Figure 5.4. In the former, the two branches are almost vertical and nearly parallel over an appreciable range of gas uptake, whereas in the later they remain nearly horizontal and parallel over a wide range of p/p_o. In certain respects *Type H2* and *H3* may be regarded as intermediate between these two extremes. A feature common to many hysteresis loops is that the steep region of the desorption branch leading to the lower closure point occurs at a relative pressure which is almost independent of the nature of the porous adsorbent

82
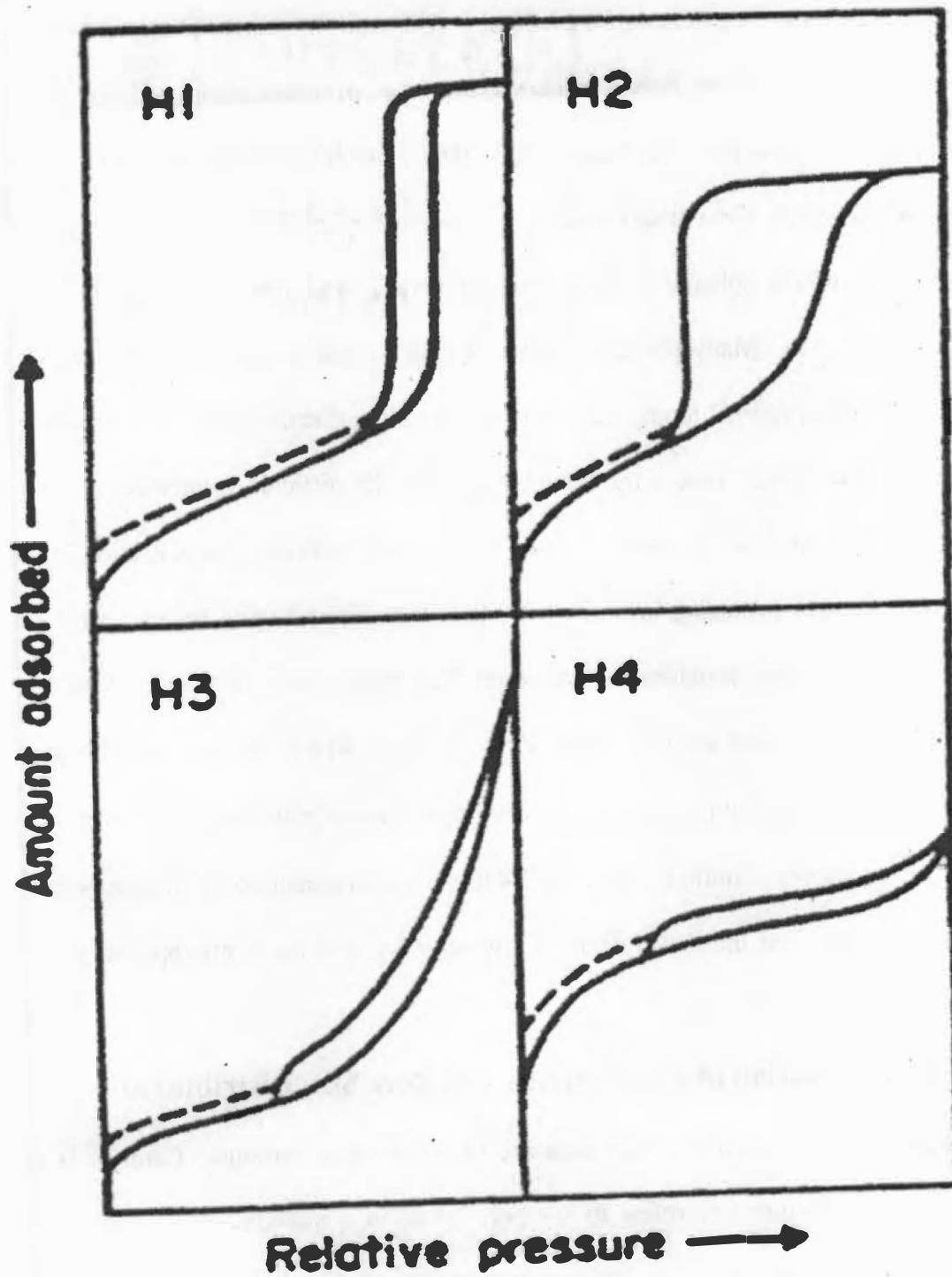
Figure 5.4: Four types of hysteresis loops.

but depends mainly on the nature of the adsorbate. Although the effect of various factors on adsorption hysteresis is not fully understood, the shape of hysteresis loops have often been identified with specific pore structures. Thus, *Type H1* is often associated with porous materials known, from other evidence, to consist of agglomerates or compacts of approximately uniform spheres in fairly regular arrays, and hence to have narrow distributions pore size. Many porous sorbents such as inorganic oxide gels and porous glasses tend to give *Type H2* loops, but in such systems the distribution of pore size and shape is not well-defined. Indeed the *H2* loop is especially difficult to interpret. In the past, it was attributed to a difference in mechanism between condensation and evaporation processes occurring in pores with narrow necks and wide bodies, but it is now recognized that this provides as over-simplified picture and the role of network effects must be taken into account. The *Type H3* loop, which does not exhibit any limiting adsorption at high p/p_o, is observed with aggregates of plate-like particles giving rise to slit-shaped pores. Similarly, the *Type H4* loop is often associated with narrow slit-like pores, but in this case the *Type I* isotherm character is indicative of microporosity.

5.5 The Determination of Pore Volume and Pore Size Distribution

Most solids with high surface area are to some extent porous. Porosity is a concept related to texture and refers to the pore space in a material. The total pore volume, V_{total}, is often derived from the amount of vapor adsorbed at a relative pressure close to unity by assuming that the pores are then filled with condensed adsorbate in the normal liquid state.

84

The determination of pore volume and pore size distribution from BET isotherms was suggested by Barrett, Joyner, and Halenda in 1951 [112]. This is based on the Kelvin equation:

$$\frac{1}{r_1} + \frac{1}{r_2} = -\frac{RT}{\sigma V} \ln\left(\frac{P}{P_0}\right) \tag{5.19}$$

This equation relates the principle radii, r_1 and r_2, of curvature of the liquid meniscus in the pore at the relative pressure, p/p_0, at which condensation occurs. σ is the surface tension of the liquid condensate and V is its molar volume. In using this approach to obtain the pore radius two fundamental assumptions are necessary:

1. The pores are cylindrical and the curvature of the meniscus in the cylindrical pores is directly related to the pore width.

2. The amount of adsorbate in equilibrium with the gas phase is retained by the Adsorbent by two mechanisms: (a) physical adsorption on the pore walls, and (b) capillary condensation in the inner capillary volume.

In the cylindrical pores, the meniscus is hemispherical and $r_1 = r_2$. Rearrangement of the Kelvin equation and replacement of $\left(\dfrac{1}{r_1} + \dfrac{1}{r_2}\right)$ by $\dfrac{2}{r_k}$ gives :

$$r_k = \frac{2\sigma V}{RT \ln(P/P_0)} \tag{5.20}$$

In the context of physisorption, it is expedient to classify pores according to their sizes: (i) pore with widths exceeding about 50 nm ($500\,\overset{\circ}{\text{A}}$) are called macropores; (ii)

pores of widths between 2 nm (20 Å) and 50 nm (500 Å) are called mesopores; (iii)

pores with widths not exceeding about 2 nm (20 Å) are called micropores.

CHAPTER 6

RESULTS AND DISCUSSIONS

The combustion activity (light-off curve) of uranium oxide based catalysts have been determined for a range of typical VOCs which are chemically different in nature. The compounds investigated include toluene, chlorobenzene and trichloroethylene respectively. The conversions were measured at a constant flow rate of 140 cc/min (0.15% toluene, 0.30% O2, He balance) and using 0.1 g catalyst, the Gas Hourly Space Velocity (GHSV) was calculated as follows:

$$GHSV = \frac{F}{W} = \frac{140\,ml/min}{0.1g\,catalyst} \times \frac{60\,min}{hr} = 84,000 \ mlg^{-1}h^{-1} \tag{6.1}$$

Where F is the flow rate per hour and W is the weight of catalyst.

The vapor pressure of VOC was estimated by using the Antoine Equation as follows:

$$Log_{10}P^* = A - \frac{B}{T+C} \tag{6.2}$$

Where P^* is the vapor pressure in mm Hg and A, B, and C are empirical constant [113] that varies from one substance to another. T is the temperature in $^{\circ}$C. By using Antoine Equation, the vapor pressure of toluene, chlorobenzene and trichloroethylene at 0 $^{\circ}$C, was calculated as follows:

$$Log_{10}P^* = 6.95334 - \frac{1343.943}{0+219.377} = 0.827 \qquad P^*_{toluene} = 6.717 \ mm \ Hg \tag{6.3}$$

$$Log_{10}P^* = 7.10690 - \frac{1500.0}{0+224.0} = 0.4105 \qquad P^*_{chlorobenzenee} = 2.573 \ mm \ Hg \tag{6.4}$$

$$\text{Log}_{10}\, P^* = 6.5183 - \frac{1018.60}{0 + 192.70} = 1.232 \qquad P^*_{\text{trichloroethylene}} = 17.07 \text{ mm Hg} \tag{6.5}$$

By knowing the vapor pressure of toluene, chlorobenzene and trichloroethylene, the concentration of each can be calculated by the following method in the flow system:

$$\frac{P^*_{\text{toluene}}\,(6.717 \text{ mm Hg})}{760 \text{ mm Hg}} \times \frac{21\,\text{ml}}{140\,\text{ml/min}} \times 10^6 = 1325\,\text{ppm} \tag{6.6}$$

$$\frac{P^*_{\text{chlorobenzene}}\,(2.573 \text{ mm Hg})}{760 \text{ mm Hg}} \times \frac{21\,\text{ml}}{140\,\text{ml/min}} \times 10^6 = 508\,\text{ppm} \tag{6.7}$$

$$\frac{P^*_{\text{trichloroethylene}}\,(17.07) \text{ mm Hg}}{760 \text{ mm Hg}} \times \frac{21\,\text{ml}}{140\,\text{ml/min}} \times 10^6 = 3369\,\text{ppm} \tag{6.8}$$

Assuming ideal gas law, the %volume of water in the reactant stream at syringe flow rate of Q ml/min and total flow rate of 140 ml/min, was calculated as follows:

$$\frac{Q\,\text{ml}}{\text{min}} \times \frac{1\,\text{g H}_2\text{O}}{1\,\text{ml H}_2\text{O}} \times \frac{1\,\text{mole H}_2\text{O}}{18\,\text{g H}_2\text{O}} \times \frac{22400\,\text{ml}}{1\,\text{mole H}_2\text{O at STP}} = Q \times 1244.44\,\frac{\text{ml}}{\text{min}}\,\text{water in stream}$$

$$\frac{Q \times 1244.44\,\dfrac{\text{ml}}{\text{min}}}{(Q \times 1244.44 + 140)\,\dfrac{\text{ml}}{\text{min}}} \times 100 = \%\,\text{by volume H}_2\text{O vapor entering into reactor.} \tag{6.9}$$

Blank reactions in an empty reactor and using a catalyst bed of frit silica used to produce the supported catalysts indicated that activity for the combustion of all VOCs at Gas Hourly Space Velocity (GHSV) of 84,000 $\text{mlg}^{-1}\text{h}^{-1}$ was negligible.

6.1 Oxidation of Toluene

6.1.1 Efficacy of Mixed (U_3O_8 – SiO_2) Catalysts U_3O_8

The BET surface area of U_3O_8 was <0.1 m^2/g. Two XRD were run, one before and one after run in the reactor. In both cases, the samples were calcined at 800 °C. Before the reaction, the sample shows sharp peaks due to U_3O_8. Every peak can be assigned to U_3O_8, but all are shifted to slightly higher angle, impling a smaller lattice constant and probably reduced sample. No peaks due to UO_2 observed. It also does not fit to UO_3. After reaction the sample showed decreased peak intensity, perhaps due to sample poisoning, but also a broad amorphous peak. Peaks again were assignable to U_3O_8, with no sign of UO_2. The T_{50} was 520 °C.

Mesoporous Silica (SiO_2)

The idea was to compare the activity of mesoporous silica based catalyst with variable mole ratio of uranyl nitrate hexahydrate. For this purpose, a pure SiO_2 sample was synthesized. The final calcination temperature was 800 °C. The BET surface area (See Figure A.1) was 221.8 cm^2/g. The XRD before the reaction shows sharp peaks aligned with SiO2. The T_{50} was 550 °C.

U-Meso-5 (Uranium Mesoporous Silica)

The monolithic mesostructure uranium oxide based catalyst was formed at final calcinations temperature of 800 °C. The mole ratio of U:Si was 1:10. The BET surface

area (see Figure A.2) was 224.6 m^2/g. The XRD measurements of the calcined catalyst before experiment indicated that the uranium is present as U_3O_8. This catalyst performed poorly. After reaction, this catalyst was examined by XRD. The XRD in Figure 6.1 clearly demonstrated that this catalyst contained a fluorite phase of UO_2. This phase is associated with the poor activity of this catalyst. It is not clear why this catalyst contained such high quantities of UO_2 phase. This catalyst did show 50% toluene light-off at 425 °C.

Meso-6 (Uranium Mesoporous Silica)

The mole ratio of U:Si was 1:20. The BET surface area (See Figure A.3) was 233 m^2/g. Two XRD were run, one before and one after the reaction. In both cases, the samples was calcined at 800 °C. Before the reaction, the sample showed peaks due to U_3O_8, but there was a very high background. Peaks are very close to predicted angle, suggesting lattice constant is comparable to U_3O_8 without reduction. There is no sign of UO_2. After reaction, exhibited the same peak with present of U_3O_8, but no sign of UO_2. This catalyst was very stable at the beginning, but after long run did show some deactivation at 575 to 600 °C. This deactivation was recovered by heating in oxygen for an hour.
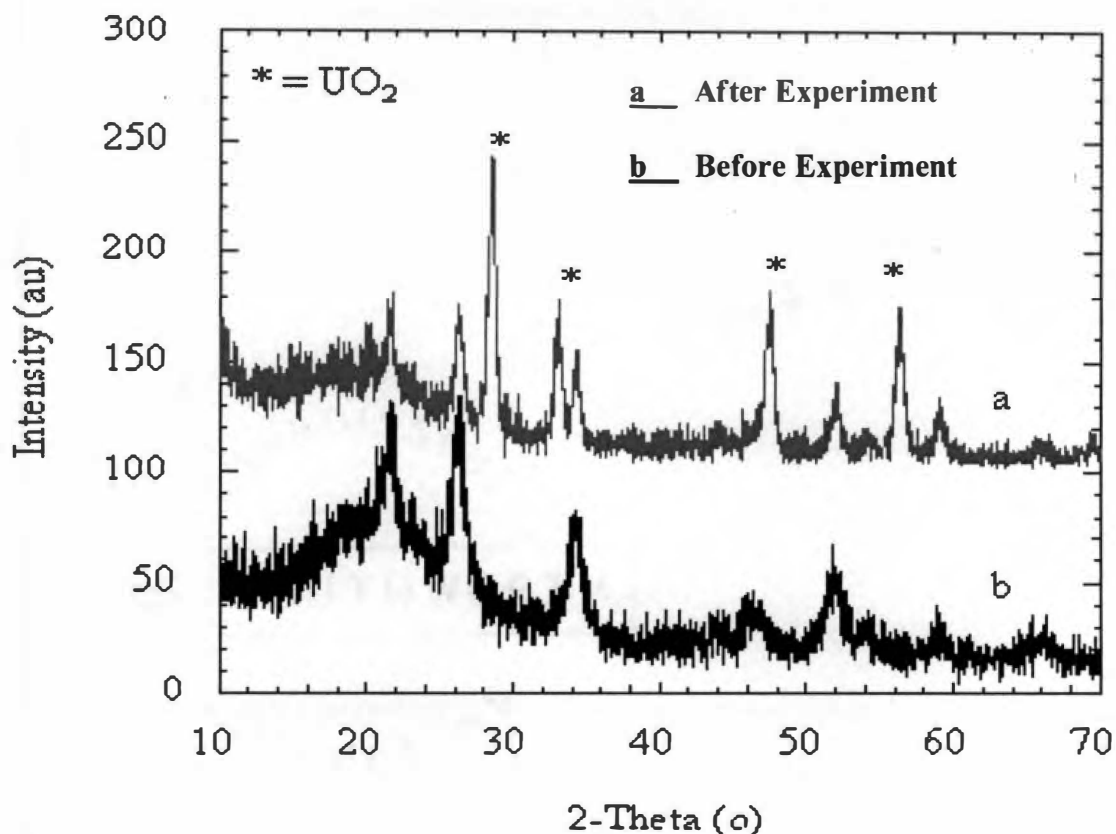
Figure 6.1: XRD spectra identifying the active U_3O_8 phase and inactive UO_2 phase present in U-Meso-5.

It was considered very important to control the concentration of toluene independently in the reaction stream, since in a technical application, the concentration of VOC may be variable. It was important to be able to confirm the catalyst activity with respect to this variable. This was accomplished by adding another gas flow line and reconfiguring the reactor streams with three individual flow rates. After modification, the activity vs. concentration of toluene was determined. The results are shown in Figure 6.2. The plot reveals that decreasing conversion as toluene concentration increases as might be expected for a fixed flow rate.
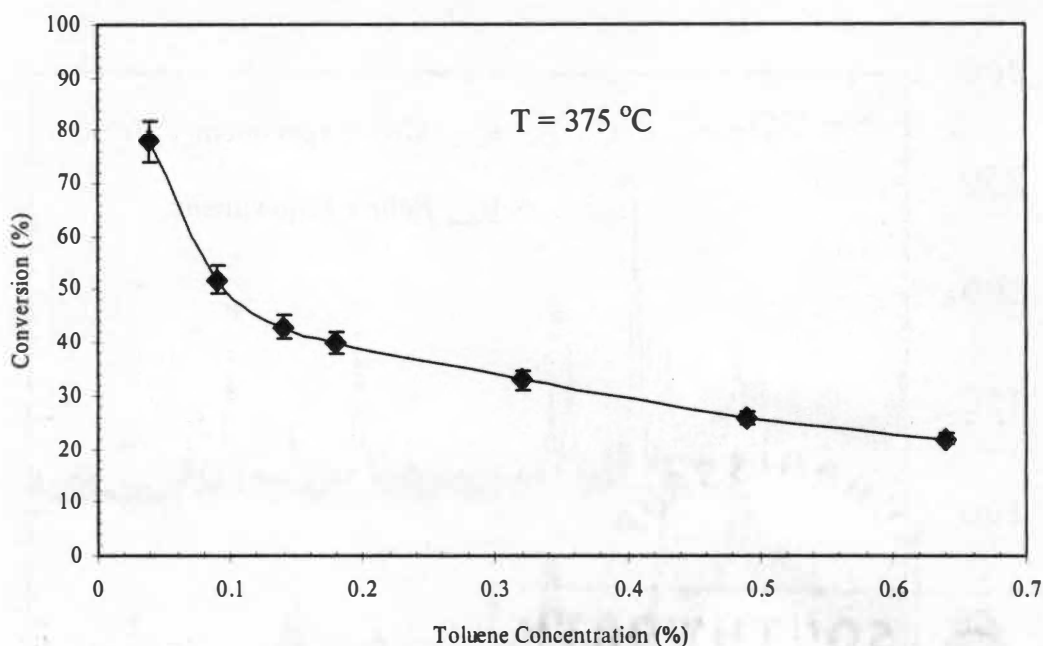
Figure 6.2: The conversion of toluene as a function of toluene concentration in the exit reactor stream.

The Mass Spectrometric analysis indicates that toluene is converted almost entirely to CO_2 and H_2O, but there is evidence for small amount of xylene and CO in the exhaust streams. This catalyst showed 50% toluene light-off at 410 °C. A comparison of the activity of this catalyst with U_3O_8, SiO_2, and U-Meso-5 is shown in Figure 6.3. The plot indicates that loading as low as 1:20 uranium to silicon give high activity probably due in part to high dispersion of uranium. The results for pure U_3O_8 catalyst suggest that uranium loading is not as important as surface area and preparation methods.
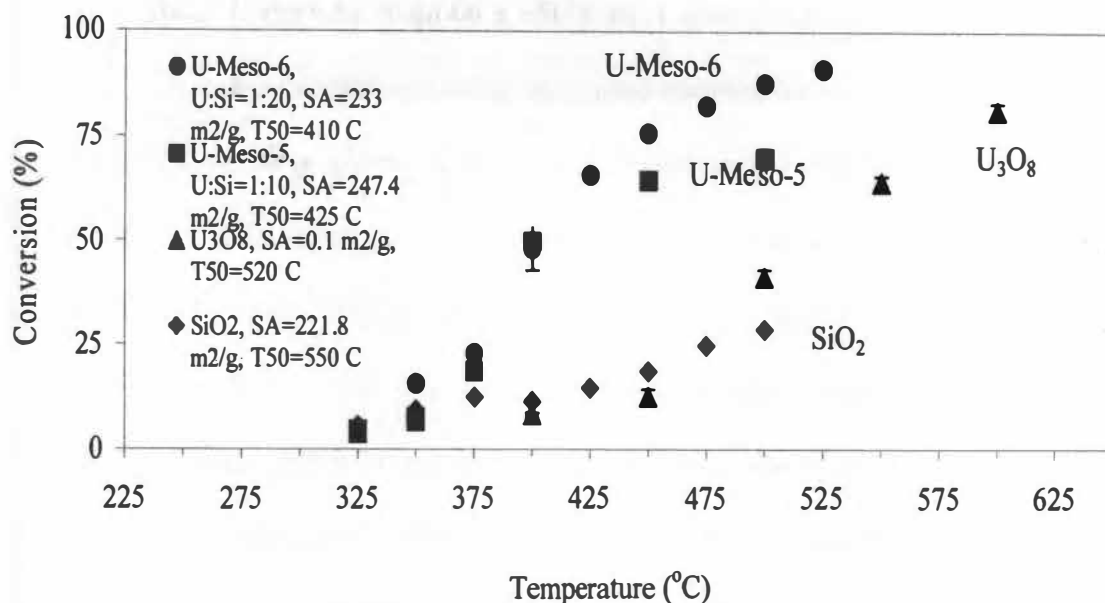
Figure 6.3: Comparison of catalytic performance (U_3O_8, SiO_2, U-Meso-5, and U-Meso-6) for destruction of toluene.

6.1.2 Effect of Chromium Doping on Catalyst Efficiency

U-Cr-Meso-19, 21 (Chromium + Uranium Mesoporous Silica) and MesoCr-22 (Chromium + Mesoporous Silica)

It is well known that Cr is an active element for oxidation of VOC. The idea was to add a small amount of the Cr which through synergistic interactions may promote the activity of the uranium oxide, perhaps by enhancing the ability of the uranium to transfer oxygen, or by stabilizing a smaller uranium oxide particle size. Cr based catalysts were prepared by different synthetic methodologies and compared for their catalytic activity. In a synthetic method, a silica supported uranium oxide catalyst without Cr was first synthesized using co-assymbly method as described previously with a U:Si mole ratio of 1:20. Then, it was calcined at 800 °C accordingly. This material was post impregnated with Cr and calcined at 600 °C. The BET surface area was 253.4 m²/g. The post-

93

impregnated was done in such a way to produce a comparable weight loading of Cr (4.9%) onto the silica supported uranium catalyst as in the co-synthesis catalyst.

In a second approach, Cr was added into the co-assembly synthesis of the silica supported uranium. After synthesis, the resulting catalyst was calcined at 800 °C. The BET surface area (See Figure A.4) was 203 m^2/g and pore volume of 0.29 cm^3/g suggesting that mesoporosity is achieved in the co-synthesis. The synthesis mole ratio of Cr:U:Si was about 1:1:20, which computes to a Cr loading of 4.9%. Detailed loading calculations are given in appendix B.7. XRD of this catalyst indicates that uranium is present as U_3O_8, but Cr is not visible due to its low concentration of or it is existing as very small particle.

In addition to above two catalysts, another sample was synthesized using co-assambly synthesis in which as silica supported Cr was prepared with no uranium oxide. The BET surface area was 207 m^2/g (See Figure A.5). The synthesis concentration is about 5.9% wt Cr, comparable with Cr loading in the other two Cr containing catalysts. After calcinations at 800 °C, the presence of Cr_2O_3 was confirmed by XRD. The three Cr doped catalysts are compared with undoped uranium-silica catalyst in Figure 6.4 where toluene "light-off" curves are shown. The activity increased, as characterized by the temperature of 50% conversion, T_{50}, which decreased from 405 °C down to 375 °C. The impregnation method for doping the catalyst with Cr was not as effective as the co-synthesis method. The activity of the impregnated catalyst is dominated by the activity
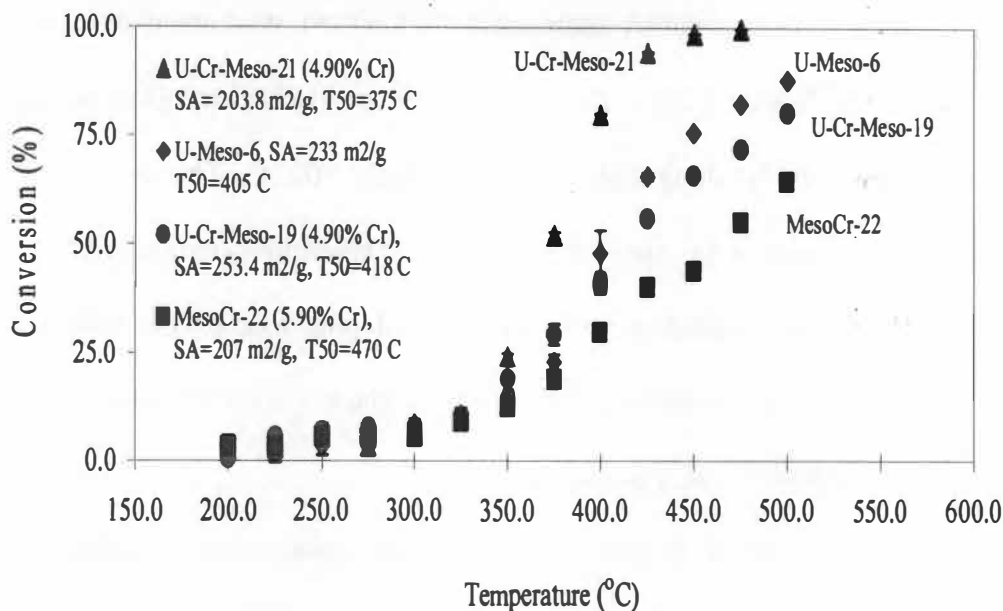
Figure 6.4: Effect of Chromium addition by co-assembly or impregnation synthesis techniques for destruction of toluene.

of the supported uranium oxide. Cr is active even without uranium when it is put onto silica using the co-assembly approach.

6.1.3 Effect of Cobalt Doping on Catalyst Efficiency

U-Co-Meso-20, 23 (Cobalt + Uranium Mesoporous Silica) and MesoCo-24 (Cobalt Mesoporous)

Similarly, post impregnation method was performed with Co loading and the resulting catalyst was calcined at 600 °C. The BET surface area was 242 m^2/g. As compared with Cr, the post-impregnation with Co has the effect of decreasing the activity. The T$_{50}$ was 440 °C.

95

In the second approach, Co was added into the co-assembly synthesis of the silica supported uranium. The synthesis mole ratio of Co:U:Si was about 1:1:20, which computes to a Co loading of 5.23%. Detailed loading calculations are given in appendix B.8. After synthesis, the resulting catalyst was calcined at 800 °C. The BET surface area was 223 m2/g (See Figure A.6). Both co-assembly and post-impregnation synthesis were performed with comparable loading. It has seen that doping with Co has little effect on the activity of co-synthesized catalyst, suggesting that the Co is not interacting with U or contributing to the activity. The T_{50} was 420 °C.

In the final approach, a different catalyst was synthesized in which as silica supported Co was prepared without uranium. The synthesis mole ratio of Co:Si was about 1:20, which computes to a Co loading of 6.44%. After calcination at 800 °C, the presence of CoO was confirmed by XRD. The BET surface area (See Figure A.7) was 224 m2/g. Interestingly, Co supported on silica without uranium is also of comparable activity as the pure uranium. These results suggest that the uranium phase and the Co phase both have comparable activity, and are not synergistically interacting. The post impregnation however may lead to large Co crystallite particles which are less active by virtue or smaller surface area and which may block access to uranium in the mesopores. The results are shown in Figure 6.5.
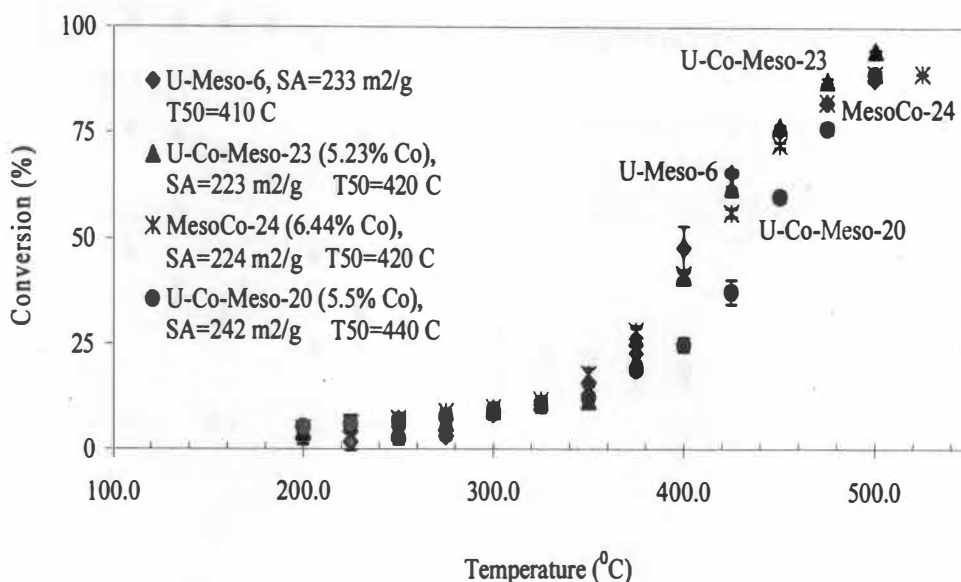
Figure 6.5: Effect of Cobalt addition by co-assembly or impregnation synthesis techniques for oxidation of toluene.

6.1.4 The Efficacy of Mixed (U_3O_8 – TiO_2) Catalyst

TiO_2-41 (Mesoporous Titanium Oxide)

Mesoporous titanium oxide catalyst was synthesized by co-assembly method according to a procedure outlined previously in chapter 4. Mesoporous titanium oxide is known to be active in oxidation reactions especially when used as a support for vanadia catalyst. The prepared titanium oxide was calcined at 400 °C, then, it was divided into three equal portions. The first portion was named TiO_2-41(400). The other two portions were calcined at 600 °C and 800 °C respectively. They were named TiO_2-41(600) and TiO_2-41(800). The purpose was to study the effect of calcinations temperature on the activity of catalyst. TiO_2-41(400) has considerable activity for oxidation of toluene. As shown in Figure 6.6, the activity of this catalyst decreases considerably when it was

97
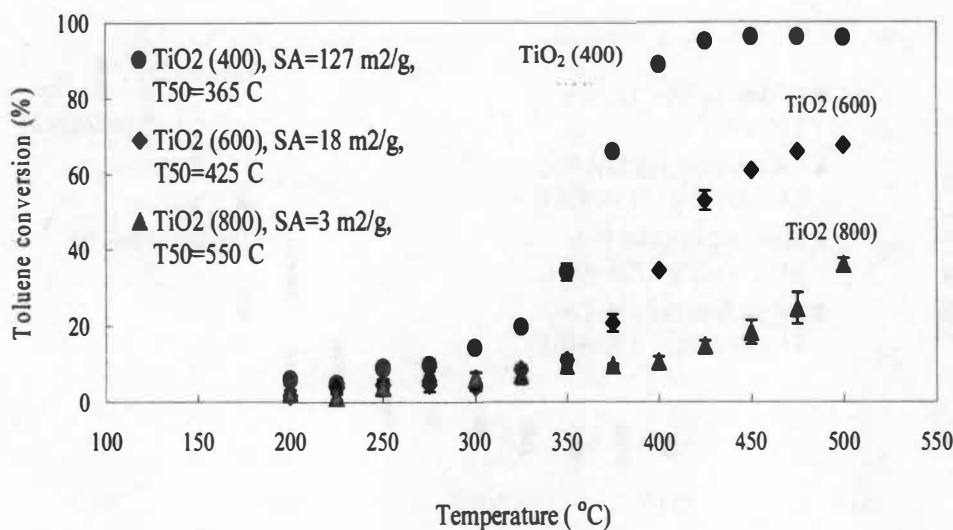
Figure 6.6: Effect of calcinations temperature upon light-off by TiO_2.

calcined above 400 °C. Calcination at 800 °C seriously degrades the titania catalysts. The

degradation is probably due to loss of surface area due to the collapse of the titania

mesoporous structure, since the BET surface area drops from 127 m^2/g down to 3 m^2/g.

The T_{50} was 365, 425, and 550 °C, for TiO_2-41(400), TiO_2-41(600), and TiO_2-41(800)

respectively. The N_2 adsorption-desorption isotherms of titania oxide are shown in

appendix A (See Figures: A.8, A.9, and A.10) at various calcinations temperature. All

three different stages of calcinations are characterized by ordered cylindrical pores, show

completely reversible Type IV isotherms with the inflection in the low relative pressure

range (P/P^o=0.40-0.90) with a H_2 type hysteresis loop, indicating mesoporous materials

and the role of network effect during calcinations. The XRD (Figure 6.7) demonstrates

that with increasing calcinations temperature, the titania crystallite size grows and

98
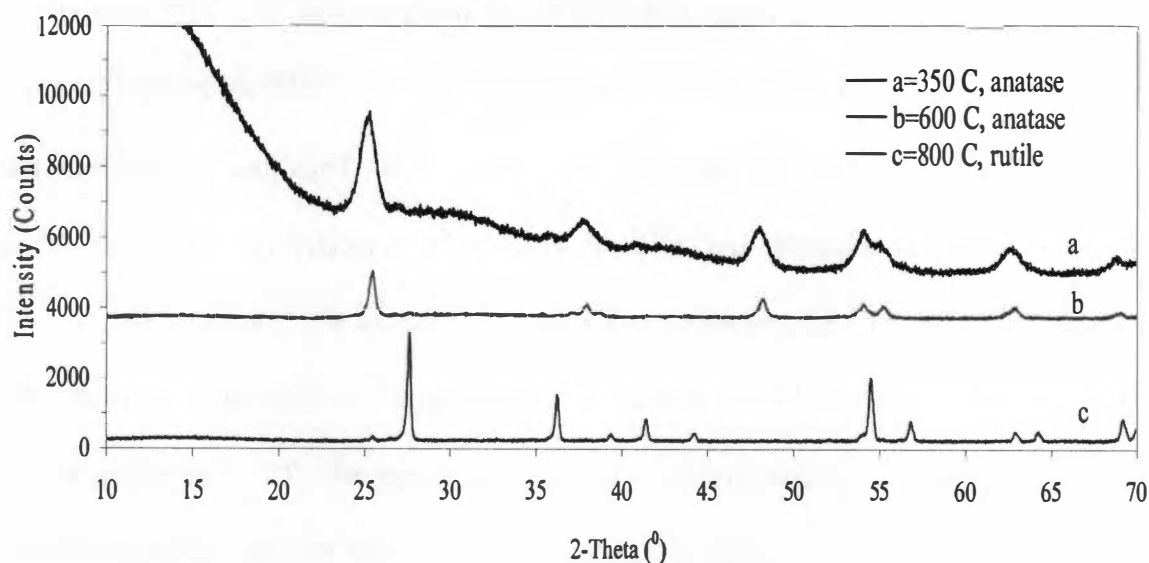
Figure 6.7: XRD pattern of TiO_2 mesoporous materials at calcinations temperature of 350 °C (a), 600 °C (b), and 800 °C (c).

converts from the anatase to the rutile titanium oxide structures which has less activity. Either the structure or the decreased surface area must be the cause of the loss of the activity.

U-Ti-Meso-(43, 42, 44, and 45) (Uranium Mesoporous Titanium Oxide)

A new type of catalyst, titania supported uranium oxide was synthesized and compared with TiO_2. The new catalyst was formed by co-assembly of uranyl nitrate with tetraethoxy titanium, and using a pluronic as a surfactant in HNO_3 solution. This synthesis has been reported in the literature for rare earth ions [101] and the present work is the first time this has been attempted with uranyl ions. The as synthesized catalyst was

calcined at 150 °C for 72 hours followed by 24 hours at 400 °C. This catalyst was divided into three equal portions. The other two portions were calcined at 600 °C and 800 °C. The first portion was named U-Ti-Meso-43(400). The other two portions were named U-Ti-Meso-43(600) and U-Ti-Meso-43(800) respectively. These catalysts, calcined at three different temperatures are shown in Figure 6.8. A conversion of 100% was achieved below 400 °C. It is seen that the catalyst improved upon calcinations to 600 °C, but, then degrades slightly after calcinations at 800 °C. The degradation is probably due to loss of surface area due to the collapse of the titania mesoporous structure, since the surface area drops from 175 down to 23 m^2/g after calcinations at 800 °C. However, it is very significant that the catalyst maintains high activity, a very important property for an oxidation catalyst. With a T_{50} of 340 °C, it is still better than uranium supported on high surface area mesoporous silica. It appears that the uranium interacts synergistically with titanium oxide and inhibits deactivation caused by sustained temperature as high as 800 °C. The activity of this catalyst was shown to be stable for days and its activity is comparable to 0.1% Pt/Al_2O_3 and therefore competitive with the more expensive preciousmetal catalyst. The comparison of BET surface areas, total pore volume, and micropore area for uranium-titanium and titanium oxide catalysts are listed in Table 6.1. Adsorption-desorption isotherms of uranium-titanium catalysts are shown in appendix A (See Figures: A.11, A.12, and A.13) for all three different stages of calcinations. The Type IV isotherms with a H_2 type hysteresis loop, indicating mesoporous materials.

Table 6.1: Catalyst BET surface area, average pore size, and total pore volume at various calcinations temperatures for U-Ti-Meso-43 and TiO$_2$-41.

Catalyst	Calcinations Temperatures (oC)	BET Surface Area (m2/g)	Total Pore Volume (cm3/g)
U-Ti-Meso-43	400	175.12	0.315
U-Ti-Meso-43	600	97.376	0.304
U-Ti-Meso-43	800	23.89	0.059
TiO2 -41	400	127.81	0.142
TiO2-41	600	18.21	0.0417
TiO2-41	800	2.953	0.0046
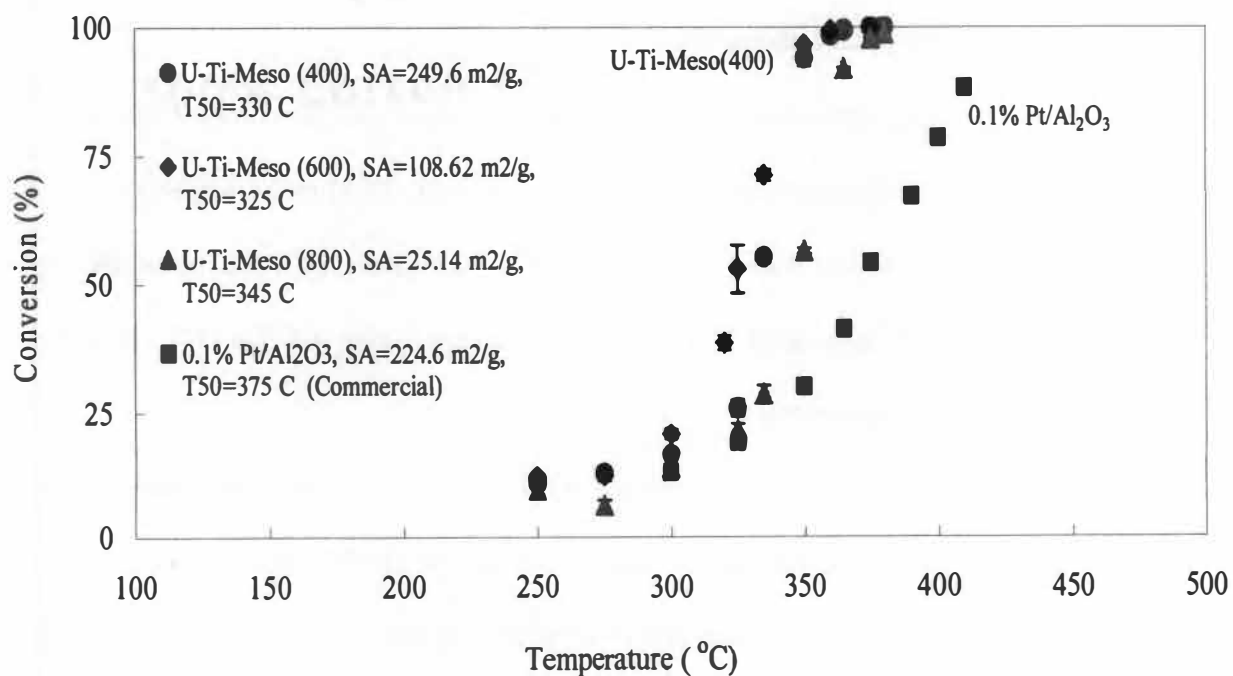
Figure 6.8: The effect of calcinations temperature upon light-off by U-Ti-Meso-43(400, 600, 800) for oxidation of toluene.

The powder X-ray diffraction pattern of the samples were recorded using a SIEMENS D5005 X-rat diffractometer, where Cu target $K\alpha$-ray ($\lambda = 0.154$ nm and operating at 40 kV and 40 mA) was used as the X-ray source. Variation of small-angle powder X-ray diffraction (XRD) patterns for uranium-titanium oxide at various stages of calcinations temperatures of 350, 600, and 800 oC are shown in Figure 6.9. All patterns are similar and they exhibit typical low angle diffraction associated with the nature of mesoporous titania oxide. It demonstrates that with increasing calcinations temperature, the titania crystallite size grows and converts from the anatase to titanium-uranium oxide ($UTiO_5$) at calcinations temperature of 800 °C. The light olive green color of $UTiO_5$ suggests that the compound is somewhat deficient in oxygen. The analytical results, however, indicate that the oxygen deficiency is minimal. Decomposition to rutile and U_3O_8, as determined by X-ray analysis, takes place above 1020 °C [114].

The ordered mesoporous structures of uranium-titanium oxides composites have been confirmed by transmission electron microscopy (TEM). TEM measurements indicated that uranium particles in the form of $UTiO_5$ were dispersed in the pores and on the external surface of titania support. All TEM images are shown in Figure 6.10 in order of their calcinations temperatures.

The mass spectrometer indicated that at lower temperature there were some byproducts. With increasing the reactor temperature above 380 °C, only carbon dioxide and water were observed. The activity of this catalyst was very stable for weeks and it is competitive with the most expensive precious metal catalyst.
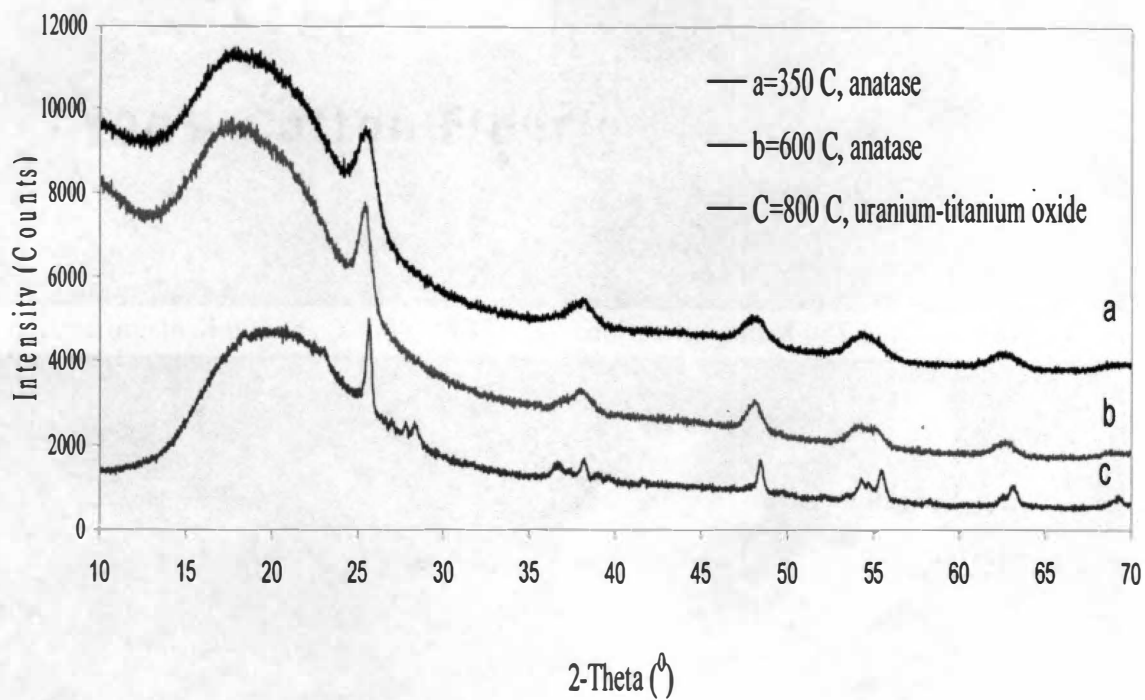
Figure 6.9: XRD pattern of U-Ti-Meso-43 at calcinations temperature of 350 °C (a), 600 °C (b), and 800 °C (c).
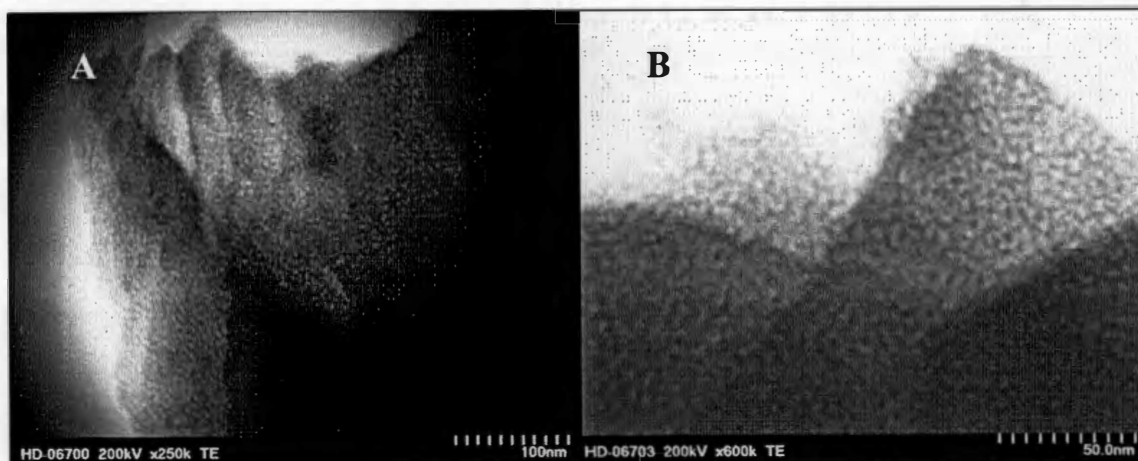
A: TEM (400 °C) at 250 K magnification   B: TEM (400 °C) at 600 K magnification
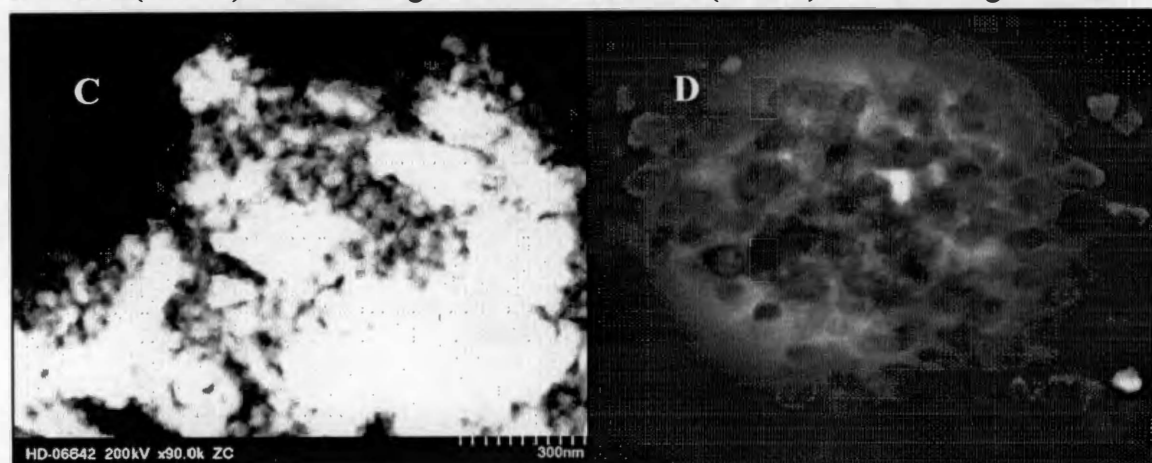
C: Z-contrast (600 °C)   D: TEM at (600 °C)
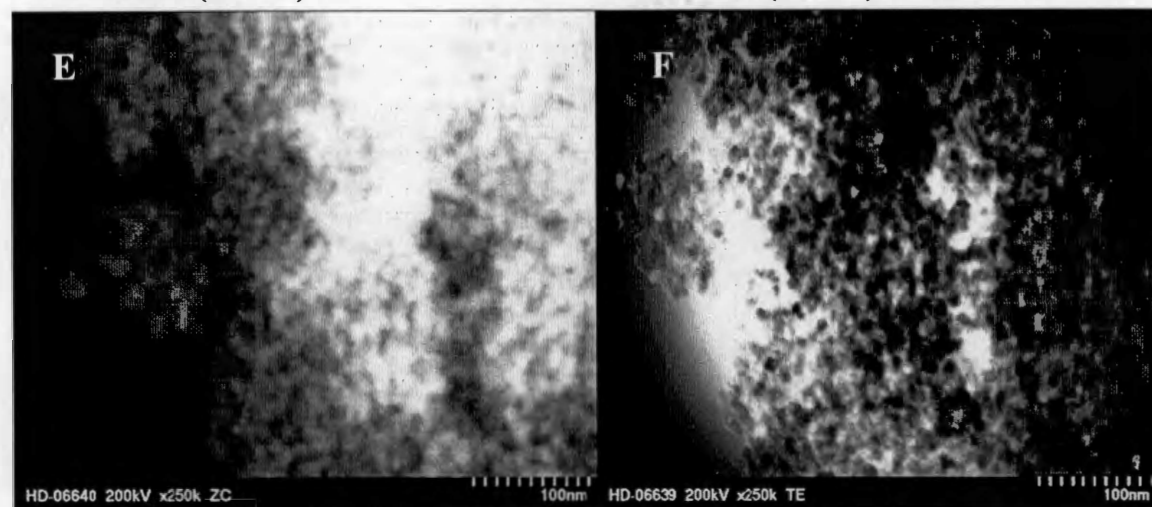
E. Z-contrast (800 °C)   F: TEM at (800 °C)

Figure 6.10: Z-contrast and TEM image of mesoporous uranium-titanium oxide catalyst (U-Ti-Meso-43).

Further syntheses were made in which the uranium was doped in different amount with titanium. Previously, it was found that uranium oxide supported on mesoporous silica yields higher activity when the uranium content was decreased from 1:20 to 1:30 (UMeso-6 and U-meso-9). Therefore, the activity of the catalyst is not straightforward to predict since it depends upon surface area or other factors besides simply the amount of uranium oxide in the catalysts and the stability of the resulting catalyst. These measurements should help determine the optimal catalyst configuration. As is evident in the Figure 6.11, the activity was decreased slightly by decreasing the loading of uranium to titanium from 1:20 to 1:30 and 1:40. On the other hand, increasing the atomic ratio of uranium to titanium from 1:20 to 1:10 slightly improved the activity as compared with others. Therefore, the relative amount of uranium oxide is evidently been optimized at 1:20. The activity decreases with decreasing loading of the uranium-to-titanium ratio from 1:20 to 1:30 and 1:40. However, the activity increases with decreasing uranium-to-titanium ratio from 1:10 to 1:20.

6.1.5 The Efficacy of Mixed U_3O_8 and K Promotor

U-MCM41-49 (Uranium+Mesoporous MCM-41), K-U-MCM41-50 (Potassium +Uranium + Mesoporous MCM-41), U-SBA-15-47 (Uranium +SBA-15), and K-U-SBA-46 (Potassium +Uranium +SBA-15).

The idea was to check the effects of potassium loading. For this purpose, two catalysts were prepared on MCM-41. First, a novel MCM-41 supported base catalyst, U-MCM-41, was synthesized with the impregnation method. U-MCM-41 was synthesized on the MCM-41 pore wall as confirmed by characterization using X-Ray diffraction, and N_2 adsorption. The BET surface area of the empty MCM-41 was 986 m^2/g, and with
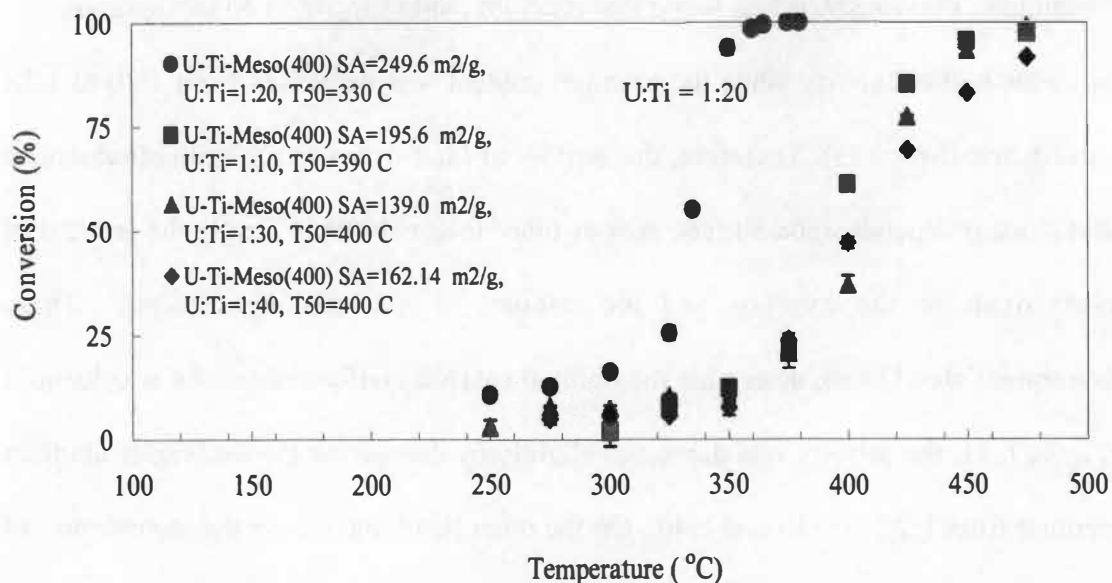
Figure 6.11: Catalyzed oxidation of toluene by variable doped uranium in U-Ti-Meso (42, 43, 44, and 45) for oxidation of toluene.

20.60 % wt loading (U:MCM-41 = 1:32) was 758 m^2/g. The calcinations temperature was 800 °C to activate the uranium. A portion of this catalyst was further doped by impregnation with potassium nitrate and calcined at 600 °C to decompose the nitrate. The BET surface area collapsed considerably to 26 m^2/g. The mole ratio of K to U-MCM-41 was 1 to 11. These two catalysts are compared in Figure 6.12. It was seen that K acts as a poison. The activity (T_{50}) was changed from 335 °C to 400 °C.

The effect of different pore sizes in the urania catalysts were compared. Two different mesoporous silica supports were impregnated with uranyl nitrate. SBA-15 has a pore size of around 5-8 nm, while MCM-41 has smaller pore sizes of 2-3 nm. The smaller pored catalyst performed slightly better, possibly due to higher uranium surface
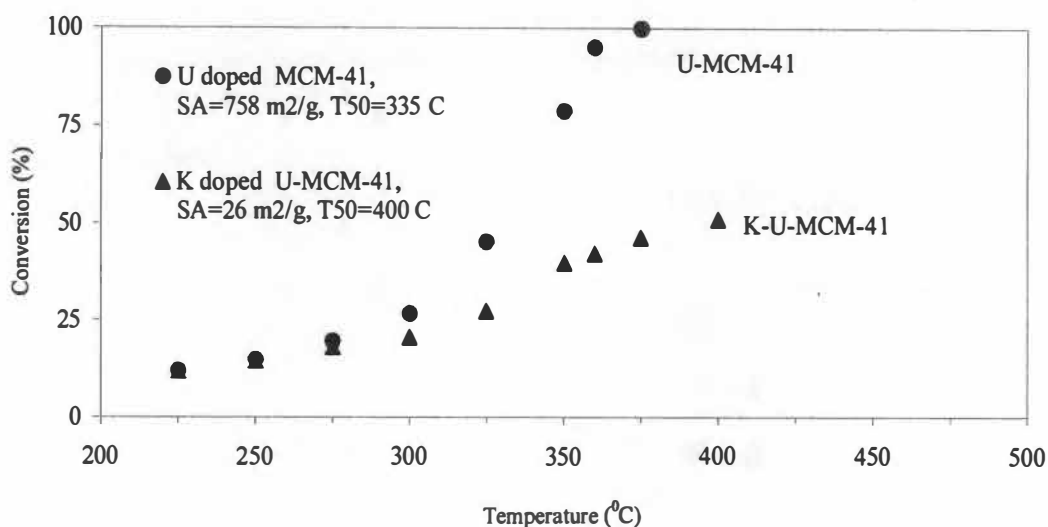
Figure 6.12: Effects of doping MCM-41 with uranium and potassium promoter for oxidation of toluene

area as seen in Figure 6.13. The T_{50} was 335 and 360 °C for U-MCM-41 and U-SBA-15 respectively. The hesteresis in the lower portion of light-off curve with U-SBA-15 was due to pressure build up in the system. This problem was corrected by modification of our system, and using a different reactor. In addition to above catalysts, another sample was synthesized by impregnation of KNO_2 with U-SBA-15. The mole ratio of K to U-SBA-15 was 1:11. It was seen that K completely destroyed the activity of catalyst.

6.1.6 Effect of Support (TiO2 – U3O8) on Platinum based Catalysts

Pt/TiO₂-56 (Platinum over Titanium Oxide) and Pt/U₃O₃-57 (Platinum over Uranium Oxide)

It is known that Pt is a highly active VOC oxidation catalyst. Studies were made of the addition of Pt to uranium oxide catalysts using incipient wetness synthesis method.
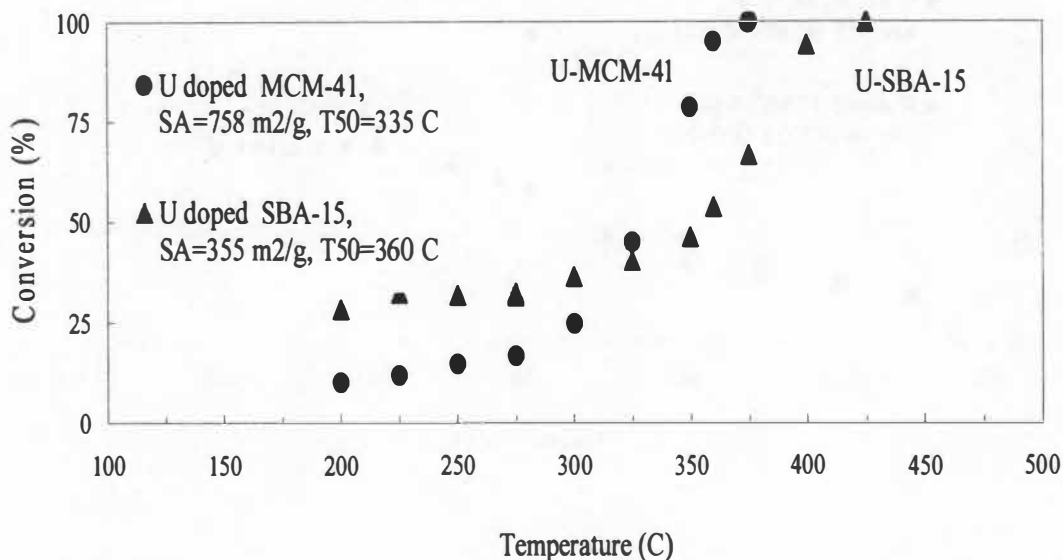
Figure 6.13: Comparison of doping uranium with SBA-15 and MCM-41 for oxidation of toluene.

In the first study, the possibility of using the uranium oxide as a support for Pt was examined. The idea was to create a bi-functional catalyst in which the VOC reacts on Pt while the uranium oxide provides a source of oxygen for the catalytic conversion. To test this possibility, uranium oxide was deposited on pure U_3O_8. In another study, Pt was deposited on pure titanium oxide, another reducible oxide. Both catalysts were calcined at 600 °C. The results are shown in Figure 6.14. It was seen that the Pt supported on titania was extremely active with light-off temperature (T_{50}) of 160 °C. Supporting Pt on uranium oxide is also very active with T_{50} near 230 °C, but it is not as good as the Pt/TiO$_2$ catalyst.

108
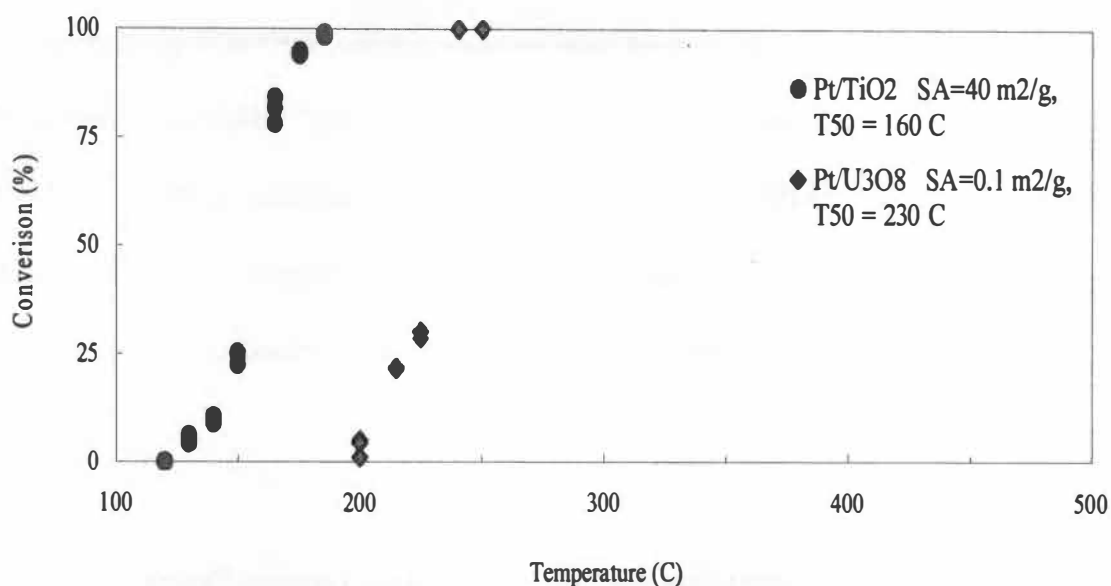
Figure 6.14: Comparison of titania (TiO₂) and urania (U₃O₈) as oxidative supports for destruction of toluene.

6.1.7 Effect of (Ti – Pt) Doping on Catalyst Efficiency

U-Ti-Si-Meso-39 (Uranium + Titanium + Mesoporous Silica)

Catalyst with good activity and stability to deactivation can be prepared from co-synthesis of uranium oxide on pores of both mesoporous silica and titania. The co-assembled mesoporous catalyst was calcined at 350 °C, then, it was divided into three equal portions. The first portion was named U-Ti-Si (350). The other two portions were calcined at 600 °C and 800 °C respectively. They were named U-Ti-Si (600) and U-Ti-Si (800). The resulting surface area was 429, 341.6, and 205.3 m²/g in order of calcinations temperatures. The first purpose was to study the improvement in the activity of catalyst by doping silica supported uranium oxide with titanium in smaller concentrations (U:Ti:Si = 1:1:20). This approach gave catalysts with activities slightly improved as

109

compared with U-Meso-6, but not as effective as the U-Ti-Meso(600). The second approach was to see the effect of calcinations temperature on the activity of catalyst. As shown in Figure 6.15, these catalysts were very stable at high temperature with constant T_{50} =390 °C. The XRD of this catalyst indicates amorphous peaks for calcination temperature of 350 °C. As calcinations temperature was increased to 600 °C, the titania crystallite size grows to anatase, then it converts to U_3O_8 and possibly to anatase at 800 °C.

U-Pt-Si-Meso-40 (Uranium + Platinum + Mesoporous Silica)

It is well known that the influence of a promoter such as Pt on the catalytic activity of a catalyst is highly considerable. A similar approach was used for preparation of this catalyst. The idea was to study the improvement in the activity of catalyst by doping silica supported uranium oxide with platinum in smaller concentrations (U:Pt:Si = 1:1:20). This approach gave catalysts with activities considerably improved as compared with U-Meso-6 as it was expected. The second approach was to see the effect of calcinations temperature on the activity of catalyst. As shown in Figure 6.16, the surface area of these catalysts has been reduced considerably as calcinations temperature was increased from 350 °C to 800 °C, resulting the loss of surface area from 477 to 247 m^2/g. The T_{50} was 170, 185, and 235 °C, for U-Pt-Si (350), U-Pt-Si (600), and U-Pt-Si (800) respectively. The mass spectrometer indicated that all exit gasses were converted to carbon dioxide and water. The XRD indicates the presence of Pt at calcinations temperature of 350 °C.
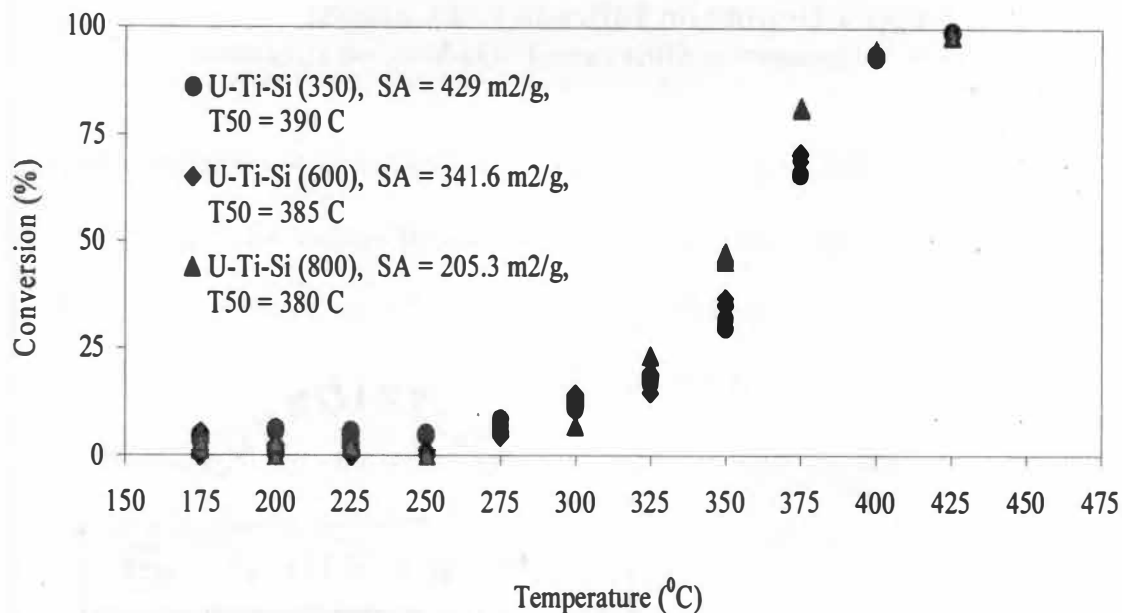
Figure 6.15: The effect of calcinations temperature upon light-off curve by U-Ti-Si-39 for oxidation of toluene.
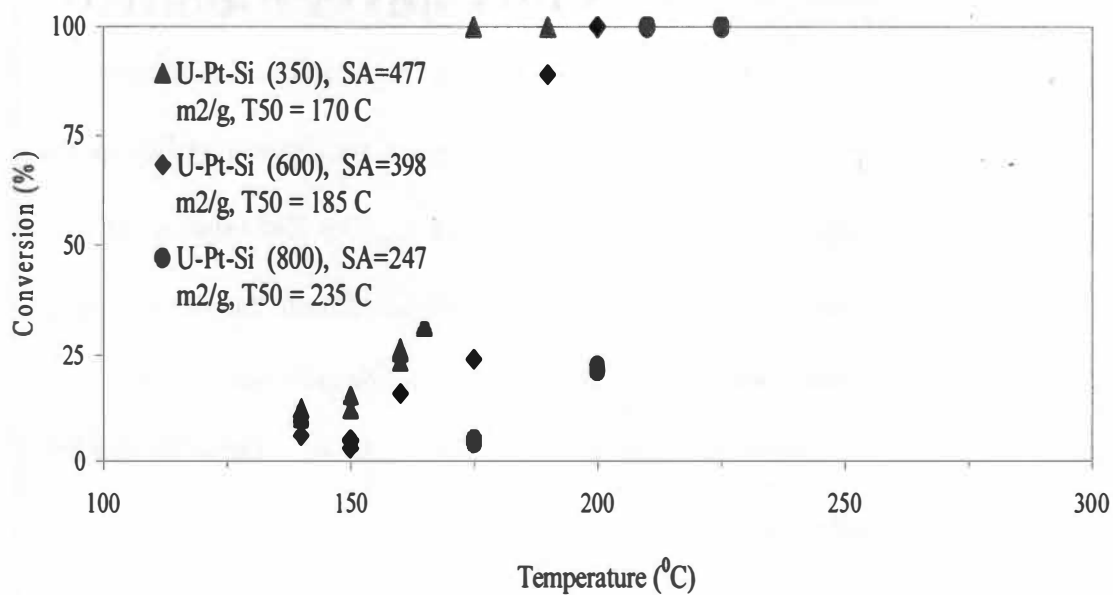
Figure 6.16: The effect of calcinations temperature upon light-off curve by U-Pt-Si-40 for oxidation of toluene.

111

6.1.8 Effect of Copper Doping on Efficiency of Catalyst
MesoCu-29 (Copper + Mesoporous Silica) and U-Cu-Meso-30 (Uranium + Copper + Mesoporous Silica)

A number of additives in low concentration are known to promote the catalytic performance of mesoporous silica. A new transition metal oxide catalyst such as CuO was co-synthesized and compared with previous catalysts. The new catalyst was formed by co-synthesis of $Cu(NO3)2$. $3H2O$ and TEOS by using a F127 surfactant in acid solution. The atom ratio of Cu:Si was 5:20. The as synthesized sample was calcined at 800 oC accordingly. A second catalyst was produced in the same way with uranium oxide. The mole ratio of U:Cu:Si was 1:5:20. The BET adsorption-desorption isotherm was 147 and 257 $m2/g$ with and without uranium respectively. It confirms that the mesoporousity has been achieved (See Figure A.14 and A.15). As shown in Figure 6.17, doping Cu with uranium oxide enhanced the activity of catalyst slightly as compared with silica supported uranium oxide. It is seen that supporting Cu on uranium oxide has light-off temperature (T_{50}) of 385 °C. Supporting Cu only on mesoporous silica is very unactive which resulted light-off temperature (T_{50}) of 540 °C. The XRD shows the presence of both U_3O_8 and CuU_3O_{10} (Copper Uranium Oxide) in the doped catalyst which indicates that uranium has slightly interacted with Cu. *Besides titanium and chromium, copper is the third oxide to interact with uranium.* Detailed synthesis calculations are given in appendix B.14.
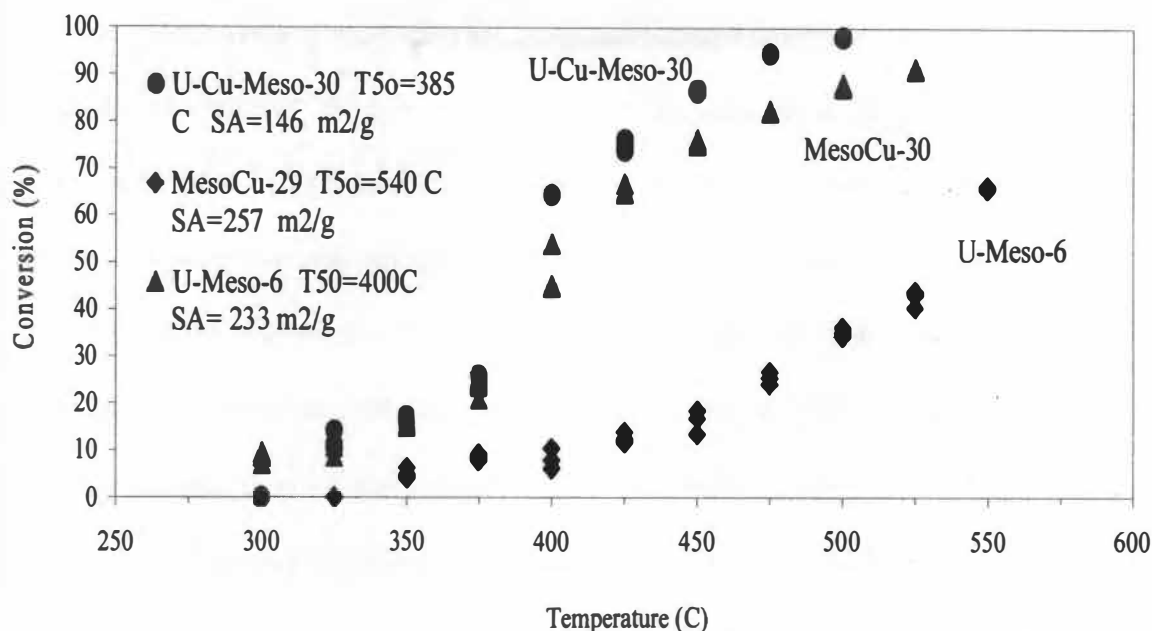
Figure 6.17: The effect of copper addition into uranium mesoporous silica supported by co-assembly method for oxidation of toluene.

6.1.9 Effect of Strontium Doping on Efficiency of Catalyst

U-Sr-Meso-33 (Uranium + Strontium + Mesoporous Silica) and MesoSr-34 (Strontium + Mesoporous Silica)

Previously, it was found that the addition of potassium in the co-synthesis destroys the mesoporous structure of the urania-silica catalyst. To better understand this with strontium, two catalysts were prepared. In the first approach, a silica supported with Sr was synthesized using the surfactant approach described previously and then calcined at 800 °C. It also had a mole ratio of Sr:Si = 1:20 which computes for a Sr to a loading of 8%. Another sample was synthesized in which one was doped with uranium oxide by co-assembly method. The mole ratio was U:Sr:Si = 1:1:20 which computes to a Sr loading of about 6.55%. The calcinations temperature was also 800 °C. The BET adsorption-

113

desorption isotherm was 94.56 and 30.77 m^2/g with and without uranium loading. The Figures A.16 and A.17 confirms that the mesoporousity has been achieved. As shown in Figure 6.18, doping Sr with uranium oxide did not enhance the activity of silica supported catalyst as compared with silica supported uranium oxide (U-Meso-6). It is very obvious that the Sr does not interacting with uranium and acts as a poison which we have seen by K previously. Supporting Sr on uranium oxide gave a light-off temperature (T_{50}) of 550 °C. Supporting Sr only on mesoporous silica resulted in an identical light-off temperature (T_{50}) of 550 °C. The XRD pattern was unclear for both cases. Similarly, doping with Zn, Al, and Li were done. There was no significant synergistic interaction between uranium and transition metal oxides.

6.1.10 Summary of Synthesis Experiments with Toluene

Table 6.2 summarizes important information about each experiment. The first column identifies the name of the catalyst. The second column describes the purposes of the experiment and details of the composition of the catalyst. The third column indicates the final temperature at which the catalyst was calcined. The fourth column gives the T_{50} for toluene [determined as the temperature at which 50% conversion of toluene to oxidation products (CO_2 and H_2O) was obtained] and provides a measure of the catalyst activity. The fifth column provides the figure number for the light-off curve for toluene with that catalyst.
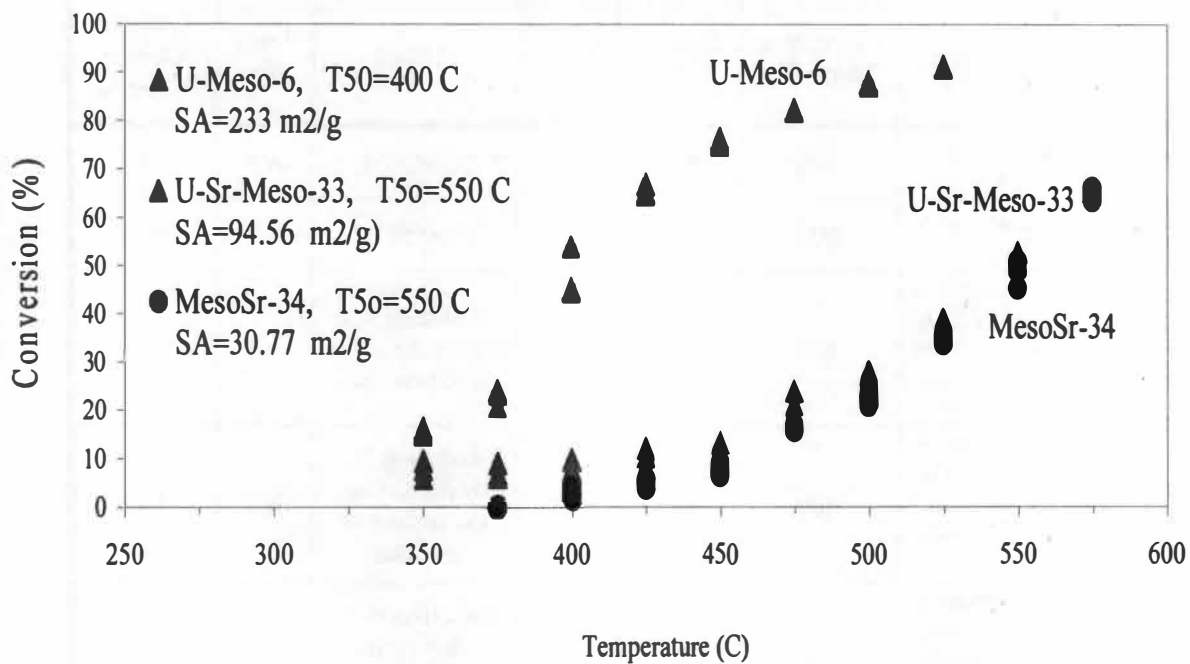
Figure 6.18: The effect of strontium addition into uranium mesoporous silica support by co-assembly method for oxidation of toluene.

Table 6.2: Summaries of compositions, calcinations temperature, T_{50}, figure number, table number, and synthesis references for all catalysts used for oxidation of toluene.

Catalyst	Purposes of synthesis and experiment	Calcination Temp. (^{0}C)	Toluene T_{50} ^{o}C	Figure No.	Finding	Table No.	Synthesis Chapter Reference
U_3O_8	Activity of U_3O_8	800	520	6.3	T_{50}=520 ^{o}C	A.1	4.4.1
SiO_2	Activity of SiO_2	600	550	6.3	T_{50}=550 ^{o}C	A.1	4.4.2
U-Meso-5	Improvement in activity of SiO_2 by doping with U at mole ratio of U:Si=1:10	800	425	6.3	Reducing T_{50} by doping silica with uranium.	A.1	4.4.3
U-Meso-6	Improvement in activity of SiO_2 by doping with U at mole ratio of U:Si=1:20	800	410	6.3	Reducing T_{50} by decreasing the content of uranium.	A.1	4.4.4
U-Cr-Meso-19 (imp.)	Improvement in activity of SiO_2 by doping with U and Cr using impregnation method	600	418	6.4	The effect of Cr doping in U-Meso-6 by impregnation.	A.2	4.4.13
U-Cr-Meso-21 (co-syn)	Improvement in activity of SiO_2 by doping with U and Cr using co-synthesis method	800	375	6.4	The effect of Cr doping in U-Meso-6 by co-synthesis.	A.2	4.4.15
MesoCr-22 (co-syn)	Comparing the activity of chromium oxide without uranium	800	470	6.4	Observing the activity of Cr-Silica based catalyst without Uraniunm.	A.2	4.4.16
U-Cr-Meso-25 (co-syn)	Comparing the activity of U-Cr-Meso-21 and U-Cr-Meso-25 by changing the mole ratio of U:Si = 1:20 to U:Si = 1:30	800	418	6.4	Differences in T_{50} by reducing uranium content in U-Cr-Meso-21.	A.2	4.4.19

116

Table 6.2: Continued.

Catalyst	Purposes of synthesis and experiment	Calcination Temp. (^{0}C)	Toluene T_{50} °C	Figure No.	Finding	Table No.	Synthesis Chapter Reference
U-Co-Meso-20 (imp)	Improvement in activity of SiO_2 by doping with U and Co using impregnation method	600	440	6.5	The effect of Co doping of U-Meso-6 by impregnation method.	A.3	4.4.14
U-Co-Meso-23 (co-syn)	Improvement in activity of SiO_2 by doping with U and Co using co-synthesis method	800	420	6.5	The effect of Co doping with U-Meso-6 by co-synthesis.	A.3	4.4.17
MesoCo-24 (co-syn)	Comparing the activity of cobalt oxide without uranium	800	420	6.5	Observing the activity of Co-Silica based catalyst without Uraniunm.	A.3	4.4.18
MesoCu-29	Comparing the activity of copper oxide without uranium	800	540	6.17	T_{50} = 540 °C for silica based copper oxide catalyst.	A.12	4.4.22
U-Cu-Meso-30	Improvement in activity of SiO_2 by doping with U and Cu using co-synthesis method and comparing with copper oxide	800	385	6.17	The effect of Uranium doping with MesoCu-29 by co-synthesis.	A.12	4.4.23
Pt/TiO$_2$-56	Using TiO_2 as a support fot Pt by impregnation.	500	160	6.14	The effect of TiO_2 as support for Pt using impregnation method.	A.9	4.4.42
Pt/U$_3$O$_8$-57	Using U_3O_8 as support for Pt by impregnation.	500	230	6.14	The effect of U_3O_8 as support for Pt and comparing with Pt/TiO$_2$-56.	A.9	4.4.43
0.1% Pt/γ alumina-59	Comparing commercial catalyst (0.1% Pt/Al2O3) with uranium-titanium	800	375	6.8	T_{50} = 375 °C for commercial catalyst.	A.5	4.4.44

117

Table 6.2: Continued.

Catalyst	Purposes of synthesis and experiment	Calcination Temp. (^{0}C)	Toluene T_{50} °C	Figure No.	Finding	Table No.	Synthesis Chapter Reference
U-MCM41-49	Doping with U to improve the activity of MCM-41	600	335	6.12	T_{50}=600 °C	A.7	4.4.35
K-UMCM41-50	Doping U-MCM-41 with K promoter to enhance the activity	600	400	6.12	The effect of promoter K on U-MCM41-49.	A.7	4.4.36
U-SBA15-47	Doping with U to improve the activity of U-SBA-15	800	360	6.13	T_{50}=360 °C	A.8	4..4.35
K-U-SBA15-46	Doping U-SBA-15 with K promoter to enhance the activity	600	Deactivated	N/A	The effect of promoter K on U-SBA15-47.	N/A	4.4.36
U-Ti-Si-39 (350)	Improvement in the activity of catalyst by doping silica supported uranium oxide with titanium at calcinations temperature of 350 °C.	350	390	6.15	T_{50}=390 °C for uranium-silica based catalyst doped with Ti in equal mole ratio of Uranium.	A.10	4.4.26
U-Ti-Si-39 (600)	The effect of calcinations temp. at 600 °C in the activity of catalyst	600	385	6.15	To find the change on T_{50} by increasing calcinations temperature of U-Ti-Si-39 from 350 to 600 ^{0}C.	A.10	4.4.26

Table 6.2: Continued.

Catalyst	Purposes of synthesis and experiment	Calcination Temp. (^{0}C)	Toluene T_{50} ^oC	Figure No.	Finding	Table No.	Synthesis Chapter Reference
U-Ti-Si-39 (800)	The effect of cacination temperature at 800 ^oC in the activity.	800	380	6.15	To find the change on T_{50} by increasing calcinations temperature of U-Ti-Si-39 from 600 to 800 ^0C.	A.10	4.4.26
U-Pt-Si-40 (350)	Improvement in the activity of catalyst by doping silica supported uranium oxide with Pt.	350	170	6.16	T_{50}=170 ^oC for uranium-silica based catalyst doped with Pt in equal mole ratio of Uranium.	A.11	4.4.27
U-Pt-Si-40 (600)	The effect of calcinations temperature at 600 ^oC in the activity of catalyst.	600	185	6.16	To find the change on T_{50} by increasing calcinations temperature of U-Pt-Si-40 from 350 to 600 ^0C.	A.11	4.4.27
U-Pt-Si-40 (800)	The effect of cacination temperature at 800 ^oC in the activity of catalyst.	800	235	6.16	To see the change on T_{50} by increasing calcinations temperature of U-Pt-Si-40 from 600 to 800 ^0C.	A.11	4.4.27
TiO$_2$-41 (400)	Using Pure TiO$_2$ as catalyst	400	365	6.6	T_{50}=365 ^0C	A.4	4.4.28

Table 6.2: Continued.

Catalyst	Purposes of synthesis and experiment	Calcination Temp. (^{0}C)	Toluene T_{50} °C	Figure No.	Finding	Table No.	Synthesis Chapter Reference
TiO$_2$-41 (600)	Effect of calcinations temperature at 600 °C for activity of pure TiO$_2$	600	425	6.6	Differences in T_{50} by increasing calcinations temperature of TiO$_2$-41 from 400 to 600 ^{0}C.	A.4	4.4.28
TiO$_2$-41 (800)	Effect of calcinations temperature at 800 °C in activity.	800	550	6.6	To see the change on T_{50} by increasing calcinations temperature of TiO$_2$-41 from 600 to 800 ^{0}C.	A.4	4.4.28
U-Ti-Meso-42 (400)	Doping TiO$_2$ with U to enhance the activity of catalyst at mole ratio of U:Ti = 1:10, TiO$_2$ considered as a support.	400	390	6.11	T_{50}=390 ^{0}C doping TiO$_2$-41 with uranium at U:Ti = 1:10	A.6	4.4.29
U-Ti-Meso-43 (400)	Doping TiO$_2$ with U to enhance the activity of catalyst at mole ratio of U:Ti = 1:20 for comparison.	400	330	6.8, 6.11	T_{50}=330 ^{0}C doping TiO$_2$-41 with uranium at U:Ti = 1:20	A.5, A.6	4.4.30
U-Ti-Meso-43 (600)	Effect of calcinations temperature at 600 °C for activity of U-Ti-Meso-43	600	325	6.8, 6.11	Effect of calcination temperature T_{50} from 330 °C to 325 °C	A.5, A.6	4.4.30
U-Ti-Meso-43 (800)	Effect of calcinations temperature at 800 °C in activity.	800	345	6.8, 6.11	To see the change on T_{50} by increasing calcinations temperature of U-Ti-Meso-43 from 600 to 800 ^{0}C.	A.5, A.6	4.4.30

Table 6.2: Continued.

Catalyst	Purposes of synthesis and experiment	Calcination Temp. (^{0}C)	Toluene T_{50} ^{0}C	Figure No.	Finding	Table No.	Synthesis Chapter Reference
U-Ti-Meso-44 (400)	Doping TiO_2 with U to enhance the activity. Changing the mole ratio from U:Ti = 1:20 to U:Ti = 1:30	400	400	6.11	To observe the differences between T_{50} of U-Ti-Meso - 43 by decreasing the mole ratio of uranium.	A.6	4.4.31
U-Ti-Meso-45 (400)	Doping TiO_2 with U to enhance the activity of catalyst at mole ratio of U:Ti = 1:40 for comparison with mole ratio of U:Ti = 1:30	400	400	6.11	To find the differences between T_{50} of U-Ti-Meso - 44 by decreasing the mole ratio of uranium.	A.6	4.4.32
U-Sr-Meso-33	Doping Sr with silica supported uranium oxide at mole ratio of U:Sr:Si = 1:1:20 to increase the activity.	800	550	6.18	To observe the change in T_{50} of U-Meso-6 by doping with Sr.	A.13	4.4.24
MesoSr-34	Comparison of the activity of Sr only on mesoporous silica at mole ratio of Sr:Si = 1:20 with U-Sr-Meso-33 which is doped with uranium.	800	550	6.18	To find the differences in T_{50} of U-Sr-Meso-33 without doping with uranium.	A.13	4.4.25

121

The sixth column (Finding) describes the most important results of the experiment. The seventh column gives the table number in the appendix containing additional information. The last column gives the chapter and section containing details of the synthesis of each catalyst.

6.2 Oxidation of Chlorobenzene

Extensive studies were made of the decomposition of chlorobenzene as catalyzed by mesoporous urania catalyst. Emphasis was placed on studying the effects of doping the catalysts with other materials including potassium, bromide, Fe, Ca and Mg. The goal was to find a way to enhance the activity of the uranium oxide catalysts.

6.2.1 The Efficacy of Mixed U_3O_8 and (K – Br) Promotor

U-Meso-10, U-Meso-11 (Potassium + Uranium mesoporous Silica) and U-Meso-12 (Bromide + Uranium Mesoporoud Silica)

Doping of uranium oxide was first tried by adding potassium into the co-synthesis of the mesoporous uranium catalysts. Potassium was used because it is a commonly promoter for various catalysts including iron catalyst used in Fischer-Tropsch catalysts and as a promoter in certain oxidation catalysts. Three different potassium precursors were tried, specifically adding potassium as a nitrate, oxalate or bromide. It was found generally the effect of potassium was to diminish the activity of the uranium catalysts. For example by adding the potassium as a nitrate, the resulting catalyst exhibited less than 8% conversion at 420 °C while undoped mesoporous uranium with the same uranium concentration gave a conversion of about 50% under the same conditions. Using

122

the oxalate and bromide precursors did not improve the activity compared to the nitrate. The oxalate yielded about 15% conversion while a corresponding undoped uranium oxide catalyst yielded 60% conversion at 440 °C. Further measurements on the bromide at increased temperature indicated that even up to 640 °C gave less than 5% conversion. Evidently, the potassium is strongly interacting with the uranium oxide and is killing its activity.

6.2.2 Effect of (Fe, Mg, Ca) Doping on Efficiency of Catalysts

U-Meso-13 (Fe + Mg + Uranium mesoporous Silica) and U-Meso-14 (Fe + Ca + Uranium Mesoporoud Silica)

In this experiment, iron was tried as an additive and it was added as a nitrate into the standard synthesis of mesoporous uranium oxide catalyst. Besides the iron, Ca or Mg was added. The Mg was added as the acetate and Ca was added as a nitrate. The relative amounts (mole ratio) of Fe, Mg or Fe, Ca and U compared to the silica support were 1:1:20. The additions of these components were found to have a slightly deleterious rather than promotional effect upon the uranium catalyst. A comparison of the conversion of chlorobenzene as a function of temperature is shown in Figure 6.19. These two catalysts showed identical 50% chlorobenzene light-off at 500 °C. The fact is that the activities are affected by the addition of Fe, Mg and Fe, Ca as compared with silica supported uranium oxide catalyst. It indicates that one of both these species are interacting with the U rather than forming a spectator phase. Further synthesis were done in which the uranium content was decreased. The activity of catalyst was slightly

123
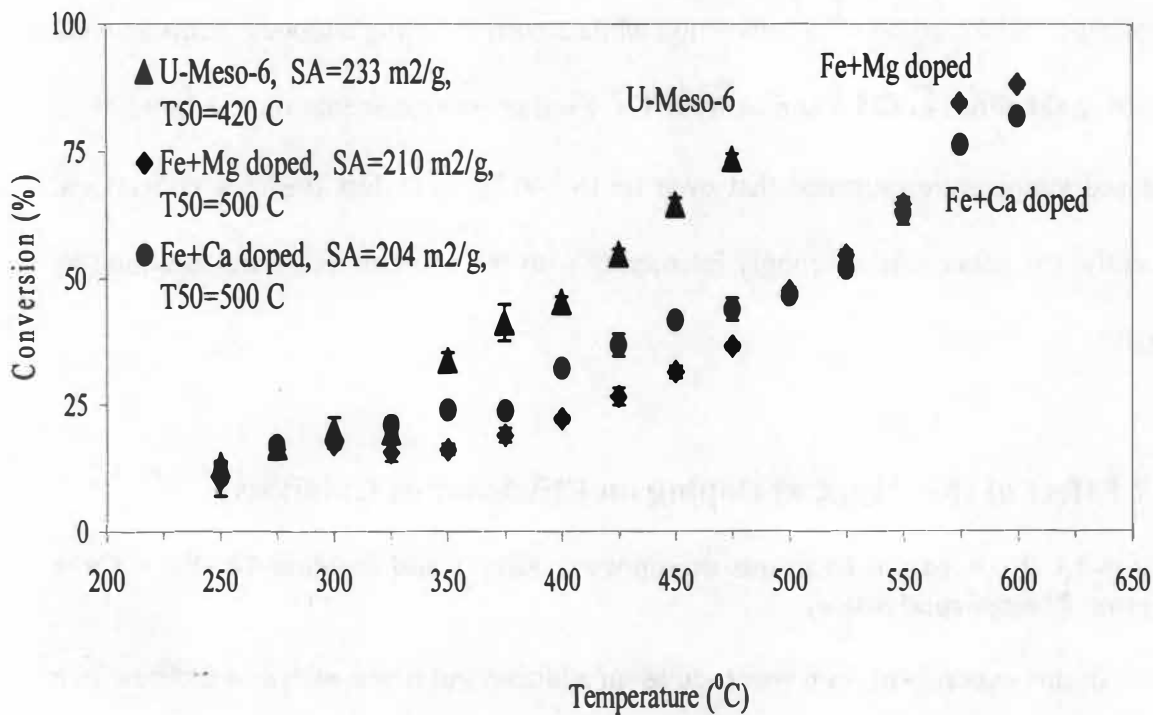
Figure 6.19: Comparison of catalyzed oxidation of chlorobenzene by pure uranium oxide catalyst and doped with (Fe+Mg or Fe+Ca) using co-assembly in mesoporous silica support.

decreased. Therefore, activity of the catalyst is not straightforward to predict since it depends upon surface area or other factors besides simply the amount of uranium oxide in the catalysts.

The BET adsorption-desorption isotherm was 210 and 204 m2/g for U-Meso-13 and U-Meso-14 respectively (See Figure A.18 and A.19). The Type IV isotherm with a H2 Type hysteresis loop, indicating the mesoporousity has been achieved. The XRD indicated that in both cases, Fe2O3 was dominant in the catalyst with a trace of U3O8. No sign of UO2 at all. The Mass Spectrometric analysis indicated the present of CO2, H2O and HCl at exit stream as expected [115]. The experimental

catalytic reactor was substantially revised. A water sparger was incorporated downstream to permit trapping of HCl or Cl2 formed during the reaction. This measure was deemed necessary for the protection of the chromatographic column. Tests were made to determine the extent that sparger would alter the determination of chlorobenzene conversion. The preliminary tests indicated that it is possible to measure chlorobenzene conversion.

6.2.3 The Efficacy of Mole Ratio (U_3O_8 – SiO_2) on Efficiency of Catalysts

U-Meso-6, U-Meso-9, U-Meso-15 and U-Meso-18 (Uranium + Mesoporous Silica)

Previously, it was found that uranium oxide supported on mesoporous silica yields higher activity than pure U_3O_8 and that the activity of the supported uranium oxide increased when the U content was decreased from 1:10 to 1:20. This seeming anomaly is attributed to the very high surface area that can be achieved in the mesoporous silica support which causes the urania to be highly dispersed both in the pores and on the external surface. During the co-synthesis, the addition of ethanol permits the fast gelation at room temperature of the reagent mixture. The gelation time can be related to cross-link polymeric chains. The high gelation rates favor the highly branched cluster aggregates of a colloidal nature, giving rise to highly cross-linked mesoporous materials [116]. The co-synthesis procedure leads to thick wall, stable mesopores with uranyl ions trapped along the walls of the pores. Having these in mind, three more catalysts were co-synthesized with mole ratio of U:Si = 1:30, 1:40, 1:50 named such as U-Meso-9, U-Meso-15 and U-Meso-18 respectively. The activity of the four modified uranium oxide
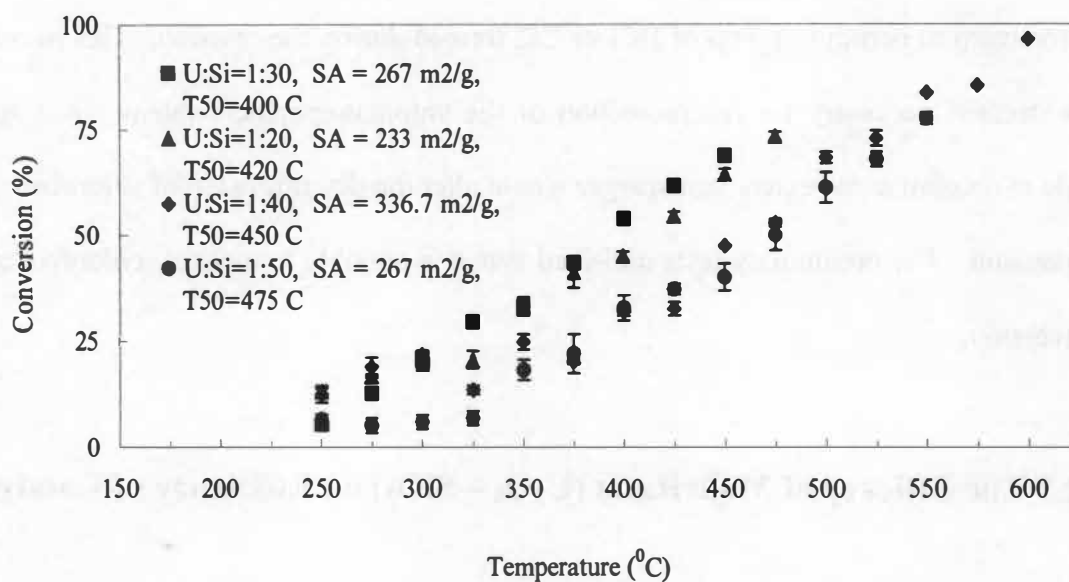
Figure 6.20: Comparison of catalyzed oxidation of chlorobenzene by various doped Uranium oxide catalysts co-assembled in mesoporous silica support.

supported on mesoporous silica catalysts vs. temperatures for oxidation of chlorobenzene are shown in Figure 6.20. The variation in the U:Si ratio indicates that optimal activity for chlorobenzene oxidation is obtained for U:Si = 1:30. For the mole ratio of U:Si = 1:20, 1:30, 1:40, and 1:50, the T50 was 420, 400, 450, and 475 oC respectively. All four catalysts had reversible Type IV isotherms with a H2 Type hysteresis loop, indicating mesoporous materials.

126
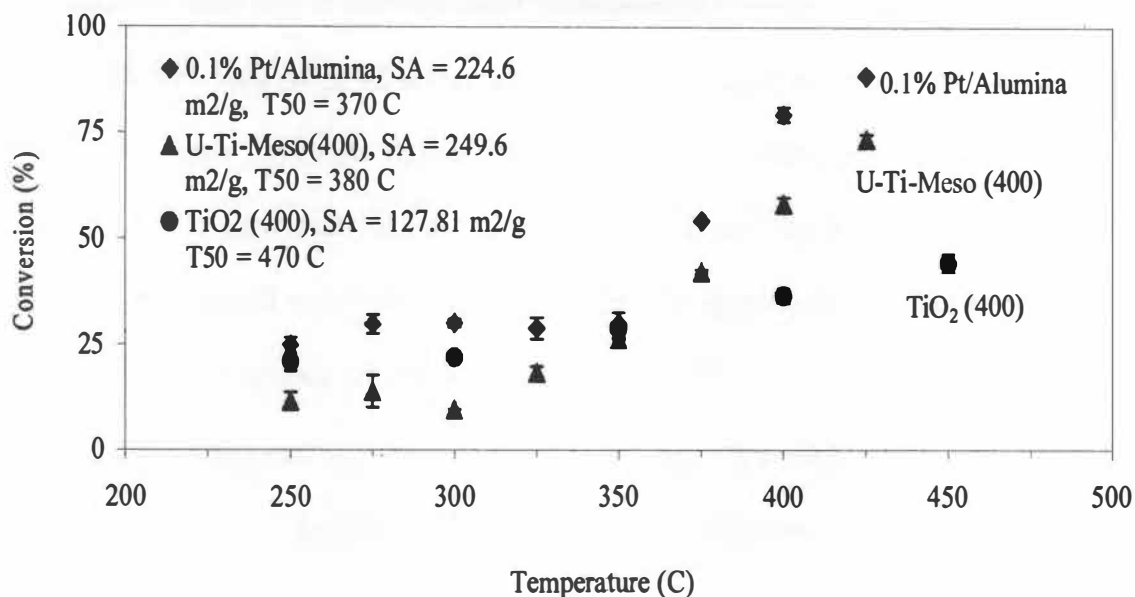
Figure 6.21: Comparison of catalyzed oxidation of chlorobenzene by 0.1% Pt/Alumina, uranium supported on mesoporous titanium oxide and pure titanium oxide catalysts.

6.2.4 Comparison of Mixed (U$_3$O$_8$ – TiO$_2$) and Platinum based Catalyst

U-Ti-Meso-43 (Uranium Mesoporous Titanium Oxide), TiO$_2$-41 (Mesoporous Titanium Oxide) and 0.1% Pt/ γ Alumina.

Previously, these catalysts were used for oxidation of toluene. Here, we compare their activity with chlorobenzene. As shown in Figure 6.21, the activity of uranium-titanium oxide catalyst was very good for decomposition of chlorobenzene as compared with pure titanium oxide catalyst. This catalyst was very stable over period of several days. By comparison, a mesoporous titanium oxide gives a conversion of about 50% at 470 °C whereas a corresponding doped titanium oxide catalyst would have around 82% conversion under the same conditions.

127

The activity of doped titanium oxide catalyst was discussed with researcher at Johnson Mathy, a manufacturer of commercial VOC catalysts based upon Pt/Alumina. They suggested that the uranium and Pt catalyst could be compared best by using Pt/Alumina powder or pellets readily available through chemical suppliers. Such samples were purchased and run in our reactor for composition with doped titanium oxide catalyst and the results indicate that titanium oxide catalyst doped with uranium oxide is competitive with 0.1% Pt/Alumina with only 10 °C differences in the T_{50} of light-off curve. The scatter in the data at low temperatures was due to hysteresis in the light-off curve leading to unstable conversion at low temperatures.

6.2.5 Summary of Synthesis Experiments with Chlorobenzene

Table 6.3 summarizes important information about each experiment. The first column identifies the name of the catalyst. The second column describes the purposes of the experiment and details of the composition of the catalyst. The third column indicates the final temperature at which the catalyst was calcined. The fourth column gives the T_{50} for chlorobenzene [determined as the temperature at which 50% conversion of chlorobenzene to oxidation products (HCl, Cl_2, CO_2 and H_2O) was obtained] and provides a measure of the catalyst activity. The fifth column provides the figure number for the light-off curve for chlorobenzene with that catalyst.

128

Table 6.3: Summaries of compositions, calcinations temperature, T_{50}, figure number, table number, and synthesis references for all catalysts used for oxidation of chlorobenzene.

Catalyst	Purposes of synthesis and experiment	Calcination Temp. (°C)	C. Benzene T_{50} °C	Figure No.	Finding	Table No.	Synthesis Chapter Reference
U-Meso-6	Improvement in activity of SiO_2 by doping with U at mole ratio of U:Si=1:20	800	420	6.19, 6.20	T_{50}=420 °C	A.14, A15	4.4.4
U-Meso-9	Improvement in activity of SiO_2 by doping with U at mole ratio of U:Si = 1:30	800	400	6.20	Reducing T_{50} of U-Meso-6 by decreasing the content of uranium.	A.15	4.4.5
U-Meso-15	Improvement in activity of SiO_2 by doping with U at mole ratio of U:Si = 1:40	800	450	6.20	Reducing T_{50} of U-Meso-9 by decreasing the content of uranium.	A.15	4.4.11
U-Meso-18	Improvement in activity of SiO_2 by doping with U at mole ratio of U :Si = 1:50	800	475	6.20	Reducing T_{50} of U-Meso-15 by decreasing the content of uranium.	A.15	4.4.12
U-Meso-10	Doping silica supported uranium oxide with KNO_3 by imp. at mole ratio of U:K:Si = 1:1:20	600	deactivated	N/A	The effect of promoter K on U-Meso-6 by method of imp. To reduce T_{50}.	N/A	4.4.6

Table 6.3: Continued.

Catalyst	Purposes of synthesis and experiment	Calcination Temp. ($^{\circ}$C)	C. Benzene T_{50} $^{\circ}$C	Figure No.	Finding	Table No.	Synthesis Chapter Reference
U-Meso-11	Doping silica supported uranium oxide with $K_2C_2O_4$ by imp. at mole ratio of U:K:Si = 1:1:20	600	Deactivated	N/A	The effect of promoter K on U-Meso-6 by method of imp. To reduce T_{50}.	N/A	4.4.7
U-Meso-12	Doping silica supported uranium oxide with KBrby imp. at mole ratio of U:Br:Si = 1:1:20	600	Deactivated	N/A	The effect of promoter Br on U-Meso-6 by method of imp. To reduce T_{50}.	N/A	4.4.8
U-Meso-13	Doping silica supported uranium oxide with (Fe+Mg) and U in mole ratio of U:Mg:Fe:Si = 1:0.5:0.5:20	600	500	6.19	Doping U-Meso-6 with (Fe+Mg) by method of imp. to reduce T_{50}	A.14	4.4.9
U-Meso-14	Doping silica supported uranium oxide with (Fe+Ca) and U in mole ratio U:Ca:Fe:Si = 1:0.5:0.5:20	600	500	6.19	Doping U-Meso-6 with (Fe+Ca) by method of imp. to reduce T_{50}.	A.14	4.4.10
0.1% Pt/ γ Alumina-59	Comparing commercial catalyst (0.1% Pt/Al_2O_3) with uranium-titanium based catalyst.	N/A	380	6.21	T_{50}=380 ^{0}C with C. Benzene as compared of T_{50}=375 ^{0}C with Toluene.	A.16	4.4.44
TiO_2-41 (400)	Using pure TiO_2 as catalyst for oxidation of chlorobenzene	400	500	6.21	T_{50}=500 ^{0}C with C. Benzene as compared of T_{50}=365 ^{0}C with Toluene.	A.16	4.4.44

Table 6.3: Continued.

Catalyst	Purposes of synthesis and experiment	Calcination Temp. ($^{\circ}$C)	C. Benzene T_{50} $^{\circ}$C	Figure No.	Finding	Table No.	Synthesis Chapter Reference
U-Ti-Meso-43 (400)	Doping TiO_2 with U to enhance the activity of catalyst at mole ratio of U:Ti = 1:20 for comparison.	400	375	6.21	T_{50}=375 ^{0}C with C. Benzene as compared of T_{50}=330 ^{0}C with Toluene.	A.16	4.4.30

The sixth column (Finding) describes the most important results of the experiment. The seventh column gives the table number in the appendix containing additional information. The last column gives the chapter and section containing details of the synthesis of each catalyst.

6.3 Oxidation of Trichloroethylene (TCE)

6.3.1 Effect of Water on (U_3O_8 – TiO_2) based Catalyst

U-Ti-Meso-43(400)

Trichloroethylene is a major pollutant found in the ground water plumes at DOEs Hanford, Paducah, and Savannah River sites. It was concluded that to test the applicability of depleted uranium catalysts for the catalytic destruction of TCE under realistic conditions. Since the proposed application is for catalytic destruction above soil vapor extraction (SVE) wells, it is required to allow for the addition of water to the reactant stream. Water is certainly going to be present in any process stream coming from a SVE and it has the potential of affecting the activity of the depleted uranium catalysts. In addition, water is expected to significantly alter the ratio of Cl_2 to HCl that is obtained as a by-product of the combustion of the TCE. Since it is expected that the desired product should be HCl, which would be trapped by a water bubbler in the process, it was decided to include the means to test this process. Also, the presence of HCl and water in the reactant streams was expected to be harmful to analysis equipment, necessitating its removal from the analysis stream.

132

The experimental catalytic reactor was substantially revised to meet the above requirements. A water injection syringe was incorporated into the reactant lines upstream from the reactor. A water sparger was incorporated downstream to permit trapping of HCl. Tests were made to determine the extent that the sparger would alter the determination of VOC conversion. Preliminary tests indicated that it is possible to measure TCE conversion. Initial tests indicated that introduction of water into the reactant stream does not interfere with the catalytic activity of the U-Ti-Meso (400). The results are shown in Figure 6.22 which indicates that comparable conversions can be obtained even in the presence of up to about 15% vol. water in the reactant stream which resulted a T_{50} of 450 °C. Seven percent water content slightly increased the activity of catalyst by having a T_{50} of 425 °C.

6.3.2 Effect of Support (U_3O_8, SiO_2, TiO_2) and Water on Lanthanum Oxide Based Catalysts

La-U-52 (Lanthanum+ Uranium) and La-Ti-53 (Lanthanum + Titanium)

These two catalysts were synthesized by IPC (in-situ polymerizable complex) method. This method was first developed by Pechini in 1967 to prepare capacitor materials focusing only on niobates, titanates and zirconates [106]. The basic chemistry involved in the IPC method is related to the formation of metal complexes as well as the dehydration reaction of an α-hydroxycarboxylic acid and a polyhydroxy alcohol. All the studies previously reported have clearly indicated that the IPC method is quite suitable for producing highly pure and homogeneous oxides at reduced temperatures (400-900 °C).
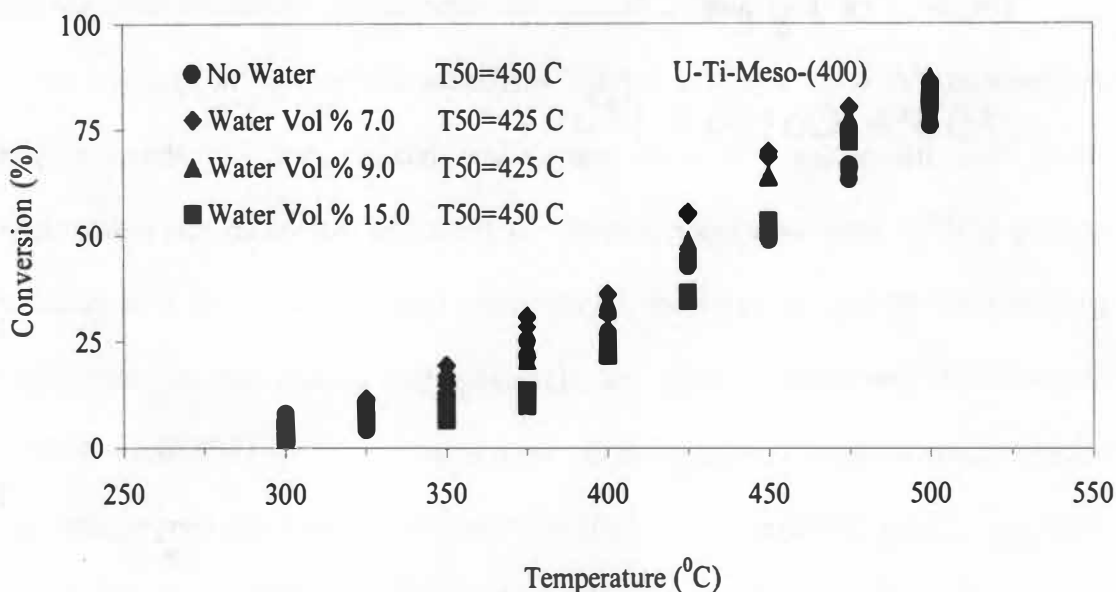
Figure 6.22: Oxidation of trichloroethylene (TCE) over U-Ti-Meso-43(400) at various water content in the reactor stream.

Lanthanum oxide based catalysts such as La_2O_3 and Ce_2O_3 showed strong activity for destructions of chlorinated hydrocarbon at temperatures between 250 and 350 °C when steam was added to the feed stream [117]. The addition of urania or titania has a synergistic interaction, which leads to a very active catalyst. In first attempt, using templated co-synthesis of uranium and lanthanum (La:U = 1:1) yields a mesoporous oxidation. A water flow rate of 1.17 ml/min (14.77% volume water) was added to the catalyst (SA = 14.75 m^2/g) with T$_{50}$ of 530 °C without presence of water for TCE feed stream for improving the activity of catalyst by removing the coke and chlorine poisoning. As shown in Figure 6.23, addition of water had no effect for improving or damaging the activity of this catalyst.

During second attempt, uranium was replaced by titanium (La:Ti = 1:1) to achieve synergistic interaction between lanthanum and titanium. This approach gave

134
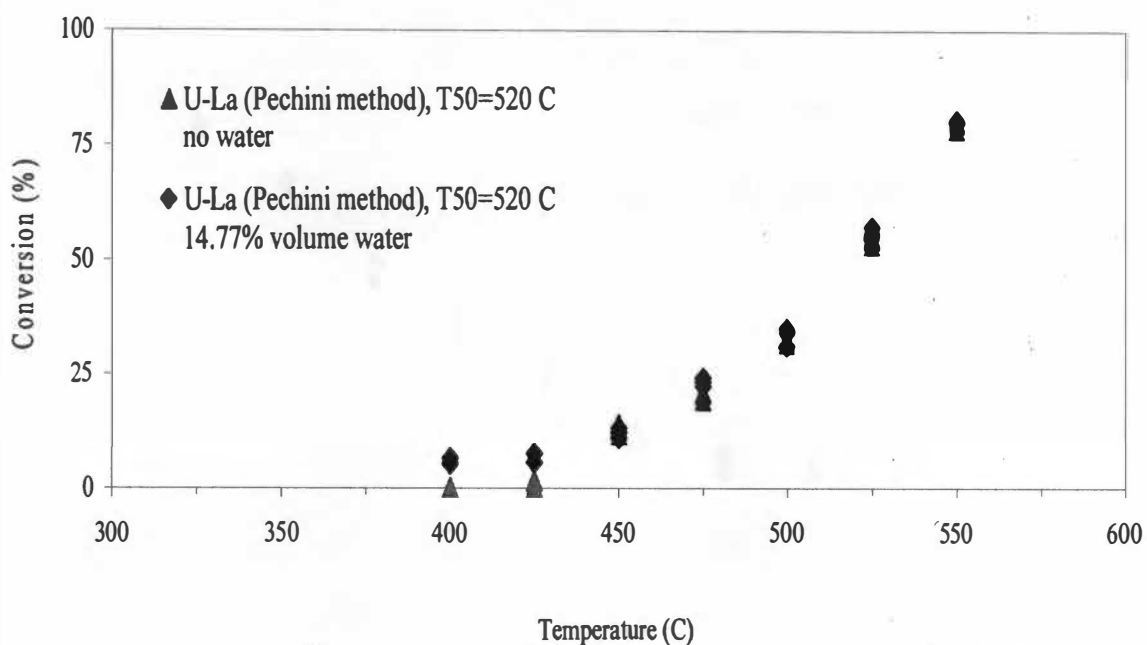
Figure 6.23: Comparison of catalyzed oxidation of trichloroethylene (TCE) by La-U-52 (Pechini method) at variable water flow rate.

catalyst with activities slightly improved as compared with U-La, but not as effective as it was expected. The addition of 14.77 % volume water had no effect on the catalyst activity. The T_{50} was 500 °C as shown in Figure 6.24. The BET surface area was 13.42 m^2/g.

U-La-Meso-27 (Lanthanum + Uranium Mesoporous SiO₂) and U-Ti-La-51 (Lanthanum + Uranium + Mesoporous TiO₂)

Catalyst with good activity and stability to deactivation can be prepared from co-synthesis of uranium oxide on pores of mesoporous silica. The co-assembled mesoporous catalyst was calcined at 800 °C. The resulting surface area was 321 m^2/g. Our purpose was to study the improvement in the activity of catalyst by doping the silica

135
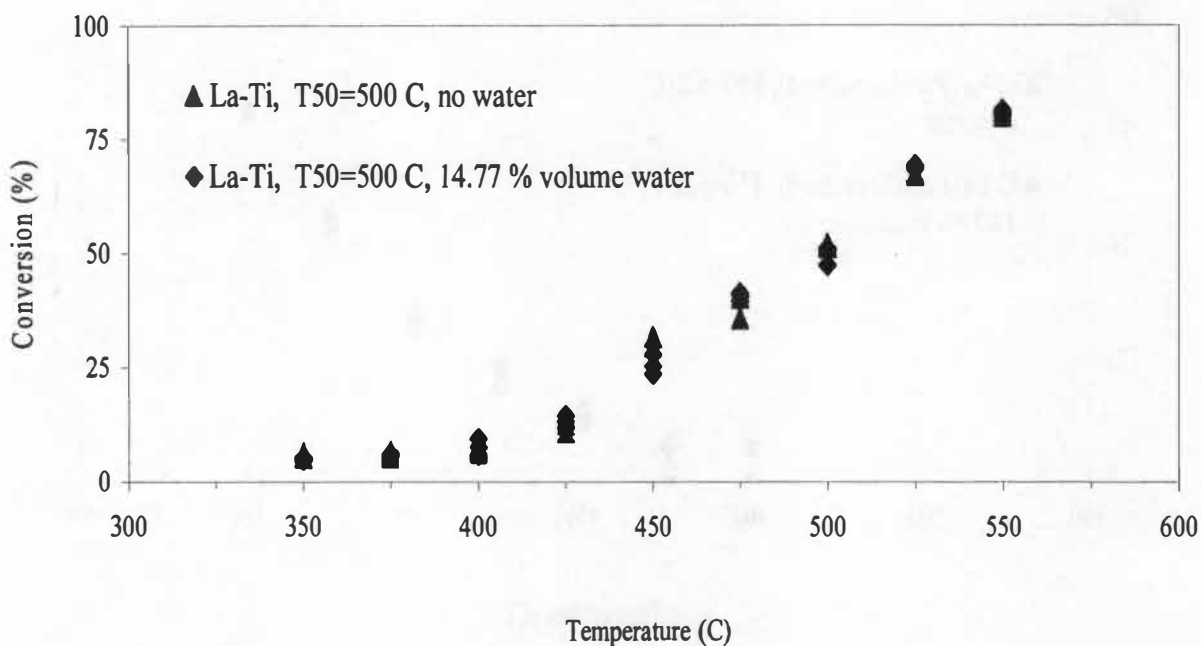
Figure 6.24: Comparison of catalyzed oxidation of trichloroethylene (TCE) by La-Ti-53 (Pechini Method) at variable water flow rate.

supported uranium oxide with lanthanum in smaller concentrations (U:La:Si = 1:0.5:20). This approach did not improve the activity of catalyst. As shown in Figure 6.25, T_{50} was 525 °C. There was no sign of deactivation for this catalyst.

A similar approach was to use titanium as a support. Titanium oxide is an active catalyst for oxidation and addition of uranium and lanthanum will have a synergistic interaction which leads to a very active catalyst. This approach gave catalysts with activities highly improved as compared with SiO_2 as a support. These two catalysts are compared in Figure 6.25. The T_{50} was 465 °C which is compatible with U-Ti-Meso (600). This catalyst also was stable at high temperature.
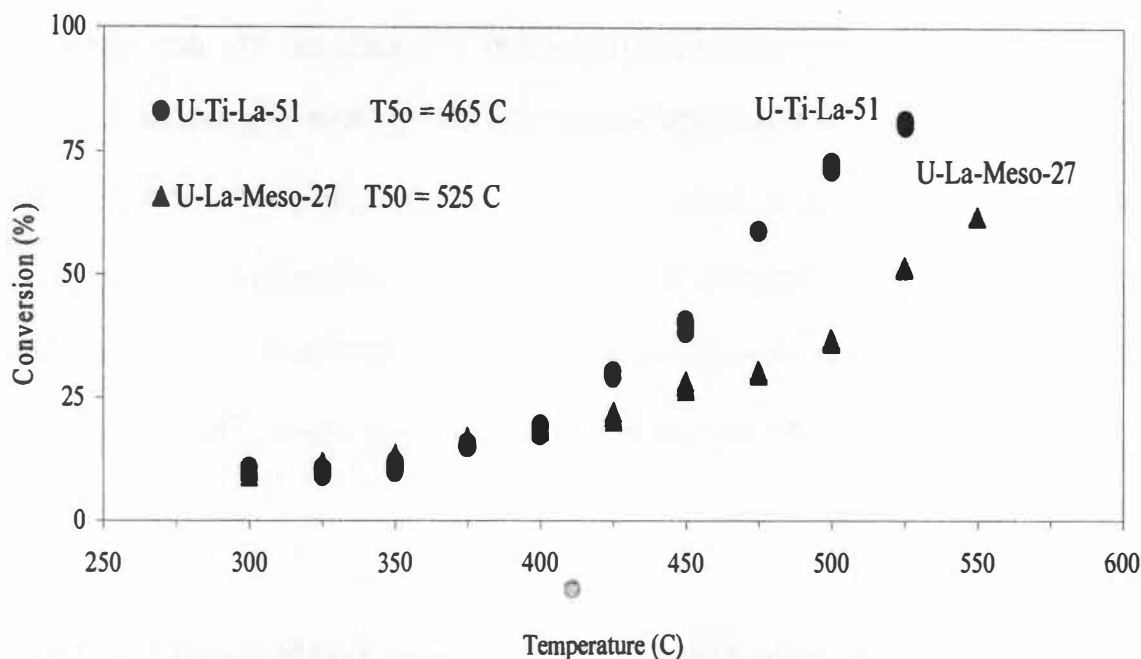
Figure 6.25: Comparison of activities for oxidation of trichloroethylene (TCE) by using two different supports (TiO$_2$, SiO$_2$) doped with uranium and lanthanum.

6.3.3 Effect of Water and Doping with Cerium on (U$_3$O$_8$ – SiO$_2$) based Catalysts

CeO2-55 (Cerium Oxide), and U-Ce-Meso-28 (Uranium + Cerium + Meso SiO2)

Emphasis was placed on studying the effects of doping the mesoporous uranium catalyst with other materials such as cerium oxide by co-assembly method. The goal was to enhance the activity of the uranium oxide catalyst. The literature indicated that addition of water also will increase the activity of cerium oxide based catalyst. Therefore, the silica supported uranium oxide (with Ce) was synthesized using the surfactant approach described before and then calcined at 800 °C. It also had a U:Ce:Si mole ratio of 1:0.5:20 respectively. The BET was 211 m^2/g. The Figure A.22 indicates that the mesostructure has been achieved. In addition to above catalyst, CeO$_2$ was prepared by

137

thermal decomposition of Ce $(NO_3)_3$. $6H_2O$ at 800 °C in static air. The BET surface area was 8 m^2/g. As shown in Figure 6.26, the addition of water slightly improved the activity of uranium based catalyst at lower temperatures, which resulted a T_{50} of 500 °C, but it has no effect at higher temperatures. It seems that the temperature of reactor plays a major rule in the activity of a catalyst when water is applied as it has been seen before [119]. The activity of CeO_2 was unchanged by addition of water. The T_{50} was 575 °C for both cases.

•

6.3.4 Effect of Water on Activity of Lanthanum Oxide based Catalyst

La$_2$O$_3$ (lanthanum Oxide)

Lanthanum oxide (La_2O_3) was prepared by thermal decomposition of La $(NO_3)_3$. $6 H_2O$ at 800 C in static air. The idea was to compare the activity of both lanthanum oxide and cerium oxide for destruction of TCE by applications of water. A series of different water flow rates were tested. As shown in Figure 6.27, the presence of water will not increase or decrease the catalytic oxidation of La_2O_3.

6.3.5 Summary of Synthesis Experiments with Trichloroethylene

Table 6.4 summarizes important information about each experiment. The first column identifies the name of the catalyst. The second column describes the purposes of the experiment and details of the composition of the catalyst. The third column (% Volume Water) specifies the percent water by volume in the reactor inlet stream.
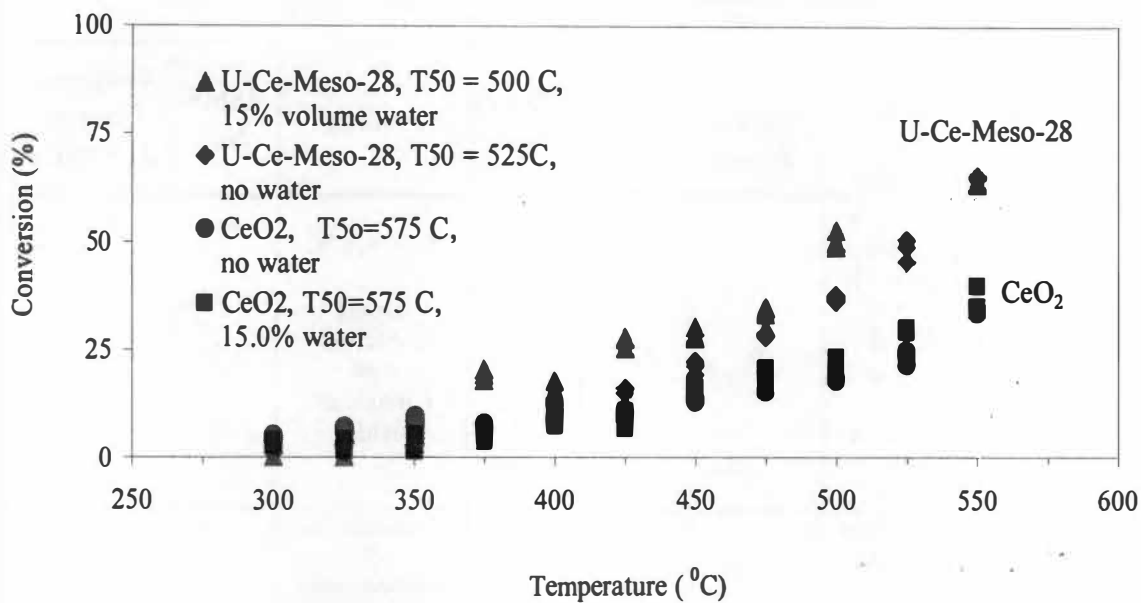
Figure 6.26: Comparison of "light-off" curve for oxidation of trichloroethylene (TCE) over CeO$_2$ and U-Ce-Meso-28 at variable water flow rates.
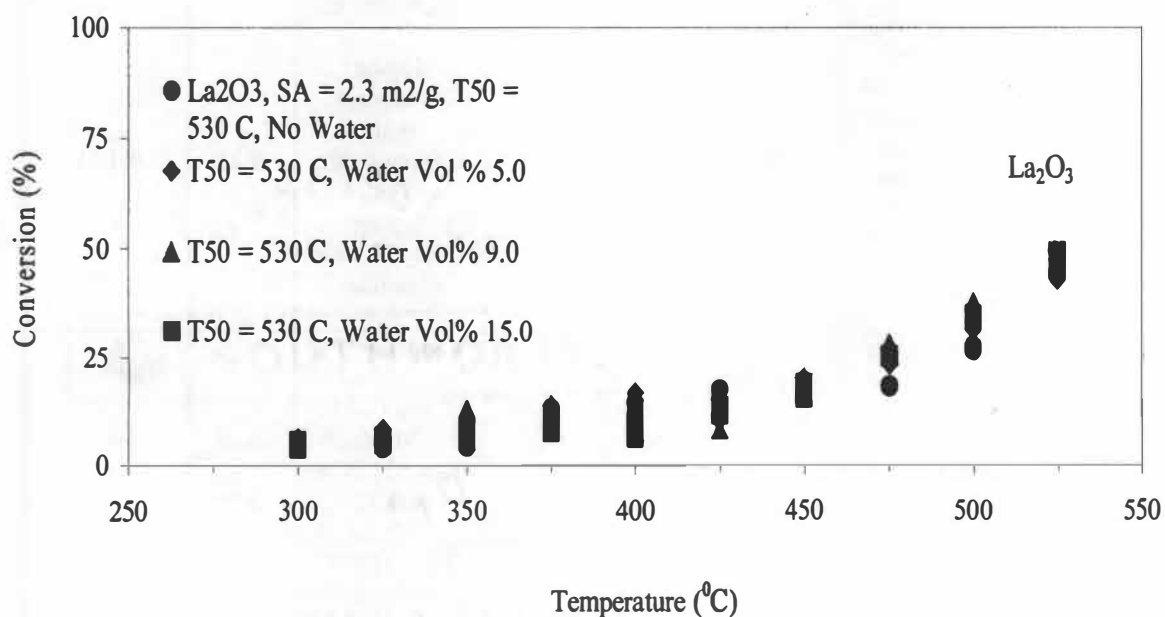
Figure 6.27: The effects of various water flow rates on the activity of La$_2$O$_3$ for destructions of trichloroethylene (TCE).

Table 6.4: Summaries of compositions, calcinations temperature, T_{50}, figure number, table number, and synthesis references for all catalysts used for oxidations of trichloroethylene.

Catalyst	Purposes of synthesis and experiment	% Volume Water	T.C.E T50 ^{o}C	Figure No.	Finding	Table No.	Synthesis Chapter Reference
U-La-Meso-27	Doping silica supported uranium oxide with La to increase the activity of catalyst at mole ratio of U:La:Si = 1:0.5 :20	0	520	6.25	T_{50} = 520 °C doping U-Meso-6 with Lanthanum oxide.	A.20	4.4.20
U-Ti-La-51	Doping titania supported uranium oxide with La to increase the activity of catalyst at mole ratio of U :Ti: La = 1:20:0.45	0	465	6.25	Reducing T_{50} of U-La-Meso-27 by doping with Titania. T_{50} was reduced from 520 °C to 465 °C.	A.20	4.4.37
U-Ce-Meso-28	Doping silica supported uranium oxide with La to increase the activity of catalyst at mole ratio of U:Ce:Si = 1: 0.5:20	0	525	6.26	T_{50} = 525 °C doping U-Meso-6 with Cerium oxide OR doping CeO_2-55 with Uranium.	A.21	4.4.21
U-Ce-Meso-28	The effect of water on the activity of U-Ce-Meso-28 at mole ratio of U:Ce:Si = 1: 0.5:20	15	500	6.26	Reducing T_{50} by application of water on U-Ce-Meso-28 from 525 °C to 500 °C.	A.21	4.4.21
CeO_2-55	Pure CeO_2 as catalyst for TCE	0	575	6.26	T_{50} = 575 °C The activity of CeO_2-55 without Uranium.	A.21	4.4.41

Table 6.4: Continued.

Catalyst	synthesis and experiment	% Volume Water	T.C.E T50 °C	Figure No.	Finding	Table No.	Synthesis Chapter Reference
CeO_2-55	The effect of water on the activity of Pure CeO_2	15	575	6.26	Reducing T_{50} by application of water on CeO_2-55, No effect.	A.21	4.4.41
La_2O_3-54	Pure La_2O_3 as catalyst for TCE	0	530	6.27	$T_{50} = 530$ °C	A.22	4.4.40
La_2O_3-54	The effect of water to increase the activity of Pure La_2O_3 at 5% volume.	5	530	6.27	Reducing T_{50} of La_2O_3-54 by application of 5% volume water in reactor inlet stream. No effect.	A.22	4.4.40
La_2O_3-54	The effect of water to increase the activity of Pure La_2O_3 at 9% volume	9	530	6.27	Reducing T_{50} of La_2O_3-54 by application of 9% volume water in reactor inlet stream. No effect.	A.22	4.4.40
La_2O_3-54	The effect of water to increase the activity of Pure La_2O_3 at 15% volume.	15	530	6.27	Reducing T_{50} of La_2O_3-54 by application of 15% volume water in reactor inlet stream. No effect.	A.22	4.4.40
La-U-52(Pechini)	Doping uranium oxide as a support with La using Pechini Method to increase the activity of catalyst by polymerization complex at mole ratio of La:U = 1:1	0	520	6.23	$T_{50} = 520$ °C	A.18	4.4.38

Table 6.4: Continued.

Catalyst	synthesis and experiment	% Volume Water	T.C.E T50 °C	Figure No.	Finding	Table No.	Synthesis Chapter Reference
La-U-52(Pechini)	The effect of water to increase the activity of Pure La-U-52 at 15% volume using uranium as a support.	15	520	6.23	Reducing T_{50} of La-U-52 by application of 15% volume water in reactor inlet stream. No effect.	A.18	4.4.38
La-Ti-53(Pechini)	Doping titanium oxide with La using Pechini Method to increase the activity of catalyst by polymerization complex at mole ratio of La:Ti = 1:1	0	500	6.24	T_{50} = 500 °C	A.19	4.4.39
La-Ti-53(Pechini)	The effect of water to increase the activity of pure La-Ti-52 at 15% volume using titanium as a support La:Ti = 1:1	15	500	6.24	Reducing T_{50} of La-Ti-53 by application of 15% volume water in reactor inlet stream. No effect. Also, comparing U (in La-U-52) and Ti (in La-Ti-53) as support for La. Ti is a better support.	A.19	4.4.39

Table 6.4: Continued.

Catalyst	synthesis and experiment	% Volume Water	T.C.E T50 °C	Figure No.	Finding	Table No.	Synthesis Chapter Reference
U-Ti-Meso-43 (400)	Doping TiO_2 with U to enhance the activity of catalyst at mole ratio of U:Ti = 1:20	0	450	6.22	comparison of T_{50} = 450 °C with T.C.E as compared of T_{50}=330 °C with Toluene and T_{50}=375 °C with C.Benzene.	A.17	4.4.30
U-Ti-Meso-43 (400)	The effect of water at 7% volume on the activity of catalyst at identical mole ratio of U:Ti = 1:20	7	425	6.22	Reducing T_{50} of U-Ti-Meso by application of 7% volume water in reactor inlet stream. T_{50} was reduced from 450 °C to 425 °C.	A.17	4.4.30
U-Ti-Meso-43 (400)	The effect of water at 9% volume on the activity of catalyst at identical mole ratio U:Ti = 1:20	9	425	6.22	Reducing T_{50} of U-Ti-Meso by application of 9% volume water in reactor inlet stream. No change in T_{50} as compared with 7% water by volume.	A.17	4.4.30
U-Ti-Meso-43 (400)	The effect of water at 15% volume on the activity of catalyst at identical mole ratio U:Ti = 1:20	15	450	6.22	Reducing T_{50} of U-Ti-Meso by application of 15% volume water in reactor inlet stream. Decreasing in T_{50} as compared with 9% water by volume. No change as compared without using water.	A.17	4.4.30

The fourth column gives the T_{50} for trichloroethylene [determined as the temperature at which 50% conversion of trichloroethylene to oxidation products (HCl, Cl_2, CO_2 and H_2O) was obtained] and provides a measure of the catalyst activity. The fifth column provides the figure number for the light-off curve for trichloroethylene with that catalyst. The sixth column (Finding) describes the most important results of the experiment. The seventh column gives the table number in the appendix containing additional information. The last column gives the chapter and section containing details of the synthesis of each catalyst.

CHAPTER 7

SUMMARY AND CONCLUSIONS

Catalytic oxidation offers a great degree of control over the reaction products and can operate with dilute effluent stream (<1% VOC), which can not be treated easily by thermal combustion or any other pollution control device. Therefore, catalytic oxidation may be considered as a promising method for energy consumption.

The literature indicated that uranium oxide has a high activity for the catalytic destruction of VOCs and halogenated VOCs (23). DOE has a surplus of depleted uranium inventory for which beneficial uses are being sought (118). Therefore, the aim of this research was to explore the possibility of tailoring depleted uranium based catalysts for use in the catalytic oxidation of VOCs.

This research consisted of synthesizing potential depleted uranium catalysts, as well as testing and structural characterization. A quartz plug flow microreactor was built to compare the catalytic performance for oxidation of toluene, chlorobenzene, and trichloroethylene. These VOCs were chosen as typical of those found in anticipated applications. In particular, toluene was selected as typical of VOC found commonly in vent air streams from operations in which volatile organic solvents are used for the manufacture of organic chemicals and polymers, cleaning and degreasing purposes in metal processing, machining and finishing, and the vent or exhaust air from air stripping process units which are used to clean ground water or soil which has been contaminated with hazardous volatile organic chemicals and solvents. Chlorobenzene was chosen as a

145

model chloro-organic compound to demonstrate the effectiveness of the uranium oxide catalysts. Chlorobenzene was selected for three reasons. First, it is listed by the US Environmental Protection Agency as one of the 318 compounds designated as VOCs. Second, chlorobenzene can be considered as a suitable chemical model reagent to probe the destruction of poly-chlorinated biphenyls (PCBs), which are common toxic compounds receiving much media attention (119). Third, chlorobenzene is a particularly stable molecule that is difficult to oxidize. Trichloroethylene also is a major pollutant found in the ground water plumes at DOEs Hanford, Paducah, and Savannah River sites.

Two key factors limiting catalytic activities of uranium oxides prepared by conventional methods are small surface area and pore size [27]. A porous material is the best candidate as supports for dispersed catalysts. Ordered mesoporous materials are one of the most exciting discoveries in the field of materials synthesis over the past decade [28].

Two methods have been used to prepare uranium-oxide catalysts supported on mesoporous oxide hosts. Impregnation or incipient wetness and most notably the templated co-synthesis of mesoporous oxides. The later method isolates urania in a highly dispersed form on a mesoporous oxide support, typically silica or titania. The structural properties of these new catalytic systems were characterized by X-ray diffraction (XRD), transmission electron microscope (TEM) and nitrogen adsorption-desorption isotherm surface area measurements (BET).

The as-synthesized catalysts were calcined and tested for the destruction of VOCs at space velocities of 84,000 $mlg^{-1}h^{-1}$. The effects of post-synthesis calcinations temperatures were also considered. A gas chromatograph was used to measure the

146

concentration of VOCs from by-pass and reactor exit streams. The catalyst activity vs. catalyst temperature was measured. This data results in so called "light-off" curves. Conversion generally increases with temperature. From light-off curves, the temperature (T_{50}) at which 50% conversion of the VOC to oxidation products (CO_2 and H_2O) is obtained, at fixed flow rates, and provides a measure of the catalyst activity. Lower T_{50} indicates higher activity. Previously, in Tables 6.2, 6.3, and 6.4, the individual activity of each catalyst was summarized. These tables give the figure number of the light-off curve, and the T_{50} for the destruction of toluene, chlorobenzene, and trichloroethylene, respectively. Tables 7.1, and 7.2 in this chapter summarize the T_{50} (50% conversion) and T_{90} (90% conversion) for all selected catalysts discussed in this work respectively.

The basis used to evaluate the catalyst performance is T_{50} (the temperature of 50% conversion) and T_{90} (the temperature of 90% conversion). A desirable T_{50} would be <325 °C while T_{90} may vary from 375 °C to 425 °C depending on the nature of the volatile organic compound (VOCs). Continuous evolutions of preparative methods have led to steady improvements in catalyst performance. XRD, BET, TEM, GC, and Mass Spectrometer indicated that supporting the U_3O_8 phase and changing the mole ratio of uranium to silica and titania modifies the structure and chemistry of the uranium oxide. Among the non-uranium based catalysts which were tested for toluene oxidations (See Table 6.2), Pt/TiO_2 was the best with a T_{50} of 160 °C and 0.1% Pt/γ Alumina was the poorest with a T_{50} of 325 °C. Among the uranium based catalysts, U-Pt-Si-40 was the best with a T_{50} of 185 °C and K-U-SBA15-46 was the poorest with complete deactivation

Table 7.1: Summaries of composition ratio, calcinations temperature, BET surface area, and T_{50} for all selected catalysts discussed in this work respectively.

Catalyst	Composition Ratio	Calcination Temp. (^{0}C)	BET (m^2/g)	Toluene T_{50} °C	C. Benzene T_{50} °C	T.C.E T_{50} °C
U_3O_8	Pure U_3O_8	800	0.1	520	N/A	N/A
SiO_2	Pure mesoporous SiO_2	600	221.8	550	N/A	N/A
U-Meso-5	U:Si = 1:10	800	247.4	425	N/A	N/A
U-Meso-6	U:Si = 1:20	800	233	410	420	N/A
U-Meso-9	U:Si = 1:30	800	267	N/A	400	N/A
U-Meso-15	U:Si = 1:40	800	336.7	N/A	450	N/A
U-Meso-18	U :Si = 1:50	800	267	N/A	475	N/A
U-Meso-10	U:K:Si = 1:1:20 imp. with KNO_3	600	4.5	N/A	Deactivated	N/A
U-Meso-11	U:K:Si = 1:1:20 imp. with $K_2C_2O_4$	600	1	N/A	Deactivated	N/A
U-Meso-12	U:Br:Si = 1:1:20 imp. with KBr	600	4	N/A	Deactivated	N/A
U-Meso-13	U:Mg:Fe:Si = 1:0.5:0.5:20	600	210	N/A	500	N/A
U-Meso-14	U:Ca:Fe:Si = 1:0.5:0.5:20	600	204	N/A	500	N/A
U-Cr-Meso-19 (imp.)	U: Cr: Si = 1:0.2:20	600	253.4	418	N/A	N/A
U-Cr-Meso-21 (co-syn)	U: Cr: Si = 1:0.2:20	800	203.8	375	N/A	N/A
MesoCr-22 (co-syn)	Cr: Si = 1:95	800	207	470	N/A	N/A
U-Cr-Meso-25 (co-syn)	U: Cr: Si =1:0.2 :30	800	201	418	N/A	N/A
U-Co-Meso-20 (imp)	U: Co: Si = 1:0.23:20	600	242	440	N/A	N/A
U-Co-Meso-23 (co-syn)	U: Co: Si = 1:0.23:20	800	223	420	N/A	N/A

Table 7.1: Continued.

Catalyst	Composition Ratio	Calcination Temp. ($^{\circ}$C)	BET (m^2/g)	Toluene T_{50} $^{\circ}$C	C. Benzene T_{50} $^{\circ}$C	T.C.E T_{50} $^{\circ}$C
MesoCo-24 (co-syn)	Co: Si = 1:85	800	224	420	N/A	N/A
U-La-Meso-27	U:La:Si = 1:0.5 :20	800	321	N/A	N/A	520
U-Ce-Meso-28	U:Ce:Si = 1: 0.5:20	800	211	N/A	N/A	525
CeO_2-55	Pure CeO_2	800	8	N/A	N/A	600
MesoCu-29	Cu:Si = 5:20	800	257.6	540	N/A	N/A
U-Cu-Meso-30	U:Cu:Si =1:5:20	800	146.76	385	N/A	N/A
Pt/TiO_2-56	TiO_2:Pt 16.4:1	500	39.7	160	N/A	N/A
Pt/U_3O_8-57	U_3O_8:Pt = 5.25:1	500	0.0921	230	N/A	N/A
0.1% Pt/ γ Alumina-59	0.1% Pt/Al_2O_3	N/A	224.6	375	380	N/A
U-Ti-La-51	U :Ti: La = 1:20:0.45	800	242.5	N/A	N/A	465
La_2O_3-54	Pure La2O3	800	2.3	N/A	N/A	530
La-U-52(Pechini)	La:U = 1:1	800	14.75	N/A	N/A	530
La-Ti-53(Pechini)	La:Ti = 1:1	800	13.42	N/A	N/A	500
U-MCM41-49	imp. Uranyl Nitrate U: MCM-41 = 1:32	600	758	335	N/A	N/A
K-MCM41-50	Imp. KNO_2 K:MCM-41 = 1:11	600	26	400	N/A	N/A
K-SBA15-46	Imp. KNO_2 K:SBA-15 = 1:11	600	112	Deactivated	N/A	N/A
U-SBA15-47	U: SBA-15 = 1:32	800	355	360	N/A	N/A
U-Ti-Si-39 (350)	U:Ti:Si =1:1:20	350	429	390	N/A	N/A
U-Ti-Si-39 (600)	U:Ti:Si =1:1:20	600	341.6	385	N/A	N/A
U-Ti-Si-39 (800)	U:Ti:Si =1:1:20	800	205.3	380	N/A	N/A

Table 7.1: Continued.

Catalyst	Composition Ratio	Calcination Temp. (°C)	BET (m²/g)	Toluene T_{50} °C	C. Benzene T_{50} °C	T.C.E T_{50} °C
U-Pt-Si-40 (350)	U :Pt:SI = 1: 0.2: 20	350	477	170	N/A	N/A
U-Pt-Si-40 (600)	U :Pt:SI = 1: 0.2: 20	600	398	185	N/A	N/A
U-Pt-Si-40 (800)	U :Pt:SI = 1: 0.2: 20	800	247	235	N/A	N/A
TiO₂-41 (400)	Pure TiO2	400	127.81	365	500	N/A
TiO₂-41(600)	Pure TiO2	600	18.21	425	N/A	N/A
TiO₂-41 (800)	Pur TiO2	800	2.95	550	N/A	N/A
U-Ti-Meso-42 (400)	U:Ti = 1:10	400	195.6	390	N/A	N/A
U-Ti-Meso-43 (400)	U:Ti = 1:20	400	249.6	330	375	465
U-Ti-Meso-43 (600)	U:Ti = 1:20	600	108.62	325	375	465
U-Ti-Meso-43 (800)	U:Ti = 1:20	800	25.14	345	375	465
U-Ti-Meso-44 (400)	U:Ti= 1:30	400	139.01	400	N/A	N/A
U-Ti-Meso-45 (400)	U:Ti = 1:40	400	162.14	400	N/A	N/A
U-Sr-Meso-33	U:Sr:Si = 1:1:20	800	94.56	550	N/A	N/A
MesoSr-34	Sr:Si = 1:20	800	30.77	550	N/A	N/A

150

Table 7.2: Summaries of composition ratio, calcinations temperature, BET surface area, and T_{90} (90% conversion) for all selected catalysts discussed in this work respectively.

Catalyst	Composition Ratio	Calcination Temp. (^{o}C)	BET (m^2/g)	Toluene T_{90} ^{o}C	C. Benzene T_{90} ^{o}C	T.C.E T_{90} ^{o}C
U_3O_8	Pure U_3O_8	800	0.1	N/A	N/A	N/A
SiO_2	Pure mesoporous SiO_2	600	221.8	N/A	N/A	N/A
U-Meso-5	U:Si = 1:10	800	247.4	N/A	N/A	N/A
U-Meso-6	U:Si = 1:20	800	233	525	535	N/A
U-Meso-9	U:Si = 1:30	800	267	N/A	525	N/A
U-Meso-15	U:Si = 1:40	800	336.7	N/A	600	N/A
U-Meso-18	U :Si = 1:50	800	267	N/A	600	N/A
U-Meso-10	U:K:Si = 1:1:20 imp. with KNO_3	600	4.5	N/A	Deactivated	N/A
U-Meso-11	U:K:Si = 1:1:20 imp. with $K_2C_2O_4$	600	1	N/A	Deactivated	N/A
U-Meso-12	U:Br:Si = 1:1:20 imp. with KBr	600	4	N/A	Deactivated	N/A
U-Meso-13	U:Mg:Fe:Si = 1:0.5:0.5:20	600	210	N/A	625	N/A
U-Meso-14	U:Ca:Fe:Si = 1:0.5:0.5:20	600	204	N/A	625	N/A
U-Cr-Meso-19 (imp.)	U: Cr: Si = 1:0.2:20	600	253.4	N/A	N/A	N/A
U-Cr-Meso-21 (co-syn)	U: Cr: Si = 1:0.2:20	800	203.8	420	N/A	N/A
MesoCr-22 (co-syn)	Cr: Si = 1:95	800	207	N/A	N/A	N/A
U-Cr-Meso-25 (co-syn)	U: Cr: Si =1:0.2 :30	800	201	N/A	N/A	N/A
U-Co-Meso-20 (imp)	U: Co: Si = 1:0.23:20	600	242	500	N/A	N/A
U-Co-Meso-23 (co-syn)	U: Co: Si = 1:0.23:20	800	223	490	N/A	N/A

151

Table 7.2: Continued.

Catalyst	Composition Ratio	Calcination Temp. ($^{\circ}$C)	BET (m^2/g)	Toluene T$_{90}$ $^{\circ}$C	C. Benzene T$_{90}$ $^{\circ}$C	T.C.E T$_{90}$ $^{\circ}$C
MesoCo-24 (co-syn)	Co: Si = 1:85	800	224	500	N/A	N/A
U-La-Meso-27	U:La:Si = 1:0.5:20	800	321	N/A	N/A	N/A
U-Ce-Meso-28	U:Ce:Si = 1:0.5:20	800	211	N/A	N/A	N/A
CeO$_2$-55	Pure CeO$_2$	800	8	N/A	N/A	N/A
MesoCu-29	Cu:Si = 5:20	800	257.6	N/A	N/A	N/A
U-Cu-Meso-30	U:Cu:Si = 1:5:20	800	146.76	465	N/A	N/A
Pt/TiO$_2$-56	TiO$_2$:Pt 16.4:1	500	39.7	175	N/A	N/A
Pt/U$_3$O$_8$-57	U$_3$O$_8$:Pt = 5.25:1	500	0.0921	240	N/A	N/A
0.1% Pt/ γ Alumina-59	0.1% Pt/Al$_2$O$_3$	N/A	224.6	325	430	N/A
U-Ti-La-51	U :Ti: La = 1:20:0.45	800	242.5	N/A	N/A	550
La$_2$O$_3$-54	Pure La2O3	800	2.3	N/A	N/A	N/A
La-U-52(Pechini)	La:U = 1:1	800	14.75	N/A	N/A	575
La-Ti-53(Pechini)	La:Ti = 1:1	800	13.42	N/A	N/A	560
U-MCM41-49	imp. Uranyl Nitrate U: MCM-41 = 1:32	600	758	360	N/A	N/A
K-MCM41-50	Imp. KNO$_2$ K:MCM-41 = 1:11	600	26	400	N/A	N/A
K-SBA15-46	Imp. KNO$_2$ K:SBA-15 = 1:11	600	112	Deactivated	N/A	N/A
U-SBA15-47	U: SBA-15 = 1:32	800	355	400	N/A	N/A
U-Ti-Si-39 (350)	U:Ti:Si =1:1:20	350	429	425	N/A	N/A
U-Ti-Si-39 (600)	U:Ti:Si =1:1:20	600	341.6	425	N/A	N/A

Table 7.2: Continued.

Catalyst	Composition Ratio	Calcination Temp. (^{o}C)	BET (m^2/g)	Toluene T_{90} ^{o}C	C. Benzene T_{90} ^{o}C	T.C.E T_{90} ^{o}C
U-Ti-Si-39 (800)	U:Ti:Si =1:1:20	800	205.3	425	N/A	N/A
U-Pt-Si-40 (350)	U :Pt:SI = 1: 0.2: 20	350	477	175	N/A	N/A
U-Pt-Si-40 (600)	U :Pt:SI = 1: 0.2: 20	600	398	195	N/A	N/A
U-Pt-Si-40 (800)	U :Pt:SI = 1: 0.2: 20	800	247	210	N/A	N/A
TiO$_2$-41 (400)	Pure TiO2	400	127.81	365	N/A	N/A
TiO$_2$-41(600)	Pure TiO2	600	18.21	425	N/A	N/A
TiO$_2$-41 (800)	Pur TiO2	800	2.95	550	N/A	N/A
U-Ti-Meso-42 (400)	U:Ti = 1:10	400	195.6	445	N/A	N/A
U-Ti-Meso-43 (400)	U:Ti = 1:20	400	249.6	350	450	N/A
U-Ti-Meso-43 (600)	U:Ti = 1:20	600	108.62	345	N/A	N/A
U-Ti-Meso-43 (800)	U:Ti = 1:20	800	25.14	365	N/A	N/A
U-Ti-Meso-44 (400)	U:Ti = 1:30	400	139.01	450	N/A	N/A
U-Ti-Meso-45 (400)	U:Ti = 1:40	400	162.14	475	N/A	N/A
U-Sr-Meso-33	U:Sr:Si = 1:1:20	800	94.56	N/A	N/A	N/A
MesoSr-34	Sr:Si = 1:20	800	30.77	N/A	N/A	N/A

153

respectively. For chlorobenzene oxidation (See Table 6.3), U-Ti-Meso-43 was the best catalyst with a T_{50} of 375 °C and U-Meso-10, U-Meso-11, and U-Meso-12 were the poorest with complete deactivation among the uranium and non-uranium based catalysts, respectively. For the trichloroethylene (TCE) oxidation (See Table 6.4), U-Ti-Meso-43 was the best with a T_{50} of 425 °C and CeO_2-55 was the poorest with a T_{50} of 575 °C among uranium and non-uranium based catalysts.

The following conclusions are drawn from experimental results and observations:

1. The initial catalysts made at Oak Ridge National Laboratory by this group were urania in a mesoporous silica support. These catalysts were made by template co-assembly. XRD measurements indicated that the urania is present as U_3O_8. TEM measurements indicated that the U_3O_8 particles were dispersed in the silica support. Some less active catalysts contained a UO_2 phase, suggesting that U_3O_8 is the active phase. Pure U_3O_8 was found to be less active than urania supported on mesoporous silica (See Table 6.2 and 6.3). This seeming anomaly is attributed to the very high surface area that can be achieved in the mesoporous silica support which causes the urania to be highly dispersed both in the pores and on the external surface. Supported in this way, it is possible to use a much smaller amount of depleted uranium in the catalyst as shown previously in Table 6.2. Various molar ratios of U:Si were tried to see the differences in the improvement of the activity of catalyst, the results indicated that the optimal activity for chlorobenzene oxidation is obtained for U:Si = 1:30 by having the lowest T_{50} of 400 °C (See Table 6.3).

2. In order to further improve the activity of uranium oxide catalysts supported on mesoporous silica, various metal oxides such as (Cr, Co, Cu, Fe, Ca, Mg, Sr) were

doped onto the catalysts. Doping chromium oxide onto a urania supported on the mesoporous silica (Cr:U:Si = 0.2:1:20) catalyst enhances the activity slightly for toluene oxidation (T_{50} = 375 °C), but only if the chromium oxide is added in co-synthesis (U-Cr-Meso-21). Post impregnation of chromium oxide (U-Cr-Meso-19) yielded no improvement (T_{50} = 418 °C) compared to urania supported on the mesoporous silica catalysts (U-Meso-6), and without urania the mesoporous chromium oxide supported (T_{50} = 470 °C) on silica catalyst (Meso-Cr-22) was much less active. Doping copper oxide into a urania supported on mesoporous silica catalyst (U-Cu-Meso-30, Cu:U:Si = 5:1:20) also enhanced the activity (T_{50} = 385 °C) slightly as shown in Figure 6.17. As shown in Figure 6.5, cobalt oxide, appears to have comparable activity to the uranium oxide, and doping it into urania supported on mesoporous silica catalyst had little synergistic effect. Doping Sr into urania supported on mesoporous silica catalyst (U-Sr-Meso-33, Sr:U:Si = 1:1:20) decreased the catalyst activity (T_{50} = 550 °C) for toluene conversion as shown in Figure 6.18.

3. Fe, Mg, and Ca were tried as dopants for oxidation of chlorobenzene. Unfortunately, these also decreased the activity of the catalyst (T_{50} = 500 °C) as shown in Table 6.3.

4. Potassium is used as a promoter for some catalysts. However, addition of Potassium by co-synthesis to the urania supported on mesoporous silica catalyst destroyed the mesoporous structure and strongly deactivated the catalysts, whether Potassium was added as a bromide, oxalate or nitrate salt. Even post-impregnation of high surface area urania supported on mesoporous silica catalyst with Potassium salts caused loss of surface area and activity. As shown in Table 6.2, the addition of potassium to U-

155

MCM-41 and U-SBA-15 changed the T_{50} from 335 °C to 400 °C for U-MCM-41 and from 360 °C to complete deactivation for U-SBA-15. Evidently Potassium is a strong poison for depleted uranium catalysts.

5. Mesoporous titanium oxide (TiO_2) is an active catalyst for oxidation of toluene as shown in Figure 6.6. Doping with uranium has a synergistic interaction which leads to a very active catalyst. Using the template co-synthesis method to dope urania into titania (with mole ratio of U: Ti= 1:20) yields a mesoporous catalyst (U-Ti-Meso-43) with a T_{50} of 325 °C for toluene oxidation. Mesoporous titanium oxide (TiO_2) is not stable at high temperatures because of crystallization that leads to mesopore collapse as shown in Table 6.1. Interestingly, urania stabilizes the TiO_2 mesoporous framework and leads to much higher surface area and inhibits deactivation caused by sustained temperatures as high as 800 °C. The activity of the (U-Ti-Meso-43) catalyst was shown (Figure 6.8) to be stable for days and its activity is comparable to a 0.1% Pt/ γAl_2O_3 (commercial catalyst, T_{50} = 375 °C) and therefore competitive with the more expensive precious metal catalyst.

6. A second approach to achieve the U-Ti synergy was to dope a U-Meso-6 catalyst with Ti in smaller levels (U-Ti-Si-39, U:Ti:Si = 1:1:20). This approach gave catalysts with a slight improvement in activity as compared to U-Meso-6, but not as good as the U-Ti-Meso-43 catalysts. These catalysts were also stable at high temperature. In the final approach, the same procedure was followed to achieve the Pt-U synergy by doping a U-Meso-6 sample with Pt in smaller amount (U-Pt-Si-40, U:Pt:Si = 1:0.2:20) which resulted T_{50} of 170 °C. The results are shown in Table 6.2.

7. The U-Ti-Meso-43 catalyst was tested for chlorinated VOCs. This catalyst was active, although higher temperatures were required to obtain comparable conversions. Measured T_{50} was 325, 375, and 465 °C for toluene, chlorobenzene and trichloroethylene respectively. The results from quad mass spectrometer indicated that the only carbon containing byproduct besides CO_2 was benzaldehyde. Conversion to benzaldehyde depended upon temperature but it was generally less than 10%. The conversion of toluene, chlorobenzene and trichloroethylene over the U-Ti-Meso-43 catalyst (Table 7.1) indicated that the efficiency of destruction for the above VOCs decreases in the following order:

toluene > chlorobenzene > trichloroethylene

8. The effect of water on the conversion of U-Ti-Meso-43 catalyst was tested for oxidation of trichloroethylene as shown in Figure 6.22. This is also important because, in an application for soil vapor extraction, the reactant stream will be saturated in water. Addition of water as high as 15 volume % did not interfere with catalytic conversion (T_{50} = 450 °C) and appeared to enhance $HCl:Cl_2$ product ratios.

9. The addition of water for increasing the activities of U-Ce-Meso-28, CeO_2-55 and La_2O_3-54 were tried. The results indicated that there was no improvement in the activities of catalysts as shown in Table 6.4.

10. The overall results indicated that urania supported on titania are more efficient, corrosion resistant due to water addition and stable at very high temperature than silica supported catalyst even in the presence of water as high as 15% by volume (Table 6.4). For both of titania and silica based catalysts, the optimum mole ratio of U to Ti and U to Si was 1:20.

11. From various synthesis and characterization techniques applied to produce active urania catalysts, we have learned that mesoporous synthesis provides:

- increased activity

- a more efficient use of uranium

- U linked Ti gives the highest activity to date

- stability to deactivation even in the presence of large amounts of water and

uranium catalysts are a viable potential use for depleted uranium stockpiles, but it is not

as active as a platinum catalyst.

CHAPTER 8

RECOMMENDATIONS FOR FUTURE RESEARCH

The completion of tables 7.1 and 7.2 are fully recommended in order to make a comprehensive conclusion about the most effective and least effective catalyst with toluene, chlorobenzene and trichloroethylene.

The impregnation method can be modified by various techniques like pressurizing, vacuum treatment, or acoustic activation. This way, all gases trapped in the pores of mesoporous materials can be removed and facilitate the impregnation process. Research is needed to develop this technique.

U-Ti-meso-43 was considered as the best uranium-titanium based catalyst synthesized and tested in this work. The honeycomb monolithic structure of this catalyst has the potential to be used as commercial catalyst for SVE or in other applications, but should be tested for other compounds.

REFERENCES

1. Edward, C.M.; Mukhopadhyay, N. VOC Control: Current Practices and Future Trends, Chemical Engineering Progress, July, 1993.

2. Horsley, J.A. Catalytica Environmental Report No. E4, Catalytica Studies Division, Mountain View, CA, 1993.

3. USEPA *Code of Federal Regulations,* Title 40, Part 51, 100(s).

4. Bacon, G.; Ramon, L.; Liang, K. "*Control Particulate and Metal HAPs*" *Chem. Eng. Prog.* December 1997.

5. US Environmental Protection Agency Toxic Release Inventory. Rep. 745-8-96002, US EPA, Washington, DC, June 1996.

6. Molina, M.J.;Rowland, F.S. *Nature* 249 (1974) 810.

7. Chemistry in Britain, February 1997.

8. Jennings, M.S.; Palazzolo, M.A. N.E. Krohn, R.M. Parks, R.S. Berry, Fidler, in: Noyes (Ed.), Catalytic Incineration for the Control of Volatile Organic Compound Emission, *Pollut. Technol. Rev.*, 121 (1985).

9. Mukhopadhyay, N.; Moretti, E.C. Current and potential future industrial practices for controlling volatile organic compounds, center for waste control management, New York, 1993.

10. Brown, J.J.; Erickson, M.D.; Beskid, N.J; *Haz. Waste Haz. Mat.* 1993, 10, 335-345.

11. Siegrist, R.L.; VanEe, J.J. U.S. EPA *Environmental Monitoring Systems Laboratory.* 1994.

12. Kerr, J.M. *Environ. Sci. Technol.* 1990, 24, 172-173.

13. Hewitt, A.D.; Miyares, P.H.; Leggett, D.C.; Jenkins, T.F. *Environ. Sci. Technol.* 1992, 26, 1932-1938.

14. Kawi, S.; Te, M. *Catal. Today* 44 (1998), P. 101.

15. Zhao, X.S.; Ma, Q.; Lu, G.Q.M. Energy fuels 12 (1998) 1051.

16. Stuart H. Taylor, Catherine S. Heneghan, Graham J. Hutchings, Ian D. Hudson, Catalysis Today 59 (2000) 249-259.

17. Kevin A. Frankel, Ben W.-L. Jang, James J. Spivey, George W. Roberts, *Applied Catalysis* A: General 205 (2001) 263-278.

18. Fogler, S. H. Catalysis and catalytic reactors. *Elements of Chemical Reaction Engineering.* Second edition. Prentice Hall P T R, Englewood Cliffs, New Jersey1992; pp. 243.

19. Haggin, J. *Chem. Eng. News* 1995, July 10, 25.

20. Spivey, J. J. *Ind. Eng. Chem. Res.* 1987, 26, 2165.

21. Chatterjee, S.; Greene, H. L. *J. Catal.* 1991, 130, 76.

22. Petrosius, S. C.; Drago, R. S.; Young, V.; Grunewald, G. C. *J. Am. Chem. Soc.* 1993, 115, 6131.

23. Hutchings, G.J.; Heneghan, C.S.; Hudson, I.D.; Taylor, S.H. Nature, 1996, 384, 341-343.

24. Hutchings, G.J.; Heneghan, C.S.; Hudson, I.D.; Taylor, S.H., *Heterogeneous Hydrocarbon Oxidatio;* Waren, B. K., Oyama, S. T., American Chemical Society, Washington, D.C., 1996, pp. 59-75.

25. Hutchings, G.J.; Heneghan, C.S.; Oleary, S.; Taylor, S.H.; Hudson, I.D.; Boyd, V.J. "The destruction of volatile organic compounds using uranium oxides based

catalysts", abstract in 2nd world congress on environmental catalysis, AIChE, 1998.

26. Nozaki, F.; Ohki, K. Bull. *Chem. Soc. Japan.* 1972, 45, 3473.

27. Vidya, K.; Dapurkar, S.E.; Selvam, P.; Badamali, D.; Kumar; Gupta, N.M. *J. Mol. Catal, 2002,* 181, 91.

28. Kresge, C.T.; Leonowicz, M.E.; Roth, W.J.; Vartuli, J.C.; Beck, J.S. Nature, 1992, 359, 710.

29. Huo, Q.; Margolese, D.I.; Stucky, G.D. *Chem. Mater.* 8 (1996), P. 1147.

30. Corma, A. "Microporous to Mesoporous Molecular Sieve Materials and Their Use in Catalysis" *Chem. Rev.* 1997, 97, 2373.

31. Voudrias, E.A. Global Nest: the int. J. vol 3, No 1, pp 1-10, 2001.

32. Nyer, Evan K. *Practical techniques for Groundwater and Soil Remediation.* Lewis Publisher, London. 1993.

33. Mackay, D.; Cherry, J.A. Groundwater Contamination: Pump-and treat remediation, *Environmental Science and Technology,* 1989, 23, 630-636.

34. Kavanaugh, M.C. National Research Council, Committee on Ground Water Cleanup Alternatives. *Alternatives for Groundwater Cleanup.* National Academy Press. Washington. 1994.

35. Dupont, R.R.; Doucette, W.J.; R.E. Assessment of *In Situ* Bioremediation Potential and Application of Bioventing at a Fuel-Contaminated Site. Robert E. Hinchee and Robert F. Olfenbuttel (ed.) *In Situ* Bioreclamation. Butterworth-Heinemann, MA. Pp. 262-282.

36. Urlings, L.G.C.M.; Spuy, F.; Coffa, S.; Van Vree, H.B.R.J. 1991. Soil Vapor Extraction of Hydrocarbons: *In Situ* and On-Site Biological Treatment. Robert E. Hinchee and Robert F. Olfenbuttel. *In Situ* Bioreclamation. Butterworth-Heinemann, Stoneham, MA. Pp. 321-336.

37. Cole, G.M. 1994. Assessment and Remediation of Petroleum Contaminated Sites. CRC Press. Boca Raton, Florida.

38. EPA/540/S-94/501, February, 1994.

39. A. *Technical Requirements for On-Site Thermal Desorption of Soil Media Contaminated with Hazardous Chlorinated Organics, September, 1997.*

    B. *Technical Requirements for On-Site Low Temperature Thermal Treatment of Non-Hazardous soils Contaminated with Petroleum/Coal Tar/Gas Plant Wastes, December, 1997.*

    C. *Technical Requirements for On-Site Low Temperature Thermal Desorption of Solid Media and Low Level Mixed Waste Contaminated With Mercury and/or Hazardous Chlorinated Organics, September, 1998.*

40. Satterfield, C.N.: *Heterogeneous Catalysis in Practice*, McGraw-Hill, Inc. New York, 1980.

41. Wentz, C.A.: *Hazardous Waste Management*, 2nd ed., McGraw-Hill, Inc. New York, 1995.

42. Slejko, F.L., *Adsorption Technology*, Marcel Dekker, New York, 1985.

43. Suzuki, M., *Adsorption Engineering*, Elsevier, Amsterdam, 1990.

44. Silverman, L., Billings, C.E. and Dennis, R., "*Performance of the model K electro-polar filte*", USAEC Report NYO 1592, Harvard University, 1954.

45. Thomas, J. W., and E. J. Woodfin, *"Electrified fibrous air filter"*, *AIEE Transactions*, **78**, 276, 1959.

46. Bogarduos, H. F., R.C. Clark, J. K. Thomspon, and G. H. Fielding, *"Enhancement of filter media performance by corona-free electric fields"*, Presented at the 13th AEC Air Cleaning Conference, August 1974.

47. Fielding, G.H.,H.F. Bogardus, R.C. Clark, and J.K. Thompson, "Electrically Augmented Filtration of Aerosols", in ACS Symp. Ser. **17**, 1975.

48. Barker, R. E, Granular electrofiltration. Ph.D. Diss., University of Tennessee, 1988.

49. Harriott, G.M. and Saville D.A. *"Electrically stimulated aerosol filtration in packed beds"*, *AIChE J*, **26**, 325, 1971.

50. Waterman, L. C. *"Electrical Coalescers"*, *Chem. Eng. Prog.*, **61**, 51-57,1965.

51. Muller, D.J., *"Electrostatic granular bed filter development program"*, Paper presented at 2nd Annual Contractors' Meeting on Contaminant Control in Hot Coal Derived Gas Streams, pp. 75-85, Morgantown, WV, 17-19 February 1982.

52. Henry, F.S. and Ariman T. *"Numeric modeling of electrically enhanced fibrous filtration"*. ASTM Committee F-21, *Fluid Filtration: Gas,* **1**, 13, 1986.

53. Accomazzo, M.A. and Grant D.C. *"Mechanisms and devices for filtration of critical Process gases"*. *Fluid Filtration: Gas,* **1**, ASTM STP *975, 402*, 1986.

54. Barker, R. E, Brunson, R. R, Clinton, S. D, and Watson J. D, Granular electrofiltration. Separations Technology, vol. 1, 1991.

55. The DuPont publication "Air Emissions Control Technologies: A Guide to Technology Selection and Economics", Dyer, J.A.; Mulholland K.L. 1994.

56. Richardson, J.T., *Principles of Catalyst Development*. Plenum Press, New York, New York, 1989.

57. Orchin, M., Homogeneous Catalysis: A Wedding of Theory and Experiment, *Catal. Rev.,* **26**, 59 (1984).

58. Andrew, S.S.P., CHEMTECH 9 (1979) 180.

59. Delmon, B.; Jacobs, P.; Poncelet, G. *Preparation of Catalyst 1, Studies in Surface Science and Catalysis*, vol. 1, Elsevier, Amsterdam, 1976.

60. Maxwell, I.A. in: Hightower, J.W.; Delgass, W.N.; Iglesia, E.; Bell, A.T., Proceedings of the 11th International Congress on Catalysis, *Studies in Surface Science and Catalysis,* vol. 101, Elsevier, Amsterdam, 1996, p.1.

61. Baiker, A., in: Hightower, J.W.; Delgass, W.N.; Iglesia, E.; Bell, A.T., Proceedings of the 11th International Congress on Catalysis, *Studies in Surface Science and Catalysis,* vol. 101A, Elsevier, Amsterdam, 1996, p.51.

62. LePage, J.F., in: Ertl, G.; Knozinger, H.; Weitkamp, J., Handbook of Heterogeneous Catalysis, vol. 1, Wiley/VCH, New York/Weinheim, 1997, p. 49.

63. Hutchings, G.J.; Bethell, D.; McGuire, N.; Bulman Page, P.C.; Robinson, D.; Willock, D.J.; Hancock, F.; King, F., *Curr. Top. Catal.* **2** (1999), p.39.

64. Davies, M.E. in: Corma, A.; Melo, F.V.; Mendorioz, S.; Fierro, J.L.G. Proceedings of the 12th International Congress on Catalysis, *Studies in Surface Science and Catalysis,* vol. 130A, Elsevier, Amsterdam, 2000, p.49.

65. Schwarz, J.M.; Contescu, C.; Contescu, A., Chem. Rev. 95 (1995), p. 477.

66. Schlogl, R., in: Ertl, G.; Knozinger, H.; Weitkamp, J., Handbook of Heterogeneous Catalysis, vol. 1, Wiley/VCH, New York/Weinheim, 1997, p. 54.

67. Courty, Ph.; Marcilly, Ch., in: Poncelet, G.; Grange, P.; Jacobs, P.A., Preparation of Catalysts III, *Studies in Surface Science and Catalysis*, vol. 16, Elsevier, Amsterdam, 1983, P.485.

68. Perego, C.; Villa, P.L. *Catal. Today* **34** (1997), p. 281.

69. Schuth, F.; Unger, K., in: Ertl, G.; Knozinger, H.; Weitkamp, J., Handbook of Heterogeneous Catalysis, vol. 1, Wiley/VCH, New York/Weinheim, 1997, p. 72.

70. Twigg, M.V. Catalysis Handbook, 2nd ed., Wolfe, London, 1989.

71. Brinker, C.J.; Scherer, G.W. Sol-Gel Science, Academic Press, New York, **1990**.

72. Ko, E.I., in: Ertl, G.; Knozinger, H.; Weitkamp, J. Handbook of Heterogeneous Catalysis, vol. 1, Wiley/VCH, New York/Weinheim, 1997, p.86.

73. Livage, J.; Henry, M.; Sanchez, C. *Prog. Solid State Chem*. **18** (1988), p.259.

74. Komiyama, M. Design and Preparation of Impregnated Catalysts, *Catal. Rev.* 27, 1985, p. 341

75. Clearfield, A. *Chem. Rev.,* 1988, 88, 125.

76. Che, M.; Clause, O.; Marcilly, Ch. In : Ertl, G.; Knozinger, H.; Weitkamp, J. Handbook of Heterogeneous Catalysis, vol. 1, Wiley/VCH, New York/Weinheim, 1997, p. 191.

77. Herron, N.; Wang, Y.; Eddy, M.M.; Stucky, G.D.; Cox, D.E.; Moler, K.; Bein, T. *J. Am. Chem.. Soc.* **1989,** 111, 530.

78. Chen, W.; Lin, Z.; Wang, Z.; Lin, L. *Solid State Comm.* **1996,** 100, 101.

79. Badeei, A.R.; Bonneviot, L. *Inorg. Chem* 1998, 37, 4142.

80. Zhao, D.; Huo, Q.; Feng, J.; Chmelka, B.F.; Stucky, G.D. *J. Am. Chem. Soc.,* **1998,** 120, 6024.

81. Huo, Q.; Margolese, D.I; Ciesla, U.; Feng, P.; Gier, T.E.; Sieger, P.; Leon, R.; Petroff, P.M; Schuth, M.; Stucky, G.D. *Nature,* **1994**, 368, 317.

82. Rabinowitch, E.; Belford, R.L. *"Spectroscopy and Photochemistry of Uranyl Compounds"*, Pergamon Press Book, New York, 1964.

83. Acres, G.J.K.; Bird, A.J.; Jenkins, J.W.; King, F. The Design and Preparation of Supported Catalysts, *Catalysis*, Vol. 4, p. 1, Royal Society of Chemistry, London, 1981.

84. Hoekstra, J.: U.S. Patent 3,388,077 (to U.O.P).

85. Henck, L.L.; West, J.K. *Chem. Rev.* **90**, 1990, p.33.

86. Suib, S.L. *Chem. Rev.* **93**, 1993, p. 803.

87. Bhatia, S. Zeolite Catalysts: Principles and Applications, CRC Press, Boca Raton, FL, 1990.

88. Richardson, J.T. Principles of Catalyst Development, Plenum Press, New York, 1989.

89. Winyall, M.E., in: Leach, B.E., Applied Industrial Catalysis, vol. 3, Academic Press, New York, 1984, p. 43.

90. Richardson, J.T.; Dubus, R.J. Preparation Variables in Nickel Catalysts, J. Catal. 1978, 54, p. 207.

91. Doesburg, E.B.M.; van Hooff, J.H.C, in: Moullijn, J.A.; van Leeuven, P.W.N.M.; van Santen, R.A., Catalysis: An Integrated Approach to Homogeneous, Heterogeneous and Industrial Catalysis, Studies in Surface Science and Catalysis, vol. 79, Elsevier, Amsterdam, 1993, Chapter 8.

92. Fulton, J.W., *Chem. Eng.* 1986, **12**, p. 97.

93. Stiles, A.V. Catalyst Manufacture, Marcel Dekker, New York 1983

94. Cahen, R.M.; Andre, M.J.; Debus, H.R. Process for the production of spherical Catalyst Supports, *Preparation of Catalysts II* (Delmon, B.; Grange, P.; Jacobs, P.; Poncelet, G.), p. 585, Elsevier, Amsterdam 1979.

95. Jiratova, K.; Janacek, L.; Schneider, P. Influence of Aluminum Hydroxide Peptization on Physical Properties of Alumina Extrudates, *Preparation of Catalysts III* (Poncelet, G.; Grange, P.; Jacobs, P.A), p. 653, Elsevier, Amsterdam 1983.

96. Ramsey, w., *Proc. Roy. Soc.* A76 111, 1905.

97. McNair, H.M.; Bonelli, E.J. *Basic Gas Chromatography*, Varian Aerograph, Walnut Creek, California, 1969.

98. Dilts, R.V. *Analytical Chemistry*, p. 512, D. Van Nostrand Company, New York, N.Y, 1974.

99. Ameteck, Process and Analytical Inatruments Division, 150 Freeport Rd, Pittsburgh, PA 15238.

100. March, R.E.; Hughes R.J. *Quadrupole* Storage Muss Spectrometry; Wiley: New York, 1989; Chapter 2.

101. Frindell, K.L.; Bartl, M.H.; Popitsch, A.; Stucky, G.D. Angew. Chem. Int. Ed. 2002, 41(6), 960.

102. Zhao, D.; Huo, Q.; Feng, J.; Chmelka, B. F.; Stucky, G. D.; J. Am. Chem. Soc., **1998**, 120, 6024.

103. Badamali, S.K.; Selvam, P.; Surf, S. Sci. Catal. 113, **1998**, 749.

104. Schmidt, M.; Stocker, D.; Akporiaye, D.; Torstad, E.H.; Olsen, A. Microporous Mater. 5, **1995**, 1.

105. Badamali, S.K. Ph.D. Thesis, IIT Bombay, Mumbai, **1999**.

106. Kakihana, M.; Yoshimura, M. Bull. Chem. Soc. Jpn., 72, 1427-1443 (1999).

107. McBain, J.W.Z. *Phys. Chem.* 1909, 38,471.

108. Adamson, A. W. *Physical Chemistry of Surfaces*; Wiley, New York, 1982, 4th Ed, Chapter 15.

109. Langmuir, I. *J. Am. Chem. Soc.* 1918, 40, 1361.

110. Brunauer, S.; Emmett, P.H.; Teller, E. *J. Am. Chem. Soc.* **1938**, 309.

111. Brunaur, S.; Deming, L.S.; Deming, W.S.; Teller, E. J. Am. Chem. Soc. 1940, 62, 1723.

112. Barrett, E.P.; Joyner, L.G.; Halenda, P.P. *J. Am. Chem. Soc.* **1951**, 73, 373.

113. Lange's Handbook of Chemistry, 14th Edition, McGraw-Hill, Inc. N.Y

114. Marshall, R.H.; Hoekstra, H.R. *J. Inorg. Nucl. Chem.,* **1965**. Vol. 27, pp. 1947 to 1950.

115. Jones, J.; Ross, J.R.G. Catal. Today 35 (1997) 97

116. Carati, A.; Ferraris, G.; Guidotti, M.; Moretti, G.; Psaro, R.; Rizzo, C. Catalysis Today 77 (2003) pp. 315-323

117. Price, P.R.; Haire, M.J.; Croff, A.G. "Depleted Uranium Uses R & D Program," Waste Management 2001 Symposium, Tucson, Arizona, February 25 – March 1, 2001.

118. Meharg, A.A.; Osborn, D. Nature **1995**, *375*, 353-354.

119. Li, W.; Lin, Y.; Zhang, Y. Catalysis Today **2003**, *83*, 239-245.

APPENDIX A

Table A.1: Comparison of catalytic performance by (U$_3$O$_8$, SiO$_2$, U-Meso-5, and U-Meso-6) for the destruction of toluene.

Temperature (°C)	% Conversion SiO$_2$	Ave. Conv.	Std. dev. s	% Conversion U$_3$O$_8$	Ave. Conv.	Std. dev. s	% Conversion U-Meso-5 U:Si = 1:10	Ave. Conv.	Std. dev. s	% Conversion U-Meso-6 U:Si = 1:20	Ave. Conv.	Std. dev. s
325.0	6.2	5.6	0.6	3.4	3.9	0.5	4.2	4.5	0.5			
325.0	5.0			4.1			4.8					
325.0	5.6			4.3								
350.0	9.0	9.4	1.1	6.2	6.8	1.0	8.8	7.5	1.1	14.9	15.7	0.8
350.0	9.2			6.3			7.0			15.6		
350.0	11.0			8.0			6.7			16.5		
375.0	11.7	12.4	0.7				19.2	18.6	0.6	23.5	22.9	1.7
375.0	12.3						18.6			20.9		
375.0	13.1						18.0			24.2		
400.0	9.6	11.4	1.5	8.4	8.3	0.4	50.5	49.7	1.0	44.7	48.0	5.2
400.0	12.0			8.6			49.9			45.3		
400.0	12.5			7.8			48.6			54.0		
425.0	16.0	14.6	1.2							65.4	65.7	1.1
425.0	13.8									64.9		
425.0	14.0									66.9		
450.0	19.6	18.7	0.8	10.5	12.4	1.9	64.2	64.5	0.7	75.7	75.7	0.7
450.0	18.2			12.6			63.9			75.1		
450.0	18.2			14.2			65.2			76.4		
475.0	24.1	24.8	0.6							82.1	82.3	0.2
475.0	25.1									82.3		
475.0	25.1									82.5		
500.0	28.4	28.5	1.1	39.5	41.2	1.8	68.8	69.9	1.1	88.2	87.8	0.4
500.0	29.7			41.0			71.0			87.4		
500.0	27.5			43.6			69.9			87.9		
525.0										91.2	91.3	0.2
525.0										91.5		
525.0										91.1		
550.0				65.5	64.1	1.5						
550.0				64.2								
550.0				62.5								
600.0				82.5	81.3	1.8						

Table A.2: Effect of Chromium addition by co-assembly or impregnation synthesis techniques for destruction of toluene.

Temperature (°C)	% Conversion U-Meso-19 (Cr) imp.	Ave. % Conv	Std dev σ	% Conversion U-Meso-21 (Cr) co-syn.	Ave. % Conv	Std dev σ	% Conversion Meso-22 (Cr) co-syn.	Ave. % Conv	Std dev σ	% Conversion U-Meso-6 co-syn.	Ave. % Conv	Std dev σ
200.0	0.0	0.7	1.2	2.8	2.7	0.4	0.3	3.2	2.5	1.7	2.8	1.7
200.0	0.0			2.2			4.4			5.2		
200.0	2.0			3.1			4.9			1.6		
225.0	6.1	5.4	1.0	2.4	3.0	0.5	0.4	3.4	2.8	0.0	1.7	2.0
225.0	5.7			3.2			4.1			1.1		
225.0	4.2			3.4			5.9			4.0		
250.0	5.9	6.7	1.7	6.5	5.7	0.9	6.1	5.6	0.5	1.2	3.4	2.1
250.0	5.5			5.8			5.0			3.7		
250.0	8.6			4.7			5.6			5.4		
275.0	8.6	7.7	1.0	3.2	3.4	0.5	5.6	5.5	0.6	2.2	3.3	1.0
275.0	7.8			3.0			6.0			4.0		
275.0	6.7			4.1			4.9			3.7		
300.0	7.2	6.2	1.0	6.5	7.9	1.2	5.3	5.5	0.2	7.2	8.5	1.2
300.0	5.2			8.3			5.5			9.6		
300.0	6.2			9.0			5.6			8.8		
325.0	11.2	10.2	1.9	11.6	9.3	2.0	10.0	9.1	2.0	10.8	10.5	1.7
325.0	11.3			8.1			10.4			8.8		
325.0	8.0			8.1			6.8			12.1		
350.0	19.6	19.0	0.8	24.9	24.2	0.7	11.1	12.6	1.5	14.9	15.7	0.8
350.0	19.3			23.7			12.5			15.6		
350.0	18.1			24.0			14.0			16.5		
375.0	31.7	29.4	2.4	52.8	52.1	0.7	18.6	18.9	0.7	23.5	22.9	1.7
375.0	29.3			51.6			18.3			20.9		
375.0	27.0			51.8			19.7			24.2		
400.0	44.0	41.1	2.6	80.3	79.9	0.4	30.2	29.7	0.6	44.7	48.0	5.2
400.0	40.0			79.6			29.8			45.3		
400.0	39.3			79.8			29.1			54.0		
425.0	57.5	56.0	1.3	94.5	94.1	0.3	41.0	40.1	1.1	65.4	65.7	0.9
425.0	55.0			94.0			40.5			64.9		
425.0	55.5			93.9			38.9			66.9		
450.0	67.4	66.0	1.1	98.4	98.5	0.1	43.4	43.8	0.8	75.7	75.7	0.7
450.0	65.6			98.5			44.7			75.1		
450.0	65.2			98.6			43.3			76.4		
475.0	72.2	72.0	0.3	99.7	99.6	0.0	55.0	55.2	0.7	82.1	82.3	0.2
475.0	72.0			99.6			54.5			82.3		
475.0	71.6			99.6			55.9			82.5		
500.0	80.6	80.3	0.4				65.2	64.5	0.6	88.2	87.8	0.4
500.0	80.0						64.4			87.4		
500.0	79.4						64.1			87.9		
525.0										91.2	91.2	0.0
525.0										91.5		
525.0										91.1		

173

Table A.3: Effect of Cobalt addition by co-assembly or impregnation synthesis techniques for oxidation of toluene.

Temperature (°C)	% Conversion U-Co-Meso-20 imp.	Ave. % Conv.	Std dev σ	% Conversion U-Co-Meso-23 co-syn.	Ave. % Conv.	Std dev σ	% Conversion MesoCo-24 co-syn.	Ave. % Conv.	Std dev σ	% Conversion U-Meso-6 co-syn.	Ave. % Conv.	Std dev σ
200.0	4.5	5.2	0.7	4.3	4.1	1.0	5.4	4.8	1.5	1.7	2.8	1.7
200.0	5.3			3.0			3.0			5.2		
200.0	5.9			4.9			5.9			1.6		
225.0	5.2	6.0	2.0	6.5	6.0	0.6	4.9	6.1	1.1	0.0	1.7	2.0
225.0	4.5			5.3			7.2			1.1		
225.0	8.2			6.2			6.3			4.0		
250.0	5.4	7.0	1.1	3.7	4.1	0.8	7.2	7.4	0.8	1.2	3.4	2.1
250.0	7.6			5.0			8.3			3.7		
250.0	7.8			3.5			6.7			5.4		
275.0	9.1	7.9	1.7	8.7	6.5	2.1	8.3	9.0	0.6	2.2	3.3	1.0
275.0	6.7			6.2			9.2			4.0		
275.0	7.6			4.5			9.6			3.7		
300.0	8.8	9.5	0.6	9.6	9.4	1.6	10.4	10.0	0.4	7.2	8.5	1.2
300.0	9.9			10.8			10.1			9.6		
300.0	9.7			7.7			9.7			8.8		
325.0	11.9	11.1	0.7	10.8	11.3	1.4	11.1	11.8	0.8	10.8	10.5	1.7
325.0	10.6			13.0			11.8			8.8		
325.0	10.8			10.3			12.6			12.1		
350.0	12.7	12.4	0.4	12.2	11.6	0.7	16.1	17.8	1.5	14.9	15.7	0.8
350.0	12.0			11.7			18.8			15.6		
350.0	12.3			10.8			18.5			16.5		
375.0	18.5	19.0	1.0	24.5	26.7	2.1	27.1	28.4	1.1	23.5	22.9	1.7
375.0	20.2			28.8			28.6			20.9		
375.0	18.3			26.8			29.3			24.2		
400.0	24.2	24.8	1.7	40.5	41.2	0.9	42.7	41.8	0.9	44.7	48.0	5.2
400.0	23.5			41.0			41.6			45.3		
400.0	26.7			42.2			41.1			54.0		
425.0	39.6	37.5	2.9	62.2	62.2	0.4	55.2	56.4	1.0	65.4	65.7	0.9
425.0	38.8			62.5			57.0			64.9		
425.0	34.2			61.8			56.9			66.9		
450.0	61.0	59.9	1.1	76.3	76.7	0.4	72.2	72.3	0.6	75.7	75.7	0.7
450.0	59.9			76.7			72.9			75.1		
450.0	58.8			77.1			71.7			76.4		
475.0	77.8	76.2	1.4	88.2	87.6	0.5	82.5	82.5	0.2	82.1	82.3	0.2
475.0	75.6			87.5			82.6			82.3		
475.0	75.2			87.1			82.2			82.5		
500.0	90.6	89.0	1.3	94.6	94.6	0.2	89.5	89.2	0.4	88.2	87.8	0.4
500.0	88.2			94.8			89.3			87.4		
500.0	88.4			94.4			88.8			87.9		
525.0							89.4	89.3	0.0	91.2	91.2	0.0
525.0							89.3			91.5		
525.0							89.3			91.1		

174

Table A.4: Effect of calcinations temperature (400, 600, and 800 °C) upon light-off for oxidation of toluene by TiO_2.

Temperature (°C)	% Conversion TiO2 (400C)	Ave. % Conv.	Std. dev. σ	% Conversion TiO2 (600C)	Ave. % Conv.	Std. dev. σ	% Conversion TiO2 (800C)	Ave. % Conv.	Std. dev. σ
200.0	5.7	6.0	1.1	2.0	1.7	1.3	3.3	2.7	0.5
200.0	7.1			0.0			2.7		
200.0	5.1			3.2			2.2		
225.0	3.0	4.7	1.5	4.5	3.8	1.1	2.2	1.4	0.8
225.0	5.7			3.0			1.4		
225.0	5.5			3.2			0.6		
250.0	8.9	8.9	0.6	6.1	4.6	1.4	4.2	4.0	1.4
250.0	8.3			3.3			5.3		
250.0	9.5			4.4			2.5		
275.0	10.6	9.7	1.6	5.9	4.6	1.8	8.1	7.7	1.5
275.0	10.5			3.3			6.1		
275.0	7.9			3.6			8.9		
300.0	14.2	14.4	0.9	5.4	4.1	1.1	7.8	6.4	1.4
300.0	15.4			3.2			5.1		
300.0	13.7			3.9			6.2		
325.0	21.1	20.0	1.3	9.1	8.5	0.8	4.3	7.2	2.5
325.0	18.6			7.6			8.4		
325.0	20.2			8.6			8.8		
350.0	32.0	34.4	2.2	12.4	11.2	1.4	11.7	9.8	1.7
350.0	36.3			11.4			8.5		
350.0	34.9			9.7			9.2		
375.0	66.0	66.1	0.2	23.4	20.9	2.3	9.5	9.8	0.4
375.0	66.3			19.0			10.0		
375.0	66.1			20.3			8.6		
400.0	89.2	89.1	0.2	34.8	34.8	0.4	9.6	10.9	1.3
400.0	89.0			35.2			10.7		
400.0	88.9			34.3			12.3		
425.0	95.5	95.2	0.2	50.3	53.3	2.6	13.5	15.0	1.3
425.0	95.2			54.7			15.6		
425.0	95.0			54.8			15.8		
450.0	96.5	96.4	0.2	60.8	61.2	0.4	15.0	18.6	3.2
450.0	96.2			61.5			20.5		
450.0	96.0			61.4			20.4		
475.0	96.6	96.4	0.1	66.4	66.1	0.3	27.4	24.8	4.1
475.0	96.4			65.9			27.0		
475.0	96.3			66.0			20.1		
500.0	96.3	96.2	0.2	68.0	67.7	0.3	38.2	36.4	1.5
500.0	96.0			67.6			35.4		
500.0	96.4			67.4			35.7		

Table A.5: Effect of calcinations temperature (400, 600, and 800 °C) upon light-off curve by U-Ti-Meso-43 for oxidation of toluene.

Temperature (°C)	% Conversion U-Ti-Meso (400C)	Ave. % Conv.	Std dev. σ	% Conversion U-Ti-Meso (600C)	Ave. % Conv.	Std dev. σ	% Conversion U-Ti-Meso (800C)	Ave. % Conv.	Std dev. σ	% Conversion 0.1% Pt/Al$_2$O$_3$	Ave % Conv.	Std. dev. σ
250.0	11.8	10.7	1.2	12.6	12.0	0.8	9.1	9.4	0.8			
250.0	9.4			12.3			8.8					
250.0	10.8			11.2			10.3					
275.0	13.5	12.7	0.7	12.5	12.3	1.1	7.5	6.3	1.0			
275.0	12.1			11.1			5.6					
275.0	12.4			13.2			5.8					
300.0	15.6	16.4	0.9	21.9	20.6	1.1	13.9	13.8	0.3	12.5	12.	0.5
300.0	17.4			19.8			14.0			13.3		
300.0	16.1			20.1			13.6					
320.0				39.2	38.5	1.4						
320.0				38.6								
320.0				36.5								
325.0	27.3	25.8	1.7	56.9	52.9	4.7	22.9	21.7	1.1	18.5	18.	0.5
325.0	26.1			54.0			21.1			19.2		
325.0	24.0			47.7			21.0					
335.0	56.3	55.2	0.9	72.4	71.2	1.1	29.9	28.6	1.6			
335.0	54.5			70.9			29.0					
335.0	54.8			70.3			26.8					
350.0	95.8	94.0	1.5	97.1	96.7	0.4	56.9	56.4	0.5	30.4	30.	0.5
350.0	93.3			96.6			56.6			29.6		
350.0	93.0			96.3			55.9					
360.0	98.5	98.4	0.0	99.4	99.3	0.1						
360.0	98.5			99.3								
360.0	98.4			99.3								
365.0	99.4	99.4	0.0				92.2	92.1	0.1	40.3	41.	1.3
365.0	99.4						92.1			42.1		
365.0	99.4						92.0					
375.0	100.0	100.	0.0	100.0	100.	0.0	97.9	97.9	0.0	54.4	54.	0.2
375.0	100.0			100.0			97.9			54.0		
375.0	100.0			100.0			97.9					
380.0	100.0	100.	0.0				99.0	98.9	0.1			
380.0	100.0						98.9					
380.0	100.0						98.9					
390.0										66.4	67.	1.0
390.0										67.9		
390.0												
400.0										77.4	78.	1.5
400.0										79.6		
410.0										87.6	88.	0.9
410.0										88.9		

176

Table A.6: Catalyzed oxidation of toluene by variable doped uranium in U-Ti-Meso-42, 43, 44, and 45 for oxidation of toluene.

Temperature (°C)	% Conversion U-Ti-Meso (400) U:Ti =1:10	Ave. % Conv.	Std. dev. σ	Percent Conversion U-Ti-Meso (400) U:Ti =1:20	Ave. % Conv.	Std. dev. σ	Percent Conversion U-Ti-Meso (400) U:Ti =1:30	Ave. % Conv.	Std. dev. σ	Percent Conversion U-Ti-Meso (400) U:Ti =1:40	Ave. % Conv.	Std. dev. σ
250.0				11.8	10.7	1.2	1.4	3.1	1.6			
250.0				9.4			3.3					
250.0				10.8			4.6					
275.0				13.5	12.7	0.7	7.6	7.9	0.3	3.7	5.0	1.3
275.0				12.1			8.1			5.2		
275.0				12.4			8.0			6.3		
300.0	0.0	2.0	3.5	15.6	16.4	0.9	8.2	7.4	0.7	5.1	5.9	1.2
300.0	6.0			17.4			7.0			5.3		
300.0	0.0			16.1			7.0			7.3		
325.0	9.7	8.4	1.5	27.3	25.8	1.7	10.9	10.	0.5	6.6	5.7	0.8
325.0	6.7			26.1			10.0			5.7		
325.0	8.7			24.0			10.4			5.0		
335.0				56.3	55.2	0.9						
335.0				54.5								
335.0				54.8								
350.0				95.8	94.0	1.5	9.0	9.5	0.5	9.3	7.6	1.8
350.0				93.3			9.6			7.7		
350.0	13.0	12.	1.4	93.0			10.0			5.7		
360.0	13.3			98.5	98.4	0.0						
360.0	10.7			98.5								
360.0				98.4								
365.0				99.4	99.4	0.0						
365.0				99.4								
365.0				99.4								
375.0	16.7	21.	4.1	100.0	100.	0.0	20.0	20.	0.9	24.0	24.	0.2
375.0	23.1			100.0			21.7			24.0		
375.0	24.4			100.0			21.0			24.3		
380.0				100.0	100.	0.0						
380.0				100.0								
380.0				100.0								
400.0	62.2	61.	0.8				35.3	37.	1.9	48.2	47.	1.3
400.0	60.8						39.0			47.7		
400.0	60.7						37.8			45.7		
425.0	84.5	85.	0.6				77.6	77.	0.3	69.6	69.	0.3
425.0	85.3						77.1			69.4		
425.0	85.7						77.1			69.0		
450.0	95.5	95.	0.2				93.6	93.	0.0	83.1	83.	0.2
450.0	95.9						93.6			83.0		
450.0	95.8						93.6			83.3		
475.0	96.7	97.	0.7				98.5	98.	0.3	91.1	91.	0.4
475.0	97.5						99.0			91.9		

Table A.7: The effects of doping MCM-41 with uranium and potassium promoter for oxidation of toluene.

Temperature (°C)	% Conversion (MCM-41)	% Conversion (MCM-41) Impregnated with KNO2
200.00	14.18	14.44
200.00	10.43	13.63
200.00	6.00	11.74
225.00	11.66	11.84
225.00	9.50	11.72
225.00	14.54	12.26
250.00	14.75	16.23
250.00	15.30	14.16
250.00	14.19	13.00
275.00	18.48	15.01
275.00	17.96	18.86
275.00	22.10	20.30
300.00	25.00	17.36
300.00	27.67	23.88
300.00	27.14	20.60
325.00	43.22	25.50
325.00	40.82	25.08
325.00	51.38	30.70
350.00	77.98	39.75
350.00	78.25	41.52
350.00	80.00	37.97
360.00	92.30	
360.00	95.97	
360.00	97.08	
375.00	99.82	45.10
375.00	99.90	48.40
375.00	99.85	46.01
400.00		53.17
400.00		50.10
400.00		49.64

Table A.8: Comparison of doping uranium with SBA-15 and MCM-41 for oxidation of toluene.

Temperature (°C)	% Conversion (MCM-41) doped with U	% Conversion (SBA-15) doped with U
200.00	14.18	29.25
200.00	10.43	25.73
200.00	6.00	30.25
225.00	11.66	30.27
225.00	9.50	33.96
225.00	14.54	32.63
250.00	14.75	31.03
250.00	15.30	31.57
250.00	14.19	34.45
275.00	18.48	31.09
275.00	17.96	29.85
275.00	22.10	32.54
300.00	25.00	40.61
300.00	27.67	36.51
300.00	27.14	36.90
325.00	43.22	35.70
325.00	40.82	41.24
325.00	51.38	44.65
350.00	77.98	47.40
350.00	78.25	45.14
350.00	80.00	46.44
360.00	92.30	
360.00	95.97	
360.00	97.08	
375.00	99.82	64.13
375.00	99.90	68.80
375.00	99.85	67.06
400.00		91.70
400.00		94.33
400.00		92.86
425.00		99.96
425.00		99.97
425.00		99.96

179

Table A.9: Comparison of titania (TiO_2) and urania (U_3O_8) as oxidative supports for Pt for oxidation of toluene.

Temperature (°C)	% Conversion Pt/U_3O_8	% Conversion Pt/TiO2
120		0.00
120		0.00
120		0.00
130		5.92
130		6.13
130		4.43
140		9.70
140		10.44
140		8.93
150		22.46
150		24.12
150		25.15
165		81.67
165		78.16
165		84.15
175		94.81
175		94.00
175		94.45
185		98.60
185		98.60
185		98.83
200	5.00	
200	4.30	
200	1.00	
215	21.37	
215	21.85	
215	21.7	
225	28.6	
225	30.14	
225	29.92	
240	100	
240	100	
240	100	
250	100	
250	100	

Table A.10: The effect of calcinations temperature (350, 600, and 800 °C) upon light-off curve by U-Ti-Si-39 for oxidation of toluene.

Temperature (°C)	% Conversion U-Ti-Si (350 °C)	% Conversion U-Ti-Si (600 °C)	% Conversion U-Ti-Si (800 °C)
175.00	0.00	0.00	6.90
175.00	2.60	0.00	4.45
175.00	3.67	2.80	0.50
200.00	3.90	0.00	4.76
200.00	4.76	0.00	1.50
200.00	0.00	5.26	3.03
225.00	5.60	0.00	0.00
225.00	6.13	2.42	3.20
225.00	1.40	1.30	2.70
250.00	5.53	0.70	1.80
250.00	4.66	1.50	2.40
250.00	2.72	0.00	1.82
275.00	4.72	0.00	0.00
275.00	4.60	1.10	0.00
275.00	4.96	0.00	0.00
300.00	8.40	5.60	7.00
300.00	7.10	4.30	6.83
300.00	6.87	5.06	7.74
325.00	10.82	14.33	6.90
325.00	13.06	12.17	13.65
325.00	13.43	11.95	13.18
350.00	18.25	19.08	23.31
350.00	18.60	14.70	20.62
350.00	16.88	17.14	19.86
375.00	29.72	34.83	46.70
375.00	32.00	35.30	47.50
375.00	31.89	40.70	41.50
400.00	65.90	70.61	81.36
400.00	65.88	70.91	81.65
400.00	65.83	69.10	81.75
425.00	93.80	93.87	94.84
425.00	93.17	94.27	95.03
425.00	93.20	93.76	95.09
450.00	99.16	99.18	98.42
450.00	99.05	99.11	98.37
450.00	98.95	99.02	98.27

Table A.11: The effect of calcinations temperature (350, 600, and 800 °C) upon light-off curve by U-Pt-Si-40 for oxidation of toluene.

Temperature (C)	% Conversion U-Pt-Si (350 °C)	% Conversion U-Pt-Si (600 °C)	% Conversion U-Pt-Si (800 °C)
140.00	12.55		
140.00	11.25		
140.00	10.06	6.00	
150.00	15.62	3.00	
150.00	12.51	5.10	
150.00	12.27	4.60	
160.00	25.80	16.10	
160.00	26.45	14.65	
160.00	23.60	12.00	
165.00	32.06		
165.00	32.00		
165.00	31.55		
175.00	100.00	26.30	5.16
175.00	100.00	22.60	4.20
175.00	100.00	24.50	5.27
190.00	100.00	86.10	
190.00	100.00	89.40	
190.00	100.00	87.12	
200.00		100.00	22.50
200.00		100.00	21.60
200.00		100.00	21.30
210.00			100.00
210.00			100.00
210.00			100.00
225.00			100.00
225.00			100.00
225.00			100.00

Table A.12: The effect of copper addition into uranium mesoporous silica support by co-assembly method for oxidation of toluene.

Temperature (°C)	% Conversion UMesoCu(29)	% Conversion MesoCu(30)	% Conversion UMeso(6)
300.00	0.00	0.00	7.17
300.00	0.00	0.00	9.55
300.00	0.00	0.00	8.75
325.00	10.40	0.00	10.75
325.00	14.20	0.00	8.75
325.00	11.20	0.00	12.12
350.00	17.20	4.85	14.94
350.00	16.52	4.20	15.60
350.00	16.12	6.31	16.46
375.00	23.20	7.85	23.48
375.00	26.00	8.52	20.93
375.00	25.26	9.16	24.15
400.00	64.30	7.86	44.70
400.00	64.60	10.36	45.30
400.00	64.26	6.10	54.00
425.00	73.86	11.60	65.42
425.00	74.84	12.42	64.85
425.00	76.30	13.80	66.93
450.00	86.35	13.50	75.70
450.00	86.52	16.77	75.09
450.00	86.80	18.46	76.40
475.00	94.46	26.74	82.13
475.00	94.74	24.07	82.32
475.00	94.75	25.47	82.52
500.00	98.08	35.15	88.18
500.00	98.04	34.32	87.40
500.00	98.02	36.21	87.94
525.00		40.55	91.16
525.00		43.16	91.46
525.00		44.00	91.14
550.00		65.80	
550.00		66.31	
550.00		66.30	

Table A.13: The effect of Strontium addition into uranium mesoporous silica support by co-assembly method for oxidation of toluene.

Temperature (°C)	% Conversion UMesoSr(33)	% Conversion MesoSr(34)	% Conversion UMeso(6)
350.00	5.90		14.94
350.00	7.81		15.60
350.00	9.46		16.46
375.00	9.00	0.00	23.48
375.00	6.10	0.00	20.93
375.00	6.80	0.00	24.15
400.00	6.92	1.80	44.70
400.00	7.50	2.86	45.30
400.00	9.66	3.90	54.00
425.00	8.06	5.82	65.42
425.00	10.43	3.90	64.85
425.00	12.14	5.40	66.93
450.00	10.70	8.40	75.70
450.00	11.92	6.55	75.09
450.00	13.40	7.04	76.40
475.00	24.05	16.50	82.13
475.00	18.94	15.77	82.32
475.00	21.30	17.00	82.52
500.00	27.60	21.02	88.18
500.00	27.00	23.06	87.40
500.00	28.18	21.11	87.94
525.00	39.00	33.80	91.16
525.00	35.92	35.46	91.46
525.00	37.65	35.22	91.14
550.00	50.01	45.40	
550.00	51.00	49.03	
550.00	52.82	50.97	
575.00		63.73	
575.00		65.05	
575.00		66.34	

Table A.14: Comparison of catalyzed oxidation of chlorobenzene by pure uranium oxide catalyst and doped with (Fe +Mg or Fe+ Ca) using co-assembly in mesoporous silica support.

Temperature (°C)	% Conversion U-Meso-13 Fe+Mg U:Si=1:20	Ave. % Conv.	Std. dev. s	% Conversion U-Meso-14 Fe+Ca U:Si=1:20	Ave. % Conv.	Std. dev. s	% Conversion U-Meso-6 U:Si=1:20	Ave. % Conv.	Std. dev. s
250	10.70			13.88			12.75		
250	8.70	10.14	1.25	7.61	11.20	3.23	12.85	13.18	0.67
250	11.00			12.10			13.96		
275	17.77			17.72			16.35		
275	15.75	16.31	1.27	15.80	17.08	1.12	16.70	16.78	0.48
275	15.41			17.74			17.30		
300	17.27			17.56			18.70		
300	17.77	17.32	0.41	17.74	18.16	0.90	22.82	20.26	2.23
300	16.94			19.20			19.26		
325	16.86			21.07			18.40		
325	13.86	15.60	1.56	22.74	20.96	1.83	21.15	19.60	1.40
325	16.10			19.09			22.45		
350	16.10			24.57			32.22		
350	16.25	16.11	0.14	22.80	23.98	1.02	33.93	33.80	1.52
350	15.98			24.57			35.26		
375	19.70			25.30			37.06		
375	18.52	18.95	0.65	23.50	23.80	1.40	43.75	41.22	3.63
375	18.65			22.56			42.86		
400	22.62			31.70			44.00		
400	21.06	22.12	0.92	32.80	32.17	0.57	45.23	45.15	1.12
400	22.70			32.01			46.24		
425	26.11			38.66			53.89		
425	24.67	26.60	2.20	35.31	36.83	1.70	54.26	54.60	0.91
425	29.00			36.52			55.63		
450	31.68			40.65			64.21		
450	31.80	31.52	0.37	42.90	41.57	1.18	63.06	64.30	1.30
450	31.10			41.16			65.64		
475	34.20			43.80			74.53		
475	36.88	36.56	2.21	44.10	43.86	0.20	73.20	73.44	0.98
475	38.60			43.70			72.60		
500	48.56			45.73					
500	46.98	47.35	1.07	46.73	46.61	0.82			
500	46.51			47.37					
525	53.40			52.68					
525	55.10	54.36	0.87	50.70	51.75	0.99			
525	54.60			51.87					
550	63.50			61.40					
550	62.75	64.41	2.27	62.64	62.65	1.26			
550	67.00			63.93					
575	84.94			76.30					
575	83.84	84.24	0.60	75.77	75.98	0.28			
575	83.96			75.89					
600	87.63			81.44					
600	88.30	87.96	0.47	82.48	81.66	0.73			

Table A.15: Comparison of catalyzed oxidation of chlorobenzene by various doped uranium oxide catalyst co-assembled in mesoporous silica support.

Temperature (°C)	(%) Conversion U-meso-6 U:Si = 1:20	Ave. % Conv.	Std. dev. s	(%) Conversion U-meso-9 U:Si = 1:30	Ave. % Conv.	Std. dev. s	(%) Conversion U-meso-15 U:Si = 1:40	Ave. % Conv.	Std. dev. s	(%) Conversion U-meso-18 U:Si = 1:50	Ave. % Conv.	Std. dev. s
250	12.75			4.75			10.31			5.5		
250	12.85	13.2	0.7	6.33	5.4	0.8	13.01	12.5	2.0	7.89	6.5	1.2
250	13.96			5.25			14.23			6.2		
275	16.35			12.50			17.50			7.11		
275	16.70	16.8	0.5	11.95	12.7	0.8	18.00	19.0	2.2	3.88	5.1	1.8
275	17.30			13.56			21.50			4.2		
300	18.70			22.96			21.85			7.4		
300	22.82	20.3	2.2	20.22	20.8	2.0	21.56	21.8	0.3	6.18	5.9	1.6
300	19.26			19.06			22.10			4.15		
325	18.40			29.54			13.08			6.3		
325	21.15	20.7	2.1	30.41	29.6	0.9	12.72	13.5	1.0	5.6	6.9	1.7
325	22.45			28.70			14.62			8.74		
350	32.22			33.06			23.23			17.6		
350	33.93	33.8	1.5	34.64	32.9	1.9	26.88	24.8	1.9	20.9	18.2	2.4
350	35.26			30.88			24.35			16.2		
375	37.06			43.86			20.55			25.3		
375	43.75	41.2	3.6	44.34	43.4	1.2	19.70	20.1	0.6	27.7	22.1	4.6
375	42.86			42.90			22.12			24.6		
400	44.00			53.48			30.80			32.42		
400	45.23	45.2	1.1	53.40	53.8	0.6	32.67	31.9	1.0	29.9	32.8	3.0
400	46.24			54.50			32.19			36		
425	53.89			61.14			31.77			35.8		
425	54.26	54.6	0.9	61.16	61.6	0.8	31.67	32.6	1.5	37.6	37.2	1.3
425	55.63			62.50			34.37			38.2		
450	64.21			69.44			47.05			36.4		
450	63.06	64.3	1.3	68.03	68.7	0.7	45.16	47.3		42.1	40.1	3.2
450	65.64			68.57			49.71			41.8		
475	74.53						52.03			54		
475	73.20	73.4	1.0				52.61	52.8	0.9	47	49.9	3.7
475	72.60						53.85			48.7		
500							67.56			60		
500							69.85	68.3	1.4	65.3	61.2	3.7
500							67.41			58.3		
525							72.42			69.8		
525							74.76	72.8	1.8	67.7	67.9	1.8
525							71.25			66.2		
550							83.55			78.4		
550							83.41	83.7	0.3	78.6	77.7	1.4
550							84.05			76		
575							85.32					
575							85.50	85.5	0.2			
575							85.66					
600							96.66					
600							96.16	96.4	0.3			
600							96.38					

186

Table A.16: Comparison of catalyzed oxidation of chlorobenzene by 0.1% Pt/Alumina, uranium supported on mesoporous titanium oxide and pure titanium oxide catalysts.

Temperature (°C)	% Conversion U-Ti-Meso-(400)	Ave. % Conv.	Std. dev. σ	% Conversion TiO_2 (400)	Ave. % Conv.	Std. dev. σ	% Conversion 0.1% Pt/Alumina	Ave. % Conv.	Std. dev. σ
250.00	10.76			19.75			26.08		
250.00	13.95	11.54	2.14	19.40	20.9	2.3	23.64	24.86	1.73
250.00	9.90			23.55					
275.00	17.95						28.18		
275.00	15.89	13.95	3.83				31.28	29.73	2.2
275.00	16.41								
300.00	9.54			21.34			29.40	30	0.92
300.00	9.54	9.54	0.00	22.50	21.97	0.6	30.70		
300.00				22.07					
325.00	17.23	18.3	1.48				30.60	28.84	2.5
325.00	19.32						27.07		
325.00									
350.00	26.26	26.4	0.20	26.35			30.37	29.98	0.54
350.00	26.55			26.50	28.66	3.87	29.60		
350.00				33.14					
375.00	41.81	42.12	0.44				54.36		
375.00	42.44						54.02	54.1	0.22
375.00							53.93		
400.00	57.17	58.2	1.44	36.60			77.44		
400.00	59.21			34.65	36.47	1.75	80.87	79.3	1.73
400.00				38.14			79.58		
425.00	74.31	73.53	1.10				87.56		
425.00	72.76						88.90	88.22	0.67
425.00							88.21		
450.00				46.40					
450.00				44.12	44.22	2.12			
450.00				42.16					
475.00									
475.00									
475.00									
500.00									
500.00									
500.00									

Table A.17: Oxidation of trichloroethylene (TCE) over U-Ti-Meso-43 at various water content in the reactant stream.

Temperature (^{0}C)	% Conversion (No Water)	% Conversion (Water = 7 vol.%)	% Conversion (Water = 9 vol.%)	% Conversion (Water = 15 vol.%)
300.00	6.22	4.70	4.40	2.50
300.00	6.00	5.83	4.00	3.90
300.00	7.90	6.80	3.35	4.50
325.00	4.46	11.62	6.06	7.17
325.00	5.80	11.13	8.13	6.27
325.00	6.00	11.02	8.70	9.18
350.00	7.50	19.23	14.45	6.60
350.00	8.00	14.74	16.50	8.00
350.00	9.22	16.77	17.40	11.33
375.00	21.86	28.55	20.71	10.10
375.00	21.54	31.10	23.44	13.45
375.00	25.31	30.67	21.00	11.12
400.00	24.43	31.45	32.68	22.03
400.00	25.55	36.36	34.66	21.88
400.00	27.18	36.15	33.05	22.42
425.00	42.88	55.48	45.94	36.50
425.00	44.17	55.01	47.90	34.77
425.00	45.27	45.53	48.79	35.48
450.00	49.05	69.84	63.90	52.68
450.00	51.87	68.70	64.18	51.33
450.00	53.00	68.46	64.21	53.30
475.00	63.50	80.18	76.92	73.30
475.00	65.84	80.56	77.48	73.71
475.00	66.70	80.56	78.10	72.30
500.00	76.52	86.10	86.76	82.36
500.00	76.15	86.90	86.41	82.80
500.00	79.36	86.23	87.55	83.53

Table A.18: Comparison of catalyzed oxidation of trichloroethylene (TCE) by La-U-52 (Pechini method) at variable water flow rate.

Temperature (^{0}C)	% Conversion (U-La) without water	% Conversion (U-La) 14.77% volume water
400.00	0.00	5.32
400.00	0.00	6.40
400.00	0.00	5.22
425.00	0.00	7.46
425.00	0.00	7.45
425.00	1.50	5.55
450.00	13.14	10.85
450.00	14.05	12.20
450.00	11.50	13.15
475.00	20.62	22.26
475.00	19.17	23.27
475.00	20.92	24.11
500.00	32.86	31.15
500.00	31.65	35.03
500.00	32.58	33.95
525.00	53.24	55.72
525.00	54.50	54.67
525.00	55.25	57.14
550.00	78.50	79.87
550.00	79.76	80.19
550.00	80.43	80.36

Table A.19: Comparison of catalyzed oxidation of trichloroethylene (TCE) by La-Ti-53 (Pechini method) at variable water flow rates.

Temperature ($^{\circ}$C)	% Conversion by LaTi, no water	% Conversion by LaTi with 14.77% volume water
350.00	5.41	5.32
350.00	5.20	4.85
350.00	6.42	5.15
375.00	5.96	6.10
375.00	5.43	5.64
375.00	6.73	5.89
400.00	6.31	5.90
400.00	6.83	7.55
400.00	6.62	9.40
425.00	10.80	11.77
425.00	12.60	14.42
425.00	14.41	13.23
450.00	29.56	23.60
450.00	31.70	25.25
450.00	31.58	27.90
475.00	35.70	39.46
475.00	40.40	40.65
475.00	40.19	41.22
500.00	51.20	47.36
500.00	51.61	50.57
500.00	52.08	51.00
525.00	67.52	68.46
525.00	67.47	68.83
525.00	67.00	69.34
550.00	80.00	80.63
550.00	80.90	80.20
550.00	81.30	81.34

Table A.20: Comparison of activities for oxidation of trichloroethylene (TCE) by using two different supports (TiO_2 or SiO_2) doped with uranium and lanthanum.

Temperature (°C)	% Conversion (U-La-Meso-27)	% Conversion (U-Ti-La-51)
300.00	10.15	10.86
300.00	9.07	8.94
300.00	10.21	9.50
325.00	11.67	9.22
325.00	11.25	9.10
325.00	11.80	10.60
350.00	12.22	9.90
350.00	13.04	11.92
350.00	13.54	11.18
375.00	16.62	15.01
375.00	16.47	15.86
375.00	16.95	15.71
400.00	19.01	17.45
400.00	18.40	19.01
400.00	19.72	19.50
425.00	21.45	29.13
425.00	20.28	30.32
425.00	22.18	30.45
450.00	27.45	40.00
450.00	28.38	38.31
450.00	26.55	40.77
475.00	29.66	59.00
475.00	29.66	58.82
500.00	36.71	72.91
500.00	36.30	71.93
500.00	36.93	71.28
525.00	51.27	81.48
525.00	51.50	80.78
525.00	51.60	80.26
550.00	61.95	
550.00	61.90	
550.00	62.01	

Table A.21: Comparison of "light-off" curve for oxidation of trichloroethylene (TCE) over CeO_2-55 and U-Ce-Meso-28 at variable water flow rates.

Temperature (°C)	% Conversion (CeO_2) no water	% Conversion (CeO_2) 15% volume water	% Conversion U-Ce-Meso(28) no water	% Conversion U-Ce-Meso(28) 15% volume water
300.00	4.08	2.40	1.12	0.00
300.00	3.70	2.49	2.26	0.00
300.00	5.02	4.05	4.50	0.00
325.00	6.91	3.96	3.53	0.00
325.00	3.15	1.50	3.62	0.00
325.00	5.97	2.83	5.36	0.00
350.00	8.41	5.43	4.40	5.00
350.00	7.10	1.52	4.44	4.60
350.00	9.40	2.83	5.50	3.16
375.00	7.85	4.38	5.70	17.84
375.00	7.28	6.89	6.95	19.16
375.00	7.85	3.70	7.72	20.33
400.00	9.17	7.40	10.06	14.56
400.00	8.60	7.55	10.80	15.66
400.00	8.46	8.44	12.12	17.71
425.00	9.34	6.80	14.85	25.33
425.00	11.09	10.75	16.00	27.50
425.00	8.62	10.85	16.01	27.83
450.00	13.16	16.30	19.13	27.70
450.00	12.94	14.72	21.12	28.67
450.00	13.92	14.53	22.31	30.34
475.00	15.20	15.88	28.00	33.37
475.00	19.53	20.85	28.60	34.82
475.00	18.02	18.02	28.75	30.00
500.00	17.84	19.81	36.32	52.67
500.00	18.60	23.01	37.60	50.00
500.00	18.78	23.40	37.00	48.85
525.00	21.42	29.23	45.44	
525.00	23.78	29.26	48.90	
525.00	24.81	30.18	50.50	
550.00	33.67	35.0	64.66	63.50
550.00	33.82	35.17	65.30	63.53
550.00	34.70	40.0	65.20	64.16

Table A.22: The effects of various water flow rates on the activity of La_2O_3 for destructions of trichloroethylene (TCE).

Temperature (°C)	% Conversion No Water	% Conversion 4.66% Volume water	% Conversion 9.0% Volume water	% Conversion 4.66% Volume water
300.00	4.21	5.94	4.36	3.98
300.00	5.00	5.70	4.88	5.62
300.00	4.50	6.30	5.30	4.90
325.00	4.00	6.18	6.23	6.10
325.00	4.00	8.40	7.20	5.74
325.00	5.66	6.35	8.11	4.93
350.00	4.40	5.40	9.61	5.71
350.00	4.30	5.70	9.67	8.40
350.00	5.66	8.90	12.80	8.90
375.00	8.53	10.87	13.89	9.63
375.00	10.80	11.98	13.16	7.60
375.00	13.20	13.70	12.19	9.14
400.00	14.40	16.85	7.63	6.30
400.00	11.90	15.13	10.76	9.80
400.00	11.04	13.60	11.87	9.30
425.00	11.90	14.25	12.82	11.64
425.00	14.40	14.23	12.35	13.25
425.00	17.50	14.37	8.26	13.63
450.00	16.50	16.13	18.18	15.56
450.00	19.00	17.25	18.73	17.70
450.00	19.60	20.12	20.32	19.01
475.00	18.20	23.64	26.03	25.10
475.00	18.40	25.87	28.27	25.60
475.00	18.06	23.37	25.08	24.96
500.00	27.74	31.47	36.93	33.66
500.00	27.72	33.06	37.80	35.05
500.00	26.43	31.95	36.60	34.98
525.00	47.30	47.28	47.46	49.40
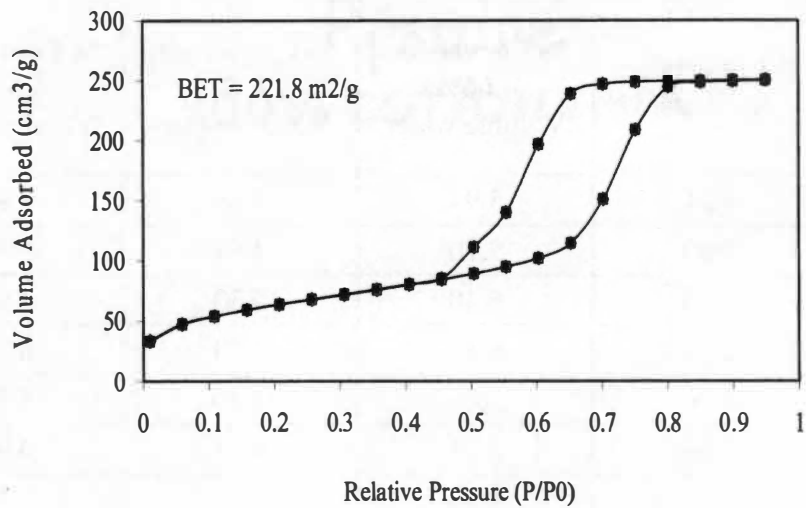
Figure A.1: BET adsorption-desorption isotherm for mesoporous SiO_2.
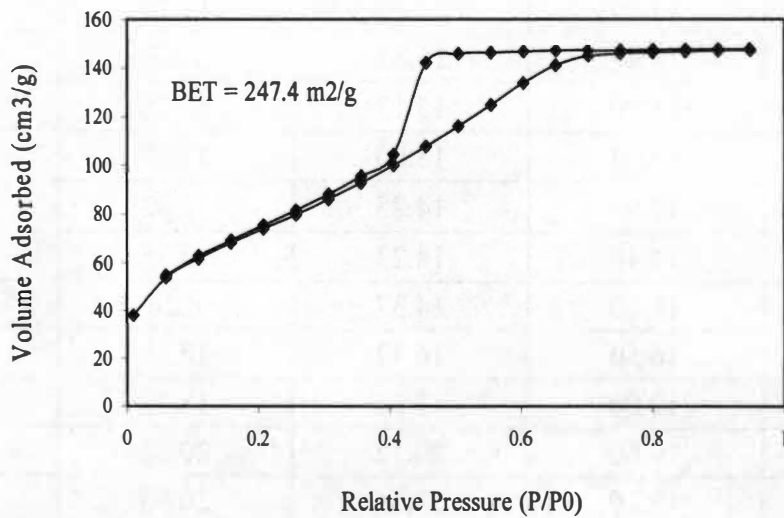
Figure A.2: BET adsorption-desorption isotherm for U-Meso-5 (U:Si = 1:10)
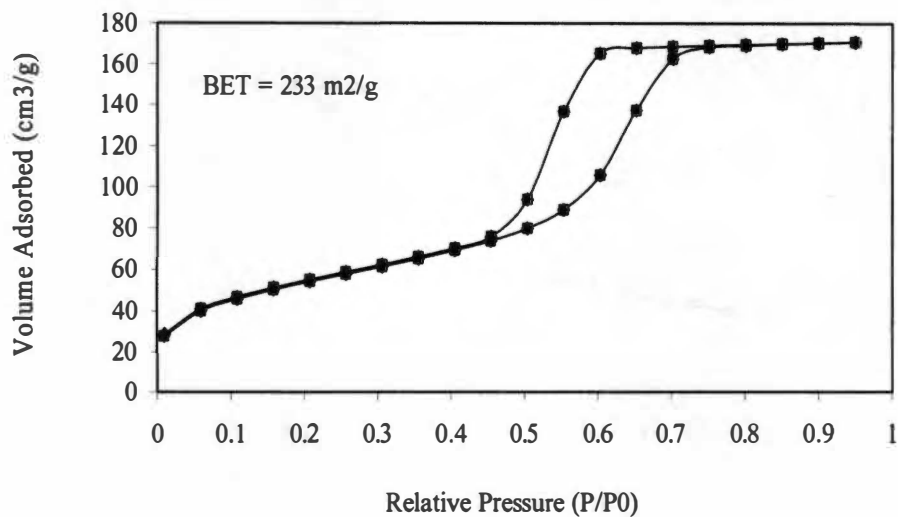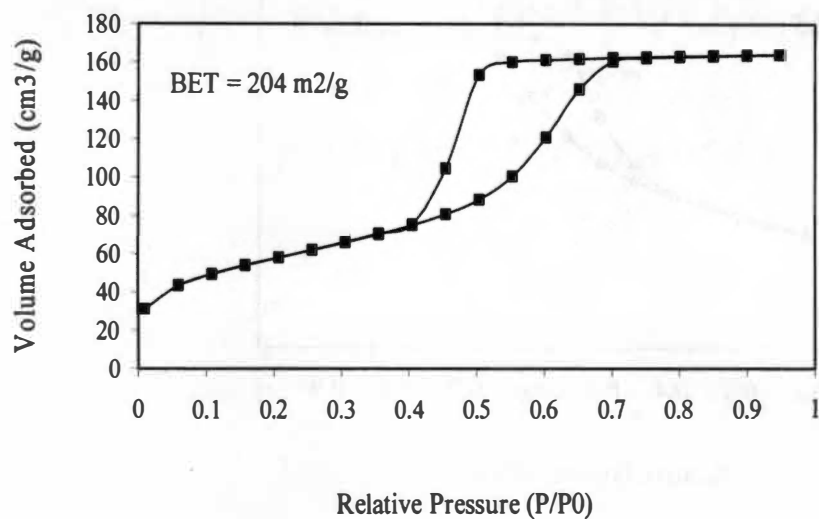
Figure A.3: BET adsorption-desorption isotherm for U-Meso-6 (U:Si = 1:20)
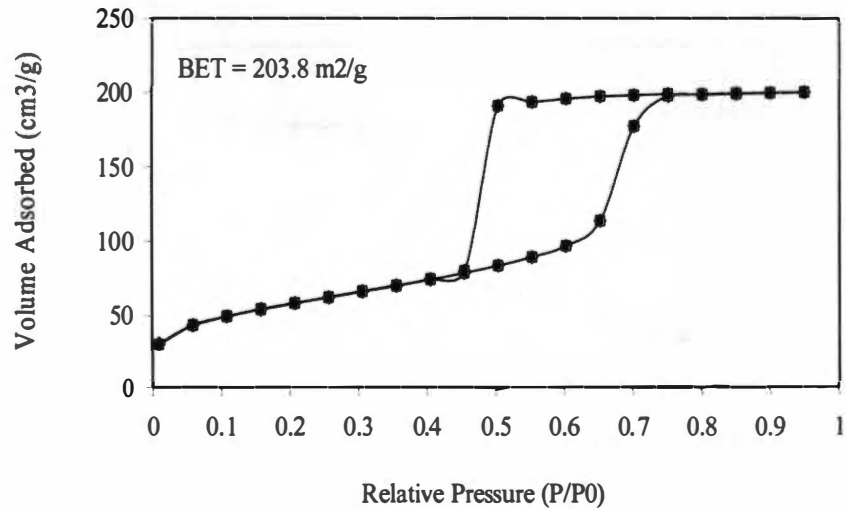
Figure A.4: BET adsorption-desorption isotherm for U-Cr-Meso-21. (U:Cr:Si = 1:0.2:20).
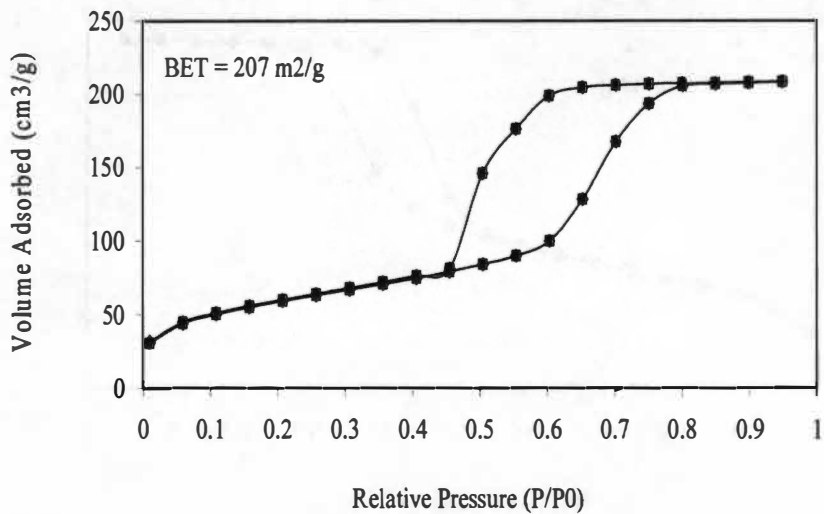
Figure A.5: BET adsorption-desorption isotherm for MesoCr-22 (Cr:S i = 1:95)
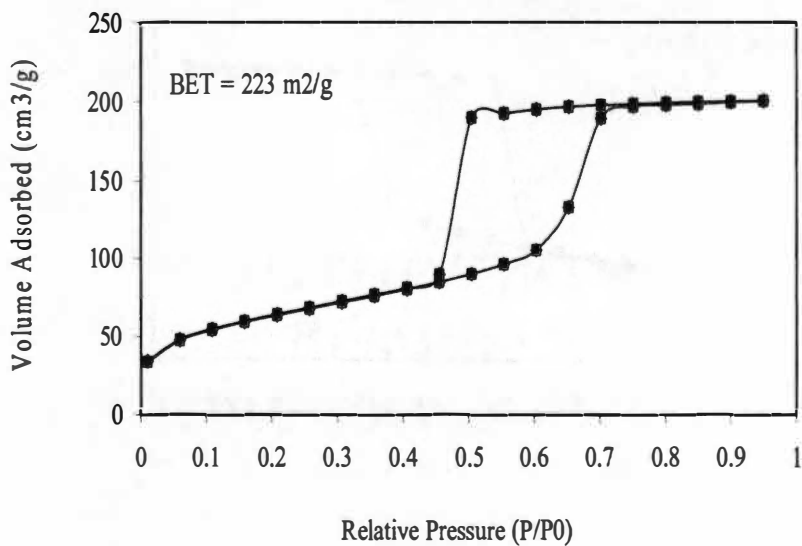
Figure A.6: BET adsorption-desor[tion isotherm for U-Co-Meso-23 (U:Co:Si = 1:0.23:20)
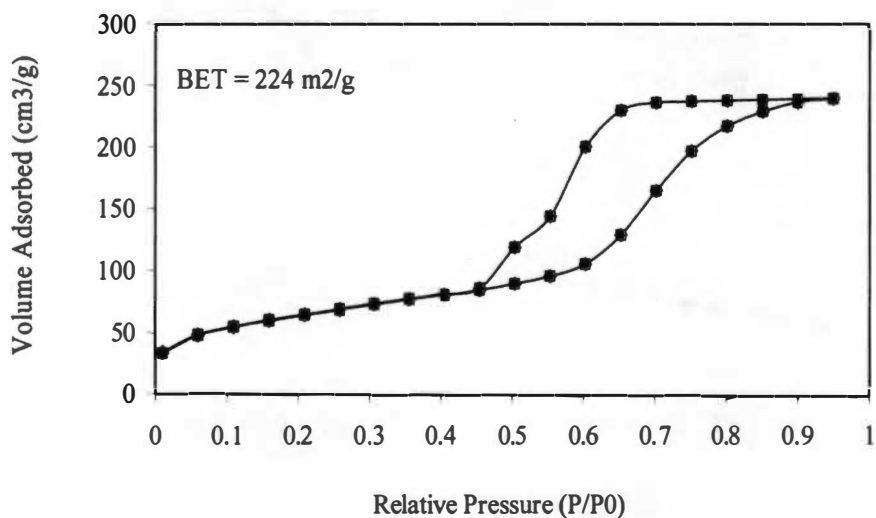
Figure A.7: BET adsorption-desorption isotherm for MesoCo-24 (Co:Si = 1:85)
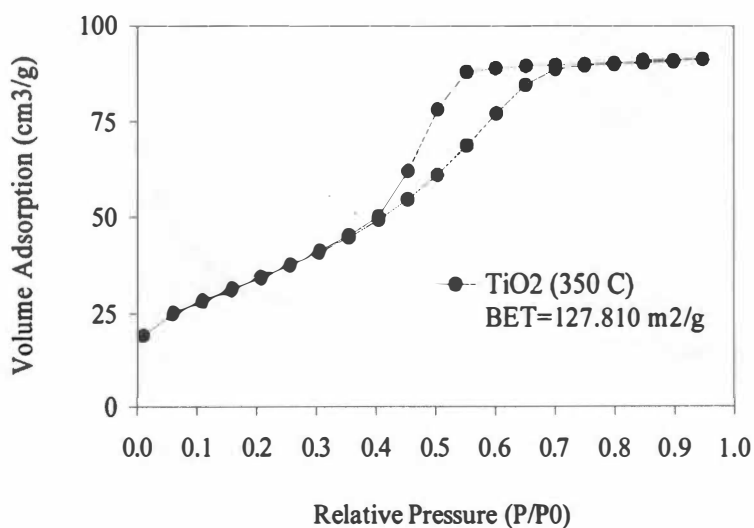
Figure A.8: BET adsorption-desorption isotherm for pure TiO_2 at calcinations temperature of 350 °C.
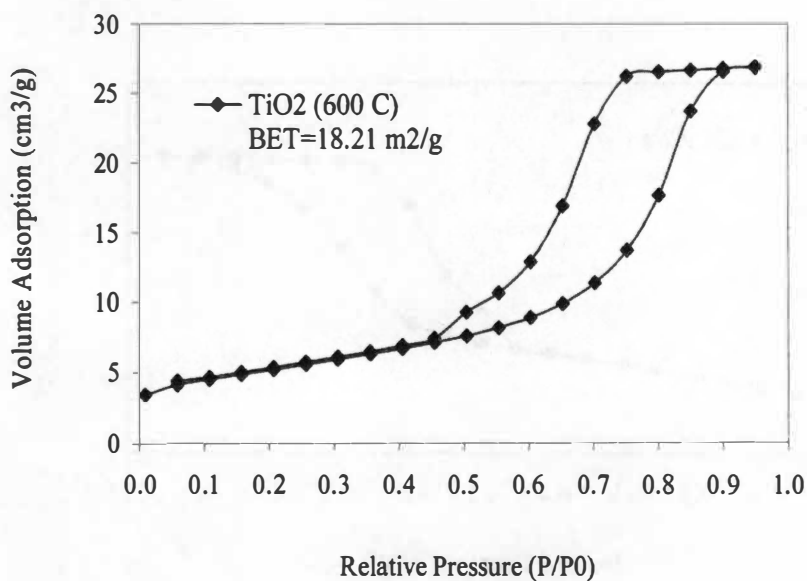
Figure A.9: BET adsorption-desorption isotherm for pure TiO_2 at calcinations temperature of 600 °C.
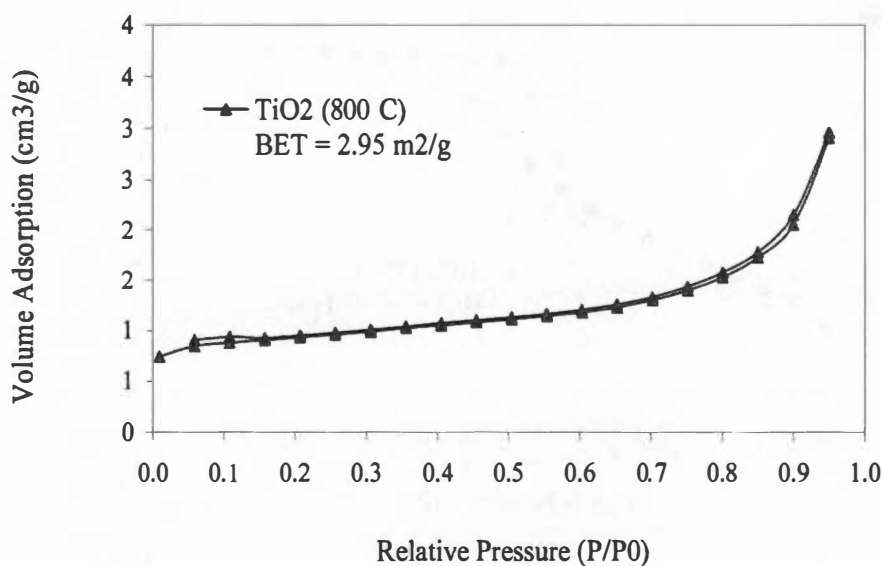
FigureA.10: BET adsorption-desorption isotherm for pure TiO_2 at calcinations temperature of 800 °C.
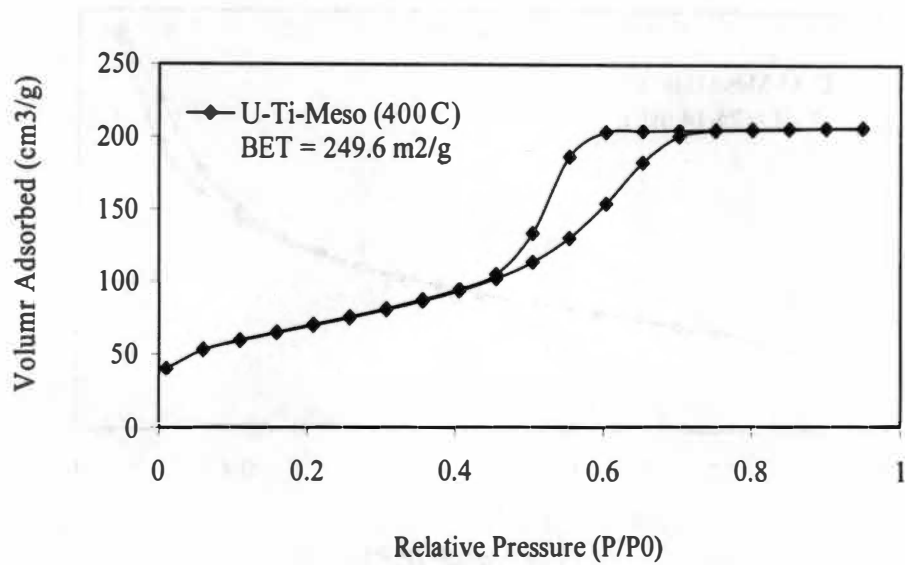
Figure A.11: BET adsorption-desorption isotherm for U-Ti-Meso (400) at calcinations temperature of 400 °C.
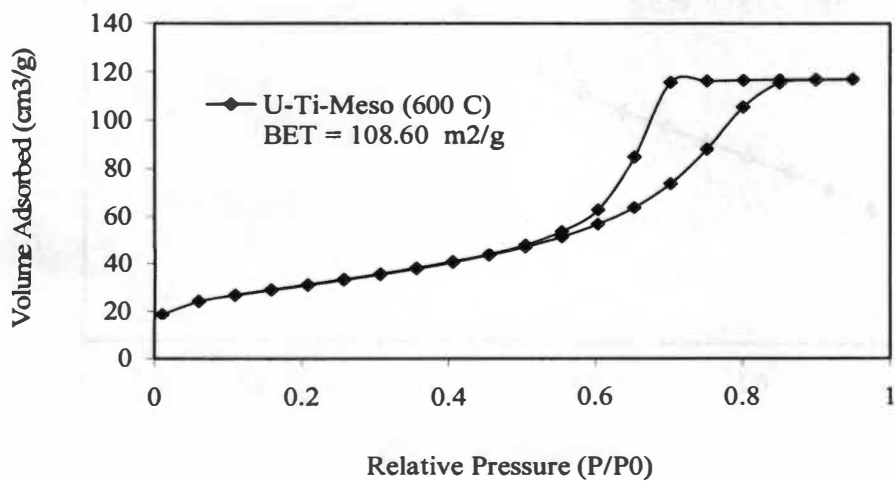
Figure A.12: BET adsorption-desorption isotherm for U-Ti-Meso (600) at calcinations temperature of 600 °C.
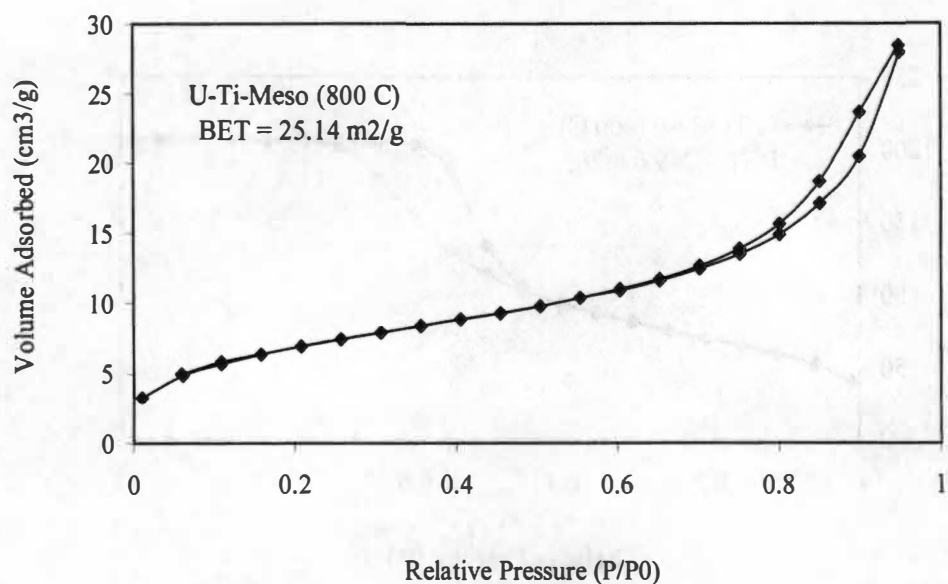
Figure A.13: BET adsorption-desorption isotherm for U-Ti-Meso (800) at calcinations temperature of 800 °C.
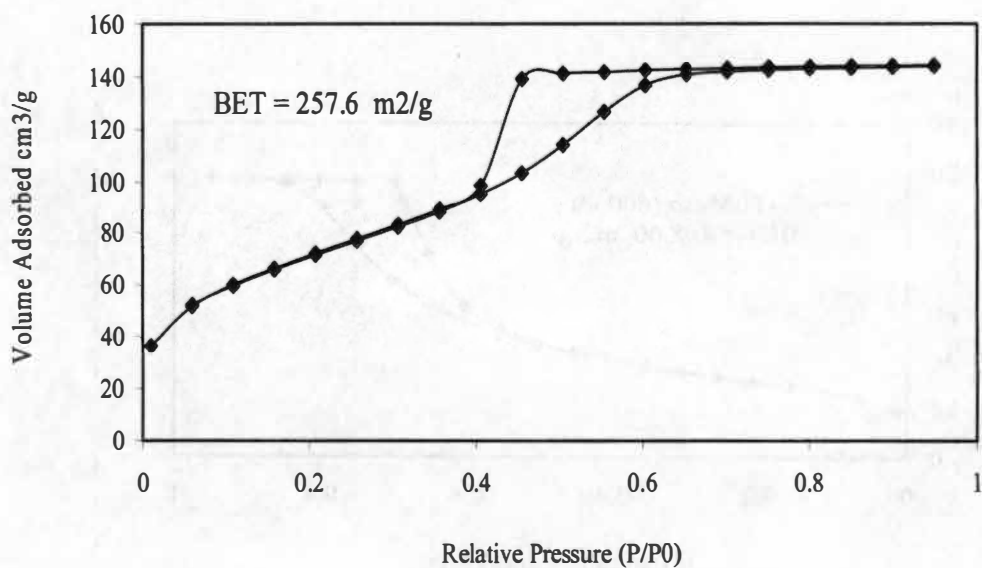
Figure A.14: BET adsorption-desorption isotherm for Meso-Cu-30 at calcinations temperature of 800 °C.
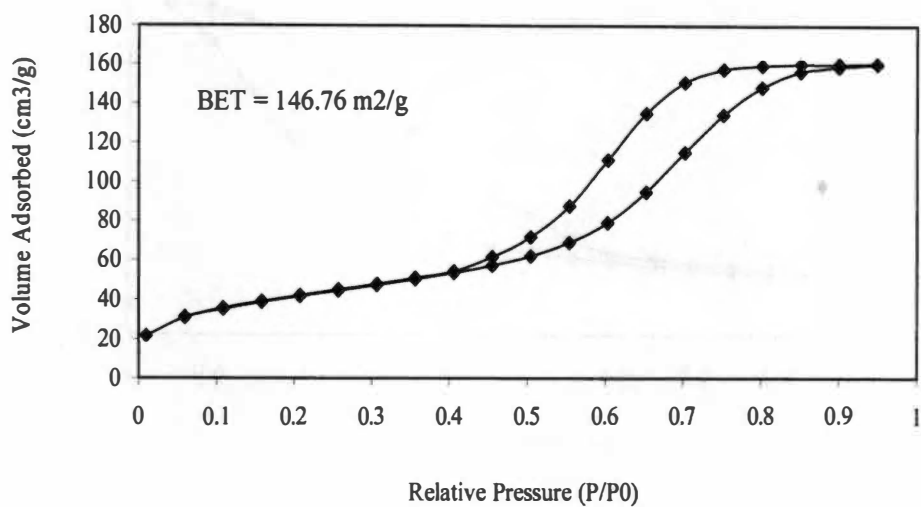
Figure A.15: BET adsorption-desorption isotherm for U-Cu-Meso-29 at calcinations temperature of 800 °C.
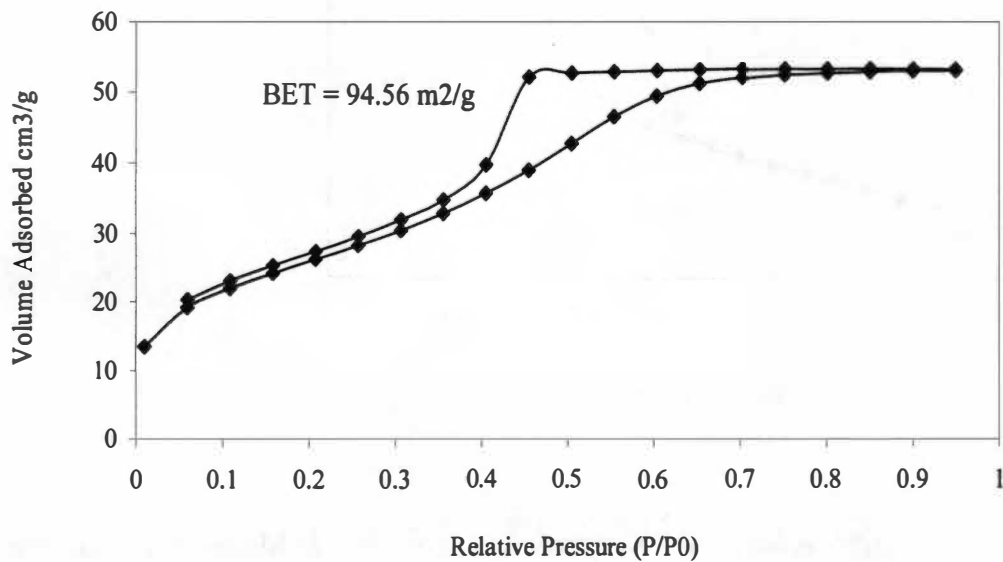
Figure A.16: BET adsorption-desorption for U-Sr-Meso-33 at calcinations temperature of 800 °C.
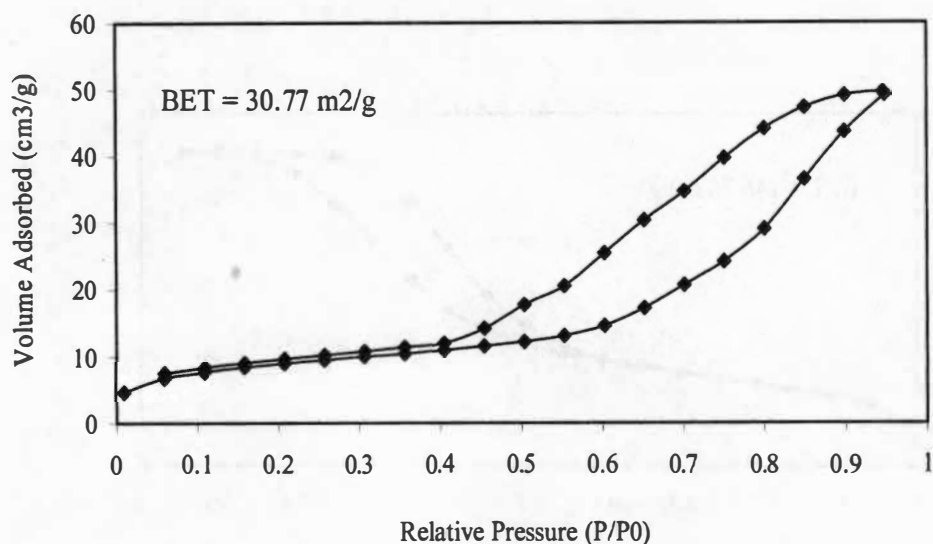
Figure A.17: BET adsorption-desorption for MesoSr-34 at calcinations temperature of 800 °C.
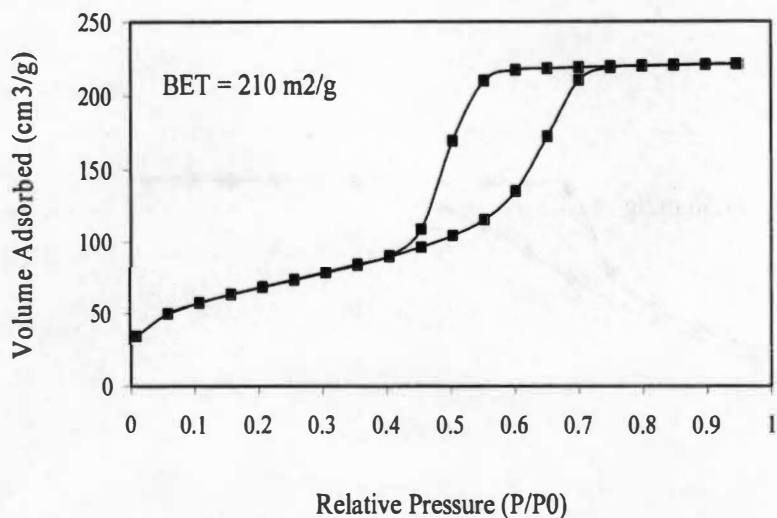
Figure A.18: BET adsorption-desorption isotherm for U-Meso-13 at calcinations temperature of 800 ^{0}C (U:Mg:Fe: FiguSi = 1:0.5:0.5:20)

Figure A.19: BET adsorption-desorption isotherm for U-Meso-14 (U:Ca:Fe:Si = 1:0.5:0.5:20)
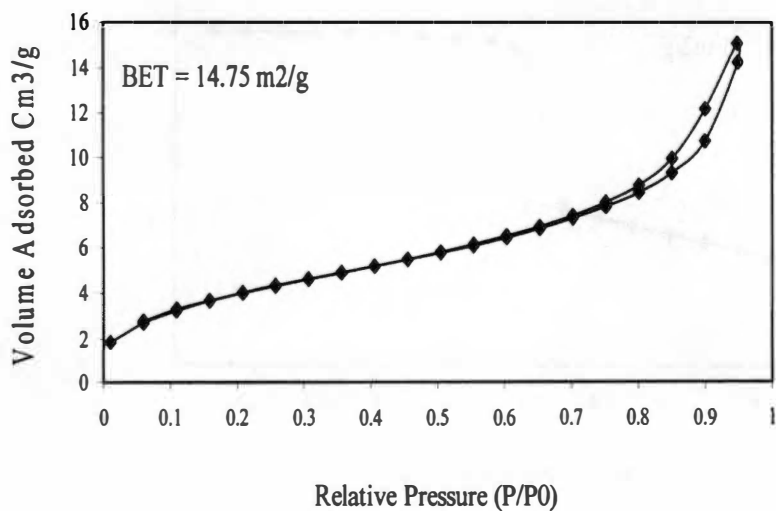
Figure A.20: BET adsorption-desorption isotherm for La-U-52 (Pechini Method).
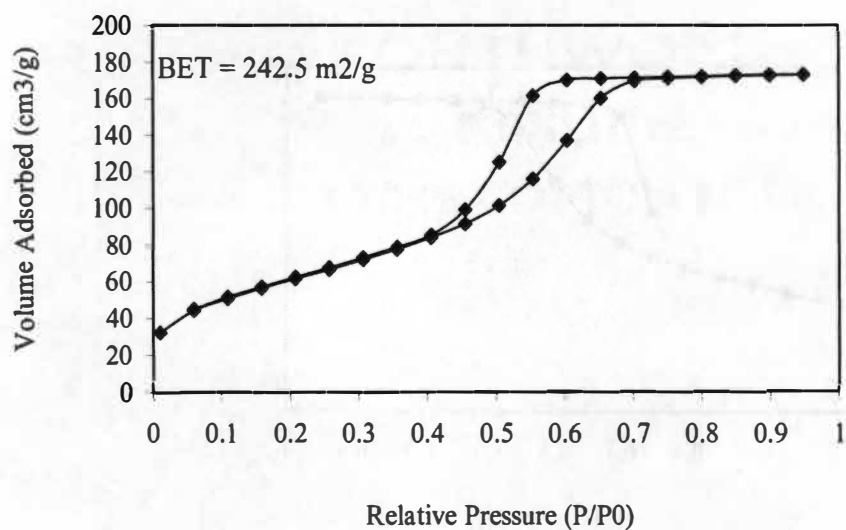
A.21: BET adsorption-desorption isotherm for La-Ti-53 catalyst (U:Ti:La = 1:20:0.45)
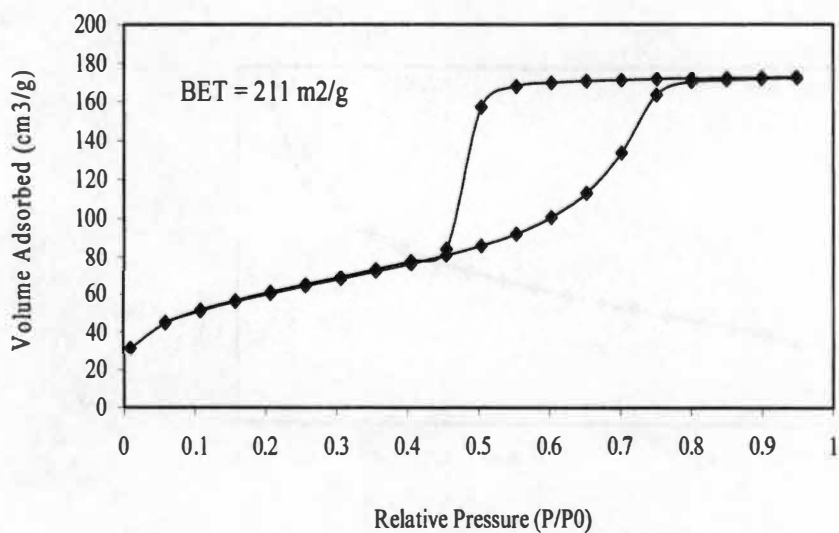
Figure A.22: BET adsorption-desorption isotherm for U-Ce-Meso-28 at calcinations temperature of 800 °C.

APPENDIX B

B.1 Synthesis calculations for SiO2.

Tetraethoxysilane (TEOS) = 2 ml
Pluronic F127 (BASF) surfactant = 0.75
Butanol = 0.5 ml
Cyclohexane = 0.5 ml
Ethanol = 2 ml

$$2 \text{ ml TEOS} \times \frac{0.934g}{1 \text{ ml TEOS}} \times \frac{1 \text{ mole TEOS}}{208.34 \text{ g}} = 0.008966 \text{ g - mole TEOS produced}$$

0.008966 g-mole TEOS $\times \dfrac{60.0 \text{ g SiO}_2}{1 \text{ mole SiO}_2} = 0.538 \text{ g SiO}_2$ produced at the end of

experiment.

B.2 Synthesis calculation for U-Meso-5.

U:Si = 1:10 mole ratio
Tetraethoxysilane (TEOS) = 2 ml
Pluronic F127 (BASF) surfactant = 0.75
Butanol = 0.5 ml
Cyclohexane = 0.5 ml
Ethanol = 2 ml
$UO_2(NO_3)_2 . 6 H_2O = 0.45$ g as follows:

$$2 \text{ ml TEOS} \times \frac{0.934g}{1 \text{ ml TEOS}} \times \frac{1 \text{ mole TEOS}}{208.34 \text{ g}} = 0.008966 \text{ g - mole TEOS produced}$$

0.008966 g-mole TEOS $\times \dfrac{60.0 \text{ g SiO}_2}{1 \text{ mole SiO}_2} = 0.538 \text{ g SiO}_2$ produced at the end of

experiment.

$$0.008966113 \text{ g - mole TEOS} \times \frac{1 \text{ mole U}}{10 \text{ mole Si}} = 0.000896611 \text{ g - mole Uranyl Nitrate}$$

0.000896611 g-mole Uranyl Nitrate $\times$

$$\frac{502 \text{ g.}}{1 \text{ g - mole } UO_2(NO_3)_2 . 6 H_2O} = 0.45 \text{ g Uranyl Nitrate required for experiment.}$$

$$0.000896611 \text{ g - mole Uranyl nitrate} \times \frac{842 \text{ g}}{1 \text{ g - mole } U_3O_3} \times \frac{1}{3 \text{ U}} = 0.251 \text{ g U at the end}$$

Total weight = 0.538 g (Si) + 0.251 g (U) = 0.789g
Si = 68%
U = 32%   by weight

B.3 Synthesis calculation for U-Meso-6.

U:Si = 1:20 mole ratio
Tetraethoxysilane (TEOS) = 2 ml
Pluronic F127 (BASF) surfactant = 0.75
Butanol = 0.5 ml
Cyclohexane = 0.5 ml
Ethanol = 2 ml
$UO_2(NO_3)_2.6H_2O$ = 0.225 g as follows:

$$2 \text{ ml TEOS} \times \frac{0.934g}{1\,\text{ml TEOS}} \times \frac{1\,\text{mole TEOS}}{208.34\,\text{g}} = 0.008966 \text{ g - mole TEOS produced}$$

$$0.008966 \text{ g-mole TEOS} \times \frac{60.0\,\text{g SiO}_2}{1\,\text{mole SiO}_2} = 0.538 \text{ g SiO}_2 \text{ produced at the end of}$$

experiment.

$$0.008966113 \text{ g - mole TEOS} \times \frac{1\,\text{mole U}}{20\,\text{mole Si}} = 0.000448306 \text{ g - mole Uranyl Nitrate}$$

0.000448306 g-mole Uranyl Nitrate ×

$$\frac{502\,\text{g.}}{1\,\text{g - mole UO}_2(NO_3)_2.6H_2O} = 0.225 \text{ g Uranyl Nitrate required for experiment.}$$

$$0.000448306 \text{ g - mole Uranyl nitrate} \times \frac{842\,\text{g}}{1\,\text{g - mole U}_3O_3} \times \frac{1}{3\,\text{U}} = 0.126 \text{ g U at the end}$$

Total weight = 0.538 g (Si) + 0.1260 g (U) = 0.664 g
Si = 80%
U = 20%   by weight

All mixtures were stirred over night, then it was dried at room temperature in an open vial for 7 days. After drying, the raw catalyst was annealed at 150 C for 6 hours to build mesoporous structures, then it was heated at 600 C for additional 6 hours, and finally it was calcined at 800 C for 8 hours intentionally to remove the template and making U_3O_8 for higher activity.

B.4 Synthesis calculation for U-Meso-9.

U:Si = 1:30 mole ratio
Tetraethoxysilane (TEOS) = 2 ml
Pluronic F127 (BASF) surfactant = 0.75
Butanol = 0.5 ml
Cyclohexane = 0.5 ml
Ethanol = 2 ml
$UO_2(NO_3)_2 . 6 H_2O = 0.15$ g as follows:

$$2 \text{ ml TEOS} \times \frac{0.934g}{1 \text{ ml TEOS}} \times \frac{1 \text{ mole TEOS}}{208.34 \text{ g}} = 0.008966 \text{ g - mole TEOS produced}$$

$$0.008966 \text{ g-mole TEOS} \times \frac{60.0 \text{ g SiO}_2}{1 \text{ mole SiO}_2} = 0.538 \text{ g SiO}_2 \text{ produced at the end of}$$

experiment.

$$0.00896613 \text{ g - mole TEOS} \times \frac{1 \text{ mole U}}{30 \text{ mole Si}} = 0.00029887 \text{ g - mole Uranyl Nitrate}$$

0.00029887 g-mole Uranyl Nitrate ×

$$\frac{502 \text{ g.}}{1 \text{ g - mole } UO_2(NO_3)_2 . 6 H_2O} = 0.150 \text{ g Uranyl Nitrate required for experiment.}$$

$$0.00029887 \text{ g - mole Uranyl nitrate} \times \frac{842 \text{ g}}{1 \text{ g - mole } U_3O_3} \times \frac{1}{3 \text{ U}} = 0.084 \text{ g U at the end}$$

Total weight = 0.538 g (Si) + 0.084 g (U) = 0.622 g
Si = 86.50%
U = 13.50% by weight

B.5 Synthesis calculation for U-Meso-15

U:Si = 1:40 mole ratio
Tetraethoxysilane (TEOS) = 2 ml
Pluronic F127 (BASF) surfactant = 0.75
Butanol = 0.5 ml
Cyclohexane = 0.5 ml
Ethanol = 2 ml
$UO_2(NO_3)_2 . 6 H_2O = 0.1125$ g uranyl nitrate as follows:

$$2 \text{ ml TEOS} \times \frac{0.934g}{1 \text{ ml TEOS}} \times \frac{1 \text{ mole TEOS}}{208.34 \text{ g}} = 0.008966 \text{ g - mole TEOS produced}$$

0.008966 g-mole TEOS $\times \dfrac{60.0 \text{ g SiO}_2}{1 \text{ mole SiO}_2} = 0.538 \text{ g SiO}_2$ produced at the end of experiment.

$$0.008966113 \text{ g - mole TEOS} \times \frac{1 \text{ mole U}}{40 \text{ mole Si}} = 0.000224153 \text{ g - mole Uranyl Nitrate}$$

0.000224153 g-mole Uranyl Nitrate $\times$

$$\frac{502 \text{ g.}}{1 \text{ g - mole UO}_2(\text{NO}_3)_2 . 6 \text{ H}_2\text{O}} = 0.1125 \text{ g Uranyl Nitrate required for experiment.}$$

$$0.000224153 \text{ g - mole Uranyl nitrate} \times \frac{842 \text{ g}}{1 \text{ g - mole U}_3\text{O}_3} \times \frac{1}{3 \text{ U}} = 0.063 \text{ g U at the end}$$

Total weight = 0.538 g (Si) + 0.063 g (U) = 0.601 g
Si = 89.50%
U = 10.50%   by weight

B.6 Synthesis calculation for U-Meso-18

U:Si = 1:50 mole ratio
Tetraethoxysilane (TEOS) = 2 ml
Pluronic F127 (BASF) surfactant = 0.75
Butanol = 0.5 ml
Cyclohexane = 0.5 ml
Ethanol = 2 ml
$UO_2(NO_3)_2 . 6 H_2O =$ 0.09 g uranyl nitrate as follows:

$$2 \text{ ml TEOS} \times \frac{0.934g}{1 \text{ ml TEOS}} \times \frac{1 \text{ mole TEOS}}{208.34 \text{ g}} = 0.008966 \text{ g - mole TEOS produced}$$

0.008966 g-mole TEOS $\times \dfrac{60.0 \text{ g SiO}_2}{1 \text{ mole SiO}_2} = 0.538 \text{ g SiO}_2$ produced at the end of experiment.

$$0.008966113 \text{ g - mole TEOS} \times \frac{1 \text{ mole U}}{50 \text{ mole Si}} = 0.000179322 \text{ g - mole Uranyl Nitrate}$$

0.000179322 g-mole Uranyl Nitrate $\times$

$$\frac{502 \text{ g.}}{1 \text{ g - mole UO}_2(\text{NO}_3)_2.6\text{ H}_2\text{O}} = 0.0900 \text{ g Uranyl Nitrate required for experiment.}$$

$$0.0001793 \text{ g - mole Uranyl nitrate} \times \frac{842 \text{ g}}{1 \text{ g - mole U}_3\text{O}_3} \times \frac{1}{3 \text{ U}} = 0.05 \text{ g U at the end}$$

Total weight = 0.538 g (Si) + 0.05 g (U) = 0.588 g
Si = 91.50%
U = 8.50%   by weight

B.7 Synthesis calculation for U-Cr-Meso-21.

U:Si = 1:20 mole ratio
Tetraethoxysilane (TEOS) = 2 ml
Pluronic F127 (BASF) surfactant = 0.75
Butanol = 0.5 ml
Cyclohexane = 0.5 ml
Ethanol = 2 ml
CrCl$_3$.6 H$_2$O = 0.12 g (see calculation)
$UO_2(NO_3)_2.6\text{ H}_2\text{O} = 0.225$ g as follows:

$$2 \text{ ml TEOS} \times \frac{0.934 g}{1 \text{ ml TEOS}} \times \frac{1 \text{ mole TEOS}}{208.34 \text{ g}} = 0.008966 \text{ g - mole TEOS produced}$$

$$0.008966 \text{ g-mole TEOS} \times \frac{60.0 \text{ g SiO}_2}{1 \text{ mole SiO}_2} = 0.538 \text{ g SiO}_2 \text{ produced at the end of}$$

experiment.

$$0.008966113 \text{ g - mole TEOS} \times \frac{1 \text{ mole U}}{20 \text{ mole Si}} = 0.000448306 \text{ g - mole Uranyl Nitrate}$$

0.000448306 g-mole Uranyl Nitrate ×

$$\frac{502 \text{ g.}}{1 \text{ g - mole UO}_2(\text{NO}_3)_2.6\text{ H}_2\text{O}} = 0.225 \text{ g Uranyl Nitrate required for experiment.}$$

$$0.000448306 \text{ g - mole Uranyl nitrate} \times \frac{842 \text{ g}}{1 \text{ g - mole U}_3\text{O}_3} \times \frac{1}{3 \text{ U}} = 0.126 \text{ g U at the end}$$

$$0.008966113 \text{ g - mole TEOS} \times \frac{1 \text{ mole Cr}}{20 \text{ mole Si}} = 0.000448306 \text{ g - mole CrCl}_3.6\text{ H}_2\text{O}$$

$$0.0004483 \text{g-mole CrCl}_3 6\text{H}_2\text{O} \times \frac{266.35 \text{ g}}{1\text{g-mole CrCl}_3.6\text{H}_2\text{O}} = 0.1194\text{g CrCl}_3 6\text{H}_2\text{O required for exp.}$$

$$0.0004483 \text{g-mole CrCl}_3 6\text{H}_2\text{O} \times \frac{151.992\text{g}}{1\text{g-mole Cr}_2\text{O}_3} \times \frac{1}{2\text{Cr}} = 0.034\text{ g Cr at the end of}$$

calcinatio at 800 ^{0}C.

Note: $CrCl_3 6H_2O$ will change into Cr_2O_3 after calcinations.

Total weight = 0.538 g S i + 0.034 Cr + 0.126 g U = 0.698 g

Si = 77%
Cr = 4.90
U = 18.1

B.8 Synthesis calculation for U-Co-Meso-24.

U:Si = 1:20 mole ratio
Tetraethoxysilane (TEOS) = 2 ml
Pluronic F127 (BASF) surfactant = 0.75
Butanol = 0.5 ml
Cyclohexane = 0.5 ml
Ethanol = 2 ml
$CoCl_2.6 H_2O$ = 0.107 g (see calculation below)
$UO_2(NO_3)_2.6 H_2O$ = 0.225 g as follows:

$$2 \text{ ml TEOS} \times \frac{0.934\text{g}}{1\text{ml TEOS}} \times \frac{1 \text{mole TEOS}}{208.34 \text{ g}} = 0.008966 \text{ g-mole TEOS produced}$$

$$0.008966 \text{ g-mole TEOS} \times \frac{60.0 \text{ g SiO}_2}{1 \text{mole SiO}_2} = 0.538 \text{ g SiO}_2 \text{ produced at the end of}$$

experiment.

$$0.008966113 \text{ g-mole TEOS} \times \frac{1 \text{mole U}}{20 \text{ mole Si}} = 0.000448306 \text{ g-mole Uranyl Nitrate}$$

0.000448306 g-mole Uranyl Nitrate ×

$$\frac{502 \text{ g.}}{1\text{g-mole UO}_2(\text{NO}_3)_2.6\text{H}_2\text{O}} = 0.225 \text{ g Uranyl Nitrate required for experiment.}$$

$$0.000448306 \text{ g - mole Uranyl nitrate} \times \frac{842 \text{ g}}{1 \text{ g - mole } U_3O_3} \times \frac{1}{3 \text{ U}} = 0.126 \text{ g U at the end}$$

$$0.008966113 \text{ g - mole TEOS} \times \frac{1 \text{ mole Co}}{20 \text{ mole Si}} = 0.000448306 \text{ g - mole CoCl}_2.6 \text{ H}_2\text{O}$$

$$0.00044836 \text{ g - mole CoCl}_2.6 \text{H}_2\text{O} \times \frac{237.84 \text{ g}}{1 \text{ g - mole CoCl}_2.6 \text{H}_2\text{O}} = 0.107 \text{ g CoCl}_2.6 \text{H}_2\text{O required for exp.}$$

$$0.00044836 \text{ g - mole CoCl}_2.6 \text{H}_2\text{O} \times \frac{165.866 \text{ g}}{1 \text{ g - mole Co}_2\text{O}_3} \times \frac{1}{2 \text{ Co}} = 0.037 \text{ g Co at the end of calcinatin}$$

Note: $CoCl_2.6H_2O$ turns into Co_2O_3 after calcinations at 800 °C.

Total weight = 0.538 g S i + 0.037 Co + 0.126 g U = 0.701 g

Si = 76%
Co = 5.23
U = 18.77

B.9 Synthesis calculation for TiO₂.

P123 (surfactant) = 1.25 g
2-Propanol = 14 g
$Ti(OC_2H_5)_4$ = 3.0 g
2,4-Pentanedione = 0.53 g
Ethanol = 2.0 g

$$3.0 \text{ g } Ti(OC_2H_5)_4 \times \frac{\text{g - mole } Ti(OC_2H_5)_4}{228.0 \text{ g (F.W)}} = 0.01315 \text{ g - mole } Ti(OC_2H_5)_4$$

$$0.01315 \text{ g mole } Ti(OC_2H_5)_4 \frac{1 \text{ g mole TiO}_2}{1 \text{ g mole } Ti(OC_2H_5)_4} \times \frac{79.90 \text{ g (M.W)}}{1 \text{ g mole TiO}_2} = 1.05 \text{ g TiO}_2$$

produced after calcinations.

%wt Ti = 74
%wt U = 26

B.10 Synthesis calculation for U-Ti-Meso-42.

U:Ti = 1: 10 (mole ratio)

The following materials have been used for the synthesis of precursor:

Titanium (IV) ethoxide = 3 g
2, 4- Pentanedione = 0.53 g
2-Propanol = 4 g

After 2 hours steering, it was added to the following solutions:

1.25 g of P123 surfactant was dissolved in 14 g of 2-propanol and steering for 2 hours. 0.530 g of $UO_2(NO_3)_2 \cdot 6H_2O$ was added to this solution. The PH of mixture including the precursor and surfactant was adjusted to 2 by addition of 4 ml HNO_3. The total sol solution was steered for 2 days. Then, it was transferred to an open tray, drying under ambient conditions for 10 days. The trunk sample was annealed at 150 C for 72 hours, then, it was calcined at 350 C for 24 hours to remove the templates. The prepared catalyst was divided into three equal portions. The other two portions were calcined at 600 C and 800 C respectively.

Calculations are as follows:

Titanium (IV) ethoxide $\{Ti(OC_2H_5)_4\}$ = 3.0 g

$$\frac{3\,g\,Titanium\,(IV)\,ethoxide}{227.9\,g\,(MW)} \times \frac{1\,mole\,UO_2(NO_3)_2 \cdot 6H_2O}{10\,mole\,Titanium\,(IV)\,etoxide} \times \frac{502\,g\,(MW)}{1\,mole\,UO_2(NO_3)_2 \cdot 6H_2O} = 0.66\ g\ required$$

$UO_2(NO_3)_2 \cdot 6H_2O$ for the above mole ratio in this experiment.

$$\frac{0.66\,g}{502\,g\,(MW)}\,Uranyl\,nitrate \times \frac{842\,g}{1\,g\text{-}mole\,U_3O_3} \times \frac{1}{3\,U} = 0.369\ g\ U\ at\ the\ end\ produced$$

$$\frac{3\,g\,Ti(OC_2H_5)_4}{227.9\,g\,(MW)} \times \frac{1\,mole\,TiO_2}{1\,mole\,Ti(OC_2H_5)_4} \times \frac{79.90\,g\,TiO_2}{1\,mole\,TiO_2} \times \frac{1\,Ti}{1\,TiO_2} = 1.05\ g\ TiO_2\ after\ calcinations$$

Total catalyst produced = 1.05 (TiO_2) + 0.369 (U_3O_8) = 1.419 g total (weight of catalyst).

B.11 Synthesis calculation for U-Ti-Meso-43.

U: Ti
1: 20

The following materials have been used for the synthesis of precursor:

Titanium (IV) ethoxide = 3 g
2, 4- Pentanedione = 0.53 g
2-Propanol = 4 g

After 2 hours steering, it was added to the following solutions:

1.25 g of P123 surfactant was dissolved in 14 g of 2-propanol and steering for 2 hours. 0.265 g of $UO_2(NO_3)_2.6H_2O$ was added to this solution. The PH of mixture including the precursor and surfactant was adjusted to 2 by addition of 4 ml HNO3. The total sol solution was steered for 2 days. Then, it was transferred to an open tray, drying under ambient conditions for 10 days. The trunk sample was annealed at 150 C for 72 hours, then, it was calcined at 350 C for 24 hours to remove the templates. The prepared catalyst was divided into three equal portions. The other two portions were calcined at 600 C and 800 C respectively.

Calculations are as follows:

Titanium (IV) ethoxide $\{Ti(OC_2H_5)_4\}$ = 3.0 g

$$\frac{3\,g\,Titanium\,(IV)\,ethoxide}{227.9\,g\,(MW)} \times \frac{1\,mole\,UO_2(NO_3)_2.6H_2O}{20\,mole\,Titanium\,(IV)\,etoxide} \times \frac{502\,g\,(MW)}{1\,mole\,UO_2(NO_3)_2.6H_2O} = 0.330\,g\,required$$

$UO_2(NO_3)_2.6H_2O$ for the above mole ratio.

$$\frac{0.330\,g}{502\,g\,(MW)}\,Uranyl\,nitrate \times \frac{842\,g}{1\,g\text{-}mole\,U_3O_3} \times \frac{1}{3\,U} = 0.185\ g\,U\,at\,the\,end\,produced$$

$$\frac{3\,g\,Ti(OC_2H_5)_4}{227.9\,g\,(MW)} \times \frac{1\,mole\,TiO_2}{1\,mole\,Ti(OC_2H_5)_4} \times \frac{79.90\,g\,TiO_2}{1\,mole\,TiO_2} = 1.05\,g\,TiO_2\,produced\,at\,the\,end\,of\,exp.$$

Total catalyst produced = 1.05 (TiO_2) + 0.185 (U_3O_8) = 1.235

%wt Ti = 85
%wt U = 15

B.12 Synthesis calculation for U-Ti-Meso-44.

U: Ti
1: 30

The following materials have been used for the synthesis of precursor:

Titanium (IV) ethoxide = 3 g
2, 4- Pentanedione = 0.53 g
2-Propanol = 4 g

After 2 hours steering, it was added to the following solutions:

1.25 g of P123 surfactant was dissolved in 14 g of 2-propanol and steering for 2 hours. 0.177 g of $UO_2(NO_3)_2 . 6H_2O$ was added to this solution. The PH of mixture including the precursor and surfactant was adjusted to 2 by addition of 4 ml HNO3. The total sol solution was steered for 2 days. Then, it was transferred to an open tray, drying under ambient conditions for 10 days. The trunk sample was annealed at 150 C for 72 hours, then, it was calcined at 350 C for 24 hours to remove the templates. The prepared catalyst was divided into three equal portions. The other two portions were calcined at 600 C and 800 C respectively.
Calculations are as follows:

Titanium (IV) ethoxide $\{Ti(OC_2H_5)_4\}$ = 3.0 g

$$\frac{3\,g\,Titanium\,(IV)\,ethoxide}{227.9\ g\,(MW)} \times \frac{1\,mole\,UO_2(NO_3)_2 . 6H_2O}{30\,mole\,Titanium\,(IV)\,etoxide} \times \frac{502\,g\,(MW)}{1\,mole\,UO_2(NO_3)_2 . 6H_2O} = 0.220\,g\,required$$
$UO_2(NO_3)_2 . 6H_2O$ for the above mole ratio.

$$\frac{0.220\,g}{502\,g\,(MW)}\,Uranyl\,nitrate \times \frac{842\,g}{1\,g\text{-}mole\,U_3O_3} \times \frac{1}{3\,U} = 0.123\ g\,U\,at\,the\,end\,produced$$

$$\frac{3\,g\,Ti(OC_2H_5)_4}{227.9\,g\,(MW)} \times \frac{1\,mole\,TiO_2}{1\,mole\,Ti(OC_2H_5)_4} \times \frac{79.90\,g\,TiO_2}{1\,mole\,TiO_2} = 1.05\,g\,TiO_2\,produced\,at\,the\,end\,of\,exp.$$

Total catalyst produced = 1.05 (TiO_2) + 0.123 g (U_3O_8) = 1.173 g catalyst produced

%wt Ti = 89.5
%wt U = 10.5

B.13 Synthesis calculation for U-Ti-Meso-45.

U: Ti
1: 40

The following materials have been used for the synthesis of precursor:

Titanium (IV) ethoxide = 3 g
2, 4- Pentanedione = 0.53 g
2-Propanol = 4 g

After 2 hours stirring, it was added to the following solutions:

1.25 g of P123 surfactant was dissolved in 14 g of 2-propanol and steering for 2 hours. 0.132 g of $UO_2(NO_3)_2.6H_2O$ was added to this solution. The PH of mixture including the precursor and surfactant was adjusted to 2 by addition of 4 ml HNO₃. The total sol solution was steered for 2 days. Then, it was transferred to an open tray, drying under ambient conditions for 10 days. The trunk sample was annealed at 150 C for 72 hours, then, it was calcined at 350 C for 24 hours to remove the templates. The prepared catalyst was divided into three equal portions. The other two portions were calcined at 600 C and 800 C respectively.

Calculations are as follows:

Titanium (IV) ethoxide $\{Ti(OC_2H_5)_4\}$ = 3.0 g

$$\frac{3\,g\,Titanium\,(IV)\,ethoxide}{227.9\ g\,(MW)} \times \frac{1\,mole\,UO_2(NO_3)_2.6H_2O}{40\,mole\,Titanium\,(IV)\,etoxide} \times \frac{502\,g\,(MW)}{1\,mole\,UO_2(NO_3)_2.6H_2O} = 0.165 \text{ g required}$$

$UO_2(NO_3)_2.6H_2O$ for the above mole ratio.

$$\frac{0.165\,g}{502\,g\,(MW)} \text{Uranyl nitrate} \times \frac{842\,g}{1\,g\text{-}mole\,U_3O_8} \times \frac{1}{3\,U} = 0.092 \text{ g U at the end produced}$$

$$\frac{3\,g\,Ti(OC_2H_5)_4}{227.9\,g\,(MW)} \times \frac{1\,mole\,TiO_2}{1\,mole\,Ti(OC_2H_5)_4} \times \frac{79.90\,g\,TiO_2}{1\,mole\,TiO_2} = 1.05 \text{ g } TiO_2 \text{ produced at the end of exp.}$$

Total catalyst produced = 1.05 (TiO_2) + 0.092 (U_3O_8) = 1.14 g catalyst produced

%wt Ti = 91.93
%wt U = 8.07

B.14 Synthesis calculation for U-Cu-Meso-30.

This catalyst was made in the following procedure:

The mole ratio U : Si : Cu was 1 : 20 : 5 respectively. The chemicals are as follows:

TEOS = 2 ml, F127 = 0.75 g, Uranyl nitrate = 0.225 g, Ethanol = 2 ml, HNO_3 = 2 ml
Cyclohexane = 0.5 ml, Butanol = 0.5 ml
$Cu(NO_3)_2 \cdot 3H_2O$ = 0.5415 g based on the following calculations:

$$2 \text{ ml TEOS} \times \frac{0.934g}{1\text{ ml TEOS}} \times \frac{1\text{ mole TEOS}}{208.34\text{ g}} = 0.008966 \text{ g - mole TEOS produced}$$

$$0.008966 \text{ g-mole TEOS} \times \frac{60.0\text{ g SiO}_2}{1\text{ mole SiO}_2} = 0.538 \text{ g SiO}_2 \text{ produced at the end of}$$

experiment.

$$0.008966113 \text{ g-mole Si} \times \frac{5\text{ mole Cu}}{20\text{ mole Si}} = 0.002241 \text{ g - mole Cu (NO}_3)_2 .3\,H_2O \text{ is required}$$

$$0.002241528 \text{ g-mole Cu (NO3)}_2. 3H_2O \times$$

$$\frac{241.60\text{ g}}{1\text{ mole Cu(NO}_3)_2.3\,H_2o} = 0.5415 \text{ g Cu(NO}_3)_2.3\,H_2O \text{ must be weighed}$$

$$\frac{0.5415 \text{ g Cu(NO}_3)_2.3\,H_2O}{241.60\text{ g (MWt)}} \times \frac{1\text{ mole CuO}}{1\text{ mole Cu(NO}_3)_2.3H_2O} \times \frac{79.54\text{ g}}{1\text{ mole CuO}} = 0.1783 \text{ g CuO was produced}$$

Calculation of required uranyl oxide hexahydrate as follows:

$$0.008966113 \text{ g - mole TEOS} \times \frac{1\text{ mole U}}{20\text{ mole Si}} = 0.000448306 \text{ g - mole Uranyl Nitrate}$$

0.000448306 g-mole Uranyl Nitrate ×

$$\frac{502\,g.}{1\,g\text{-mole}\,UO_2(NO_3)_2.6\,H_2O} = 0.225\,g \text{ Uranyl Nitrate required for experiment.}$$

$$0.000448306\,g\text{-mole Uranyl nitrate} \times \frac{842\,g}{1\,g\text{-mole}\,U_3O_3} \times \frac{1}{3\,U} = 0.1263\,g\,U \text{ at the end}$$

Total weight = 0.538 g (Si) + 0.1783 g (Cu) + 0.1263 g (U) = 0.8426 g

Si = 63.85%   Cu = 21.16%   U = 15%   by weight

All mixtures were stirred over night, then it was dried at room temperature in an open vial for 7 days. After drying, the raw catalyst was annealed at 150 C for 6 hours to build mesoporous structures, then it was heated at 600 C for additional 6 hours, and finally it was calcined at 800 C for 8 hours intentionally to remove the template and making U_3O_8 for higher activity.

MesoCu (30)

This catalyst was made in the following procedure without uranyl nitrate:

The mole ratio Si : Cu , 20 : 5 respectively. The chemicals are as follows:

TEOS = 2 ml, F127 = 0.75 g, Ethanol = 2 ml, HNO_3 = 2 ml

Cyclohexane = 0.5 ml, Butanol = 0.5 ml

$Cu(NO_3)_2. 3H_2O$ = 0.5415 g based on the following calculations:

$$2\,ml\,TEOS \times \frac{0.934\,g}{1\,ml\,of\,TEOS} \times \frac{1\,mole\,TEOS}{208.34\,g\,TEOS} = 0.008966\,g\text{-mole TEOS}$$

$$0.008966\,g\text{-mole TEOS} \times \frac{60.0\,g\,SiO_2}{1\,mole\,SiO_2} = 0.538\,g\,SiO_2 \text{ produced at the end of}$$

experiment.

$$0.008966113\,g\text{-mole Si} \times \frac{5\,mole\,Cu}{20\,mole\,Si} = 0.002241\,g\text{-mole Cu}\,(NO_3)_2.3\,H_2O \text{ is required}$$

0.002241528 g-mole Cu (NO3)$_2$. 3H$_2$O $\times$

$$\frac{241.60\,g}{1\,mole\,Cu(NO_3)_2.3\,H_2o} = 0.5415\,g\,Cu(NO_3)_2.3\,H_2O\ \text{must be weighed}$$

$$\frac{0.5415\,g\,Cu(NO_3)_2.3\,H_2O}{241.60\,g\,(MWt)} \times \frac{1\,mole\,CuO}{1\,mole\,Cu(NO_3)_2.3H_2O} \times \frac{79.54\,g}{1\,mole\,CuO} = 0.1783\,g\,CuO\ \text{was produced}$$

Total weight = 0.538 g (Si) + 0.1783 g (Cu) = 0.7163 g total weight of catalyst was produced.

Si = 75.10%   Cu = 24.90%   by weight

All mixtures were stirred over night, then it was dried at room temperature in an open vial for 7 days. After drying, the raw catalyst was heated at 150 C for 6 hours to build mesoporous structures, then it was calcined at 600 C for additional 6 hours, and finally it was calcined at 800 C for 8 hours to make CuO.

B.15 Synthesis calculation for U-Sr-Meso-33.

This catalyst was made in the following procedure:

The mole ratio U : Si : Sr was 1 : 20 : 1 respectively. The chemicals are as follows:

TEOS = 2 ml, F127 = 0.75 g, Uranyl nitrate = 0.225 g, Ethanol = 2 ml, HNO$_3$ = 2 ml
Cyclohexane = 0.5 ml, Butanol = 0.5 ml
SrCl$_2$.6 H$_2$O = 0.12 g based on the following calculations:

$$2\,ml\,TEOS \times \frac{0.934g}{1\,ml\,TEOS} \times \frac{1\,mole\,TEOS}{208.34\,g} = 0.008966\,g\text{-}mole\,TEOS\ \text{produced}$$

0.008966 g-mole TEOS $\times \dfrac{60.0\,g\,SiO_2}{1\,mole\,SiO_2} = 0.538\,g\,SiO_2$ produced   at   the   end   of

experiment.

$$0.008966113 \text{ g-mole Si} \times \frac{1 \text{ mole Sr}}{20 \text{ mole Si}} = 0.0004483 \text{ g - mole SrCl}_2.6\text{H}_2\text{O is required}$$

0.0004483 g-mole SrCl$_2$. 6H$_2$O $\times$

$$\frac{266.62 \text{ g}}{1 \text{ mole SrCl}_2.6\text{H}_2\text{o}} = 0.12 \text{ g SrCl}_2.6\text{H}_2\text{O must be weighed}$$

$$\frac{0.12 \text{ g SrCl}_2.6\text{H}_2\text{O}}{266.62 \text{ g (MWt)}} \times \frac{1 \text{ moleSrO}}{1 \text{ moleSrCl}_2.6\text{H}_2\text{O}} \times \frac{103.62 \text{ g}}{1 \text{ moleSrO}} = 0.0466 \text{ g SrO was produced}$$

Calculation of required uranyl oxide hexahydrate as follows:

$$0.008966113 \text{ g - mole TEOS} \times \frac{1 \text{ mole U}}{20 \text{ moleSi}} = 0.000448306 \text{ g - mole Uranyl Nitrate}$$

0.008966113 g-mole Uranyl Nitrate $\times$

$$\frac{502 \text{ g.}}{1 \text{ g - mole UO}_2(\text{NO}_3)_2.6\text{H}_2\text{O}} = 0.225 \text{ g Uranyl Nitrate required for experiment.}$$

$$0.000448306 \text{ g - mole Uranyl nitrate} \times \frac{842 \text{ g}}{1 \text{ g - mole U}_3\text{O}_3} \times \frac{1}{3 \text{ U}} = 0.1263 \text{ g U at the end}$$

Total weight = 0.538 g (Si) + 0.0466 g (Sr) + 0.1263 g (U) = 0.7107 g
Si = 75.7%   Sr = 6.55%   U = 17.75%   by weight

All mixtures were stirred over night, then it was dried at room temperature in an open vial for 7 days. After drying, the raw catalyst was annealed at 150 C for 6 hours to build mesoporous structures, then it was heated at 600 C for additional 6 hours, and finally it was calcined at 800 C for 8 hours intentionally to remove the template and making U$_3$O$_8$ for higher activity.

MesoSr (34)

This catalyst was made in the following procedure without uranyl nitrate:

The mole ratio Si : Sr , 20 : 1 respectively. The chemicals are as follows:

TEOS = 2 ml, F127 = 0.75 g, Ethanol = 2 ml, HNO$_3$ = 2 ml
Cyclohexane = 0.5 ml, Butanol = 0.5 ml
SrCl$_2$.6 H$_2$O = 0.12 g based on the following calculations:

$$2 \text{ ml TEOS} \times \frac{0.934 \text{ g}}{1 \text{ ml of TEOS}} \times \frac{1 \text{ mole TEOS}}{208.34 \text{ g TEOS}} = 0.008966 \text{ g - mole TEOS}$$

0.008966 g-mole TEOS $\times \dfrac{60.0\,\text{g SiO}_2}{1\,\text{mole SiO}_2} = 0.538\,\text{g SiO}_2$ produced at the end of experiment.

0.008966113 g-mole Si $\times \dfrac{1\,\text{mole Sr}}{20\,\text{mole Si}} = 0.0004483\,\text{g - mole SrCl}_2.\,6\,\text{H}_2\text{O}$ is required

0.0004483 g-mole $SrCl_2$. $6H_2O \times$

$\dfrac{266.62\,\text{g}}{1\,\text{mole SrCl}_2.\,6\,\text{H}_2\text{o}} = 0.12\,\text{g SrCl}_2.\,6\,\text{H}_2\text{O}$ must be weighed

$\dfrac{0.12\,\text{g SrCl}_2.6\,\text{H}_2\text{O}}{266.62\,\text{g (MWt)}} \times \dfrac{1\,\text{mole SrO}}{1\,\text{mole SrCl}_2.6\text{H}_2\text{O}} \times \dfrac{103.62\,\text{g}}{1\,\text{mole SrO}} = 0.0466\,\text{g SrO}$ was produced

Total weight = 0.538 g (Si) + 0.0466 g (Sr) = 0.5846 g total weight of catalyst was produced.

Si = 92%   Sr = 8%   by weight

All mixtures were stirred over night, then it was dried at room temperature in an open vial for 7 days. After drying, the raw catalyst was heated at 150 C for 6 hours to build mesoporous structures, then it was calcined at 600 C for additional 6 hours, and finally it was calcined at 800 C for 8 hours to make SrO.

VITA

Cyrus K. Riahi-Nezhad was born in suburb of the city of Noor (Vanoosh) near the coast of Caspian Sea located in Mazenderan province in the North of Iran (Persia). He attended Reza Pahlavi and Shareef High School in Chalous, Mazenderan and obtained his high-school diploma with honors in 1973. After finishing his tour of duty (Army) in fall of 1976, he came to U.S.A to pursue his undergraduate and graduate studies in Chemical Engineering. In 1990, he earned his B.S in Chemical Engineering from Tennessee Technological University. In December 2001, he obtained his first Master of Science in Chemical Engineering from University of Tennessee at Knoxville. In August 2004, he obtained his second Master of Science in Environmental Engineering from University of Tennessee at Knoxville He is currently a U.S Citizen and is employed in Chemical Sciences Division at the Oak Ridge National Laboratory. He is a member of American Institute of Chemical Engineers (AIChE) and American Institute of Environmental Engineering (AIEE).